Natural Resources Canada
Ressources naturelles Canada

High-Resolution Interpolation of Climate Scenarios for Canada Derived from General Circulation Model Simulations

D.T. Price, D.W. McKenney, L.A. Joyce,
R.M. Siltanen, P. Papadopol, and K. Lawrence

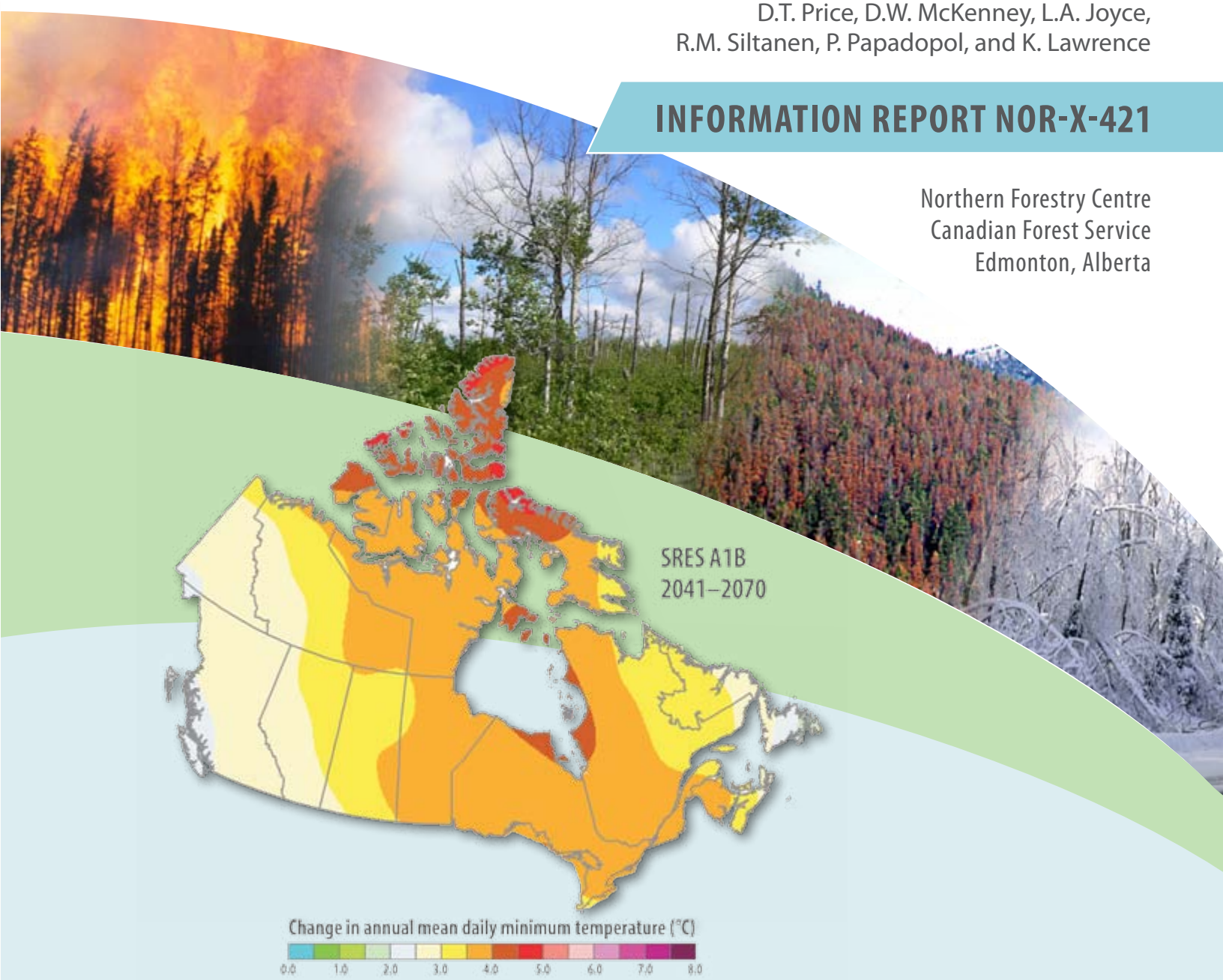

INFORMATION REPORT NOR-X-421

Northern Forestry Centre
Canadian Forest Service
Edmonton, Alberta

Published in partnership with the US Forest Service
Rocky Mountain Research Station, Fort Collins, Colorado, November 2011

Canada

The Northern Forestry Centre is one of five centres of the Canadian Forest Service, which has its headquarters in Ottawa, Ontario. This centre undertakes the regional delivery of national projects.

The Canadian Forest Service's main objective is research in support of improved forest management for economic, social, and environmental benefits to all Canadians.

Le Centre de foresterie du Nord constitue l'un des cinq établissements du Service canadien des forêts, dont l'administration centrale est à Ottawa (Ontario). Le Centre entreprend la réalisation régionale de projets nationaux.

Le Service canadien des forêts s'intéresse surtout à la recherche en vue d'améliorer l'aménagement forestier afin que tous les Canadiens puissent en profiter aux points de vue économique, social et environnemental.

Cover Photo credits: Natural Resources Canada (fire and mountain pine beetle damage), Ted Hogg, Natural Resources Canada (effects of drought), and Lina Breton, Province of Quebec (ice damage).

High-Resolution Interpolation of Climate Scenarios for Canada Derived from General Circulation Model Simulations

D.T. Price[1], D.W. McKenney[2], L.A. Joyce[3],
R.M. Siltanen[1], P. Papadopol[2], and K. Lawrence[2]

INFORMATION REPORT NOR-X-421

Canadian Forest Service
Northern Forestry Centre
2011

[1]Natural Resources Canada, Canadian Forest Service, Northern Forestry Centre, 5320 – 122 Street, Edmonton, Alberta T6H 3S5
[2]Natural Resources Canada, Canadian Forest Service, Great Lakes Forestry Centre, 1219 Queen Street East, Sault Ste. Marie, Ontario P6A 2E5
[3]US Department of Agriculture Forest Service, Rocky Mountain Research Station, 240 West Prospect, Fort Collins, Colorado 80526, USA

Natural Resources Canada
Canadian Forest Service
Northern Forestry Centre
5320–122 Street
Edmonton, Alberta T6H 3S5

Catalogue No. Fo133-1/421E-PDF
ISBN 978-1-100-19272-7
ISSN 0831-8247

For an electronic version of this report, visit the Canadian Forest Service Publications site at http://cfs.nrcan.gc.ca/publications

TTY: 613-996-4397 (Teletype for the hearing-impaired)
ATS: 613-996-4397 (appareil de télécommunication pour sourds)

Library and Archives Canada Cataloguing in Publication

High-resolution interpolation of climate scenarios for Canada derived from general circulation model simulations [electronic resource] / David T. Price ... [et al.].

(Information report ; NOR-X-421)
Electronic monograph in PDF format.
Co-published by: US Forest Service, Rocky Mountain Research Station.

ISBN 978-1-100-19272-7
Cat. no.: Fo133-1/421E-PDF

1. Climatic changes--Canada--Forecasting.
2. Climatic changes--Environmental aspects--Canada--Forecasting.
3. Greenhouse effect, Atmospheric--Canada--Forecasting.
4. Global warming--Canada--Forecasting.
5. Greenhouse gases--Canada--Forecasting.
6. Climatic normals--Canada--Forecasting.
I. Price, David Thomas, 1954-
II. Northern Forestry Centre (Canada)
III. Rocky Mountain Research Station (Fort Collins, Colo.)
IV. Series: Information report (Northern Forestry Centre (Canada) : Online) NOR-X-421

QC903.2 C3 H53 2011 551.6971 C2011-980126-4

Price, D.T.; McKenney, D.W. ; Joyce, L.A. ; Siltanen, R.M.; Papadopol, P. ; Lawrence, K. 2011.
***High-Resolution Interpolation of Climate Scenarios for Canada Derived from General Circulation Model Simulations*.**
Nat. Resour. Can., Can. For. Serv., North. For. Cent., Edmonton, AB.
Inf. Rep. NOR-X-421.

ABSTRACT

Projections of future climate were selected for four well-established general circulation models (GCMs) forced by each of three greenhouse gas (GHG) emissions scenarios recommended by the Intergovernmental Panel on Climate Change (IPCC), namely scenarios A2, A1B, and B1 of the IPCC *Special Report on Emissions Scenarios*. Monthly data for the period 1961–2100 were downloaded mainly from the web portal of the Coupled Model Intercomparison Project (Phase 3) of the Program for Climate Model Diagnosis and Intercomparison, and subsets of data covering North America were extracted. Scenario data sets were produced for monthly mean daily maximum and minimum temperatures, precipitation, solar radiation, wind speed, and vapor pressure. All variables were expressed as changes relative to the simulated monthly means for 1961–1990, which corrected for GCM bias in reproducing past climate and allowed future projected trends to be compared directly. The downscaling procedure used the ANUSPLIN software package to fit a two-dimensional spline function to each month's change data for each climate variable at a spatial resolution of 5 arcminutes (0.0833°) longitude and latitude. The resulting scenarios were surprisingly consistent, with differences resulting from different GHG forcings being generally greater than those resulting from different GCMs, although the consistency varied spatially. The A2 emissions scenario invariably generated the greatest warming by 2100, and the B1 scenario the least. Canada's far north was projected to undergo the greatest regional increases in temperature and precipitation, and the southeast and west coastal regions the least, with intermediate warming in midcontinental regions. All models projected increases in precipitation that were generally correlated with the projected increases in temperature, although with greater differences in spatial and seasonal patterns. Changes in vapor pressure were similarly correlated with changes in temperature and precipitation, whereas solar radiation was projected to decline slightly in regions where the increase in precipitation was particularly pronounced. Gridded data sets will be made available as a resource to researchers and others needing high-resolution data for studies of the impacts of climate change. A companion report and data set will be issued by the US Department of Agriculture Forest Service for the continental United States and Alaska.

RÉSUMÉ

On a choisi les projections du climat futur pour quatre modèles de circulation générale (MCG) bien établis, forcés selon trois scénarios d'émissions de gaz à effet de serre (GES) recommandés par le Groupe d'experts intergouvernemental sur l'évolution du climat (GIEC), soit les scénarios A2, A1B et B1 définis dans le *Rapport spécial sur les scénarios d'émissions* du GIEC. On a téléchargé les données mensuelles pour la période de 1961 à 2100 depuis le portail Web du projet d'intercomparaison de modèles couplés (phase 3) du programme de diagnostic et d'intercomparaison de modèles climatiques (*Program for Climate Model Diagnosis and Intercomparison*), puis on a extrait des sous-ensembles de données couvrant l'Amérique du Nord. Des ensembles de données sur les scénarios ont été produits pour les températures quotidiennes maximales et minimales moyennes mensuelles, les précipitations, le rayonnement solaire, la vitesse du vent et la pression de vapeur. Toutes les variables ont été exprimées comme des changements par rapport aux moyennes mensuelles simulées pour la période de 1961 à 1990, ce qui a corrigé le biais du MCG dans la reproduction du climat antérieur et a permis de comparer directement les tendances projetées. La procédure de réduction d'échelle a nécessité l'utilisation du progiciel ANUSPLIN pour ajuster une fonction spline bidimensionnelle aux changements de données de chaque mois, et ce, pour chacune des variables climatiques à une résolution spatiale de 5 minutes d'arc (0,0833º) en longitude et latitude. Les scénarios qui en ont découlé étaient étonnamment cohérents, les différences qui résultaient des divers forçages de GES étant généralement supérieures à celles résultant des différents MCG, bien que la consistance varie sur le plan spatial. Le scénario d'émissions A2 a invariablement généré le réchauffement le plus marqué d'ici 2100, alors que le scénario B1 a généré le réchauffement le plus faible. Il a été projeté que le Grand Nord canadien connaîtrait les plus fortes hausses régionales de température et de précipitation, et les régions côtières du sud-est et de l'ouest connaîtraient les hausses les plus faibles, pendant que les régions du centre du continent subiraient un réchauffement moyen. Tous les modèles ont projeté des augmentations des précipitations qui étaient généralement corrélées aux augmentations projetées des températures, bien qu'avec de plus grandes différences des profils spatiaux et saisonniers. De façon similaire, les changements de pression de vapeur ont été corrélés aux changements de température et de précipitation, alors que l'on a projeté que le rayonnement solaire diminuerait légèrement dans les régions où l'augmentation des précipitations serait particulièrement importante. Les ensembles de données maillées sont des ressources qui seront rendues disponibles aux chercheurs et autres intervenants qui ont besoin de données à haute résolution pour des études sur les impacts des changements climatiques. Un rapport d'accompagnement et un ensemble de données seront émis par l'US Department of Agriculture Forest Service pour les besoins de la partie continentale des États-Unis et de l'Alaska

ACKNOWLEDGMENTS

We acknowledge the support provided by the global climate modeling community and their willingness to contribute and share data through web-based data archives, notably the data portal for the Coupled Model Intercomparison Project (Phase 3) of the Program for Climate Model Diagnosis and Intercomparison. In addition, we greatly appreciate the provision of data by the following organizations and individuals:

- in Canada, the Canadian Centre for Climate Modelling and Analysis
- in the United States, the US National Center for Atmospheric Research and G. Strand of the University Corporation for Atmospheric Research
- in Australia, the Commonwealth Scientific and Industrial Research Organisation (CSIRO), particularly M. Collier, M. Dix, and T. Hirst of the Marine and Atmospheric Research Division
- in Japan, the Center for Climate System Research, the University of Tokyo, the National Institute for Environmental Studies, and the Frontier Research Center for Global Change

This research used data provided by the Community Climate System Model (CCSM) project (http://www.cesm.ucar.edu/models/ccsm3.0), supported by the Directorate for Geosciences of the US National Science Foundation and the Office of Biological and Environmental Research of the US Department of Energy. Any redistribution of CCSM data must include this data acknowledgment statement. Similarly, the authors of the current document request that any users of the scenario data presented in this report also provide appropriate acknowledgments to the respective general circulation model groups, as identified above. We also acknowledge the support of the US Department of Agriculture (USDA) Forest Service for this research. A. Schloss of the Complex Systems Research Center, University of New Hampshire, provided a key reference. We greatly appreciate the time invested by many reviewers of this or the USDA report, namely Robert Bailey, Nick Crookston, Ray Drapek, Mike Flannigan, Alisa Gallant, Louis Iverson, Mark Johnston, Jorge Ramirez, Roger Simmons, and Peter Thornton. Finally, we wish to acknowledge the editorial team: Peggy Robinson, who provided a complete technical edit of this document, and Brenda Laishley and Sue Mayer of Natural Resources Canada, who coordinated its production.

KEYWORDS AND METADATA

Climate scenario, general circulation model, GCM, downscaling, interpolation, ANUSPLIN, National Center for Atmospheric Research, NCAR, Community Climate System Model, CCSM, Canadian Centre for Climate Modelling and Analysis, CCCma, Coupled Global Climate Model, CGCM, Commonwealth Scientific and Industrial Research Organisation, CSIRO, Climate System Model, Center for Climate System Research, CCSR, National Institute for Environmental Studies, NIES, Model for Interdisciplinary Research on Climate, MIROC.

CONTENTS

APPENDIX

FIGURES

TABLES

EXECUTIVE SUMMARY

Researchers from the Canadian Forest Service and the US Department of Agriculture (USDA) Forest Service collaborated in the production of a suite of downscaled climate scenarios covering the continental United States and Canada. Each scenario was derived from a simulation carried out with a state-of-art general circulation model (GCM) for which results were available from the Coupled Model Intercomparison Project (Phase 3) of the Program for Climate Model Diagnosis and Intercomparison. The following four GCMs were selected on the basis of data available in 2008 and because they were well recognized within the global GCM community: the Third Generation Coupled Global Climate Model, version 3.1, medium resolution (CGCM31MR), developed by the Canadian Centre for Climate Modelling and Analysis; the Australian Commonwealth Scientific and Industrial Research Organisation's Mark 3.5 Climate System Model (CSIROMK35); the Model for Interdisciplinary Research on Climate, version 3.2, medium resolution (MIROC32MR), developed by the Japanese Center for Climate System Research; and the Community Climate System Model, version 3.0 (NCARCCSM3), developed by the US National Center for Atmospheric Research.

Monthly time-series data were obtained for each GCM, representing both the 20th century (1961–2000) and three scenarios of greenhouse gas (GHG) emissions for the 21st century, developed for the Intergovernmental Panel on Climate Change Third and Fourth Assessment Reports, namely scenarios A2, A1B, and B1 of the *Special Report on Emissions Scenarios* (Nakićenović et al. 2000). These scenarios offer a range of values for potential global mean surface warming, from a minimum of 1.8°C associated with the B1 scenario, through 2.8°C for the A1B scenario, to 3.4°C in the A2 scenario, for the period 2090–2100 relative to 1980–1999 (Solomon et al. 2007). In each case, data for simulated climate variables were downloaded and computer programs used to extract and manipulate subsets covering Canada and the continental United States (i.e., excluding Hawaii). The climate variables included monthly mean daily maximum and minimum temperatures, precipitation, incident surface solar radiation, and wind speed. Two other variables, monthly mean specific humidity and sea-level barometric pressure, were used to calculate monthly mean vapor pressure as a sixth variable. Each monthly value at each GCM grid node was normalized either by subtracting (for temperature variables) or dividing by (for other climate variables) the mean of that month's values for the 30-year baseline period 1961–1990. The normalized data (or "deltas") were then formatted for input to the ANUSPLIN thin-plate spline software of Hutchinson and coworkers at the Australian National University (e.g., Hutchinson 2009). ANUSPLIN was used to fit a unique two-dimensional spline "surface" function to each month's data for each of the six normalized climate variables. The fitted spline functions were in turn used to create gridded data sets for each monthly variable covering North America at a spatial resolution of 5 arcminutes (0.0833°) longitude and latitude on a geographic projection. Data for Canada were extracted and packaged for general distribution via FTP downloads.

The normalization and interpolation procedures effectively removed any tendencies for individual GCMs to estimate observed climate incorrectly and allowed direct comparison of the downscaled projections for different GHG scenarios and different GCMs. (This approach is consistent with requirements outlined in a recent USDA Forest Service memorandum, "Draft NEPA Guidance on Consideration of the Effects of Climate Change and Greenhouse Gas Emissions", released 18 February 2010).

The downscaled data were analyzed, partly as a form of quality assessment and partly to demonstrate how the data can be used for national and regional studies of the impacts of climate change. Results for selected variables were plotted as national maps of 30-year means for the three periods 2011–2040, 2041–2070, and 2071–2100 (or 2071–2099 in the case of NCARCCSM3), where the normalized data were added to (for temperature variables) or multiplied by (for other variables) spatially interpolated climatological data for the period 1961–1990. When forced with the A2 GHG emissions

scenario, the NCARCCSM3 generally predicted the greatest warming. For Canada, the MIROC32MR generally yielded the "second warmest" scenarios, but it appeared less sensitive to higher levels of GHG forcing, so the differences between the results of A2 and A1B forcing were relatively small. In most respects, the maps of projections for temperature and precipitation indicated that the GCMs behaved rather similarly and that differences were generally too small (e.g., less than 1°C), given the range of each variable at the continental scale, to allow them to be visually discriminated for the same forcing scenario and the same 30-year period. Accordingly, a series of maps of the change fields was created. Each map showed the distribution of mean temperature increase (°C) or change in precipitation (ratio) relative to 1961–1990 for each of the three 30-year periods, according to each GCM forced by the A1B emissions scenario. In these cases, the range of values was much narrower, which allowed much easier comparison of the climate impacts according to each model.

The generally greater warming detected with the NCARCCSM3 forced by the A2 emissions scenario occurred across much of Canada. In general, the CSIROMK35 projected the least warming, and the CGCM31MR was generally intermediate between CSIROMK35 and MIROC32MR. As noted previously, the MIROC32MR projected less warming than the NCARCCSM3 with forcing by the A2 scenario; however, this pattern was reversed with forcing by the A1B scenario. All four models agreed substantially in projecting the greatest warming in the Arctic and the least in the coastal regions of British Columbia and the Atlantic provinces. Within this geographic range, the projected warming in the midcontinental regions occurred along a generally southwest-to-northeast gradient, following the existing climatic zones. In general, projected increases for monthly mean daily minimum temperatures were 0.5°C to 2.0°C greater than increases for the monthly mean daily maxima, with the largest differences occurring in the Arctic.

For precipitation, the general projected trend followed that for temperature, with the largest increases (in proportional terms) occurring in the far north, and the smallest increases in the south west part of the country and in southern Ontario. However, the largest increases in amount of precipitation were projected to occur on the Pacific coast, where annual precipitation is already much higher than anywhere else. The models differed appreciably in the projected magnitudes of change in precipitation: the Canadian model, CGCM31MR, generally projected the greatest increases, whereas the Japanese and US models, MIROC32MR and NCARCCSM3, respectively, projected the smallest increases. Furthermore, the NCARCCSM3 and, to a lesser extent, the CSIROMK35, projected significant declines in precipitation in the BC Lower Mainland and Vancouver Island, whereas the MIROC32MR projected significant decreases in southern Ontario. When the GCMs were forced by the A1B emissions scenario, most of these trends were clearly apparent as early as 2010–2040. For the western prairies, the CSIROMK35 projected significantly greater increases in precipitation by 2100, a trend supported by the CGCM31MR and, to a certain extent, the NCARCCSM3.

The area of Canada was divided into 18 ecozones, based on the Terrestrial Ecozones of Canada classification (Ecological Stratification Working Group 1995; see also Wiken 1986), with three extra subdivisions identified for the Carbon Budget Model of the Canadian Forest Sector (see Kurz et al. 2009). Area-weighted ecozonal means of the downscaled data were calculated for every monthly value for every climate variable in each of the 12 scenarios (four GCMs each forced by three GHG emissions scenarios) and were then used to calculate seasonal and annual means and totals. The seasons were defined as spring (March to May), summer (June to August), fall (September to November), and winter (December to February). These data were summarized by ecozone for each climate variable and each GHG forcing scenario to create scatter plots comparing projected changes for the 2050s and 2090s. Graphs were also generated to compare projections across models for the period 2001–2100 and to allow comparison with observed data for 1961–2008. The summarized data for all four GCMs were averaged and further summarized in a comprehensive set of tables, as a way to report "model consensus" for each variable in each ecozone with each emissions scenario.

The results of the analysis confirmed that the GCMs were in general agreement, particularly with respect to temperature, precipitation, and solar radiation,

both in terms of their relative responses to the various forcing scenarios and in the magnitudes of the changes projected for the 21st century. This is not to say that the results agreed in all cases, but the projections for individual ecozones were often consistent among the four models. Furthermore, when historical records of temperature and precipitation were compared subjectively with the model results for the period 1961–2008, the magnitude and periodicity of interannual variations, as well as the overall trends in means, appeared very similar for all GCMs in all seasons and all ecozones. There was less consistency among the models in terms of projections of changes in interannual variability over the 21st century, but changes for different seasons according to each model were proportionately similar (e.g., if increases in temperature variability for a particular ecozone were smaller in summer than in winter, this difference was likely to be seen for all four models).

Projected changes in mean vapor pressure were generally consistent with projected increases in mean temperature and were often correlated with projected increases in seasonal and annual precipitation. Interestingly, increases in vapor pressure, particularly in summer, were often correlated with slight reductions in solar radiation, consistent with a warmer atmosphere holding more water vapor and hence creating generally cloudier conditions.

The data for wind speed generally showed good agreement among the models, with little change in either interannual variability or mean wind speeds projected under any of the GHG forcing scenarios. However, this observation applied only at monthly time scales; changes in the distribution of wind speeds at daily or hourly time scales were not investigated.

In addition to the analysis of the gridded data, the GCM-projected changes in temperature and precipitation were averaged over 30-year periods and then interpolated using ANUSPLIN to the locations of climate stations in Canada and the USA. These data were then combined with observed station normals for the period 1961–1990 to create projected normals for three consecutive 30-year periods: 2011–2040, 2041–2070 and 2071–2100. A Bessel interpolation scheme was used to generate daily temperature and precipitation sequences that pass monotonically through the monthly values. This allowed for a suite of bioclimatic indicator variables to be estimated for these periods, including for example, mean growing season duration and precipitation during the growing season. These will be of value for modeling in forestry, agriculture, and ecology. Annual values of these bioclimatic variables were also generated for 2001–2100.

In summary, the suite of 12 climate scenarios provides a range of potential future climates for assessing possible impacts of a changing climate on natural resources, ecosystems, human infrastructure and communities. Each should be considered a "plausible" scenario for a specific set of assumptions captured in each GCM and in each of the IPCC SRES GHG emissions scenarios. The results are interpolated changes calculated with respect to 1961–1990 means, and gridded to a common format to facilitate handing and comparison among scenarios. Data sets are freely available from Natural Resources Canada, Canadian Forest Service.

Literature Cited

Ecological Stratification Working Group. 1995. A national ecological framework for Canada. Agric. Agri-Food Can., Res. Branch, Cent. Land Biol. Resour. Res. and Environ. Can., State Environ. Dir., Ecozone Anal. Branch, Ottawa/Hull. 125 p. + map at 1:7 500 000 scale.

Kurz, W.A.; Dymond, C.C.; White. T.M.; Stinson, G.; Shaw, C.H.; Rampley, G.J.; Smyth, C.; Simpson, B.N.; Neilson, E.T.; Trofymow, J.A.; Metsarantaa, J.; Apps, M.J. 2009. CBM-CFS3: a model of carbon-dynamics in forestry and land-use change implementing IPCC standards. Ecol. Model. 220:480–504.

Nakićenović, N.; Alcamo, J.; Davis, G.; de Vries, B.; Fenhann, J.; Gaffin, S.; Gregory, K.; Grübler, A.; Jung, T.Y.; Kram, T.; La Rovere, E.L.; Michaelis, L.; Mori, S.; Morita, T.; Pepper, W.; Pitcher, H.; Price, L.; Raihi, K.; Roehrl, A.; Rogner, H.-H.; Sankovski, A.; Schlesinger, M.; Shukla, P.; Smith, S.; Swart, R.; van Rooijen, S.; Victor, N.; Dadi, Z. 2000. Special report on emissions scenarios. A special report of Working Group III of the Intergovernmental Panel on Climate Change. Cambridge Univ. Press, Cambridge, UK, and New York, NY. 599 p. Also available from <http://www.grida.no/publications/other/ipcc_sr/?src=http://www.grida.no/climate/ipcc/>. Accessed 28 July 2010.

Solomon, S.; Qin, D.; Manning, M.; Chen, Z.; Marquis, M.; Averyt, K.B.; Tignor, M.; Miller, H.L., editors. 2007. Climate change 2007: the physical science basis. Contribution of Working Group I to the Fourth Assessment Report of the Intergovernmental Panel on Climate Change. Cambridge Univ. Press, Cambridge, UK. 996 p.

Wiken, E.B., compiler. 1986. Terrestrial ecozones of Canada. Environ. Can., Ecol. Land Classif. Ser. 19. Environ. Can. Hull, QC. 26 p.

SOMMAIRE

Les chercheurs du Service canadien des forêts et du service des forêts de l'US Department of Agriculture (USDA) ont travaillé de concert à la production d'une série de scénarios climatiques à échelle réduite couvrant la partie continentale des États-Unis et du Canada. Chaque scénario a été dérivé d'une simulation réalisée avec un modèle de circulation générale (MCG) de pointe dont les résultats étaient rendus disponibles dans le cadre du projet d'intercomparaison de modèles couplés (phase 3) du programme de diagnostic et d'intercomparaison de modèles climatiques (Program for Climate Model Diagnosis and Intercomparison). Les quatre MCG suivants ont été choisis en raison des données disponibles en 2008 et du fait qu'ils sont bien connus dans l'ensemble du milieu des MCG : le modèle couplé climatique global de troisième génération, version 3.1, à résolution moyenne (CGCM31MR), mis au point par le Centre canadien de la modélisation et de l'analyse climatique; le modèle du système climatique Mark 3.5 (CSIROMK35) de l'Australian Commonwealth Scientific and Industrial Research Organisation, un organisme scientifique national de l'Australie; le modèle pour la recherche interdisciplinaire sur le climat, version 3.2, à résolution moyenne (MIROC32MR), mis au point par le Japanese Center for Climate System Research; et, le modèle communautaire du système climatique, version 3.0 (NCARCCSM3), mis au point par l'US National Center for Atmospheric Research.

On a obtenu des données chronologiques mensuelles pour chaque MCG, représentant le 20e siècle (de 1961 à 2000) et les trois scénarios d'émissions de gaz à effet de serre (GES) pour le 21e siècle élaborés dans le cadre du Troisième et du Quatrième rapport d'évaluation pour le Groupe d'experts intergouvernemental sur l'évolution du climat, soit les scénarios A2, A1B et B1 du Rapport spécial sur les scénarios d'émissions (Nakićenović et al., 2000). Ces scénarios fournissent une gamme de valeurs du réchauffement moyen potentiel à la surface de la planète, allant de 1,8 °C avec le scénario B1, jusqu'à 3,4 °C avec le scénario A2, en passant par 2,8 °C avec le scénario A1B, pour la période de 2090–2100 par rapport à la période de 1980–1999 (Solomon et al., 2007). Dans chaque cas, on a téléchargé des données sur les variables climatiques simulées et utilisé des programmes informatiques pour extraire et manipuler les sous-ensembles de données couvrant le Canada et la partie continentale des États-Unis (c.-à-d. en excluant Hawaii). Les variables climatiques comprenaient des données sur les températures maximales et minimales quotidiennes moyennes par mois, les précipitations, le rayonnement solaire incident et la vitesse du vent. Deux autres variables, l'humidité spécifique moyenne mensuelle et la pression barométrique au niveau de la mer, ont été utilisées pour calculer la pression de vapeur moyenne mensuelle constituant la sixième variable de l'étude. Chaque valeur mensuelle à chaque nœud de la grille du MCG a été normalisée, soit en soustrayant (dans le cas des variables de température), soit en divisant par (pour les autres variables climatiques) la moyenne des valeurs pour le mois donné pour la période de référence de 30 ans, de 1961 à 1990. Les données normalisées (ou « deltas ») ont été formatées de manière à servir de données d'entrée dans le progiciel ANUSPLIN à fonction spline de type plaque mince, développé par Hutchinson et ses collègues de l'Australian National University (voir p. ex., Hutchinson, 2009). ANUSPLIN a été utilisé pour ajuster une unique fonction spline bidimensionnelle de « surface » aux données de chaque mois pour chacune des six variables climatiques normalisées. Les fonctions spline ajustées ont ensuite été utilisées pour créer des ensembles de données maillées pour chaque variable du mois couvrant l'Amérique du Nord, à une résolution spatiale de 5 minutes d'arc (0,0833º) en longitude et latitude sur une projection géographique. Les données pour le Canada ont été extraites et rassemblées pour permettre une diffusion générale par voie de téléchargements sur un site FTP.

Les procédures de normalisation et d'interpolation ont été efficaces pour enlever toutes les tendances des MCG, pris individuellement, à produire des estimations erronées du climat observé et ont permis de comparer directement les projections à échelle réduite des différents scénarios d'émissions de GES ainsi que des différents MCG. (Cette approche concorde avec les exigences formulées dans une

récente note émise par le service des forêts de l'USDA le 18 février 2010, intitulée Draft NEPA Guidance on Consideration of the Effects of Climate Change and Greenhouse Gas Emissions.)

On a analysé les données à échelle réduite, en partie pour une question d'évaluation de la qualité et en partie pour démontrer comment les données peuvent être utilisées dans le cadre d'études nationales et régionales sur les impacts des changements climatiques. Les résultats pour les variables choisies ont été reportés sur des cartes nationales des moyennes sur 30 ans, pour les périodes 2011–2040, 2041–2070, et 2071–2100 (ou 2071–2099 dans le cas du modèle NCARCCSM3), les données normalisées ayant été, soit additionnées aux données climatologiques spatiales interpolées pour la période de 1961 à 1990 (dans le cas des variables de température), soit multipliées par celles-ci (pour les autres variables climatiques). Lorsque le modèle NCARCCSM3 était forcé avec le scénario A2 d'émissions de GES, il a généralement prédit le réchauffement le plus marqué. Au Canada, le modèle MIROC32MR a habituellement donné lieu aux scénarios arrivant au deuxième rang des plus chauds, mais il a semblé moins sensible aux forçages plus intenses d'émissions de GES, de sorte que les différences dans les résultats obtenus avec les scénarios de forçage A2 et A1B étaient relativement faibles. À bien des égards, les cartes de projections des températures et des précipitations indiquaient que les MCG se comportaient de façon assez semblable et que, compte tenu de l'éventail de valeurs de chaque variable à l'échelle continentale, les différences étaient généralement trop faibles (p. ex., moins de 1 °C) pour permettre une discrimination visuelle pour un même scénario de forçage et une même période de 30 ans. En conséquence, on a créé une série de cartes des domaines de changement. Chaque carte illustrait soit la distribution de l'augmentation de la température moyenne (°C), soit le changement dans les précipitations (ratio) par rapport à 1961–1990 pour chacune des trois périodes de 30 ans, selon chaque MCG auquel était appliqué le scénario A1B de forçage des émissions de GES. Dans ces cas, l'éventail de valeurs était nettement plus restreint, ce qui a facilité la comparaison des impacts climatiques selon chaque modèle.

Le réchauffement généralement plus marqué décelé par le modèle NCARCCSM3 auquel on a appliqué le scénario A2 de forçage des émissions se produisait dans presque tout le Canada. En général, le modèle CSIROMK35 projetait le réchauffement le moins marqué, alors que le modèle CGCM31MR donnait généralement des résultats à mi-chemin entre les modèles CSIROMK35 et MIROC32MR. Ainsi qu'on l'a indiqué précédemment, le modèle MIROC32MR projetait un réchauffement moins marqué que le modèle NCARCCSM3 quand on appliquait le scénario de forçage A2; cependant, ce profil était renversé avec le scénario de forçage A1B. Les quatre modèles concordaient dans une large mesure quant à leur projection : le réchauffement le plus marqué se produisait dans l'Arctique et le moins marqué, dans les régions côtières de la Colombie-Britannique et des provinces de l'Atlantique. À l'intérieur de cette étendue géographique, le réchauffement projeté dans les régions du centre du continent se produisait le long d'un gradient allant généralement du sud-ouest au nord-est, suivant les zones climatiques existantes. En général, les augmentations projetées des températures minimales quotidiennes moyennes par mois étaient de 0,5 °C à 2,0 °C supérieures aux augmentations des températures maximales quotidiennes moyennes par mois, la différence la plus grande se produisant dans l'Arctique.

Dans le cas des précipitations, la tendance générale projetée correspondait à celle des températures; ainsi, les augmentations les plus importantes (toutes proportions gardées) se produisaient dans l'extrême nord, alors que les augmentations les plus faibles étaient observées dans la partie sud-ouest du pays et dans le sud de l'Ontario. Cependant, les modèles ont projeté que les augmentations les plus marquées, pour ce qui est des quantités de précipitations, se produiraient sur la côte du Pacifique où les précipitations annuelles sont déjà beaucoup plus importantes que partout ailleurs. Les modèles divergeaient sensiblement quant à l'ampleur des changements projetés dans les précipitations : le modèle canadien, CGCM31MR, projetait généralement les plus fortes hausses, alors que les modèles japonais et américain, MIROC32MR et NCARCCSM3, projetaient les plus faibles augmentations. En outre, le NCARCCSM3

et, dans une moindre mesure, le CSIROMK35 projetaient des diminutions importantes des précipitations dans les basses-terres continentales de la Colombie-Britannique et dans l'île de Vancouver, alors que le MIROC32MR projetait des diminutions significatives dans le sud de l'Ontario. Quand les MCG étaient forcés avec le scénario A1B d'émissions, la plupart de ces tendances étaient nettement évidentes dès 2010–2040. Pour ce qui est de l'ouest des Prairies, le modèle CSIROMK35 projetait des augmentations nettement supérieures des précipitations d'ici 2100, une tendance soutenue par le modèle CGCM31MR ainsi que, dans une certaine mesure, par le modèle NCARCCSM3.

La superficie du Canada a été divisée en 18 écozones, d'après la classification des écozones terrestres du Canada (Groupe de travail sur la stratification écologique, 1995; voir aussi Wiken, 1986), auxquelles se sont ajoutées trois subdivisions identifiées aux fins du Modèle du bilan du carbone du secteur forestier canadien (voir Kurz et al., 2009). On a calculé les moyennes, pour les écozones pondérées en fonction de la superficie, des données à échelle réduite pour chaque valeur mensuelle de chaque variable climatique, et ce, pour chacun des 12 scénarios (quatre MCG soumis à trois scénarios de forçage des émissions de GES); puis, on a utilisé les résultats pour calculer les moyennes saisonnières et annuelles ainsi que les valeurs totales. Les saisons étaient définies comme suit : printemps (de mars à mai); été (de juin à août); automne (de septembre à novembre); hiver (de décembre à février). Ces données ont ensuite été résumées pour chaque écozone en fonction de chaque variable climatique et de chaque scénario de forçage des émissions de GES de manière à créer des diagrammes de dispersion comparant les changements projetés pour les années 2050 et 2090. On a aussi généré des graphiques afin de comparer les projections des divers modèles pour la période 2001–2100 et de permettre la comparaison avec les données observées durant la période 1961–2008. On a fait la moyenne des données résumées pour les quatre MCG, puis on les a condensées davantage dans un ensemble complet de tableaux, permettant de présenter le « consensus » entre les modèles pour chaque variable dans chaque écozone avec chaque scénario d'émissions.

Les résultats de l'analyse ont confirmé que, en général, les MCG concordaient, particulièrement en ce qui concerne les températures, les précipitations et le rayonnement solaire, en ce qui a trait à leurs réponses relatives aux divers scénarios de forçage et à l'ampleur des changements projetés pour le 21e siècle. Ce qui ne veut pas dire que les résultats concordaient dans tous les cas, mais que les projections pour les écozones prises individuellement avec les quatre modèles allaient dans le même sens. De plus, lorsque l'on a comparé subjectivement les données historiques des températures et des précipitations aux résultats des modèles pour la période 1961–2008, l'ampleur et la périodicité des variations interannuelles ainsi que les tendances générales des moyennes sont apparues très semblables pour les MCG, et ce, à toutes les saisons et dans toutes les écozones. La cohérence entre les modèles était moindre pour ce qui est des projections des changements de la variabilité interannuelle au cours du 21e siècle, mais les changements au cours des saisons selon chacun des modèles étaient proportionnellement semblables (c.-à-d. que si les augmentations de la variabilité des températures pour une écozone donnée étaient plus faibles en été qu'en hiver, il est probable que cette différence ait été observée dans les quatre modèles).

Les changements projetés de la pression de vapeur moyenne concordaient généralement avec les augmentations projetées des températures moyennes et étaient souvent corrélés avec les augmentations projetées des précipitations saisonnières et annuelles. Il est intéressant de constater que les augmentations de la pression de vapeur, particulièrement en été, étaient souvent corrélées à de légères diminutions du rayonnement solaire, ce qui cadre avec le fait qu'une atmosphère plus chaude contient plus de vapeur d'eau et engendre de ce fait des conditions généralement plus nuageuses.

Les données sur la vitesse du vent étaient généralement concordantes d'un modèle à l'autre : avec tous les scénarios de forçage des émissions de GES, on a observé peu de changements de la variabilité interannuelle ou des vitesses moyennes de vent projetées. Cependant, cette observation ne s'applique qu'à une échelle mensuelle; les

changements dans la répartition des vitesses de vent à l'échelle quotidienne ou horaire n'ont pas été étudiés.

En plus de l'analyse des données maillées, on a calculé la moyenne des changements projetés de températures et de précipitation au moyen des MCG sur des périodes de 30 ans, puis, à l'aide du progiciel ANUSPLIN, on a interpolé les valeurs des changements aux emplacements des stations climatiques situées au Canada et aux États-Unis. Ces données ont ensuite été combinées aux normales observées aux stations pour la période 1961–1990 afin de générer des normales projetées pour trois périodes consécutives de 30 ans, soit 2011–2040, 2041–2070 et 2071–2100. On a utilisé la méthode d'interpolation de Bessel pour générer des séquences de températures et de précipitations quotidiennes qui passent au travers des valeurs mensuelles de façon monotone. On a ainsi pu évaluer pour ces périodes une série de variables bioclimatiques indicatrices incluant, par exemple, la durée moyenne de la saison de croissance et les précipitations durant la saison de croissance. Ces résultats seront utiles pour la modélisation dans les domaines de la foresterie, de l'agriculture et de l'écologie. Les valeurs annuelles de ces variables bioclimatiques ont aussi été générées pour la période 2001–2100.

En résumé, la série de 12 scénarios climatiques a fourni une gamme de climats futurs potentiels permettant d'évaluer les impacts possibles de changements climatiques sur les ressources naturelles, les écosystèmes, les infrastructures humaines et les collectivités. Il faut considérer chacun de ces scénarios comme étant « plausibles » pour un ensemble donné de suppositions établies dans chaque MCG et dans chaque scénario d'émissions de GES défini dans le Rapport spécial sur les scénarios d'émissions du GIEC. Les résultats sont des changements interpolés, calculés par rapport aux moyennes de 1961–1990, puis transposés dans une grille de même format pour faciliter leur manipulation et la comparaison des divers scénarios. Les ensembles de données étaient disponibles gratuitement auprès du Service canadien des forêts de Ressources naturelles Canada.

Références Bibliographiques

Ecological Stratification Working Group. 1995. A national ecological framework for Canada. Agric. Agri-Food Can., Res. Branch, Cent. Land Biol. Resour. Res. and Environ. Can., State Environ. Dir., Ecozone Anal. Branch, Ottawa/Hull. 125 p. + map at 1:7 500 000 scale.

Kurz, W.A.; Dymond, C.C.; White. T.M.; Stinson, G.; Shaw, C.H.; Rampley, G.J.; Smyth, C.; Simpson, B.N.; Neilson, E.T.; Trofymow, J.A.; Metsarantaa, J.; Apps, M.J. 2009. CBM-CFS3: a model of carbon-dynamics in forestry and land-use change implementing IPCC standards. Ecol. Model. 220:480–504.

Nakićenović, N.; Alcamo, J.; Davis, G.; de Vries, B.; Fenhann, J.; Gaffin, S.; Gregory, K.; Grübler, A.; Jung, T.Y.; Kram, T.; La Rovere, E.L.; Michaelis, L.; Mori, S.; Morita, T.; Pepper, W.; Pitcher, H.; Price, L.; Raihi, K.; Roehrl, A.; Rogner, H.-H.; Sankovski, A.; Schlesinger, M.; Shukla, P.; Smith, S.; Swart, R.; van Rooijen, S.; Victor, N.; Dadi, Z. 2000. Special report on emissions scenarios. A special report of Working Group III of the Intergovernmental Panel on Climate Change. Cambridge Univ. Press, Cambridge, UK, and New York, NY. 599 p. Also available from <http://www.grida.no/publications/other/ipcc_sr/?src=http://www.grida.no/climate/ipcc/>. Accessed 28 July 2010.

Solomon, S.; Qin, D.; Manning, M.; Chen, Z.; Marquis, M.; Averyt, K.B.; Tignor, M.; Miller, H.L., editors. 2007. Climate change 2007: the physical science basis. Contribution of Working Group I to the Fourth Assessment Report of the Intergovernmental Panel on Climate Change. Cambridge Univ. Press, Cambridge, UK. 996 p.

Wiken, E.B., compiler. 1986. Terrestrial ecozones of Canada. Environ. Can., Ecol. Land Classif. Ser. 19. Environ. Can. Hull, QC. 26 p.

INTRODUCTION

Reseachers concerned with assessing the potential impacts of anticipated changes in climate on Canadian ecosystems and infrastructure often require data extracted from projections generated by general circulation models (GCMs), as a means of exploring the range of possible environmental, social and economic consequences of different forecasts of future greenhouse gas (GHG) emissions. The GCMs represent the best available encapsulation of current expert knowledge about how the global climate system is likely to respond to GHG forcing. Hence, overall assessments of impacts should be based on a suite of these projections, as a way of examining the range of possibilities and gauging some of the uncertainty.

As reported in the Fourth Assessment Report (AR4) of the Intergovernmental Panel on Climate Change (IPCC) (see, for example, http://www.ipcc.ch/publications_and_data/publications_and_data_reports.shtml) projections of the future global climate have been developed by numerous GCM research groups around the world, using the GHG forcing scenarios recommended in the *Special Report on Emissions Scenarios* (SRES) (Nakićenović et al. 2000). We have developed a suite of high-resolution climate projections for the North American land surface (and enclosed water bodies) using a subset of the available GCM simulation results prepared for the AR4. We anticipate that these products will be of great value in conducting other studies of the impacts of climate change at regional to continental scales.

There are several major limitations to using the GCM scenario data that are available from recognized climate data archives such as the IPCC Data Distribution Centre (http://www.ipcc-data.org/) and the Program for Climate Model Diagnosis and Intercomparison (PCMDI; http://www-pcmdi.llnl.gov/). These limitations include the very coarse spatial resolution inherent in GCM output (typically a separation of 100 to 400 km between grid nodes at mid-latitudes) and the need to extract data from huge global data sets for application to smaller regions. Further problems include determining which scenarios are representative of the range of future climates projected for North America and bringing the data into a common format to allow easy comparison when used for studies assessing the impacts of climate change.

This report provides a detailed description of the process to "downscale" the results of four different GCMs, operating at a range of spatial resolutions and forced by different GHG emissions scenarios, to a common spatial resolution. The downscaling approach described here follows that reported by Price et al. (2004) and McKenney et al. (2006c) and uses the ANUSPLIN thin-plate smoothing spline-interpolation technique, a method developed at the Australian National University over the past two decades (Hutchinson 2009). The results of the current analysis covered Canada, Alaska and the conterminous 48 states of the United States. Individual grid cells measured 5 arcminutes (0.0833°) latitude and longitude or about 10 km from north to south. (Although the resolution is referred to as "10 km," this is a nominal dimension. In reality, a 5 arcminute grid cell is an approximate square measuring about 9.25 km on a side at the equator. Furthermore, the east–west dimension decreases as the cosine of the latitude [i.e., as the meridians converge toward the poles].) Each climate variable is reported here as monthly departures from simulated monthly means for the 1961–1990 baseline period. In total, data for six standard climate variables were developed in this way, for the period from 1961 to 2100 (or 2099, in the case of the GCM developed by the US National Center for Atmospheric Research): mean daily maximum and minimum temperature, precipitation, solar radiation, vapor pressure and wind speed. The advantage of this approach is that different historical climatologies can be used to construct projections of future climate (for this report, the historical climatology developed by McKenney et al. [2007] was used). Data covering the Canadian landmass were extracted from the North American coverage and reprojected to a nominal 10-km grid in the commonly used Lambert conformal conic projection (e.g., Snyder 1987). Finally, the data were bundled into manageable units for distribution via internet or on optical disks. All data sets are freely available for use by researchers and others, on request from the authors. Data for Canada

and for North America can be obtained from the CFS Northern Forestry Centre and Great Lakes Forestry Centre. Data for the continental United States, in a 5 arcminute geographic projection, are available from the archive website of the US Department of Agriculture Forest Service Rocky Mountain Research Station.

The scenario data for Canada are presented here primarily to help in investigations of the impacts of climate change on Canadian forest resources. The data will be available to other federal agencies, provincial agencies, and private sector groups (e.g., forest and tourism industries, nongovernmental organizations, and consultants), for use in studies of the effects of climate change on natural resources throughout Canada.

A companion report (Joyce et al. n.d.) provides a similar analysis for the continental United States, including Alaska, to document the US data sets.

The project reported here had the following main objectives:

1. Create a consistent set of climate projections from the output generated by four well-established GCMs for Canada forced by the A2, A1B, and B1 GHG emissions scenarios, as defined in the IPCC's SRES (Nakićenović et al. 2000).
2. Provide results as text-format geographic grids with resolution of 5 arcminutes (about 10 km), where each grid consists of the change factor (as absolute difference [for temperature] or a ratio [for all other climate variables]) for monthly mean daily minimum and maximum temperature, precipitation, solar radiation, wind speed, and vapor pressure.
3. Provide additional results as text-format geographic grids with resolution of 5 arcminutes, where each grid consists of the monthly value of a single climate variable (temperature, precipitation, solar radiation, wind speed, and vapor pressure).
4. Analyze the data sets generated in objectives 2 and 3 to demonstrate and interpret similarities and differences among the GCMs and GHG forcing scenarios for distinct regions of Canada and to highlight any problems discovered as a result of the downscaling procedures.

METHODS

Review of Spatial Downscaling of Global Climate Simulations

The various approaches to downscaling GCM outputs differ in their complexity. The more sophisticated approaches include dynamical and statistical downscaling. Of these, dynamical approaches typically use higher-resolution atmospheric circulation models (generally referred to as regional climate models) that operate over a relatively large region bounded by GCM grid cells. The atmospheric processes occurring within the domain of a regional climate model are forced by boundary conditions generated by the GCM at its usual time step. Within the domain of the regional climate model, higher-resolution representation of surface topography and more detailed parameterization of some processes are intended to allow the model to generate physically consistent simulations of weather and climate that can be validated against observed data. The validated model should be able to project more realistic regional climate than can be obtained from the GCM alone. In general, regional climate models are expensive to operate and do not provide continuous long-term projections for multiple GCM scenarios (but see the latest results of the North American Regional Climate Change Assessment Program, http://www.narccap.ucar.edu/results/rcm3-gfdl-results.html).

In contrast to dynamical downscaling, statistical downscaling is based on relationships among multiple local-scale and larger-scale meteorological observations that are used to interpret or modify the GCM outputs (e.g., Hashmi et al. 2009), often by generating a distribution of values for the location of interest. There are three broad statistical approaches: weather typing, weather generators, and regression models, the last of which are also known as transfer functions (Wilby et al. 2004; Hashmi et al. 2009; see also http://www.cics.uvic.ca/scenarios/index.cgi?More_Info-Downscaling_Background). Weather typing is based on statistical relationships between observed meteorological variables and a classification of synoptic weather patterns. The GCM-simulated changes in frequency and spatial distributions of these weather patterns are used to project changes in the same meteorological variables. Problems with this approach include its subjectivity and the possibility that the assumed relationships between observed weather patterns and climate may not hold in the future (e.g., Conway and Jones 1998), a legitimate concern, given the expectation of "novel" climates (e.g., Williams et al. 2007).

Weather generators (e.g., Semenov and Barrow 1997; Wilks and Wilby 1999) typically are used to simulate the occurrence of high-frequency climatic events, at daily or hourly time scales, typically from weekly or monthly climate statistics. Hence, such tools are not germane to spatial downscaling of GCM projections of monthly climate data but they may be useful in some impact studies that make use of data that have been spatially downscaled by another method.

Statistical transfer functions represent a range of linear or nonlinear regression methods (the latter including approaches such as artificial neural networks and genetic algorithms) to relate large-scale meteorological or climatic data (observed or generated by a GCM) to small-scale climate variables (e.g., Wilby et al. 2002). Although some of these techniques are quite powerful, and many offer the capacity to estimate daily values (rather than monthly means) coupled with physically based predictions of changes in variability and the occurrence of extreme events, Hashmi et al. (2009) noted the following limitation:

> There is no universal single statistical downscaling technique that works very well under all circumstances. According to the "Guidelines for Use of Climate Scenarios Developed from Statistical Downscaling Methods" (Wilby et al. 2004), the user should carefully select the downscaling method according to the nature of problem and predictands involved.

Simpler and more transparent methods include using the GCM output directly (e.g., from the closest grid node) and spatial interpolation to finer resolution from latitude and longitude coordinates. Such methods have been adopted for interpolating both

climate observations and GCM scenario output to fine spatial resolutions over large regions, where it is generally impractical to apply statistical downscaling methods.

Typically, the GCM data are normalized to a historical reference period, so that bias in the GCM's estimates of observed values can be removed, an approach sometimes referred to as the "delta method". Because GCMs typically have very low horizontal resolution (see Fig. 1), their representation of topographic effects on local climate is necessarily poor. For this reason, the normalized and interpolated GCM data ("delta values") should be combined with climatological data for the reference period interpolated to the same resolution. This approach provides a more localized correction to the climate scenario.

Interpolation of Climate Data with ANUSPLIN

In this study, historical climate data from point locations (weather stations) were used to develop an interpolated surface of the climatology at the spatial scale of interest. The ANUSPLIN software developed at the Australian National University (ANU) by Hutchinson and coworkers (e.g., Hutchinson 2009, http://fennerschool.anu.edu.au/publications/software/anusplin.php) has been used widely for estimating climate data as grids (or at specific locations), often, but not always, identified by latitude, longitude, and elevation. This software has been applied in many individual countries (e.g., Hutchinson 1995, 1998a, 1998b), including Canada (Price et al. 2000; McKenney et al. 2001, 2004; Hutchinson et al. 2009) and the United States (Rehfeldt 2006), and globally (New et al. 2002; Hijmans et al. 2005). The theory of ANUSPLIN has been described elsewhere, both extensively (e.g., Hutchinson and Gessler 1994; Hutchinson 1995, 1998a, 1998b, 2009; Hutchinson et al. 2009) and briefly (McKenney et al. 2004), and will not be discussed in detail here. The thin-plate spline method can be described as a multidimensional, nonparametric curve-fitting technique, although ANUSPLIN can be configured in many ways. For interpolation of climate data, the target climate variable generally is modeled as a function of various spatially varying dimensions (typically position, as represented by latitude and longitude, and topography, as represented by appropriately scaled elevation). ANUSPLIN has been applied to many climate variables at temporal resolutions ranging from a single day to a month and extending to long-term means, such as 30-year monthly normals.

Price et al. (2000) and McKenney et al. (2001) showed that ANUSPLIN performs extremely well for mean values of monthly temperature and precipitation observed over periods of 30 years or more. ANUSPLIN also has been successfully used to carry out interpolations of monthly time-series data and time series at shorter time scales (weeks to days) (McKenney et al. 2006b; Hutchinson et al. 2009). It is recognized, however, that the inherently patchy nature of rainfall (both in time and in space) generally reduces the confidence in precipitation models relative to temperature models. McKenney and coworkers in the CFS have invested considerable effort (in close collaboration with Hutchinson at ANU) in developing high-resolution climatologies covering the continental United States and Canada (e.g., McKenney et al. 2006b, 2007; Hutchinson et al. 2009).

Price et al. (2001, 2004) and Price and Scott (2006) were the first to report the use of ANUSPLIN as a method of downscaling GCM climate projections. The improvements by McKenney and Hutchinson (e.g., McKenney et al. 2006a, 2006b) were extended to interpolate time series of GCM output data as functions of grid-node latitude and longitude, with treatment of the data values simulated for each grid node as if they were climate observations at the grid-node location. Interpolated climate scenarios were derived from GCM data produced after the IPCC Third Assessment Report was published in 2001 and were documented by Price et al. (2004) and McKenney et al. (2006c). A range of climate data products has since been developed and made widely available both from the CFS Great Lakes Forestry Centre based in Ontario (http://cfs.nrcan.gc.ca/subsite/glfc-climate/climate) and by FTP from the CFS Northern Forestry Centre in Alberta.

Price et al. (2001) carried out several experiments to investigate various ANUSPLIN models and settings for spatial interpolation of GCM output, in particular relating to the use of elevation as a third independent variable. Diagnostics produced by ANUSPLIN in those tests showed relatively little impact of GCM

grid-cell elevation on the resulting spline function, likely because elevation typically is averaged across an entire GCM grid cell, such that high mountains are reduced to relatively lower-altitude plateaus. Hence, the influence of elevation on, for example, temperature, rainfall, and wind speed currently is not well captured in GCMs. This concern will have to be revisited as the spatial resolution of GCMs increases. In the present study, the four GCMs for which simulation results were obtained, are used to generate output at scales ranging from 300–400 km (e.g., Canadian Third Generation Coupled Global Climate Model, version 3.1, medium resolution [CGCM31MR]) to 100–150 km (e.g., Community Climate System Model, version 3.0 of the US National Center for Atmospheric Research [NCARCCSM3]). For these reasons, the interpolations of all GCM results presented here use only longitudinal and latitudinal gradients with a "fixed signal." It should be noted that each downscaled GCM projection is reported as change factors (i.e., delta values) relative to the means of the data simulated by the same GCM for the period 1961–1990, as a way of normalizing the data for any inherent bias between the model and reality (i.e., to remove bias in projected means, although not necessarily from the projected interannual variation). The intention is that these change factors will be combined with interpolated normals of observed climate for the period 1961–1990, which necessarily should account for topographic and elevation effects. In this way, the effects of local spatial variability on real climate are captured and can be combined with the trends in climate projected by the GCMs.

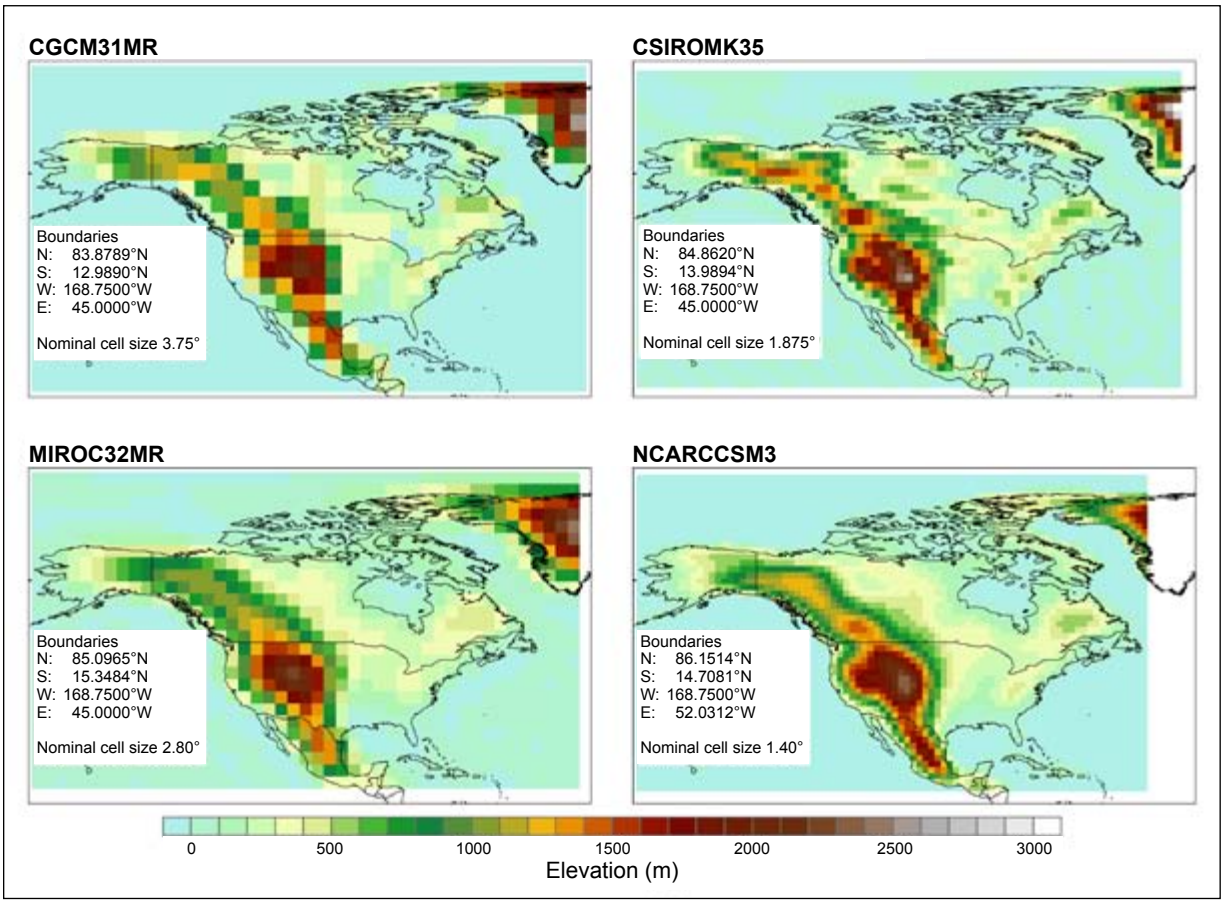

Figure 1. Comparison of grid-cell elevations for the four general circulation models used in this study, from which simulation data were used in the downscaling procedures. Note the differences in horizontal resolution, from CGCM31MR (coarsest) to NCARCCSM3 (finest). For CSIROMK35 and MIROC32MR, some ocean pixels had nonzero values. Latitude and longitude values represent the boundaries of the area of analysis with each model. CGCM31MR = Third Generation Coupled Global Climate Model, version 3.1, medium resolution; CSIROMK35 = Commonwealth Scientific and Industrial Research Organisation Climate System Model, Mark 3.5; MIROC32MR = Model for Interdisciplinary Research on Climate, version 3.2; NCARCCSM3 = Community Climate System Model, version 3.0. The boundaries indicated on each map define the rectangle of data extracted for interpolation using ANUSPLIN.

The simulated climate variables to be interpolated in this study were monthly means of daily surface temperature (minimum and maximum, denoted T_{min} and T_{max}, respectively), global downward solar radiation, and wind speed, and monthly precipitation. Monthly mean atmospheric vapor pressure was estimated from the simulated monthly mean specific humidity and sea-level barometric pressure. The monthly values (including calculated vapor pressure data) were converted to monthly change factors, with the means of the simulated monthly values for the 30-year period 1961–1990 used as a baseline. In the case of mean daily minimum and maximum temperature, the change factor was computed as the arithmetic difference between the monthly value and the corresponding 30-year mean of the same temperature variable for that month. For all other variables, the change factor was the ratio of the monthly value to the mean for that month over the period 1961–1990.

The change factors were interpolated using ANUSPLIN to create time series for the period over which the AR4 simulations were carried out (generally from 1961 to 2100). An ANUSPLIN model was generated for each monthly variable, which was then used to create gridded data covering North America at a spatial resolution of 5 arcminutes. It should be noted that the grids are simply a convenient expression of the fitted spline functions mapped over the region of interest. The spline functions have been archived and can, in principle, be used to estimate monthly values at any location given only latitude and longitude. Finally, for the Canadian landmass, the gridded data were reprojected by means of ArcGIS software (Esri, Toronto, Ontario) to the Lambert conformal conic projection (as used widely in Canadian government mapping projects; see Snyder 1987) with a nominal 10-km grid resolution.

Selection of Forcing Scenarios for GHG Emissions

The choice of GHG emissions scenarios, which were used to "force" a GCM's simulation of future climate, was limited to three global economic–demographic storylines, as described in the SRES (Nakićenović et al. 2000) and used in the IPCC AR4 reports: SRES A2, A1B, and B1 scenarios (see also http://www.grida.no/publications/other/ipcc_sr/). These scenarios offer a range of potential futures with a global mean surface warming of 1.8°C associated with the B1 scenario, 2.8°C for the A1B scenario, and 3.4°C for the A2 scenario, for 2090–2100 relative to 1980–1999 (Solomon et al. 2007).

In addition, output from each GCM was downloaded for an additional scenario, the 20C3M scenario. This fourth scenario represents the model's attempt to simulate historical climate for the 20th century, on the basis of known atmospheric forcings (GHG concentrations, ozone depletion, aerosols [including those caused by volcanic eruptions], and variations in solar output). For most climate models, results for the 20C3M scenario were made available only for the period 1961–2000, which was sufficient to allow use of the 1961–1990 period as a baseline for normalizing the future scenario data (see below).

For the current project, results were selected from the PCMDI Coupled Model Intercomparison Project Phase 3 (CMIP3) data portal at https://esg.llnl.gov:8443/index.jsp, as simulated by each of the following GCMs (see Fig. 1 for comparison of resolution; note "T" values reported in parentheses refer to the triangular truncation of the spectral transformations of each model's horizontal spherical harmonic functions [NCAR Data Support Section 2004]); see also Appendix 1.):

- CGCM31MR – Third Generation Coupled Global Climate Model, version 3.1, medium resolution (T47), developed by the Canadian Centre for Climate Modelling and Analysis (http://www.cccma.bc.ec.gc.ca/data/cgcm3/cgcm3.shtml)
- CSIROMK35 – Climate System Model, Mark 3.5 (T63), developed by Commonwealth Scientific and Industrial Research Organisation (CSIRO), Australia (Gordon et al. 2002; see also http://www-pcmdi.llnl.gov/ipcc/model_documentation/CSIRO-Mk3.5.htm)
- MIROC32MR – Model for Interdisciplinary Research on Climate, version 3.2, medium resolution (T42), developed by the Japanese Center for Climate System Research, the University of Tokyo, the Japanese National Institute for Environmental Studies, and the Frontier Research Center for Global Change (Hasumi and Emori 2004)

- NCARCCSM3 – Community Climate System Model, version 3.0 (T85), developed by US National Center for Atmospheric Research (http://www.ccsm.ucar.edu/models/ccsm3.0/)

The use of these distinct and well-established GCMs ensured that the downscaled scenarios would meet the recommended criteria for selecting and using scenarios for studies of impacts related to climate change. These criteria include the following features:

- consistency of regional scenarios with global projections;
- physical plausibility and consistency (because multiple climate variables, including radiation, wind speed, and humidity, were to be interpolated for each GCM scenario separately and provided in each data set); and
- applicability for assessing impacts (because the downscaled scenario data were reported as change factors that could be referenced to locally observed climate data).

At the time this work commenced, many GCM groups were carrying out simulations for the various AR4 emissions scenarios; however, relatively few of these groups had made data sets available for all three scenarios. This restricted the choice of GCMs quite severely, and it proved necessary to locate some data from sources other than the PCMDI CMIP3 portal for three of the four models selected (see Table). Furthermore, it was critically important when locating simulation results from different sources that they be from the same realization of each model for each GHG forcing scenario. Table 2 summarizes the runs that were selected for each GCM.

Table 1. General circulation model (GCM) data sets for scenarios from the Fourth Assessment Report of the Intergovernmental Panel on Climate Change used to create input files for interpolation by ANUSPLIN software

GCM[a]	IPCC AR4 scenarios	Monthly variables[b]	Source[c]	Time period
CGCM31MR	20C3M, A2, A1B, B1	tas, pr, rsds, uas, vas, hur, huss, psl	CMIP3	1961–2100
	20C3M, A2, A1B, B1	tasmin, tasmax	CCCma	1961–2100
CSIROMK35	20C3M, A2, A1B, B1	tas, tasmin, tasmax, pr, rsds, uas, vas, hur, huss (except B1) psl,	CMIP3	1961–2100
	B1	huss	CSIRO	2001–2100
MIROC32MR	20C3M, A2, A1B, B1	tas, tasmin, tasmax, pr, rsds, uas, vas, hur, huss, psl	CMIP3	1961–2100
NCARCCSM3	20C3M, A1B, B1	tas, tasmin, tasmax, pr, rsds, uas, vas, hur, huss, psl	CMIP3	1961–2099
	A2	tas, tasmin, tasmax, pr, rsds, uas, vas, hur, huss, psl	ESG	1961–2099

[a]CGCM31MR = Third Generation Coupled Global Climate Model, version 3.1, medium resolution; CSIROMK35 = Commonwealth Scientific and Industrial Research Organisation (CSIRO) Climate System Model, Mark 3.5; MIROC32MR = Model for Interdisciplinary Research on Climate, version 3.2; NCARCCSM3 = Community Climate System Model, version 3.0.

[b]Simulated climate variables (as defined by Program for Climate Model Diagnosis and Intercomparison [PCMDI]): tas = mean 2-m air temperature (K), tasmin = mean daily minimum 2-m air temperature (K), tasmax = mean daily maximum 2-m air temperature (K), pr = monthly precipitation (kg m^{-2} s^{-1}), rsds = surface downwelling shortwave radiation (W m^{-2}), uas = zonal wind velocity (m s^{-1}), vas = meridional wind velocity (m s^{-1}), hur = relative humidity (%), huss = surface specific humidity (kg kg^{-1}), psl = sea level pressure (Pa).

[c]Most data were downloaded from the PCMDI Coupled Model Intercomparison Project (Phase 3) (CMIP3) data portal at https://esg.llnl.gov:8443/index.jsp. The Canadian Centre for Climate Modelling and Analysis (CCCma) website serves data for CGCM31MR and other Canadian climate models (http://www.cccma.bc.ec.gc.ca/data/cgcm3/cgcm3.shtml). Daily minimum and maximum temperature data for CGCM31MR were obtained from this source because they were not available from CMIP3. The Earth System Grid (ESG) data portal of the University Corporation for Atmospheric Research (http://www.earthsystemgrid.org) serves data standardized to the specifications of the US National Center for Atmospheric Research model. The complete and consistent NCARCCSM3 data set for the A2 scenario was available only from this data portal.

Table 2. Realization (or run) numbers for each general circulation model and greenhouse gas forcing scenario selected for interpolation with ANUSPLIN

Model and scenario	Realization number	Time stamp[a]
CGCM31MR[b]		
20C3M	Run 5	Reformatted 2005-05-12—22:21:09
A2	Run 5	Reformatted 2005-05-12—22:21:09
A1B	Run 5	Reformatted 2005-05-12—22:21:09
B1	Run 5	Reformatted 2005-05-12—22:21:09
CSIROMK35[c]		
20C3M	Run 1	2006-09-20—05:09
A2	Run 1	2006-09-20—04:09
A1B	Run 1	2006-11-04—10:04
B1	Run 1	2006-09-20—04:09
MIROC32MR[d]		
20C3M	Run 3	Reformatted 2004-10-14—20:53:37
A2	Run 3	Reformatted 2004-12-14—00:22:38
A1B	Run 3	Reformatted 2004-12-14—00:02:09
B1	Run 3	Reformatted 2004-12-14—00:53:41
NCARCCSM3[e]		
20C3M	b30.030e (run 5)	2004-10-18—12:38:54 MDT[b]
A2	b30.042e (run 5)	2004-11-28—15:15:39
A1B	b30.040e (run 5)	2004-12-09—12:52:07 MST[c]
B1	b30.041e (run 5)	2005-01-26—11:05:29 EST[d]

[a]Date and time information extracted from available metadata for the run. MDT = mountain daylight time, MST = mountain standard time, EST = eastern standard time.
[b]CGCM31MR = Third Generation Coupled Global Climate Model, version 3.1, medium resolution.
[c]CSIROMK35 = Commonwealth Scientific and Industrial Research Organisation Climate System Model, Mark 3.5.
[d]MIROC32MR = Model for Interdisciplinary Research on Climate, version 3.2.
[e]NCARCCSM3 = Community Climate System Model, version 3.0.

Downloading, Extraction, and Processing of GCM Data

Standardized procedures for processing the GCM data sets were developed following those reported by Price et al. (2004). These procedures were built around interpolation of the GCM output data by means of ANUSPLIN, where the monthly data values were treated as simulated records obtained from a "virtual climate station" located at the GCM grid-node coordinates.

Because the conversion and extraction processes described in the following paragraphs had to be carried out many times (about 40 repetitions for each GCM), the processing programs were run on multiple Linux-based computers, controlled by Unix shell scripts. These scripts were edited specifically for each GCM, to account for the different spatial resolutions covering the North American domain (as shown in Fig. 1) and for other differences in the contents of the data files.

The following major steps were used in preprocessing the data for interpolation by ANUSPLIN.

Step 1

Global orography data sets for each GCM were downloaded and used to create sets of grid cell coordinates, which were stored in three individual, comma-separated value (CSV) format files: elevs world.csv, lats_world.csv, and lons_world.csv. Elevation data contained in the elevs_world.csv file had to be "naturally oriented" (i.e., west to east and north to south). The global grids for all four GCMs were flipped north to south (which meant that the processing programs had to invert them), with the west-most column at 0° longitude. The longitude coordinates stored in lons_world.csv were converted to their negative equivalents (e.g., 240.0° = 120.0° W = −120.0°). Given that the data sets provided global coverage, latitude values for the southern hemisphere stored in lats_world.csv were also converted to their negative equivalents. These CSV data files were

copied to the working directory used to extract data for the North American rectangles indicated in Fig. 1.

Step 2

GCM data files (for each climate variable and each of the four scenarios) were downloaded, generally in NetCDF format (see http://www.unidata.ucar.edu/software/netcdf/), from the websites listed in Table 2. The downloaded files were renamed to a systematic format to ensure models and scenarios were uniquely identified and to facilitate subsequent manipulation.

Step 3

Global data for each climate variable were extracted from the NetCDF files using a script called nc-readvar_to_asg.txt, which then called program nc-readvar to convert data for each variable to ASCII code with GRIB-format headers (i.e., for each monthly time step, the data were preceded by a single line containing information about the time step and the grid dimensions, as described at http://cera-www.dkrz.de/IPCC_DDC/info/Readme.grbconv). These output files were called "ASCII grids," to reflect the use of ASCII text and to refer to the data content organized on a standard geographic grid. The files were identified with the same names as used for the input NetCDF files, but with the extension "asg" replacing the extension "nc."

Step 4

Data for wind speed were extracted for those GCMs with data files containing multiple atmospheric pressure levels. Further scripts were used to call several programs, described below, to extract the required data and combine them with the GCM grid-node elevations to obtain estimates of wind velocity at the surface elevation of the GCM. Scripts called merge_ua.txt and combine_merge_ua.txt were used for the zonal (*U*) component vector of wind velocity, and scripts called merge_va.txt and combine_merge_va.txt were used for the meridional (*V*) component vector of wind velocity. The programs used to extract data and their specific functions were as follows:

nc-readvar Extract data from NetCDF file at multiple pressure levels and convert to ASCII grids for each month.

cat Concatenate ASCII data from multiple months and a single pressure level into a single time series.

asg2nc Convert ASCII time series into a NetCDF file containing the time series for a single pressure level.

nc_merge Merge data from multiple pressure levels into a single surface (i.e., where the grid-cell elevations are sufficiently high to penetrate above the bottom atmospheric pressure levels in the GCM data file). This program has switches (--or --inclusive) to allow retention of existing surface level values as they are merged with data from progressively higher atmospheric levels.

For all GCMs, the *U* and *V* component vectors of wind velocity were combined to calculate mean wind speed (*u*), using the hypotenuse calculation:

$$u = \sqrt{U^2 + V^2} \quad [1]$$

Another script, extract_merged_to_asg.txt, which again called nc-readvar, was run to create ASCII files with GRIB headers from the merged wind velocity data.

Step 5

Data for the North American rectangles (including the western part of Greenland [see Fig. 1]) were extracted from the global NetCDF data files using a script called do_gcm_subsetXXxYY.txt and from the merged global ASCII files using a script called do_gcm_subsetXXxYY_merged.txt, where XX and YY are the longitudinal and latitudinal grid dimensions, respectively, of the GCM-specific rectangle. The do_gcm_subsetXXxYY.txt script first converted the NetCDF file into ASCII format. Both scripts then called a program called gcm_subset to extract the desired North American spatial subset from the global ASCII files. Most GCM grids were "flipped," meaning that the data were organized with the southern-most grid cells at the top, so it was necessary to check for flipping and reverse as appropriate. The gcm_subset program defaults to handle the flipped grid orientation correctly, but flipping can be suppressed with a -F switch. Output files generated by gcm_subset had a suffix added to the input file name of the generic format ".XXxYY.subset." For each GCM, gcm_subset also produced the corresponding subsets of the elevs_world.csv, lats_world.csv, and lons_world.csv files that were needed to generate the grid-node coordinate information when formatting the data for input to ANUSPLIN.

Because the spatial domains, grid resolutions, and output variables differed among the four GCMs, some model-specific details are provided in the following paragraphs (see also Fig. 1 and Appendix 1):

CGCM31MR
The global domain consists of 96 longitudinal cells × 48 latitudinal cells, yielding nominal grid-cell dimensions of 3.75° longitude by 3.75° latitude at the equator. Although the longitudinal angular dimensions are constant for all grid cells, in common with most GCMs, the latitudinal angular dimensions vary with latitude. With this model, generation of a subset for North America produced a rectangular grid of 20 cells north to south and 34 cells west to east, with northerly and southerly boundaries of 83.8789°N and 12.989°N, respectively, and westerly and easterly boundaries at 168.75°W and 45.0°W, respectively.

For CGCM31MR, the variables tasmax and tasmin (defined in Table 1) were available only as daily data. These daily files were downloaded, spatial subsets were created, and the data were averaged for each month to obtain the monthly mean daily values before continuing with Step 6.

CSIROMK35
The global domain consists of 192 longitudinal cells × 96 latitudinal cells, yielding a nominal grid-cell size of 1.875° longitude × 1.865° latitude at the equator. Generation of a subset for North America produced a rectangular grid of 39 cells north to south and 67 cells west to east, with boundaries at 84.862°N, 13.9894°N, 168.75°W and 45.0°W, respectively.

MIROC32MR
The global domain consists of 128 longitudinal cells × 64 latitudinal cells, yielding a nominal cell size of 2.81° longitude × 2.79° latitude at the equator. Generation of a subset for North America produced a rectangular grid of 26 cells north to south and 45 cells west to east, with boundaries at 85.0965°N, 15.3484°N, 168.75°W, and 45.0°W, respectively.

NCARCCSM3
The global domain consists of 256 longitudinal cells × 128 latitudinal cells, yielding a nominal cell size of 1.40625° longitude × 1.400768° latitude at the equator. Generation of a subset for North America produced a rectangular grid of 52 cells north to south and 84 cells west to east, with boundaries at 86.1415°N, 14.7081°N, 168.75°W and 52.0312°W, respectively.

Step 6
The subsets of monthly GCM data grids were converted into the columnar format used for input to ANUSPLIN: annual data blocks, each comprising fields for the latitude, longitude, and elevation of the grid node, followed by 12 monthly climate values, sorted by lines in latitude and longitude order. This procedure was carried out with program gcm_processor, called by a script named gcmprocessor_GCM_XXxYY.txt, where "GCM" represents the name of the GCM, and "XXxYY" represents the longitudinal and latitudinal dimensions (i.e., number of grid cells) of its North American rectangle. The main function of gcm_processor was to normalize the GCM data in a two-pass procedure. On the first pass, gcm_processor was run using the GCM's 20th century (20C3M) results as input, to calculate 30-year means for each month during the simulated period 1961–1990. On the second pass, these calculated means were used to convert the GCM output from projections of absolute values to change factors relative to the 1961–1990 means. These means were applied to the GCM projections (A2, A1B, B1). In the case of temperature variables, the change factors were calculated by subtracting the means from the monthly values. For all other climate variables, the change factors were calculated by dividing the monthly values by the simulated 1961–1990 means. The multi_gcmproc.txt script called multiple instances of gcmprocessor_GCM_XXxYY.txt so that data for all climate variables for a single GHG emissions scenario could be handled in a single process. Specific versions of both batch files were created for each GCM and emissions scenario, which also accounted for the period of the simulation (1961–2099 for NCARCCSM3 and 1961–2100 for the other three GCMs). Each output file generated by multi_gcmproc.txt contained data for a single climate variable and a single year, because ANUSPLIN treats each month of each year as an independent data set.

Step 7
In the particular case of simulated atmospheric humidity, the preferred measure was vapor pressure (denoted *e*), which required conversion from other humidity terms simulated by the GCMs. After much

searching, complete error-free data sets of simulated specific humidity (denoted H_s) at surface elevation were obtained, though data for only 10 of the 12 GCM projections were available from PCMDI. One exception was the NCARCCSM3 model forced by the A2 emissions scenario, for which there were acknowledged errors, including complete absence of data for the 2070s decade and some absurdly high values occurring every January at several locations around the globe (including all grid cells at the South Pole and two small groups of adjacent cells in North America). The use of surface relative humidity instead of specific humidity to calculate vapor pressure was considered, but these data were also missing for the 2070s decade.

Subsequently, a complete time series of surface specific humidity data was located at the Earth System Grid data portal of the University Corporation for Atmospheric Research, although this data set also had the problem with extreme values at two locations in North America and elsewhere. To overcome this problem, a new routine was added to gcm_processor, which scanned all of the data in each month for values that were excessively high (i.e., 6.5×10^5 to 7.5×10^5 kg kg^{-1} rather than the typical values, on the order of 0.001 kg kg^{-1}). Whenever the scanning algorithm located a grid cell containing an over-range value, that value was replaced by the mean of the values in the adjacent grid cells, excluding any that were themselves over-range. Because the search algorithm worked from northwest to southeast, the means of some grid cells were derived from interpolated means in adjacent cells to the north and west. Under the circumstances, this seemed a necessary but minor compromise to provide the consistent data set needed for the ANUSPLIN interpolation to be carried out successfully.

Precipitation amounts simulated by GCMs are often highly correlated with the simulated humidity in the same or adjacent grid cells. However, no precipitation data that were clearly overrange were found in the NCARCCSM3 data for the months affected by the specific humidity problem.

A second exception was the CSIROMK35 forced by the A1B emissions scenario. In this case, data for surface specific humidity were unavailable from PCMDI but were obtained directly from CSIRO.

Because vapor pressure depends on elevation, sea-level pressure data (also simulated by each GCM) were used to provide barometric corrections for grid-cell elevation. A second custom program, anu_hum, was written to perform the conversion of humidity data extracted for each GCM to the format required for input to ANUSPLIN. This program read monthly change factors for specific humidity and corresponding change factors for sea-level pressure, recombining these values with the 1961–1990 means calculated in Step 6. The appropriate data were used to calculate monthly values of vapor pressure, which were exported to new output files, also in ANUSPLIN input format.

Vapor pressure was derived from the values for specific humidity and sea-level pressure simulated by each GCM. Steps for the conversion algorithm were as follows:

a. Read in specific humidity (H_s, kg kg^{-1}) and sea-level pressure ($P(0)$, kPa) for each GCM grid point.
b. Adjust sea-level pressure to "surface pressure" at the elevation given by the GCM orography data, using the equation of Jensen et al. (1990):

$$P(z) = P(0)\ (1.0 - 0.0065z/293.0)^{5.26} \quad [2]$$

where $P(z)$ is the atmospheric pressure (kPa) at elevation z (m).

c. Calculate surface vapor pressure at elevation z, $e(z)$, from specific humidity, H_s, and surface pressure, $P(z)$, using the following equation:

$$e(z) = P(z)\ H_s/[0.622 + H_s(1.0 - 0.622)] \quad [3]$$

where 0.622 is the ratio of the molecular weights of water vapor to air (e.g., Monteith and Unsworth 2008), and $e(z)$ and $P(z)$ are in kilopascals.

Consideration was given to limiting the calculated values of surface vapor pressure to the lesser of the value obtained from [3] and saturation at the daily minimum temperature for the same time step and GCM grid node, since it is generally unlikely that monthly mean vapor pressure would exceed saturation. However, computing saturation at the daily minimum temperature produced many instances where this assumption did not hold.

Another possibility would have been to limit vapor pressure to the lesser of the calculated value and saturation at the monthly mean daily temperature but after some further thought it was decided that a better approach would be to not attempt any limitation on the calculated value. The justifications for this decision were as follows:

- Although unlikely, it is possible that diurnal changes in vapor pressure, coupled with the curvilinear response of saturation vapor pressure to temperature, would cause a situation in which monthly mean vapor pressure exceeds saturation at daily minimum or mean temperature.
- There are likely to be differences among the GCMs in their simulation of variability and trends in vapor pressure. Limiting these values to saturation at temperatures simulated by each GCM could mask some of these differences and cause any comparison of the calculated values to be misleading.
- As for precipitation, solar radiation, and wind speed data, projected changes in monthly mean vapor pressure were normalized as ratios relative to the simulated 1961–1990 monthly means. These ratios necessarily required that future and baseline data be computed in exactly the same way; hence, even if the absolute values simulated by the GCM exceeded saturation in T_{min}, the actual vapor pressure data obtained from each downscaled scenario would depend on the baseline climatology temperature and vapor pressure data that were to be combined with the scenario change factors.
- The responsibility for determining whether the simulated climate variables are physically consistent should remain with the user of the downscaled data. It is safer, and potentially less confusing, for users of the data to account for situations where vapor pressure exceeds saturation (if needed) than it is for them to assume this will never happen.

For these reasons, the final change factors for vapor pressure were not arbitrarily limited to saturation at monthly minimum or mean temperature.

Step 8

The files of normalized monthly change factors for each GCM variable (i.e., four GCMs × three scenarios × six variables, for 72 files in total) were submitted to the CFS Great Lakes Forestry Centre, for interpolation using ANUSPLIN. At the Great Lakes Forestry Centre, ANUSPLIN models were developed for each month of normalized GCM scenario data, with the data being treated as anomalies relative to the 1961–1990 means. Because the input data were to be treated as anomalies, rather than actual climate values, a fixed-signal model, rather than a standard optimization model, was used (McKenney et al. 2006c). Notably, there are no inherent statistical relationships between these anomalies and the independent variables of longitude and latitude. A fixed signal of 60% of the data points (the GCM grid-cell values) produced reasonable results (e.g., avoiding singularities ["bulls' eyes"] in the resultant climate change scenario models). The LAPGRD program (part of the ANUSPLIN package) was used to generate the data grids from a 30 arcsecond digital elevation model of North America. This model was constructed by staff at the Great Lakes Forestry Centre using the US Geological Survey GTOPO30 digital elevation model coverage for the United States (http://eros.usgs.gov/#/Find_Data/Products_and_Data_Available/gtopo30_info) and a Canadian digital elevation model (see Lawrence et al. 2007). Log files containing summary statistics were also generated by LAPGRD. The monthly grids of interpolated change factors were generated in Esri ArcInfo ASCII format, with a cell size of 5 arcminute (300 arcsecond) latitude x 5 arcminute (300 arcsecond) longitude (about 9.25 km^2 at the equator), covering the domain from 168°W to 52°W and from 25°N to 85°N (1392 columns x 720 rows). This grid resolution matches that of many other climate data products previously produced at the Great Lakes Forestry Centre (McKenney et al. 2007). The generated monthly files were bundled and transmitted back to the Northern Forestry Centre via FTP for post-processing.

Step 9

"Subset rectangles" were extracted from the North American grids for Canada, the conterminous 48 states of the United States, and Alaska, by means of macros running in Esri ArcInfo and were packaged

for final distribution. Canadian data grids were also reprojected to the Lambert conformal conic projection (Snyder 1987) using Esri ArcInfo and converted to NetCDF files containing consecutive monthly data for each climate variable.

The normalization procedures carried out in Step 6 removed biases in the different GCMs. That is any tendency for a GCM model to over or underestimate historical climate, defined as the 1961–1990 mean, was removed and only the change relative to that period was retained. The interpolations carried out in Step 9 allowed direct comparison of the downscaled projections for different GHG scenarios and different GCMs (which operate at different spatial resolutions). These steps were consistent with requirements outlined in a recent USDA Forest Service memorandum, "Draft NEPA Guidance on Consideration of the Effects of Climate Change and Greenhouse Gas Emissions," which was released on 18 February 2010.

Use of Historical Climatology

The interpolation procedure applied to the GCM output data did not account for topographic effects, because the representation of surface orography in global-scale GCMs is typically poor (although, as Fig. 1 shows, the horizontal resolution varied substantially among the four GCMs, and it might be expected that the effects of elevation on surface climatology would be much better represented by NCARCCSM3 than by CGCM31MR). Observed climate normals for 1961–1990 were interpolated to the same grid resolution to account for topographic effects (see McKenney et al. 2007). The interpolated change factors for the GCM scenarios can be combined with these or other interpolated data grids of current climate, so that spatial variability in future climate attributable to topography is retained while the climate change trends simulated by the GCMs are captured. This approach is only an approximation of future climate, however, as there may be interactions between topography and climate change that alter the course of the local projection. Conversely, there are so many other larger sources of errors in the GCM projections that errors associated with this combination approach are unlikely to be important (see also the Discussion).

Because the interpolated GCM scenario data are consistent with IPCC selection criteria (see http://www.ipcc-data.org/ddc_scen_selection.html), and have been converted to change factors referenced to the 30-year monthly means for the simulated 1961–1990 period, they can be combined with gridded climate normals for the same 30-year period to create "absolute" values for the future projections of climate. This approach preserves the characteristics of current climate while superimposing the climate change signals simulated by each GCM for each GHG forcing scenario. A key advantage is that the user is free to combine these interpolated scenario data with any climatological data set, although these data should, of course, be for an appropriate variable averaged over the period 1961–1990 (where examples of "appropriate variables" include radiation, expressed in watts per square meter or megajoules per square meter per day; wind speed expressed in meters per second, miles per hour, or knots; and precipitation, expressed in millimeters per day or inches per month). A further advantage is that for change factors expressed as ratios (i.e., for climate variables other than temperature), the units of the historical climatology will always be retained in the combined data.

As previously noted, the CFS has constructed continental-scale gridded climatologies derived from records collected at climate stations across Canada and the continental United States since 1901 (see McKenney et al. 2006b). These data, including grids of 30-year normals and historical monthly models are freely available in various formats. In addition, historical continent-wide daily models have been constructed (see Hutchinson et al. 2009). All gridded data sets are available for download via password-protected FTP from the CFS Northern Forestry Centre upon request to the authors.

Analysis of Interpolated Climate Variables

This section describes the procedures applied to the interpolated GCM scenario data to produce the results presented in this report. The objective was to carry out a comprehensive survey of the results obtained for Canada, including the following aspects:

- compare and contrast the large-scale trends, both spatial and temporal, seen in the 12 high-resolution GCM scenarios that were produced;
- demonstrate the kinds of analyses that can be performed with these data and that might be applied to specific regions of Canada other than the ecozones identified for the current project;
- highlight the consistencies and inconsistencies among the different GCMs;
- perform quality control on the interpolated data products by locating apparent errors; and
- identify problems with GCMs and/or particular GHG forcing scenarios.

The 12 projections (three scenarios and four GCMs) each generated projected changes in monthly climate over a 100-year period, for five distinct climate variables (i.e., temperature, precipitation, solar radiation, wind speed, and humidity). Given the quantity of data, it is impossible to present in a single report all possible interpretations of the data set. Instead, selected results are presented in three ways.

The first method involved comparing and contrasting spatial variability among the different GCMs and GHG emissions scenarios and then showing the results of these analyses as a series of maps of Canada. Each series of maps depicted the averages of a key climate variable (annual or seasonal) projected for a 30-year period (2011–2040, 2041–2070, or 2071–2100), according to a single GCM and GHG emissions scenario. Initially, maps were developed to display the change factors applied to the interpolated normals for 1961–1990. However, the differences among the projections often were very subtle, because the spatial variations in projected changes are small relative to the strong climatic gradients that exist across the entire continent, resulting from latitudinal and elevational differences and from the east-to-west gradients caused by synoptic weather systems and the Rocky Mountains. The approach subsequently adopted was to show, for key variables (specifically temperature and precipitation) for a single GCM, single sets of four maps each, comparing the 1961–1990 normals with projections for each of the 30-year periods (e.g., annual mean daily maximum temperature). The temperature maps were derived by adding the means of the interpolated change factors for each 30-year period to the interpolated 1961–1990 normals (shown as the topmost map in each figure). For precipitation, the projections were derived by multiplying the means of the interpolated change factors for each 30-year period by the 1961–1990 normals. The GCM selected for this process was the Canadian CGCM31MR, forced by the A1B emissions scenario. In addition to these maps, a series of maps were prepared to compare the change factors projected by each of the four GCMs for different 30-year periods for different GHG forcings. In the latter maps, all grid-cell means were weighted to account for the number of days in each month, including leap years, and hence can be compared with historical 30-year climate normals obtained from climate station observations.

For the second method of interpreting and comparing the GCM scenarios, the interannual variation in each climate projection was examined by graphing long-term time series of key annual or seasonal variables spatially averaged for 18 ecozones, based on the Terrestrial Ecozones of Canada (Ecological Stratification Working Group 1995; see also Wiken 1986) (Fig. 2; Table 3). Each of these graphs enabled comparison of projected trends in means and interannual variability, according to each GCM scenario, for a specified variable and ecozone. In these graphs, the seasonal and annual absolute data are area-weighted spatial means of the monthly aggregated values. The area weightings were calculated as ratios for each grid cell, where the actual area was expressed relative to the mean area of all grid cells in the ecozone, as follows:

$$R_{Ai} = \frac{A_i}{A_{region}/N} \qquad [4]$$

where R_{Ai} is the area ratio for grid cell i, N is the number of grid cells in the ecozone, A_i is the area of grid cell i, and A_{region} is the total area of the ecozone, given by $\sum_{i=1}^{N} A_i$. The area A_i was calculated in steradians using the following equation:

$$A_i = \frac{\cos(\alpha+\delta/2) + \cos(\alpha-\delta/2)}{2}\delta^2 \qquad [5]$$

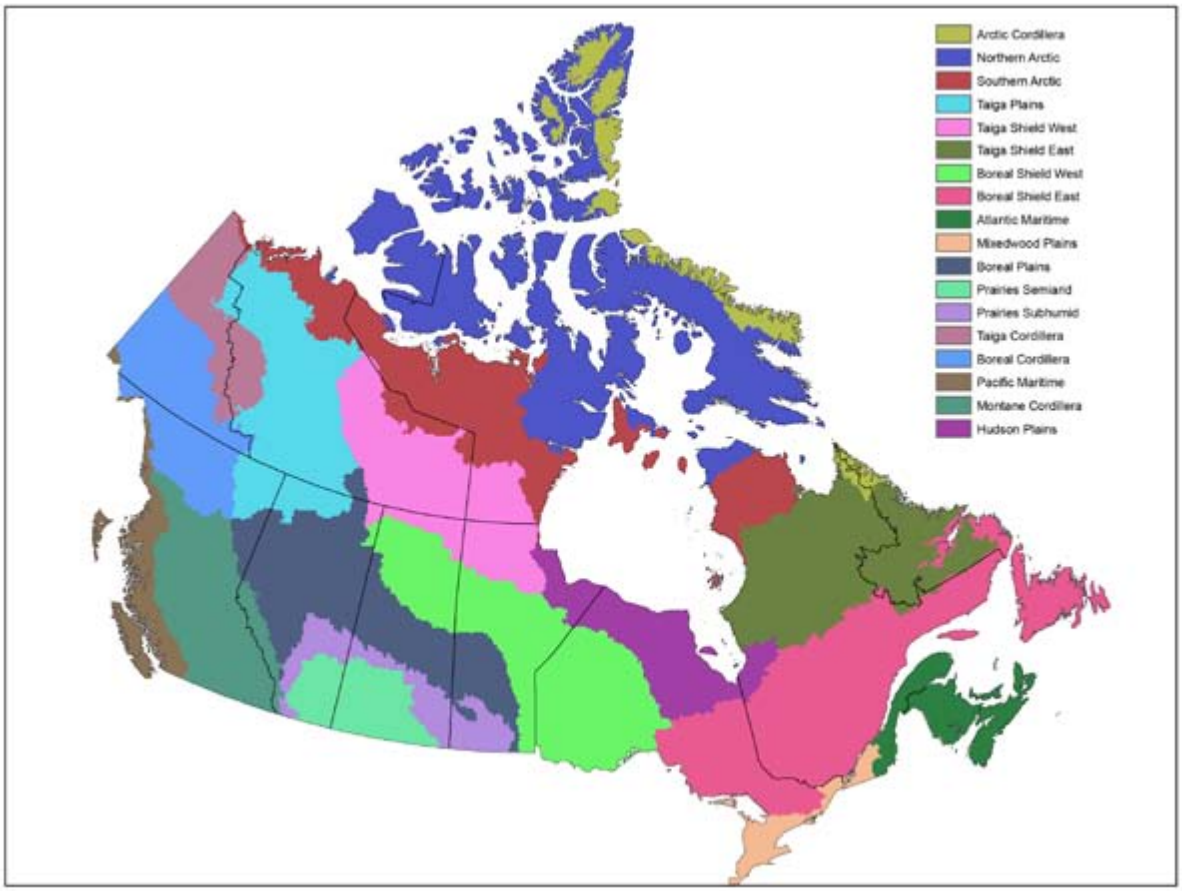

Figure 2. Terrestrial ecozones of Canada used in the climate scenario analysis, derived from the map of the Ecological Stratification Working Group (1995; see also Wiken 1986), with three additional subdivisions as used in Canada's national reporting framework for the forest carbon budget (e.g., Kurz et al. 2009).

where angle α is the latitude at the grid cell centroid, and δ is the dimension of the grid cell (latitude and longitude), expressed in radians. The area in steradians can be converted to square kilometers using a value of 6371.2213 km per radian, assuming that the earth is a perfect sphere (Kittel et al. 1995), but this is unnecessary for [4].

The graphical analysis led to a third method of presenting the results: a set of comprehensive tables summarizing results for all variables and all scenarios in each of the 18 ecozones.

Calculation of Bioclimatic Indices from the Scenario Data

As an added set of products, 30-year models of mean changes in temperature and precipitation were also developed, for the purpose of projecting changes in various bioclimatic indicators (listed in Table 4). This required several additional steps. First, ANUSPLIN surfaces for the 30-year mean change fields from each GCM scenario were created for the three future periods (2011–2040, 2041–2070, and 2071–2100). These surfaces were used to estimate projected mean changes at North American weather stations operating during the period 1961–1990. The mean changes were combined, in turn, with the station normals for the 1961–1990 period. This allowed for the generation of new ANUSPLIN surfaces of projected mean values for each future period. For these models, trivariate (position- and elevation-dependent) splines were used. The statistical signals were good because there are statistically strong elevational dependencies in the 1961–1990 models, which remained in the derived ANUSPLIN models of future climate.

With these surfaces it was possible to generate several bioclimatic variables (e.g., length of growing season, precipitation during growing season) that are often used in modeling in the fields of forestry, agriculture, and ecological impacts, and hence have greater interest to some potential users. The derived variables are possible because a daily sequence of temperature and precipitation can be generated from the primary monthly surfaces. This is done through a Bessel interpolation, whereby the daily sequence is forced to pass through the monthly means in a monotonic form (for details, see Mackey et al. 1996). It is important to understand that these data are intended to represent mean conditions, and that in any given year, "noise" would influence the actual daily sequence of bioclimatic variables.

It was recognized that some users might desire estimates of bioclimatic variables at annual time steps, rather than 30-year means. This created an additional challenge because of the previously noted greater stochasticity of individual years. After due consideration, it was decided to generate model outputs at another resolution to allow dissemination of some of the projected bioclimatic variables at annual time steps. Again, users should appreciate that these bioclimatic models do not account for stochasticity at daily and monthly time scales, but they do retain the interannual variations provided in the GCM projections. To make the data sets more manageable, these models were developed at the slightly coarser resolution of 900 arcsecond (about 30 km).

Table 3. Ecozones used in the regional analysis of general circulation model scenarios applied to Canada, based on the classification of the Ecological Stratification Working Group (1995; see also Wiken 1986), with three extra subdivisions identified by Kurz et al. (2009)[a]

Ecozone number	Ecozone name	Climate summary table
ECZ1	Arctic Cordillera	5
ECZ2	Northern Arctic	6
ECZ3	Southern Arctic	7
ECZ4	Taiga Plains	8
ECZ5a	Taiga Shield West	9
ECZ5b	Taiga Shield East	10
ECZ6a	Boreal Shield West	11
ECZ6b	Boreal Shield East	12
ECZ7	Atlantic Maritime	13
ECZ8	Mixedwood Plains	14
ECZ9	Boreal Plains	15
ECZ10a	Prairies Semiarid	16
ECZ10b	Prairies Subhumid	17
ECZ11	Taiga Cordillera	18
ECZ12	Boreal Cordillera	19
ECZ13	Pacific Maritime	20
ECZ14	Montane Cordillera	21
ECZ15	Hudson Plains	22

[a]The original Prairie ecozone was divided into semiarid and subhumid regions, denoted ECZ10a and ECZ10b, respectively (corresponding approximately to grassland prairie and aspen parkland regions). Similarly, the original Taiga and Boreal Shield ecozones were subdivided into western (ECZ5a and ECZ6a, respectively) and eastern (ECZ5b and ECZ6b, respectively) subregions.

Table 4. Variables derived from primary climate surfaces[a,b]

No.	Variable[c]	Description
1	Annual mean temperature	Annual mean of monthly mean temperatures
2	Mean diurnal temperature range	Annual mean of monthly mean daily temperature ranges
3	Isothermality	Variable 2 ÷ variable 7
4	Temperature seasonality	Standard deviation of monthly mean temperature estimates, expressed as a percentage of their mean
5	Maximum temperature of warmest period	Highest monthly maximum temperature
6	Minimum temperature of coldest period	Lowest monthly minimum temperature
7	Annual temperature range	Variable 5 – variable 6
8	Mean temperature of wettest quarter	Mean temperature of three wettest consecutive months
9	Mean temperature of driest quarter	Mean temperature of three driest consecutive months
10	Mean temperature of warmest quarter	Mean temperature of three warmest months
11	Mean temperature of coldest quarter	Mean temperature of three coldest months
12	Annual precipitation	Sum of monthly precipitation values
13	Precipitation of wettest period	Precipitation of wettest month
14	Precipitation of driest period	Precipitation of driest month
15	Precipitation seasonality	Standard deviation of monthly precipitation estimates, expressed as a percentage of their mean
16	Precipitation of wettest quarter	Total precipitation of three wettest consecutive months
17	Precipitation of driest quarter	Total precipitation of three driest consecutive months
18	Precipitation of warmest quarter	Total precipitation of three warmest months
19	Precipitation of coldest quarter	Total precipitation of three coldest months
20	Start of growing season	Date when daily mean temperature first meets or exceeds 5°C for five consecutive days in spring
21	End of growing season	Date when daily minimum temperature first falls below –2°C after 1 August
22	Growing season length	Variable 21 – variable 20
23	Total precipitation in the three months before start of growing season	Total precipitation in the three months before variable 20
24	Total growing season precipitation	Total precipitation during variable 22
25	Growing degree-days during growing season	Total degree-days during variable 22, accumulated for all days where mean temperature exceeds 5°C
26	Annual minimum temperature	Annual mean of monthly minimum temperatures
27	Annual maximum temperature	Annual mean of monthly maximum temperatures
28	Mean temperature during growing season	Mean temperature during variable 22
29	Temperature range during growing season	Highest minus lowest temperature during variable 22

[a]Modified from McKenney et al. (2006a).
[b]In all cases, the descriptions should be considered estimates rather than actual values.
[c]Variables 1–19 were generated by ANUCLIM (Houlder et al. 2000); variables 20–29 were generated by SEEDGROW (Mackey et al. 1996). The approach used by Mackey et al. (1996) creates a daily sequence of minimum and maximum temperature and precipitation, with the values forced monotonically through the monthly values. The resulting values are intended to represent mean conditions only, as the weather in any given year would be expected to produce different results, because of interannual variability.

RESULTS

Maps showing the trends in annual mean daily temperature and precipitation are presented in sets of six figures: Figs. 3–8 for daily maximum temperature, Figs. 9–14 for daily minimum temperature and Figs. 15–20 for total precipitation. In each group of figures, the first set of maps (Figs. 3, 9, and 15) shows the trends in absolute measures of temperature or precipitation according to the CGCM31MR model, forced by the A1B emissions scenario. The subsequent three figures in each set (Figs. 4–6, Figs. 10–12, and Figs. 16–18) show the changes relative to the means for 1961–1990, for each successive 30-year period, for all four GCMs, again forced by the A1B emissions scenario. The final two figures in each set (Figs. 7 and 8, Figs. 13 and 14, and Figs. 19 and 20) show the changes for the period 2071–2100 for the A2 and B1, which can be compared directly to the data for the A1B scenario in Figs. 6, 12, and 18.

For many regions, the four GCMs agreed fairly closely in their projections of temperature trends, as shown in Figs. 4–8 and 10–14 and in many of the regional (ecozonal) graphs presented in the section "Projected Climate Trends, 2000–2100." Not surprisingly, the A2 scenario generated the greatest warming across the country and the B1 scenario the least. In general, the warming projected with forcing by the B1 scenario for the period 2071–2100 was qualitatively similar to that obtained with forcing by the A1B scenario for the preceding 30-year period (compare Figs. 5 and 8 for maximum temperature and Figs. 11 and 14 for minimum temperature). The NCARCCSM3 model was the exception to this general trend, projecting a distinctly warmer climate nationwide for 2041–2070 when forced by the A1B scenario (Figs. 5 and 11) than for 2071–2099 when forced by the B1 scenario (Figs. 8 and 14).

Of the four models, MIROC32MR, forced by the A1B emissions scenario, predicted noticeably greater warming during the 21st century for most of Canada than the other three models (Figs. 4–6, 10–12). However, the NCARCCSM3 model was often a close second, and projections for annual mean minimum temperature were comparable for these two models for the 2071–2100 period with forcing by the A2 scenario (Figs. 7 and 13). The CGCM31MR model projected the least warming, whereas the CSIROMK35 model generally projected the third-warmest scenarios. The models were in strong agreement that in the north, the Arctic and Hudson Bay regions would undergo the greatest temperature increases, while the coastal regions of British Columbia and the Atlantic provinces would experience the least warming. The distribution of warming from east to west across the provinces was somewhat less consistent among the four GCMs, although the general pattern was for warming to be generally centered in Manitoba and Ontario. The MIROC32MR and NCARCCSM3 models appeared to project greater warming across eastern Canada all the way to Newfoundland, whereas the CGCM31MR and CSIROMK35 models projected similar temperature increases on both the Pacific and the Atlantic coasts. The projected warming in the midcontinental regions occurred along a general southwest-to-northeast gradient, following the existing climatic zones.

With regard to annual precipitation, the greatest proportional increases were projected to occur in the territories, particularly in the far north, but the models diverged considerably for the provinces. In general, precipitation was projected to increase, but the NCARCCSM3 model projected significant reductions in southern British Columbia (Figs. 17–20) and a more gradual decline in Saskatchewan and Manitoba. The CSIROMK35 model projected a less severe decrease in annual precipitation across much of southern British Columbia, whereas the MIROC32MR model projected drying in southern Ontario. Most of these trends were clearly apparent as early as 2011–2040 for forcing with the A1B scenario (Fig. 16). Only the CGCM31MR model projected general increases in precipitation nationwide, although the other models projected generally greater increases in the Arctic by the end of the 21st century. The CSIROMK35 model projected greater increases for the western prairies by 2100 than did the CGCM31MR model, a trend that was also seen to some extent with the NCARCCSM3 model.

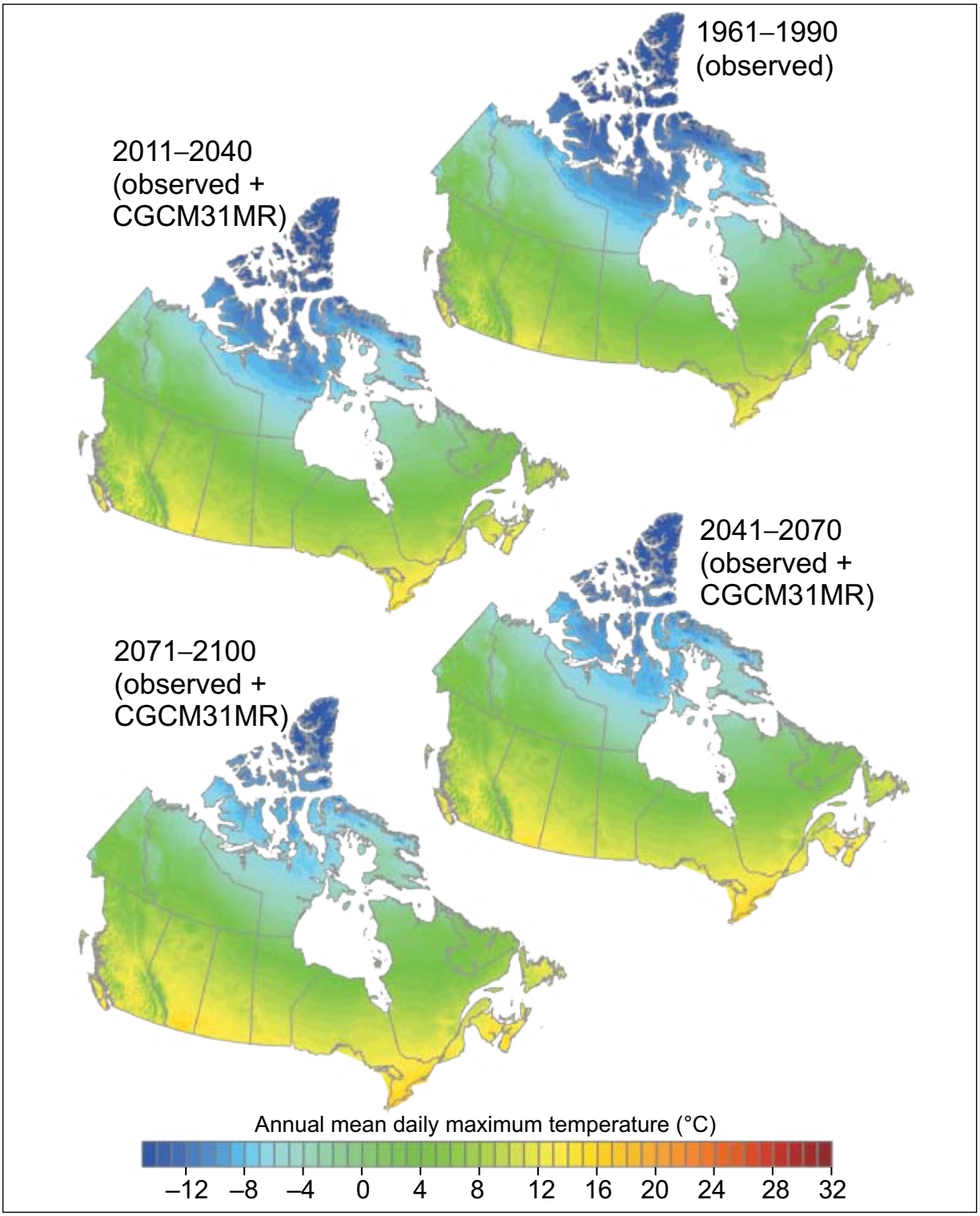

Figure 3. Maps of annual mean daily maximum temperature derived from climate station records for the period 1961–1990 and projections according to the Third Generation Coupled Global Climate Model, version 3.1, medium resolution (CGCM31MR), forced by the A1B emissions scenario, for 2011–2040, 2041–2070, and 2071–2100. The projections were derived by adding the interpolated climate normal data shown in the 1961–1990 normals map (at top) to the means of the interpolated change factors for each 30-year period.

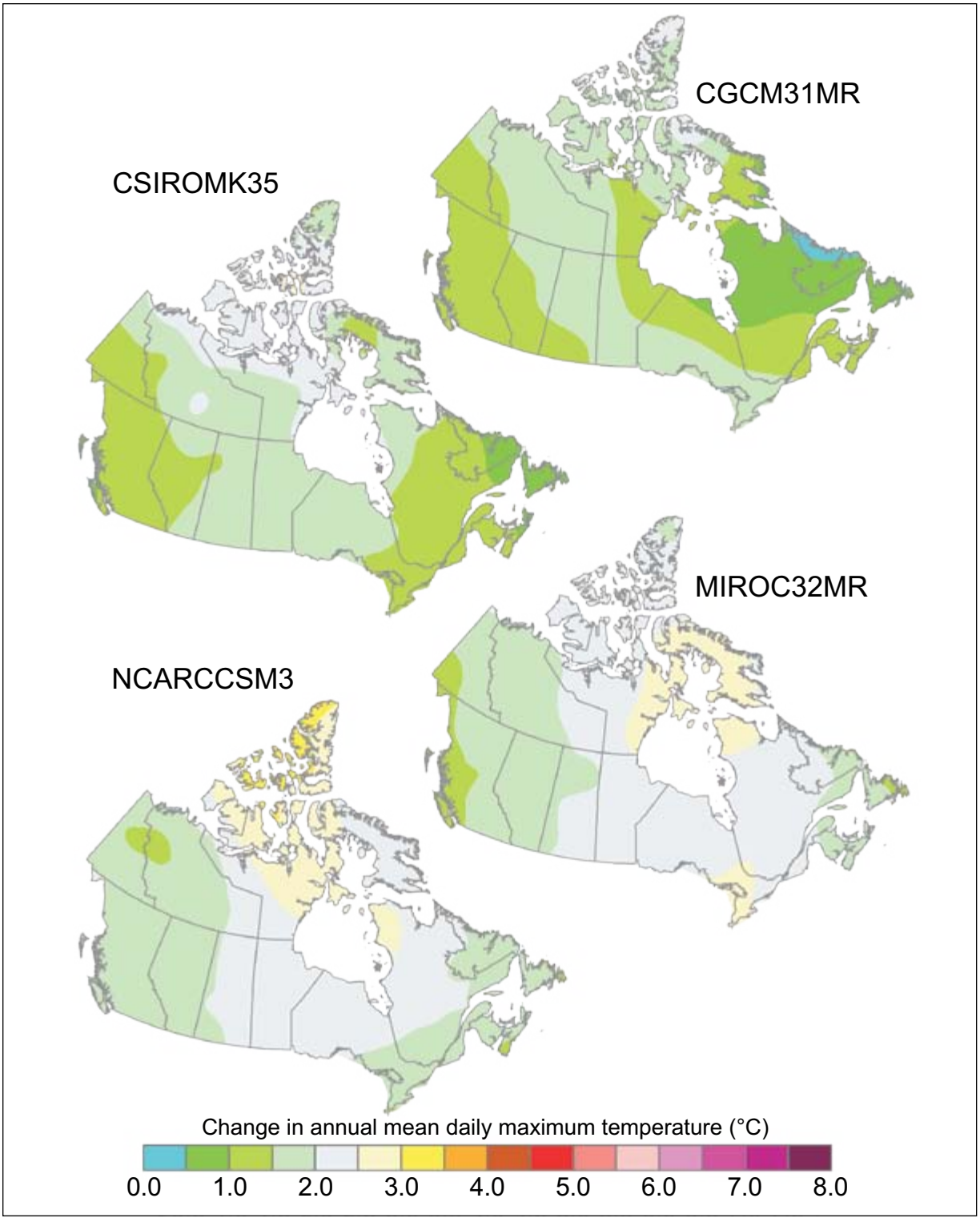

Figure 4. Projected changes in annual mean daily maximum temperature for the period 2011–2040, relative to 1961–1990, for the A1B forcing scenario, according to the four general circulation models used in this study. CGCM31MR = Third Generation Coupled Global Climate Model, version 3.1, medium resolution; CSIROMK35 = Commonwealth Scientific and Industrial Research Organisation Climate System Model, Mark 3.5; MIROC32MR = Model for Interdisciplinary Research on Climate, version 3.2, medium resolution; NCARCCSM3 = Community Climate System Model, version 3.0.

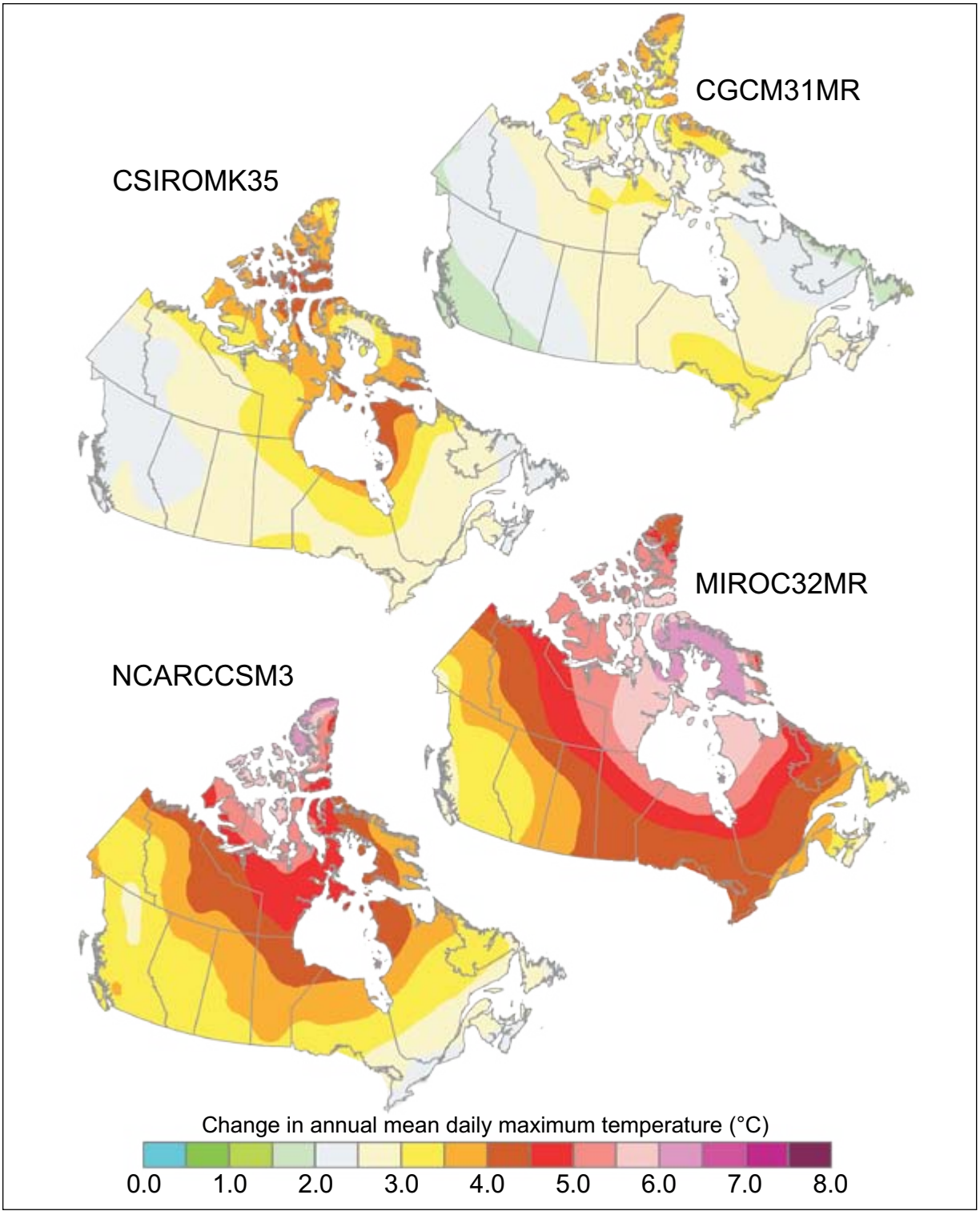

Figure 5. Projected changes in annual mean daily maximum temperature for the period 2041–2070, relative to 1961–1990, for the A1B forcing scenario, according to the four general circulation models used in this study. Model abbreviations are as in Figure 4.

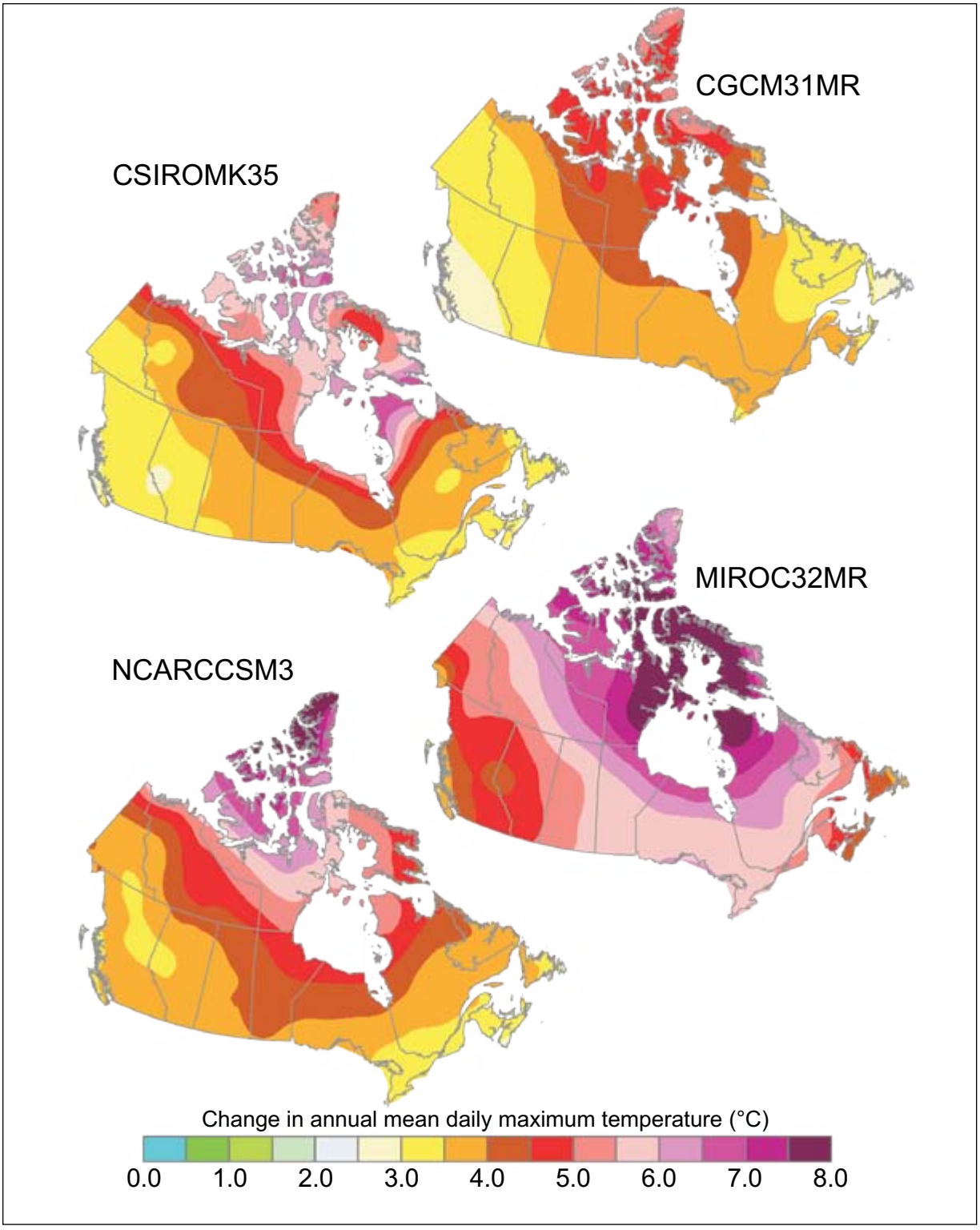

Figure 6. Projected changes in annual mean daily maximum temperature for the period 2071–2100, relative to 1961–1990, for the A1B forcing scenario, according to the four general circulation models used in this study. Model abbreviations are as in Figure 4.

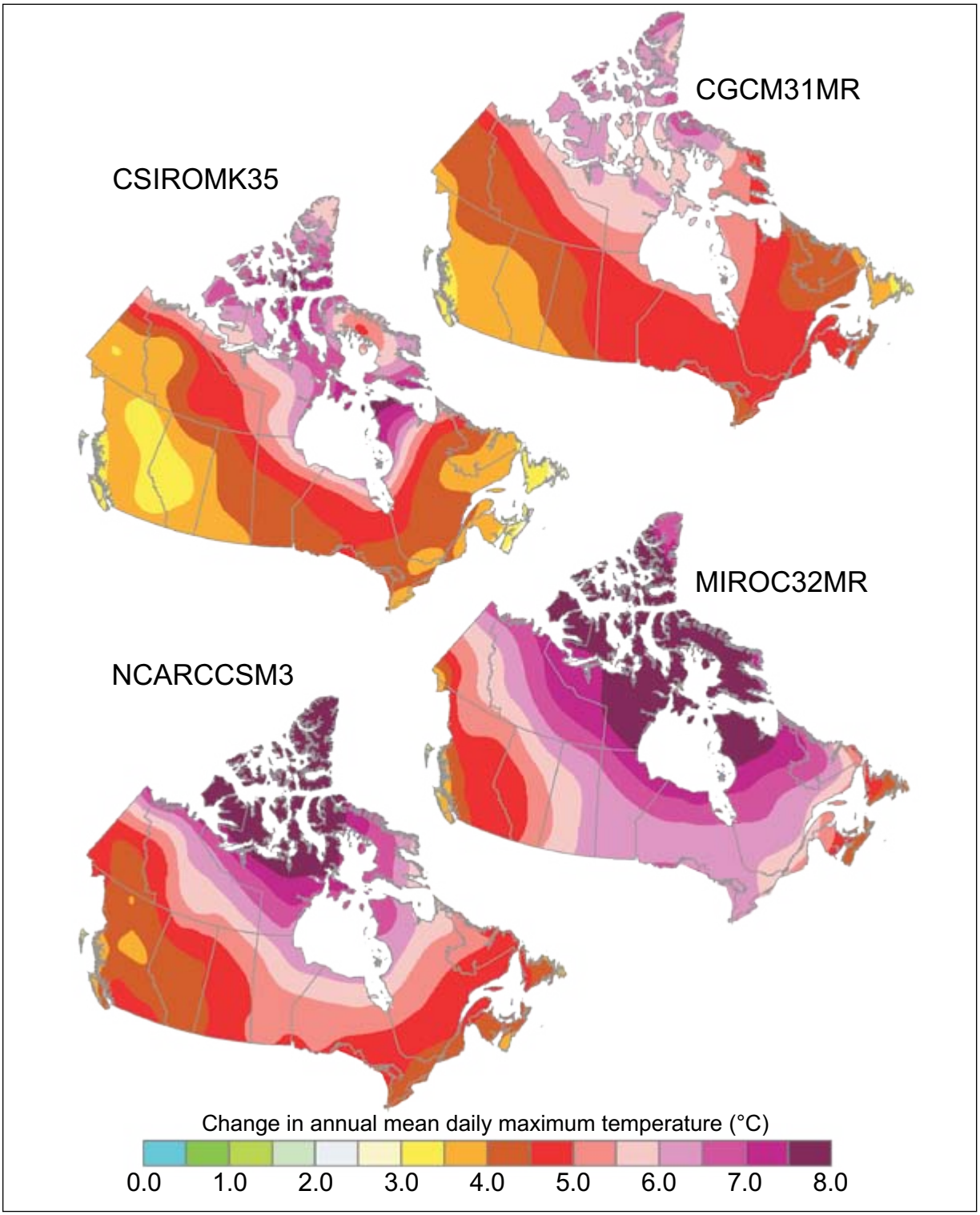

Figure 7. Projected changes in annual mean daily maximum temperature for the period 2071–2100, relative to 1961–1990, for the A2 forcing scenario, according to the four general circulation models used in this study. Model abbreviations are as in Figure 4.

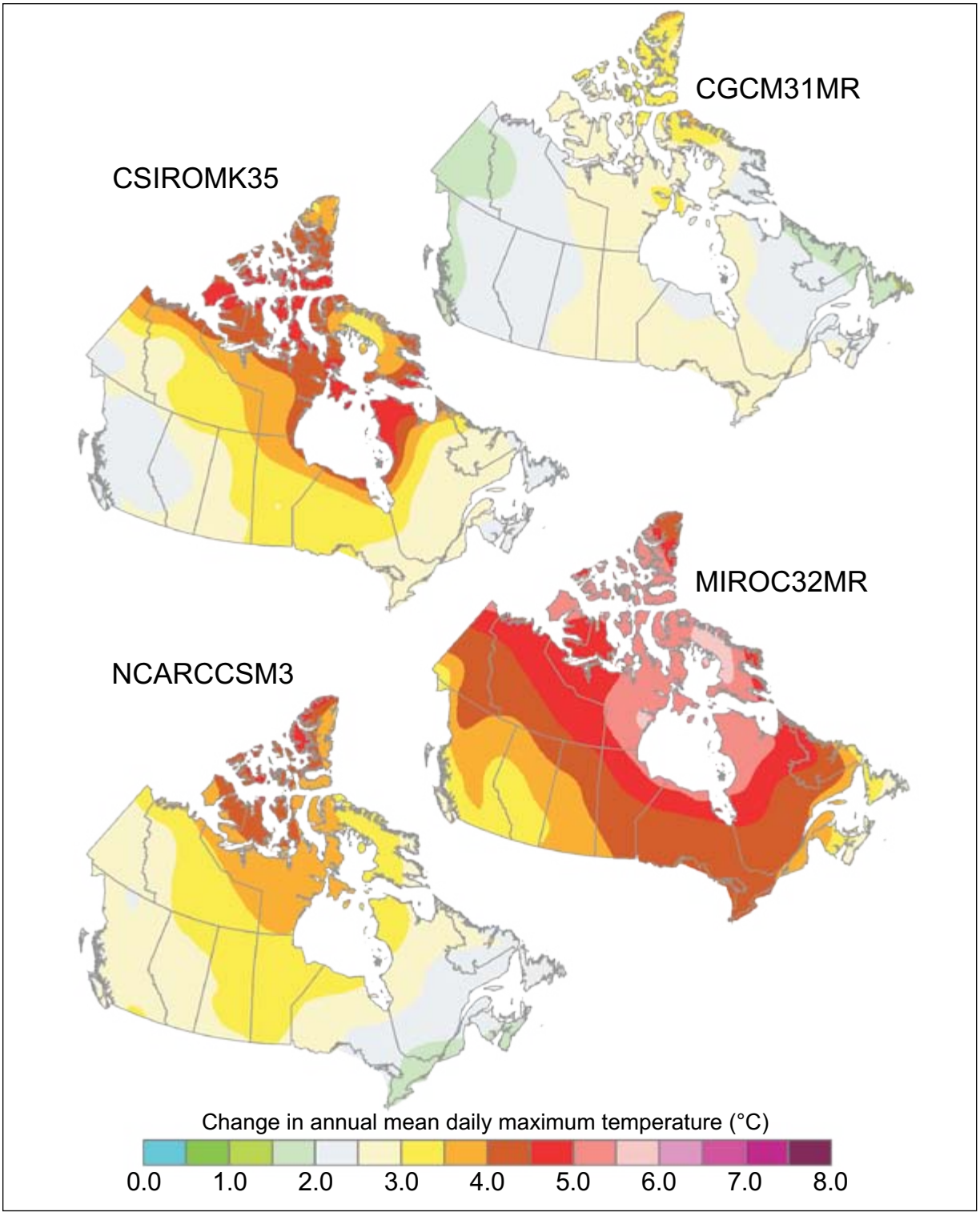

Figure 8. Projected changes in annual mean daily maximum temperature for the period 2071–2100, relative to 1961–1990, for the B1 forcing scenario, according to the four general circulation models used in this study. Model abbreviations are as in Figure 4.

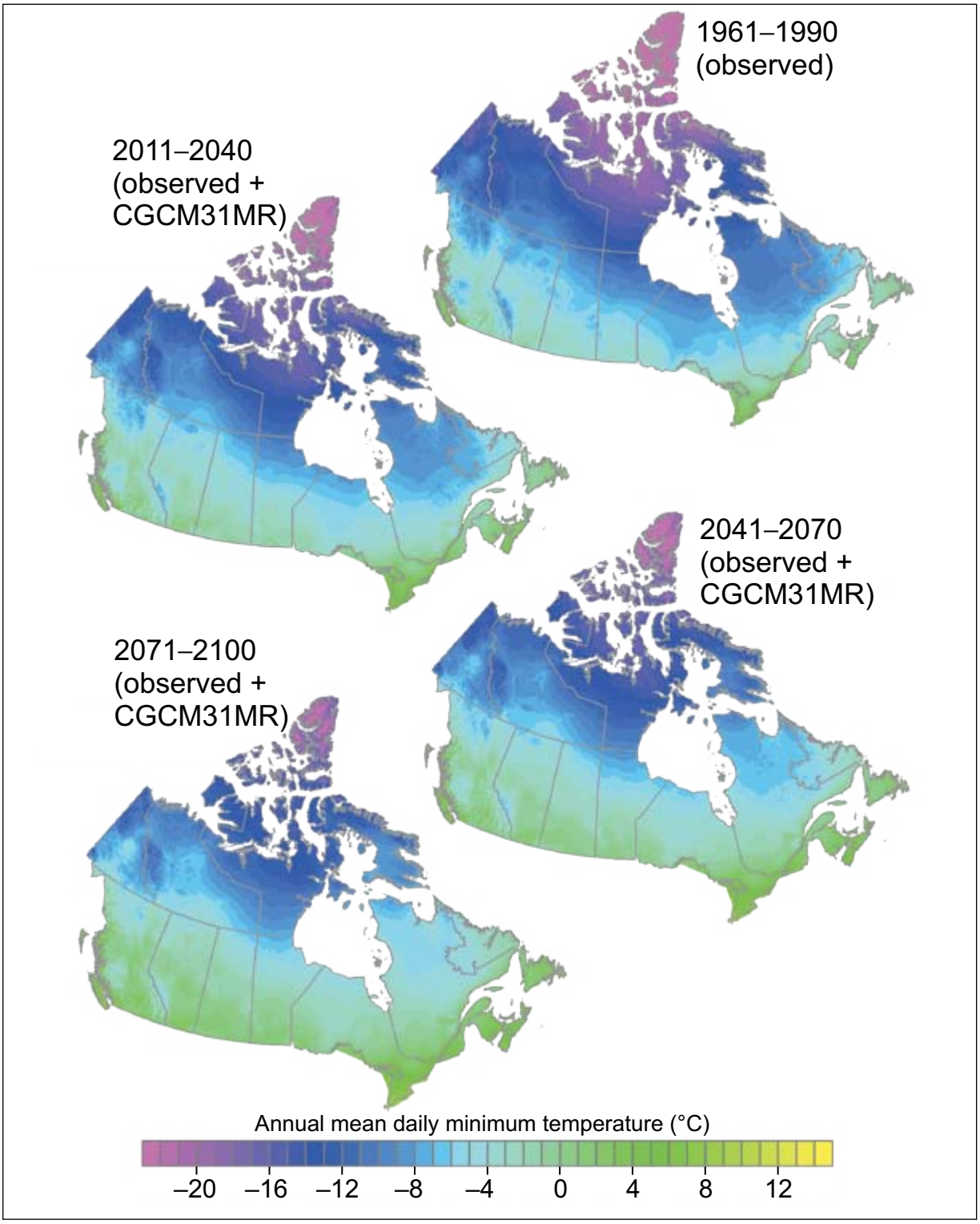

Figure 9. Maps of annual mean daily minimum temperature derived from climate station records for the period 1961–1990 and projections according to the Third Generation Coupled Global Climate Model, version 3.1, medium resolution (CGCM31MR) forced by the A1B emissions scenario, for 2011–2040, 2041–2070, and 2071–2100. The projections were derived by adding the interpolated climate normal data shown in the 1961–1990 normals map (at top) to the means of the interpolated change factors for each 30-year period.

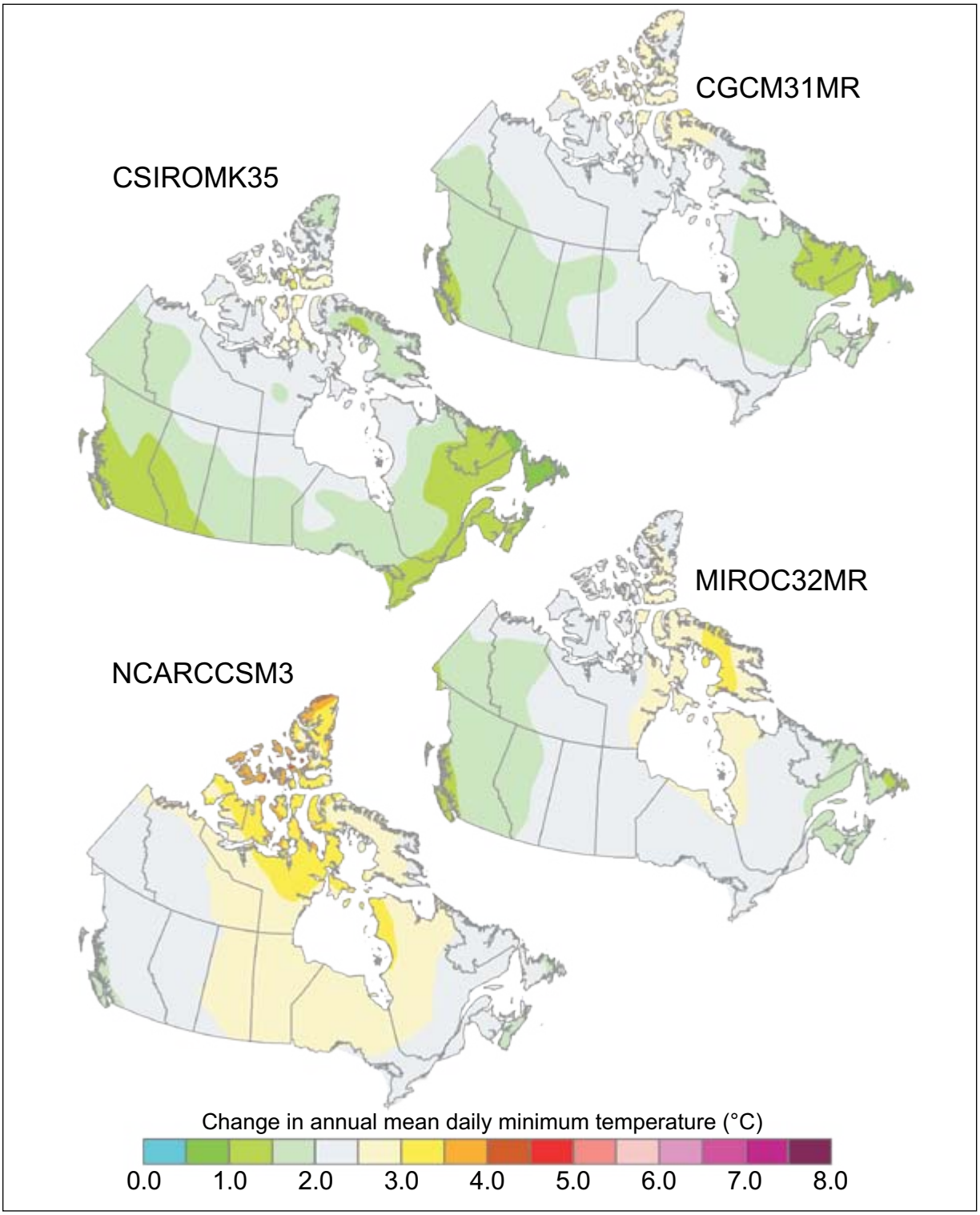

Figure 10. Projected changes in annual mean daily minimum temperature for the period 2011–2040, relative to 1961–1990, for the A1B forcing scenario, according to the four general circulation models used in this study. Model abbreviations are as in Figure 4.

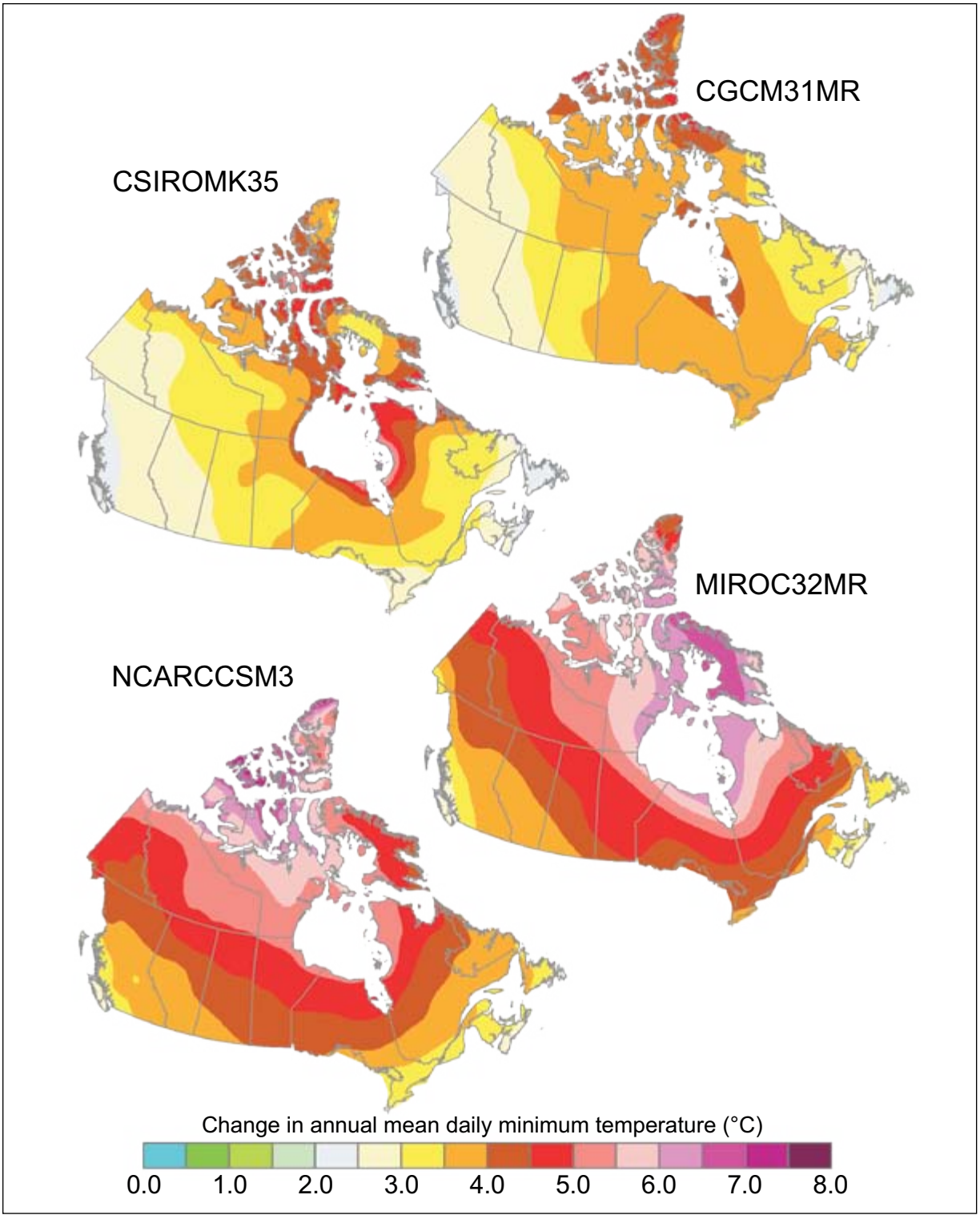

Figure 11. Projected changes in annual mean daily minimum temperature for the period 2041–2070, relative to 1961–1990, for the A1B forcing scenario, according to the four general circulation models used in this study. Model abbreviations are as in Figure 4.

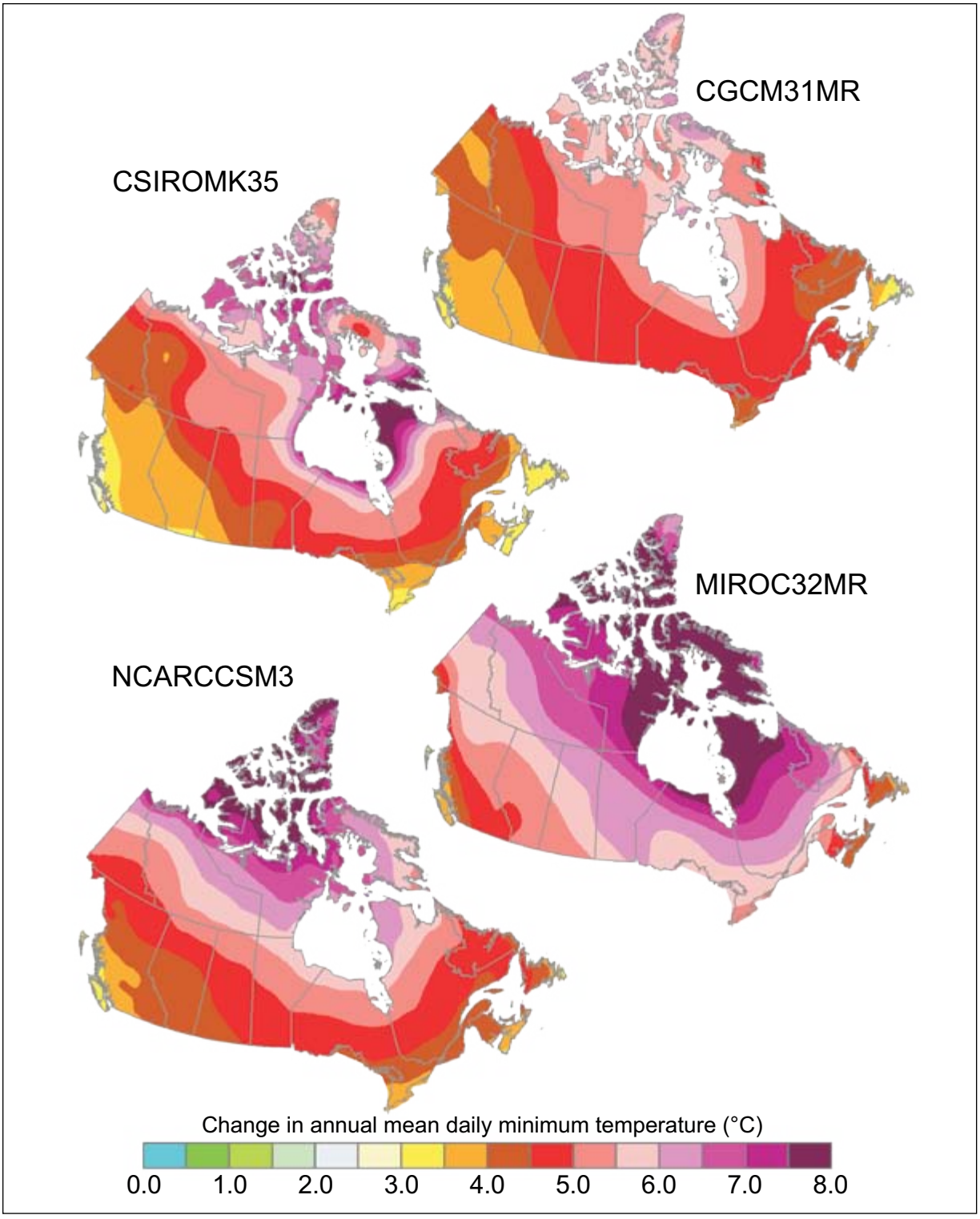

Figure 12. Projected changes in annual mean daily minimum temperature for the period 2071–2100, relative to 1961–1990, for the A1B forcing scenario, according to the four general circulation models used in this study. Model abbreviations are as in Figure 4.

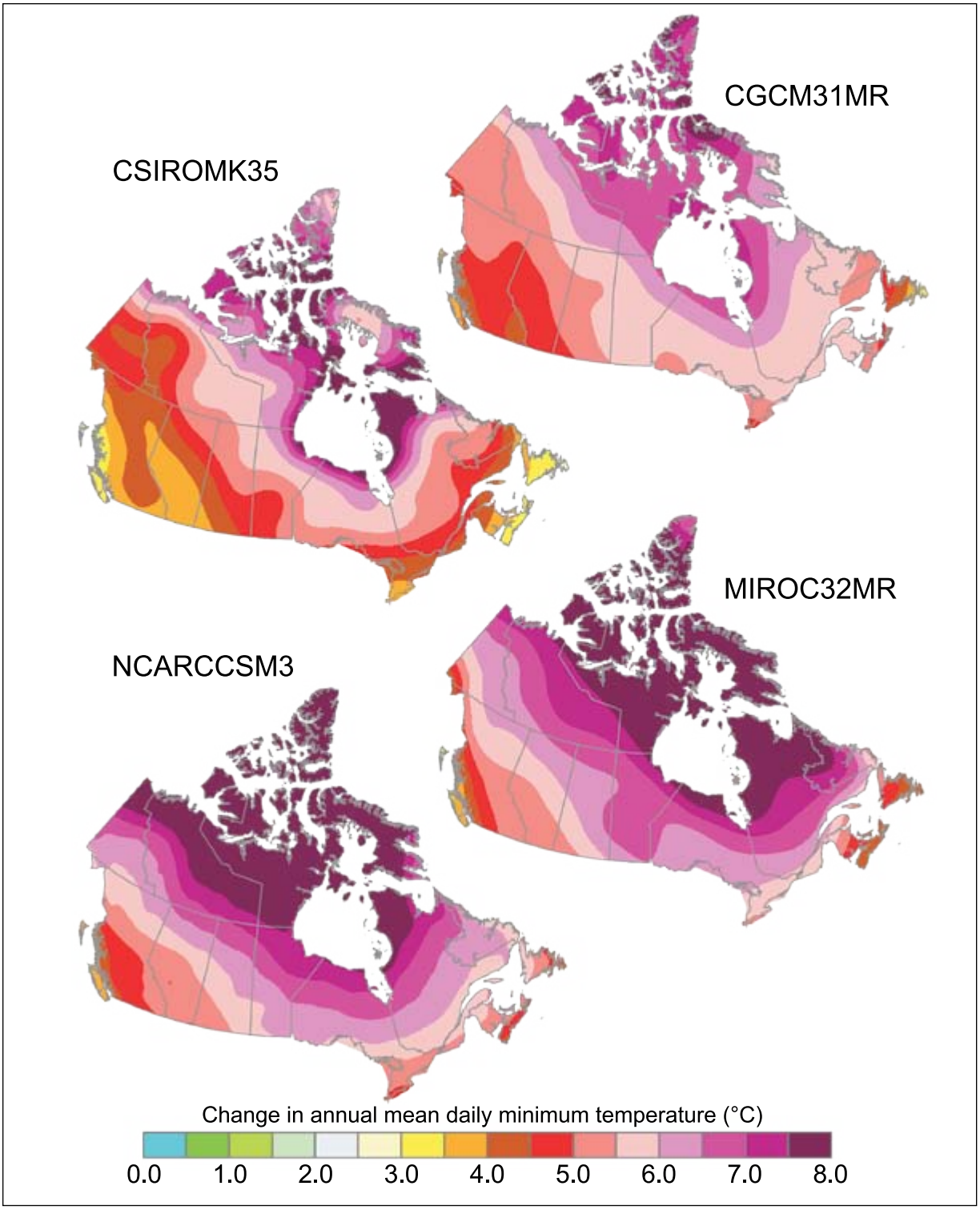

Figure 13. Projected changes in annual mean daily minimum temperature for the period 2071–2100, relative to 1961–1990, for the A2 forcing scenario, according to the four general circulation models used in this study. Model abbreviations are as in Figure 4.

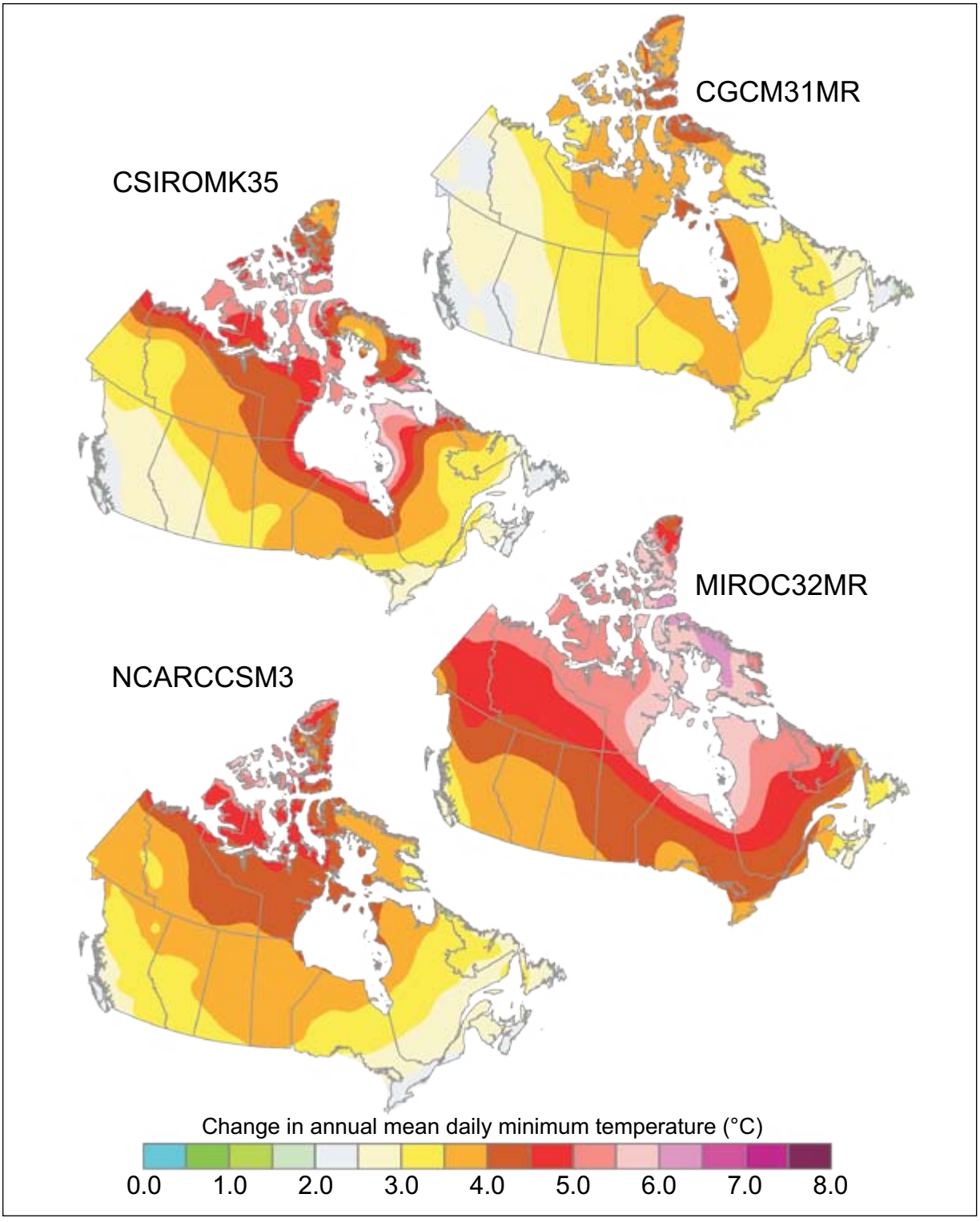

Figure 14. Projected changes in annual mean daily minimum temperature for the period 2071–2100, relative to 1961–1990, for the B1 forcing scenario, according to the four general circulation models used in this study. Model abbreviations are as in Figure 4.

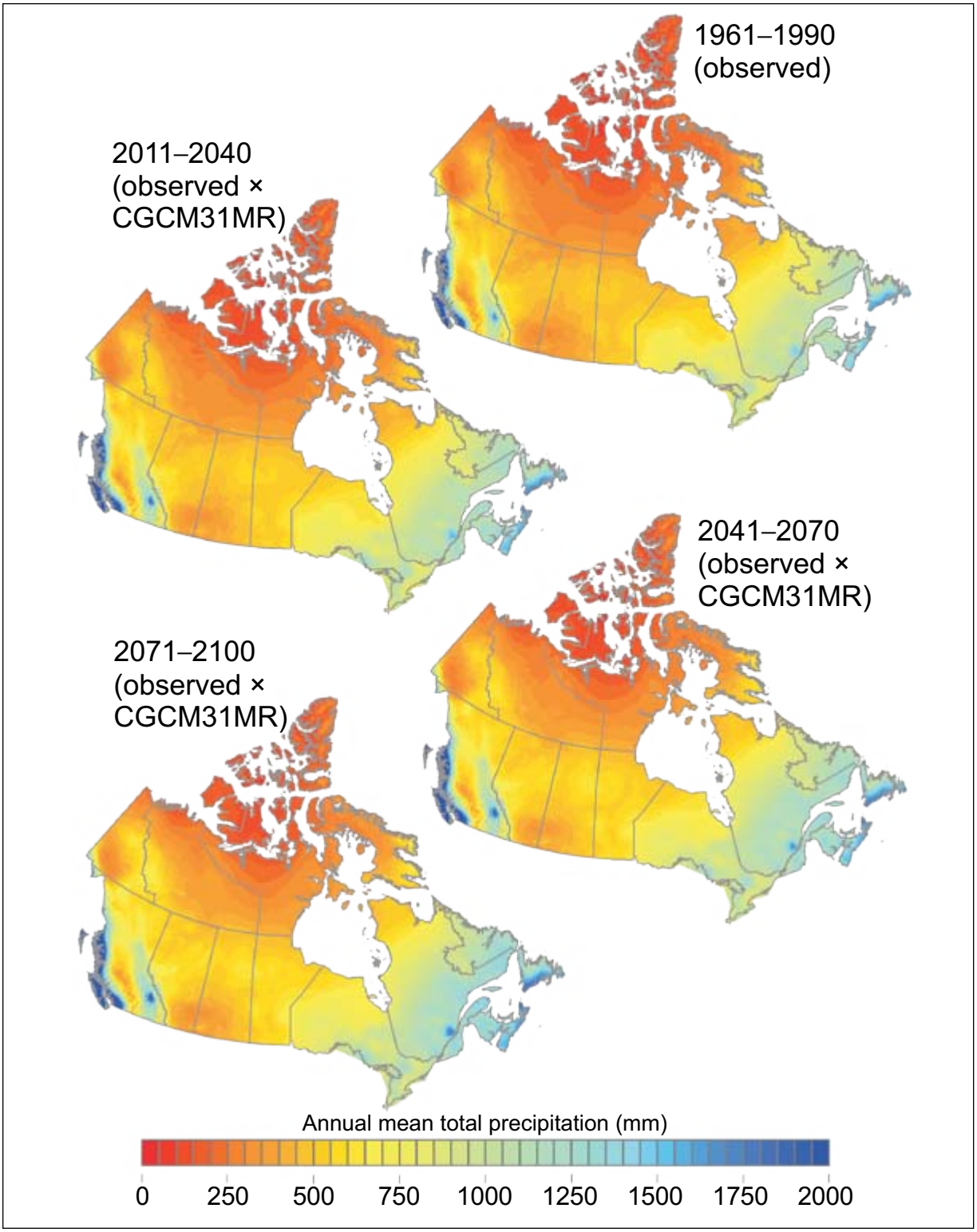

Figure 15. Maps of annual total precipitation derived from climate station records for the period 1961–1990 and projections according to the Third Generation Coupled Global Climate Model, version 3.1, medium resolution (CGCM31MR), forced by the A1B emissions scenario, for 2011–2040, 2041–2070, and 2071–2100. The projections were derived by multiplying the interpolated climate normal data shown in the 1961–1990 normals map (at top) by the means of the interpolated change factors for each 30-year period.

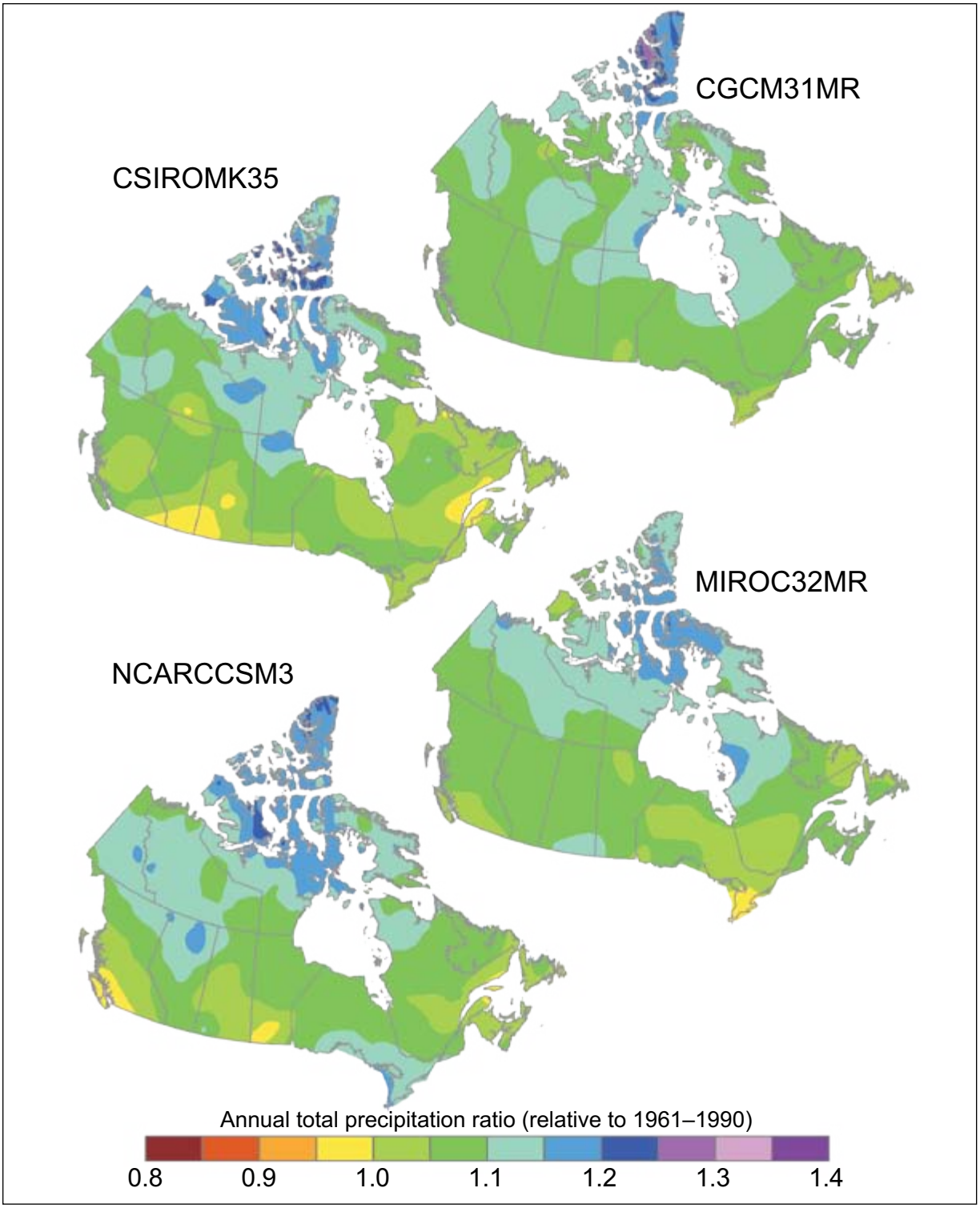

Figure 16. Projected changes in annual total precipitation for the period 2011–2040, expressed as ratios relative to the means for 1961–1990, for the A1B forcing scenario, according to the four general circulation models used in this study. Model abbreviations are as in Figure 4.

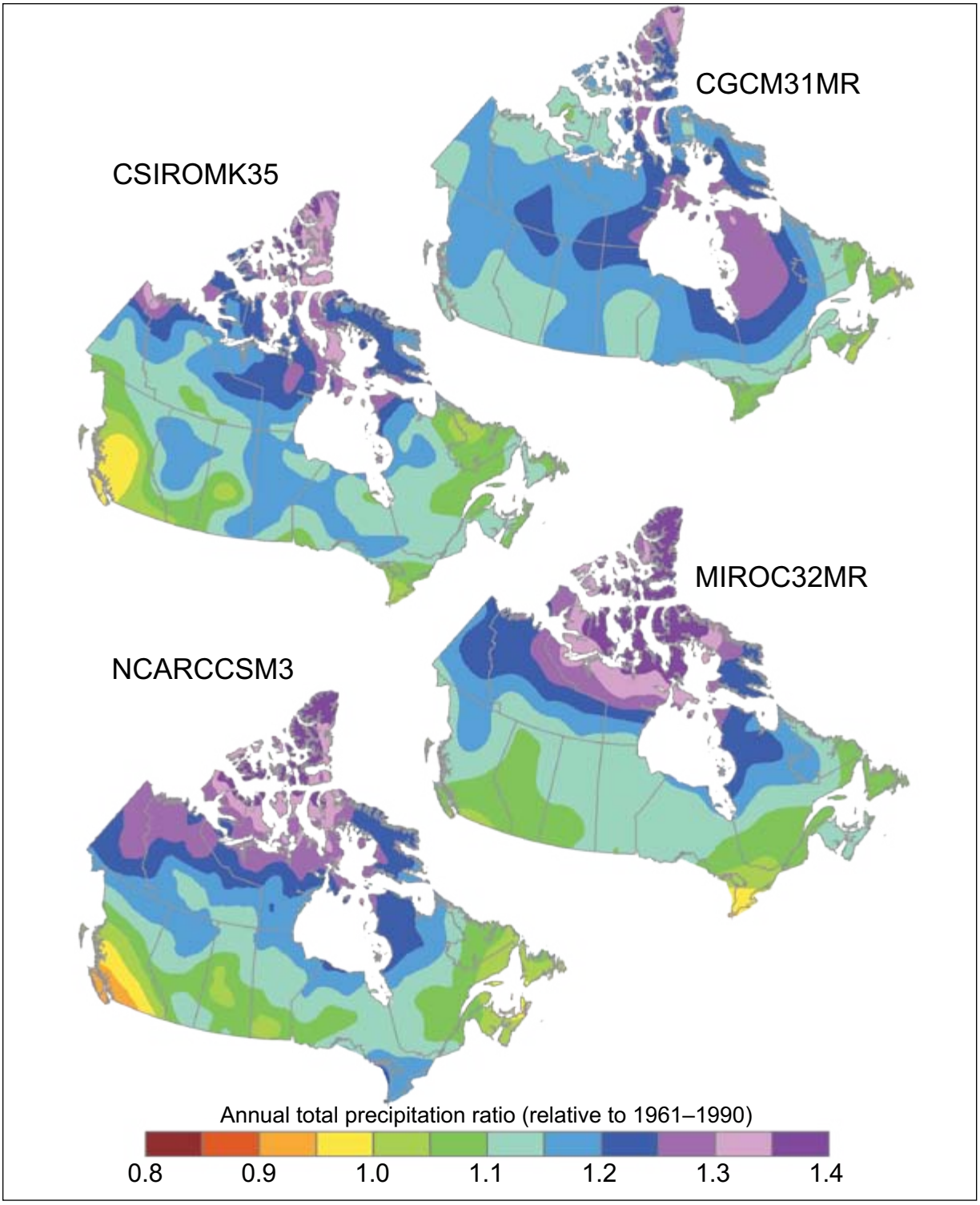

Figure 17. Projected changes in annual total precipitation for the period 2041–2070, expressed as ratios relative to the means for 1961–1990, for the A1B forcing scenario, according to the four general circulation models used in this study. Model abbreviations are as in Figure 4.

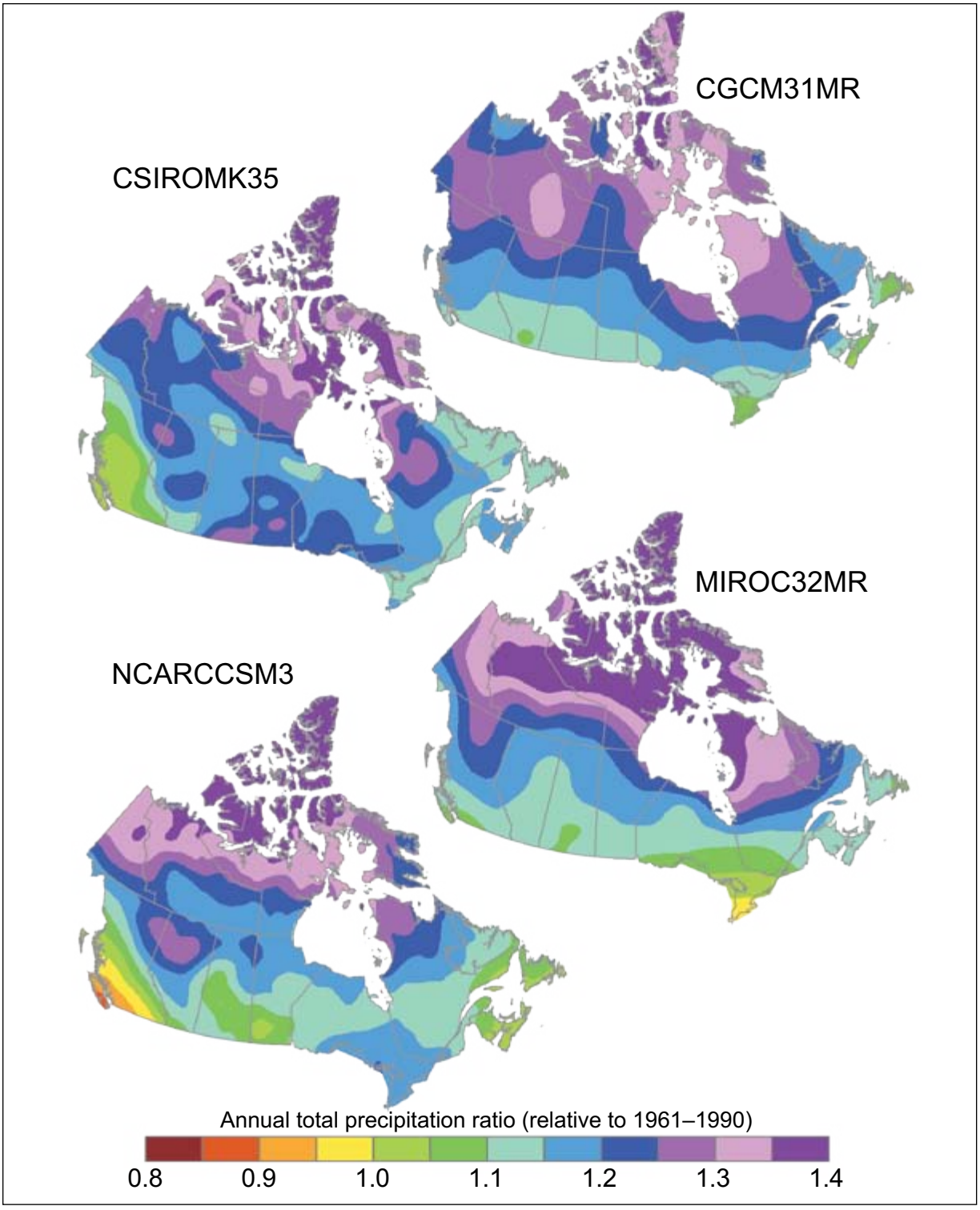

Figure 18. Projected changes in annual total precipitation for the period 2071–2100, expressed as ratios relative to the means for 1961–1990, for the A1B forcing scenario, according to the four general circulation models used in this study. Model abbreviations are as in Figure 4.

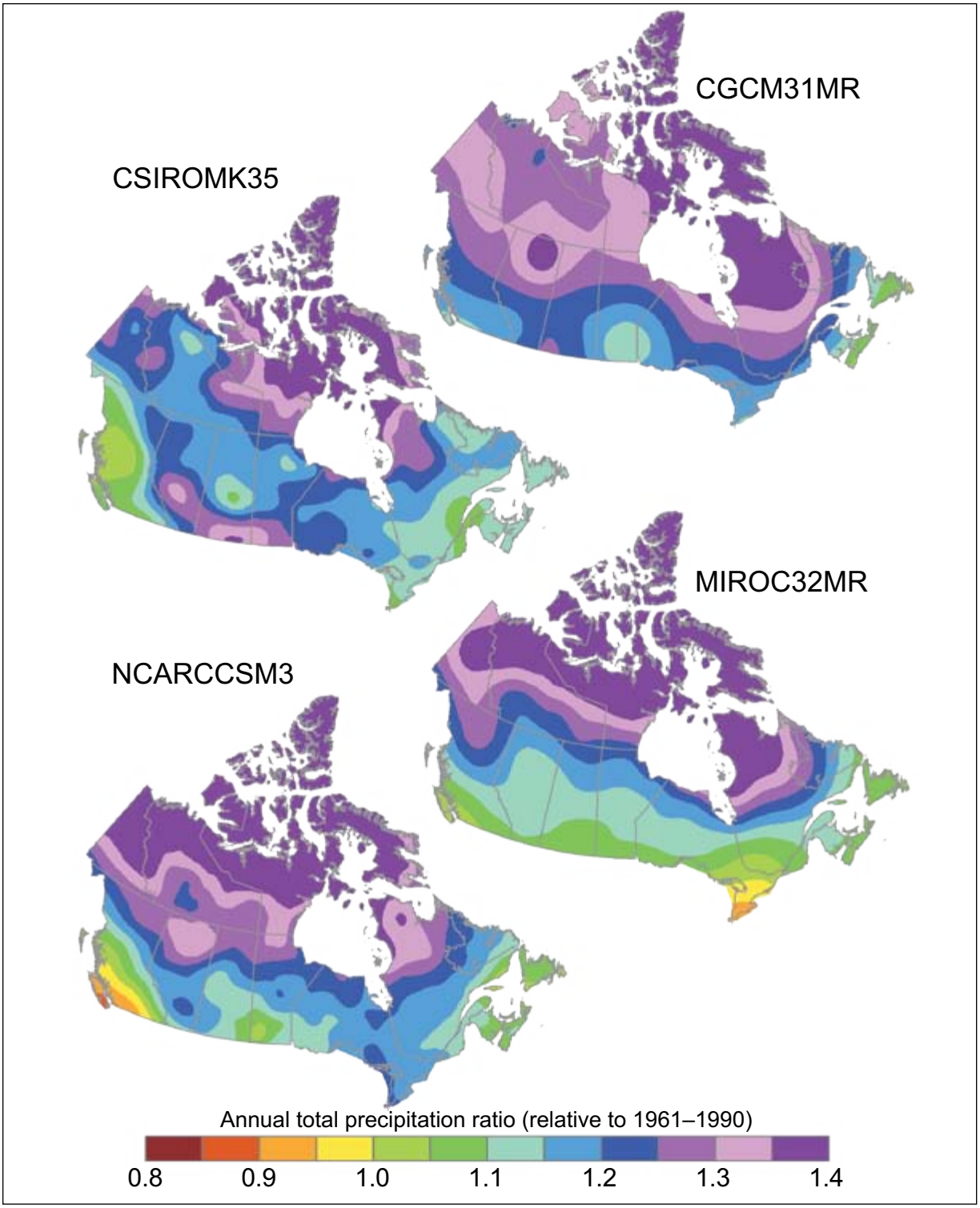

Figure 19. Projected changes in annual total precipitation for the period 2071–2100, expressed as ratios relative to the means for 1961–1990, for the A2 forcing scenario, according to the four general circulation models used in this study. Model abbreviations are as in Figure 4.

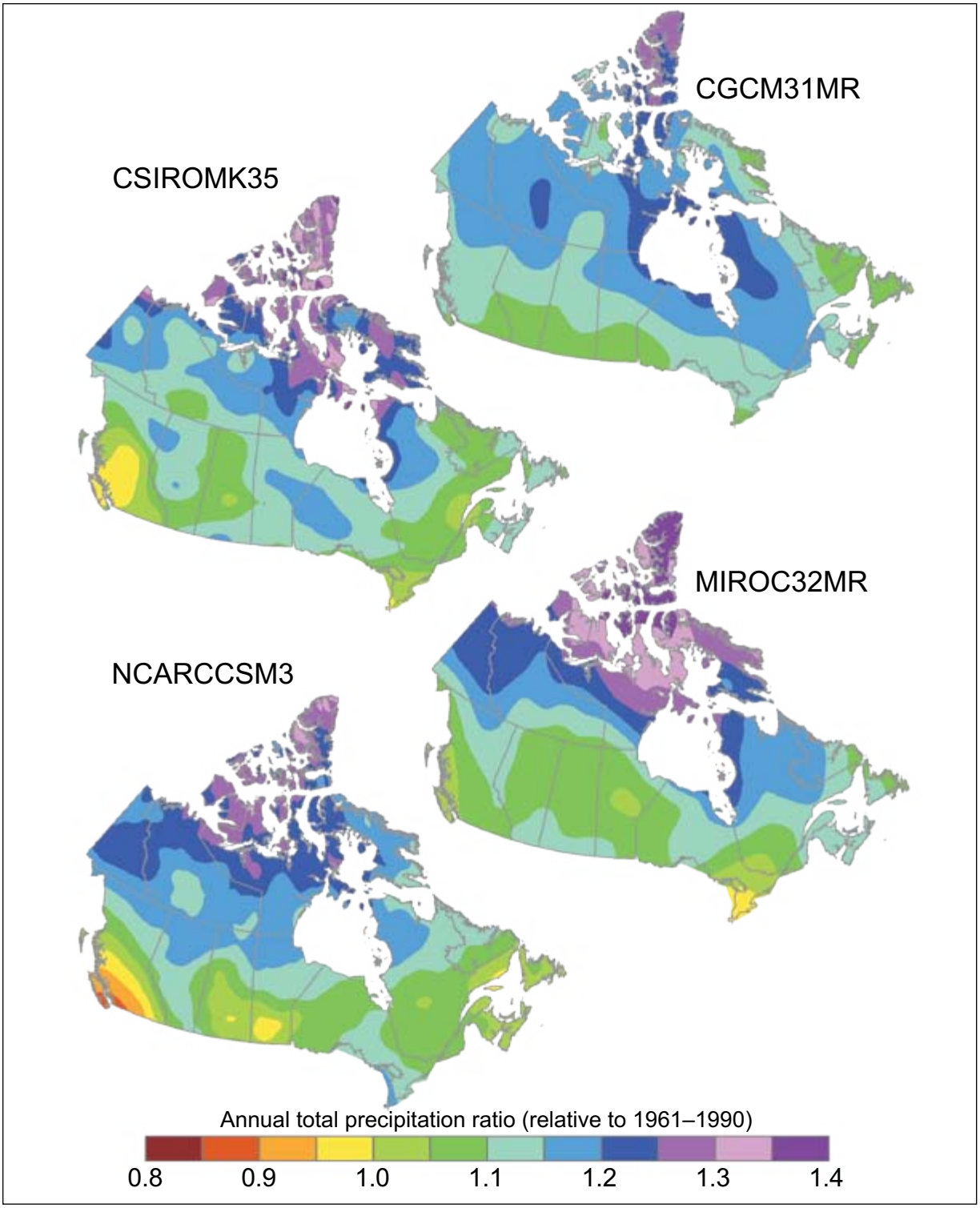

Figure 20. Projected changes in annual total precipitation for the period 2071–2100, expressed as ratios relative to the means for 1961–1990, for the B1 forcing scenario, according to the four general circulation models used in this study. Model abbreviations are as in Figure 4.

The maps presented in Figs. 3–20 serve as a guide to the spatial differences that were found in the different GCM projections of changes in temperature and precipitation. Similar maps could be generated for individual months or averaged over different periods, such as decades. It would also be possible to generate similar maps for the remaining climate variables, assuming maps of 1961–1990 normals are available.

Following this exploration of spatial differences in the projected trends, a more detailed analysis of temporal changes in area-weighted means of seasonal and annual values was performed, with computations for each of the 18 ecozones shown in Fig. 2. This analysis included a systematic production of time-series data for seasonal and annual means of each monthly variable in every ecozone for all four GCMs and all three scenarios of future GHG emissions, plus the 20th century simulations and historical temperature and precipitation measurements—a total of 8910 separate time series. Clearly, it would have been impractical to present all of these results, and therefore only a few examples will be provided here. The seasons were defined as 3-month periods: spring (March to May), summer (June to August), fall (September to November), and winter (December to February). By this definition, the winter of the final year (2100 [2099 for NCARCCSM3]) would contain only one month, and it was therefore omitted from calculations of 30-year means.

The time-series data also were imported into a series of Microsoft Excel spreadsheets and used to generate summary tables providing key information about projected changes during the 21st century (Tables 4–22), for each of the 18 ecozones shown in Fig. 2. Results for the four GCMs were averaged, on the assumption that they provide equally likely estimates of future changes. The complete spreadsheet files are available upon request to the authors.

The following discussion attempts to sample all of the available data by comparing some results obtained with each model and each GHG scenario, for each climate variable and season and for several ecozones (generally those with tree cover). First, a suite of scatter plots (Figs. 21–23) are presented to demonstrate how the four GCMs, forced by each of the three SRES scenarios, differ in their projections of climatic change for each ecozone. These plots also should be useful when selecting specific GCM scenarios to represent the range of projected changes in climate (temperature and precipitation) for a particular region of Canada. Then, a selection of graphs representing the various ecozones and seasons (Figs. 24–43) are used to highlight some specific strengths and weaknesses, where differences among the results may indicate problems with particular variables or GCMs (or both). This graphical analysis is followed by a section entitled "Interpreting the Downscaled Climate Scenarios for Individual Eczones." (for the 21st century), which is based on interpretation of the graphs and summary tables.

Comparison of Projections of Changes in Temperature and Precipitation

The scatter plots (Figs. 21–23) show mean changes in annual mean daily minimum temperature and precipitation ratio for 20-year periods centered on 2050 and 2090 (i.e., about 40 and 80 years from the present day), referenced to the 1961–1990 baseline. These plots show some expected trends and a few surprising differences from expectations. In general, the projected warming was greater for the 2090s than for the 2050s, but with greater divergence among the GCMs. More specifically, the A2 scenario almost invariably created greater warming than the A1B scenario, which in turn produced greater warming than the B1 scenario. Consistent with expectations, the models all projected the greatest warming, and generally greatest precipitation increases, for high latitudes (particularly the Arctic ecozones; Figs. 21a–21c), the least warming, and generally the smallest increases or even decreases in precipitation, for the Pacific and Atlantic Maritime ecozones (Figs. 23a and 23c), and intermediate warming and precipitation increases elsewhere.

The NCARCCSM3 model appeared most sensitive to GHG concentration, such that when forced by the A2 emissions scenario it generally projected the greatest warming. The MIROC32MR model projected similar (but generally slightly less) warming with forcing by the A2 scenario, but its sensitivity to the difference between the A2 and A1B scenarios was much smaller. Consistent with interpretations from Figs. 3–20, therefore, the general trend was for the MIROC32MR model to generate greater warming

than the other three models when forced by the A1B scenario, but to generate marginally greater warming when forced by the A2 scenario—hence making it more comparable to NCARCCSM3. The differences between the CGCM31MR and CSIROMK35 models, which generally projected less warming, were more difficult to discriminate, as these models overlapped closely in most regions. Contrary to the interpretation of the national maps in Figs. 3–14, the CSIROMK35 model often projected less warming by 2050 than the CGCM31MR model. In British Columbia, differences among the four GCMs were smaller, with the NCARCCSM3, CGCM31MR, and MIROC32MR models projecting comparable warming and the CSIROMK35 model rather less (Figs. 23a and 23b). The four models were relatively consistent in the Prairie ecozones (though showing greater divergence in the projections of precipitation; Figs. 23d and 23e) and in the Mixedwood Plains (Fig. 23f), although the CSIROMK35 model invariably projected less warming than the other three models.

There was less agreement among the models for projected changes in precipitation, and the trends varied among regions much more than was the case for temperature. However, the correlation of precipitation increase to temperature increase was clearly strongest in the Arctic ecozones (Figs. 21a–21c), and became progressively poorer with decreasing latitude. The MIROC32MR model projected the greatest increases in precipitation for the Arctic (with forcing by the A2 scenario; Figs. 21a–21c), but it was also the only GCM to project a decrease in precipitation averaged over an entire ecozone (for the Mixedwood Plains; Fig. 23f). The regional drying trends noted in Figs. 18–20, notably in southern British Columbia and southern Saskatchewan and Manitoba, represented only small portions of individual ecozones (and may have crossed ecozonal boundaries), so they did not manifest in the area-weighted ecozonal means.

Among the four GCMs, the CGCM31MR generally projected greater increases in precipitation for similar temperature changes and can be considered the "wettest model." This pattern was particularly evident in the Taiga region (Figs. 21e, 21f, and 22a). Further south, the CSIROMK35 model projected comparable or even greater increases in precipitation for the Boreal Shield and Boreal Plains (Figs. 22b, 22c, and 22e) and for the Prairies (where there was perhaps the greatest inconsistency among the four models; Figs. 23d and 23e).

The west coast regions also had relatively inconsistent results for precipitation change, among models and even among GHG forcing scenarios. This inconsistency was particularly pronounced for the Pacific Maritime ecozone, with the NCARCCSM3 model projecting very little change on average and the CGCM31MR model projecting increases of 25% (Fig. 23a).

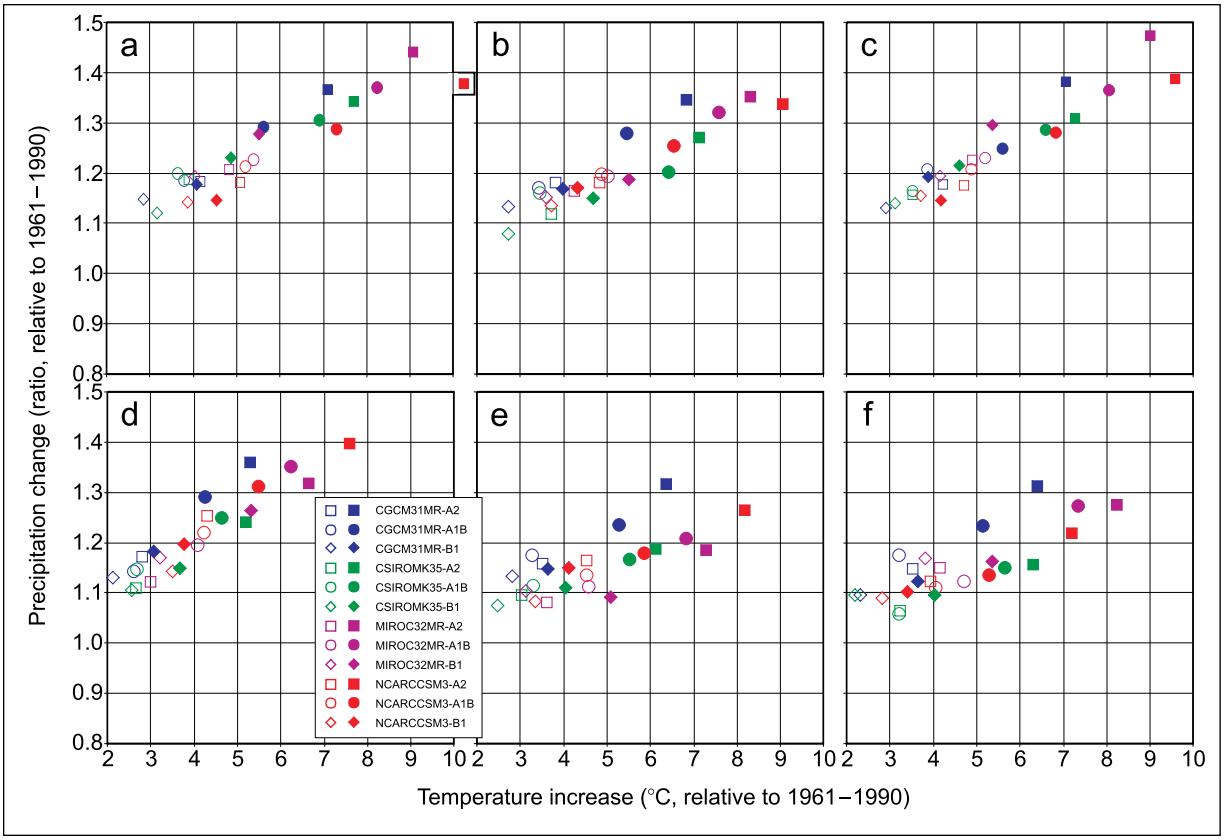

Figure 21. Scatter plots showing the changes in annual mean daily minimum temperature (*x* axis) and annual precipitation ratio (*y* axis) projected by each general circulation model, as forced by each greenhouse gas emissions scenario (A1B, B1, A2), relative to means for 1961–1990. Open symbols represent mean changes for 2040–2059, and closed symbols represent mean changes for 2080–2099. Each scatter plot shows area-weighted means for a specific Canadian terrestrial ecozone according to the subdivisions of Kurz et al. (2009): (a) Northern Arctic, (b) Southern Arctic, (c) Arctic Cordillera, (d) Taiga Cordillera, (e) Taiga Shield West, (f) Taiga Shield East. Note that the *x* axis range is shifted 2°C higher relative to Figs. 22 and 23. Model abbreviations are as in Figure 4.

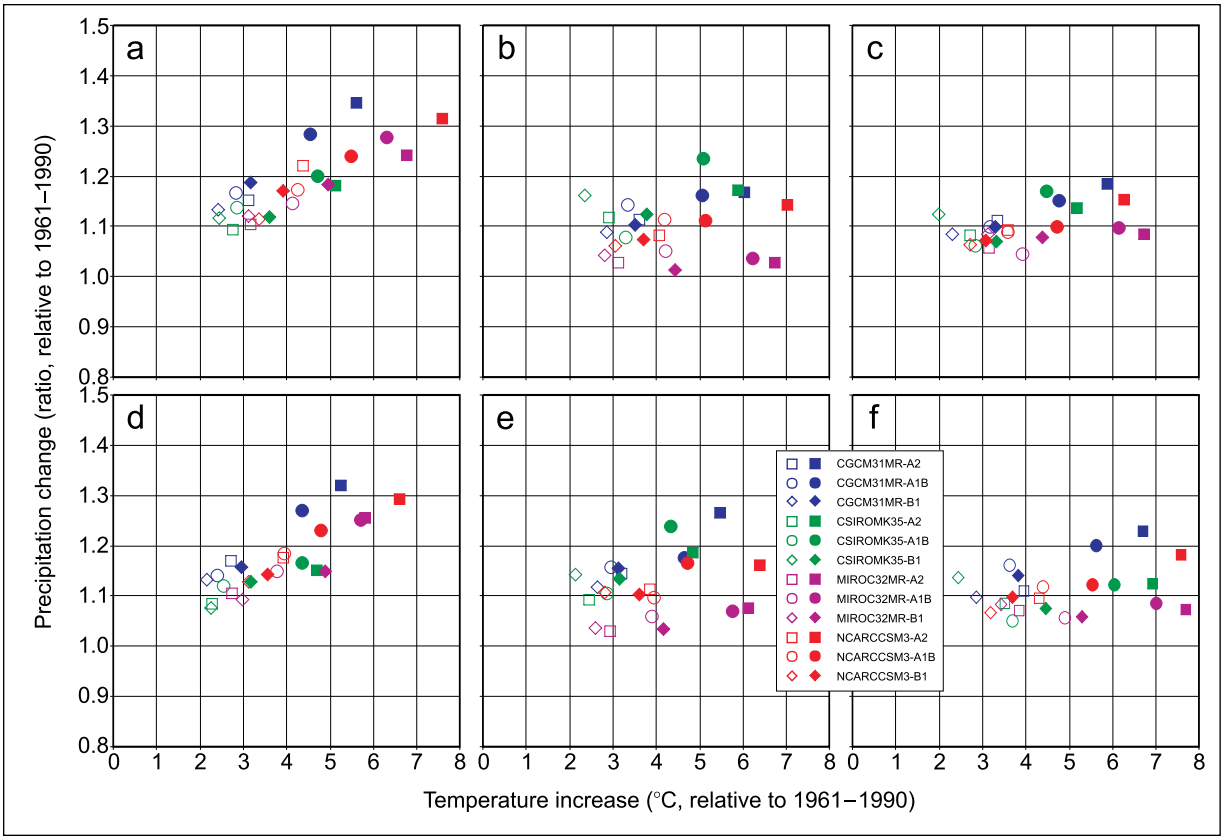

Figure 22. Scatter plots showing the changes in annual mean daily minimum temperature (*x* axis) and annual precipitation ratio (*y* axis) projected by each general circulation model, as forced by each greenhouse gas emissions scenario, relative to means for 1961–1990. Open symbols represent mean changes for 2040–2059, and closed symbols represent mean changes for 2080–2099. Each scatter plot shows area-weighted means for a specific Canadian terrestrial ecozone according to the subdivisions of Kurz et al. (2009): (a) Taiga Plains, (b) Boreal Shield West, (c) Boreal Shield East, (d) Boreal Cordillera, (e) Boreal Plains, (f) Hudson Plains. Note that the *x* axis range is shifted 2°C lower relative to Fig. 21. Model abbreviations are as in Figure 4.

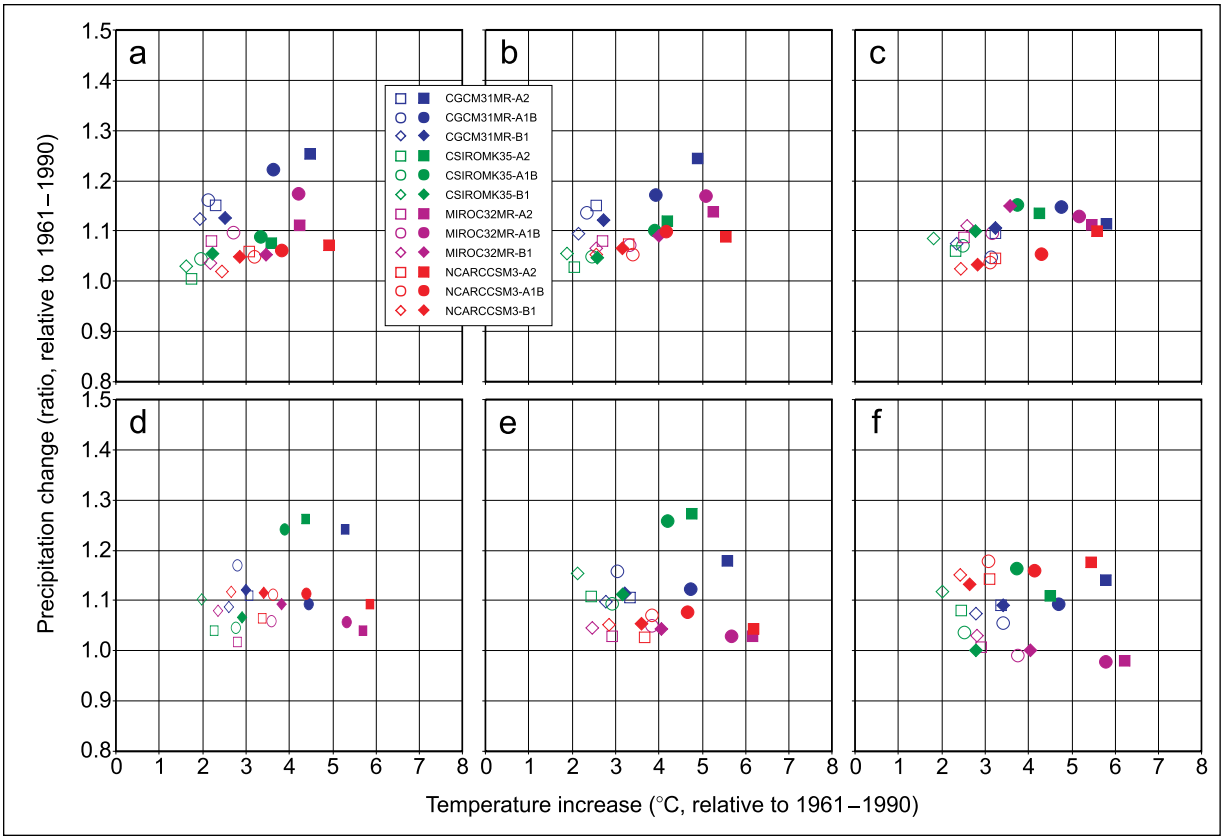

Figure 23. Scatter plots showing changes in annual mean daily minimum temperature (*x* axis) and annual precipitation ratio (*y* axis) projected by each general circulation model, as forced by each greenhouse gas emissions scenario, relative to means for 1961–1990. Open symbols represent mean changes for 2040–2059, and closed symbols represent mean changes for 2080–2099. Each scatter plot shows area-weighted means for a specific Canadian terrestrial ecozone according to the subdivisions of Kurz et al. (2009): (a) Pacific Maritime, (b) Montane Cordillera, (c) Atlantic Maritime, (d) Prairies Semiarid, (e) Prairies Subhumid, and (f) Mixedwood Plains. Note that the *x* axis range is shifted 2°C lower relative to Fig. 21. Model abbreviations are as in Figure 4.

Comparison of Simulated Interannual Variability

The leftmost panels of Figs. 24–27 (together with those of Figs. 32, 35, 38, and 41 and part "a" of Figs. 33, 36, 39, and 42) show how the four GCMs were able to capture observed interannual variability in seasonal and annual temperature and precipitation. In each figure, observed data for 1961–2008 (black line) are superimposed on the results of the GCM simulations, comprising the 20C3M scenario for the period 1961–2000 (1961–1999 for NCARCCSM3) and the three SRES GHG emissions scenarios for 2001–2008 (2000–2008 for NCARCCSM3). Although clearly there were some important differences during this 1961–2008 comparison period, the amplitudes of variation around the simulated means were generally comparable to those of the interpolated observed data, and the differences among seasons were captured well. This was also true of the differences in patterns of variability between daily minimum and maximum temperature in the summer (Fig. 24), fall (Fig. 38), and winter (Figs. 25 and 41). However, some GCMs tended to exaggerate the observed variability in the Southern Arctic, particularly in winter, notably the CGCM31MR and, to some extent, NCARCCSM3 and CSIROMK35 models (Fig. 25b). Elsewhere, the agreement between modeled and observed data was generally good, but agreement for minimum temperature was generally better than for maximum temperature. The CGCM31MR and NCARCCSM3 models both tended to exaggerate the observed variability, notably in the Prairies Subhumid ecozone (Fig. 32a) and during summer in the Atlantic Maritime (Fig. 35a). Interestingly, in the Boreal Plains during winter, the observed variability in both minimum and maximum temperature was quite dramatic, and all of the models appeared to capture this remarkably well (Fig. 41).

The quality of agreement in amplitude of variation was poorer for precipitation, both between the simulated historical and observed interpolated data and among the different GCMs. Both the NCARCCSM3 and CSIROMK35 models typically exaggerated the observed variability, whereas the CCGCM31MR and MIROC32MR models either captured variability fairly well or tended to underestimate it (Figs. 26, 27a, 33a, 36a, 39a, and 42a).

Overall, the results suggested considerable consensus among the models, particularly with regard to simulation of interannual variability of observed temperature means, but even to some extent with regard to the observed precipitation data. Hence, the GCMs appeared to capture many of the observed characteristics of these climate variables, which in turn suggests that the future scenarios can be treated as plausible projections of future climate as determined by different scenarios of future GHG emissions. The following section attempts to make some broad interpretations of the general trends for the Canadian ecozones shown in Fig. 2.

Projected Climate Trends 2000–2100

There is little doubt that the Arctic region will experience the greatest increases in temperature within Canada over the next 90 years (Figs. 21a–21c; see also Tables 5, 6, 7). Summer temperatures (both mean daily minima and mean daily maxima) in the Southern Arctic ecozone were projected to increase by 3°C to 6°C by 2100 (depending on the GHG emissions scenario and not accounting for the MIROC32MR model, which suggested much greater increases than the other three GCMs) (Fig. 24). The four models were more consistent in their projected increases for winter, which ranged from 5°C to 10°C for daily maximum temperature (Fig. 25a) to as much as 13°C for daily minimum temperature (Fig. 25b). The mean projected increases in winter for all three Arctic ecozones (based on 30-year averaging periods) were about 4.5°C to 9.5°C for maximum temperature and 5.0°C to 10.5°C for minimum temperature by 2100 (for more detail, see Tables 5, 6, and 7).

In all seasons, the agreement among the four GCMs for temperature projections was generally stronger in southern Canada than in the Arctic. As previously noted, the MIROC32MR model typically projected the largest increases in the south (except for the NCARCCSM3 model when forced by the A2 scenario) (e.g., Figs. 32 and 35). The smallest projected temperature increases were from 2.0°C to 4.0°C for daily maximum temperature and from 2.0°C to 5.0°C for daily minimum temperature during summer on the Pacific and Atlantic Maritime coasts (see Fig. 35, Tables 13 and 20). Temperatures were projected to increase similarly in the Mixedwood Plains ecozone (Fig. 38), a region already exposed to the warmest

summers in Canada, so the projections imply midsummer daytime highs regularly exceeding 40.0°C are likely (see Table 14). The midcontinental regions were projected to undergo greater warming, specifically 2°C to 5°C in the Prairies for annual T_{max} and T_{min} (see Fig. 32; see also Figs. 23d and 23e), and 2°C to 6°C for annual T_{min} in the southern boreal forest (Figs. 22d and 22e). Winter temperatures were projected to increase by 4°C to 6°C (T_{max}) and 5°C to 7°C (T_{min}) during winter in the Boreal Plains (Figs. 41–43). Even larger increases in mean annual temperatures were projected for the northern boreal and southern taiga ecozones, with daily minimum temperature projected to increase by 2°C to 6°C (Figs. 22b and 22c) and by 2.5° to 7.0°C further north in the Taiga Shield ecozone (Figs. 21e and 21f).

The four GCMs showed virtually 100% agreement in projecting increasing precipitation across Canada during the 21st century. In fact, for all 18 ecozones, the only exceptions to this general observation were the MIROC32MR projections for the most southerly Mixedwood Plains ecozone (Fig. 23f), as previously noted. (The MIROC32MR model also projected significant decreases in precipitation and generally much drier conditions than the other three GCMs for much of the central and southern United States—see Joyce et al. 2011) However, the projected increases varied regionally, with the largest (in proportional terms) occurring in the far north, ranging from 10% to 45% (Figs. 21a–21c) and the smallest (notably those simulated by the MIROC32MR model), in the range –3% to +15%, occurring in the south and east (Figs. 23c and 23f). In terms of precipitation amounts, the largest increases were projected for the Pacific Maritime ecozone. When results for all four GCMs were averaged, the trend indicated an increase in annual precipitation of 100 to 200 mm (about 5% to 10%) by 2071–2100, mainly in fall and winter (accompanied by increases in variability during these seasons; see Table 20). Notably, however, both the NCARCCSM3 and CSIROMK35 models projected significant decreases in the areas of Vancouver Island and the Lower Mainland of British Columbia (see Figs. 18–20). In comparison, annual precipitation for the Atlantic Maritime and Mixedwood Plains ecozones was projected to increase by about 50–100 mm (Tables 13 and 14).

Projected increases in precipitation for the Arctic ecozones ranged from about 35 to 100 mm, depending on the GHG emissions scenario (Tables 5, 6, and 7). The eastern Taiga Shield and Boreal Shield East ecozones were projected to become much wetter, with increases of 10%–20% (up to 160 mm per year for the eastern Taiga Shield). Similarly, the cordilleran ecozones in the west (which are subject to some influence from the Pacific Ocean) were projected to experience an increase in annual precipitation of 50 to 110 mm, depending on the scenario (Tables 18, 19, and 21). Elsewhere, the mean projected increases ranged from about 30 to about 70 mm, again depending on the emissions scenario.

Precipitation trends for all four seasons in the Pacific Maritime ecozone (Figs. 26 and 27) indicate generally good agreement among the four models (with all three forcing scenarios), in terms of both projected means and interannual year-round variation. As previously noted, both the NCARCCSM3 and CSIROMK35 models predicted generally greater extremes. The MIROC32MR model and, to some extent, the CGCM31MR model, projected slightly higher precipitation in spring, whereas the NCARCCSM3 model projected slightly lower amounts during winter (trends supported by the ranges of annual precipitation increases in Fig. 23a). There was an approximate doubling in the increase between the B1 and A1B forcing scenarios, but little obvious difference between the A1B and A2 scenarios.

The vapor pressure projections for the Taiga Shield East ecozone (Figs. 28 and 29) provide a good comparison of the results for this variable from different GCMs throughout the downscaled data set. All four models projected steady increases that correlated well with the general projected trends in temperature. In particular, the MIROC32MR model projected noticeably greater increases in vapor pressure than the other GCMs during spring and summer, whereas the NCARCCSM3 model projected somewhat higher values for fall and winter. These differences were entirely consistent with similar trends for the projected seasonal temperature trends in the Taiga Shield ecozone (not shown). Similar relationships can be seen in Figs. 32b and 34a (Prairie Subhumid ecozone), 35b and 37a (Atlantic Maritime ecozone), and 38b and 40a (Mixedwood

Plains ecozone), although in some cases the greater sensitivity of the NCARCCSM3 model to the A2 forcing scenario evidently drove the projected vapor pressure even higher than that projected by the MIROC32MR model (e.g., Figs. 38–40).

With regard to summer and winter solar radiation incident at the surface for the Boreal Shield West ecozone (Figs. 30 and 31), the four models differed slightly in the projected amplitude of interannual variability, particularly in summer (Fig. 30a), when the NCARCCSM3 and CGCM31MR models had generally more variability than the MIROC32MR and CSIROMK35 models. Of these, relative to the mean, the NCARCCSM3 model projected slightly greater values and the CGCM31MR model slightly lower values. Winter data presented in Fig. 30b show the NCARCCSM3 model producing the greatest extremes (below the mean), but the models were in good agreement both with one another and in the comparison between winter and summer variability.

Hidden within the substantial interannual variability were general increases in summer radiation that are also apparent in many of the ecozones, as seen in Tables 9–17 and 20–22. The exceptions were in the Arctic (Tables 5–7) and northern cordilleran ecozones (Tables 18 and 19), where summer radiation was generally projected to decrease. Figures 31a and 31b show 10-year moving means of the same data. Figure 31a clearly shows a trend of increasing summer radiation according to the NCARCCSM3 and MIROC32MR models, but only marginal changes according to the CGCM31MR and CSIROMK35 models. These trends were strongest with the A2 forcing scenario (particularly for the NCARCCSM3 model), but were barely detectable with the B1 scenario. All of the models projected a trend of decreasing winter radiation (Fig. 31b), with the A2 scenario causing the largest decline (see also Tables 5–22).

Wind speed data for all regions generally showed little consistent change in terms of either means or variability and no consistent sensitivity to the level of GHG warming (see also Tables 5–22 and comments in the section "Interpreting the Downscaled Climate Scenarios for Individual Ecozones"). Hence, there did not appear to be significant or consistent differences among the four GCMs for this variable.

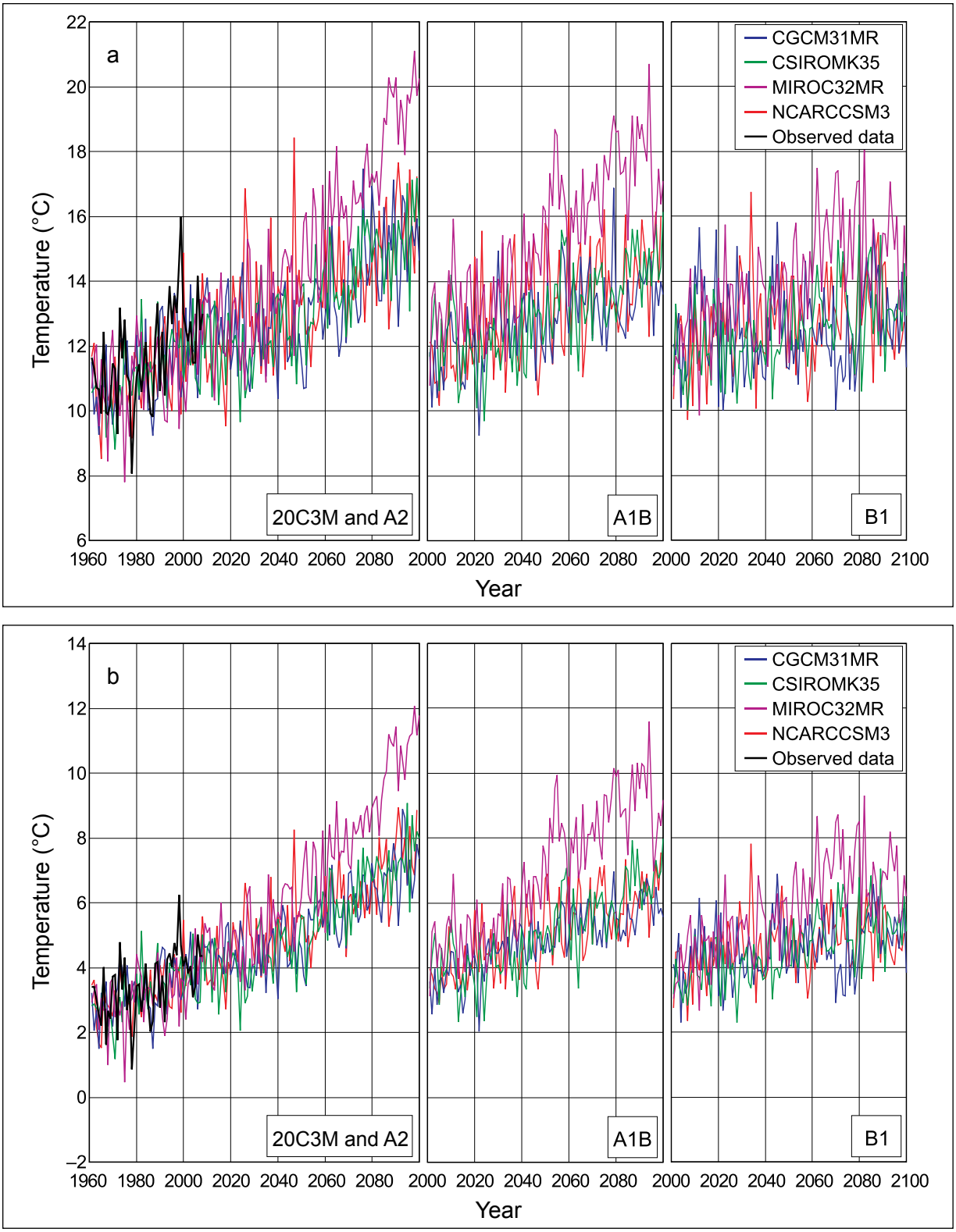

Figure 24. Projections of spatially averaged summer mean daily maximum (a) and minimum (b) temperature (°C) for the Southern Arctic ecozone for four greenhouse gas forcing scenarios, relative to interpolated observed data for 1961–2008. The simulated historical data for the period 1961–2000 (20C3M scenario) and observed data are shown only in the leftmost panels but are common to all three future projections. Model abbreviations are as in Figure 4.

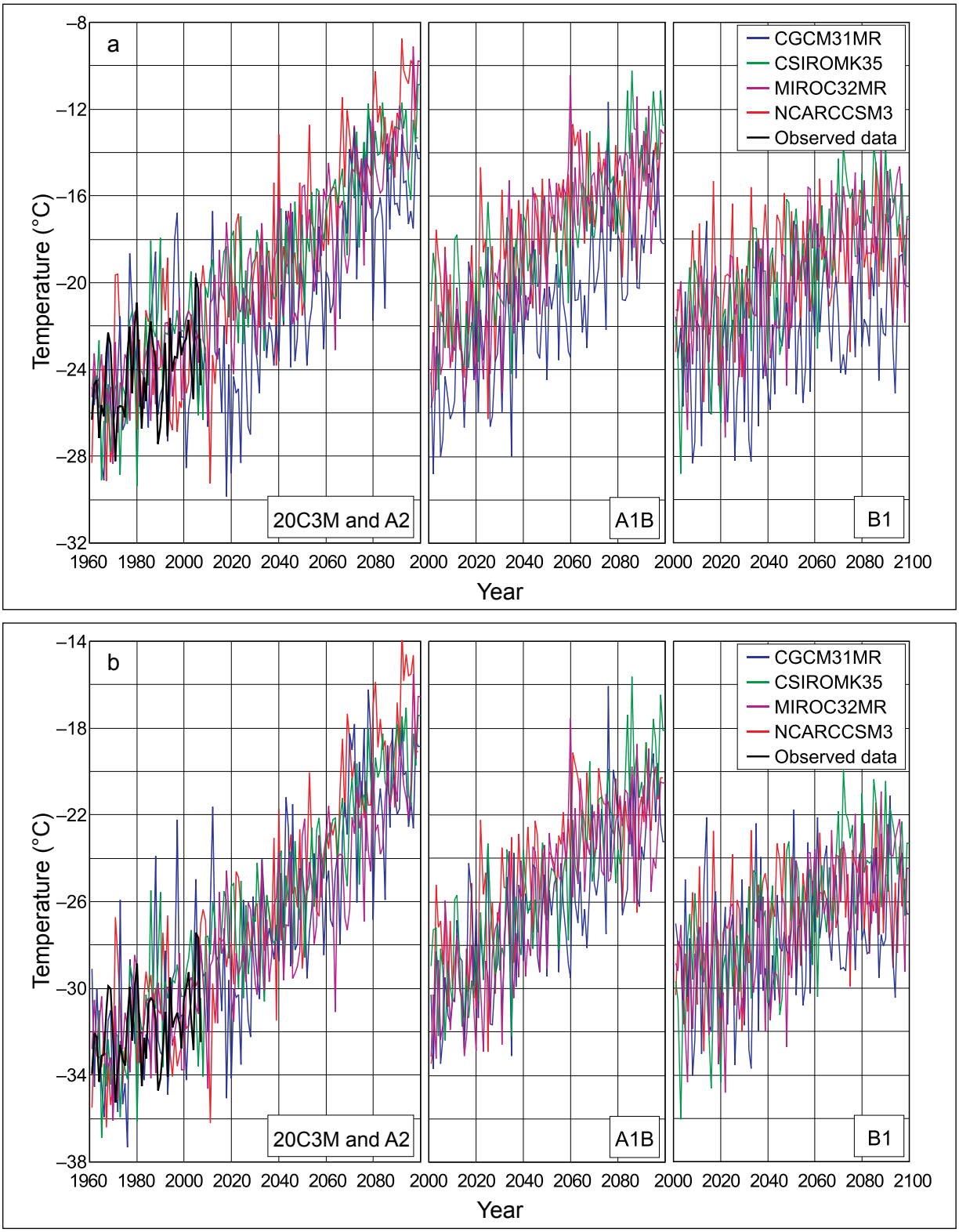

Figure 25. Projections of spatially averaged winter mean daily maximum (a) and minimum (b) temperature (°C) for the Southern Arctic ecozone for four greenhouse gas forcing scenarios, relative to interpolated observed data for 1961–2008. The scale for winter temperatures differs from that for summer temperatures shown in Fig. 24. The simulated historical data (20C3M scenario) and observed data are shown only in the leftmost panels but are common to all three future projections. Model abbreviations are as in Figure 4.

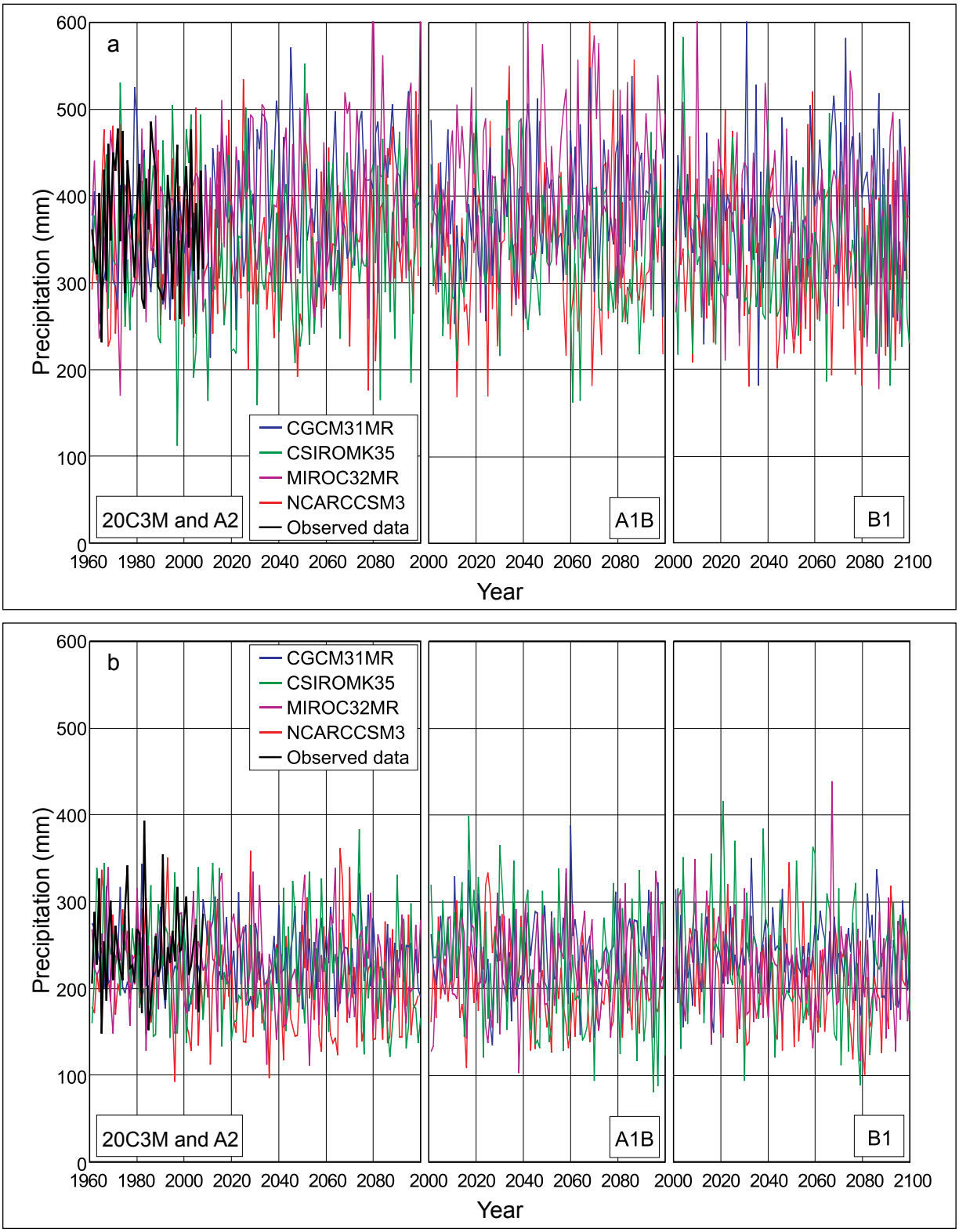

Figure 26. Projections of spatially averaged spring (a) and summer (b) total seasonal precipitation (mm) for the Pacific Maritime ecozone for four greenhouse gas forcing scenarios, relative to interpolated observed data for 1961–2008. The simulated historical data (20C3M scenario) and observed data are shown only in the leftmost panels but are common to all three future projections. Model abbreviations are as in Figure 4.

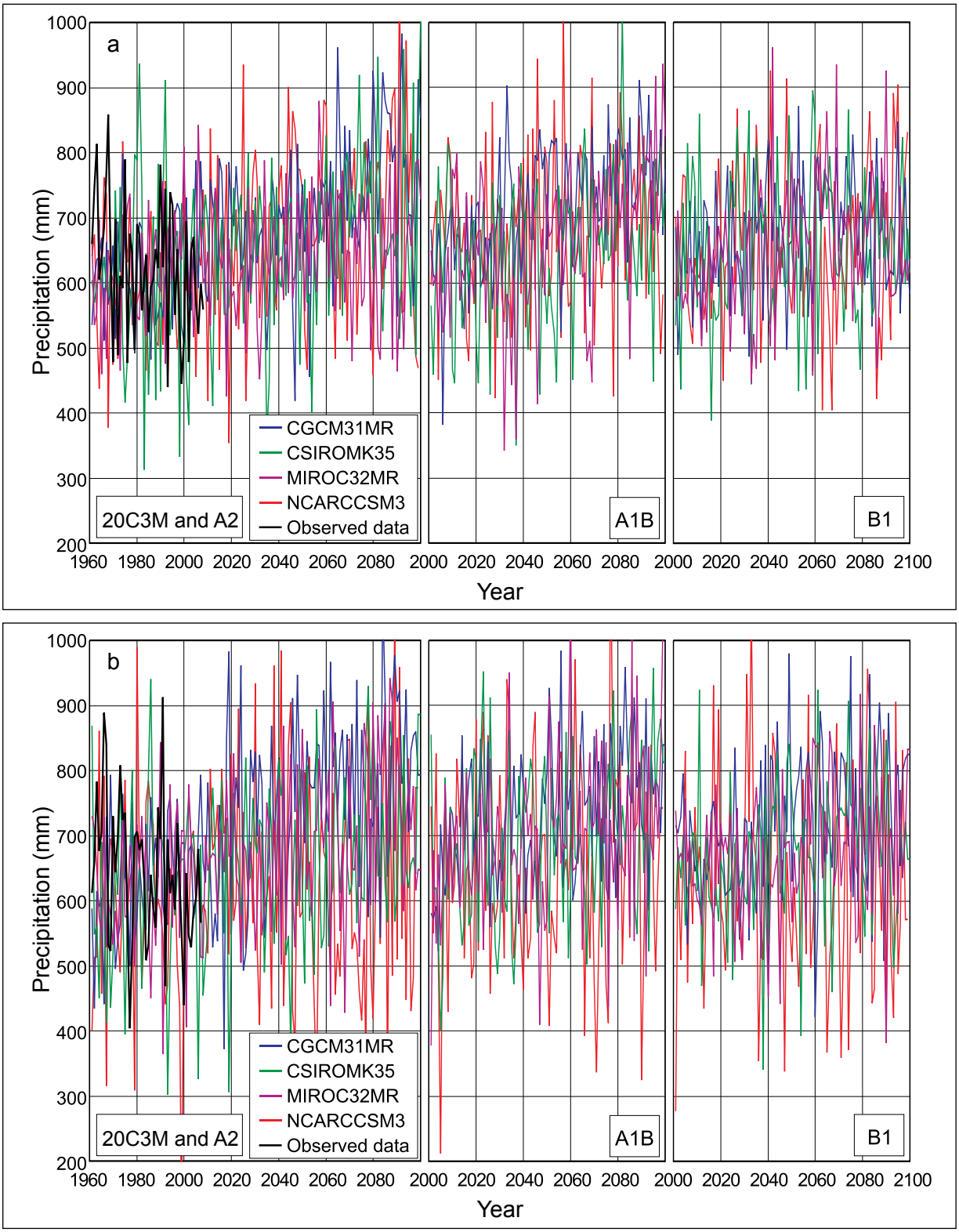

Figure 27. Projections of spatially averaged fall (a) and winter (b) total seasonal precipitation (mm) for the Pacific Maritime ecozone for four greenhouse gas forcing scenarios, relative to interpolated observed data for 1961–2008. The simulated historical data (20C3M scenario) and observed data are shown only in the leftmost panels but are common to all three future projections. Model abbreviations are as in Figure 4.

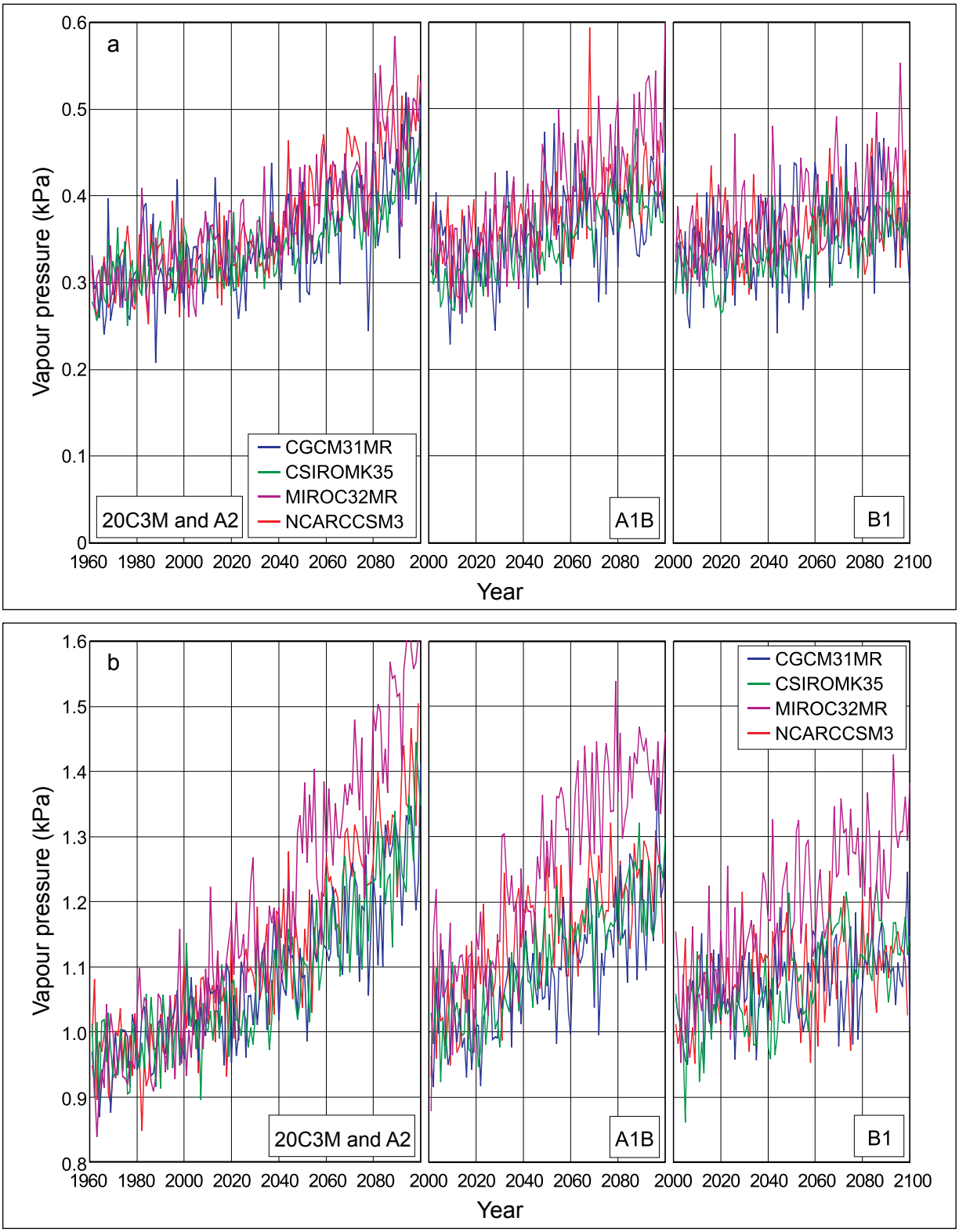

Figure 28. Projections of spatially averaged spring (a) and summer (b) mean vapor pressure (kPa) for the Taiga Shield East ecozone for four greenhouse gas forcing scenarios. The simulated historical data (20C3M scenario) are shown only in the leftmost panels but are common to all three future projections. Model abbreviations are as in Figure 4.

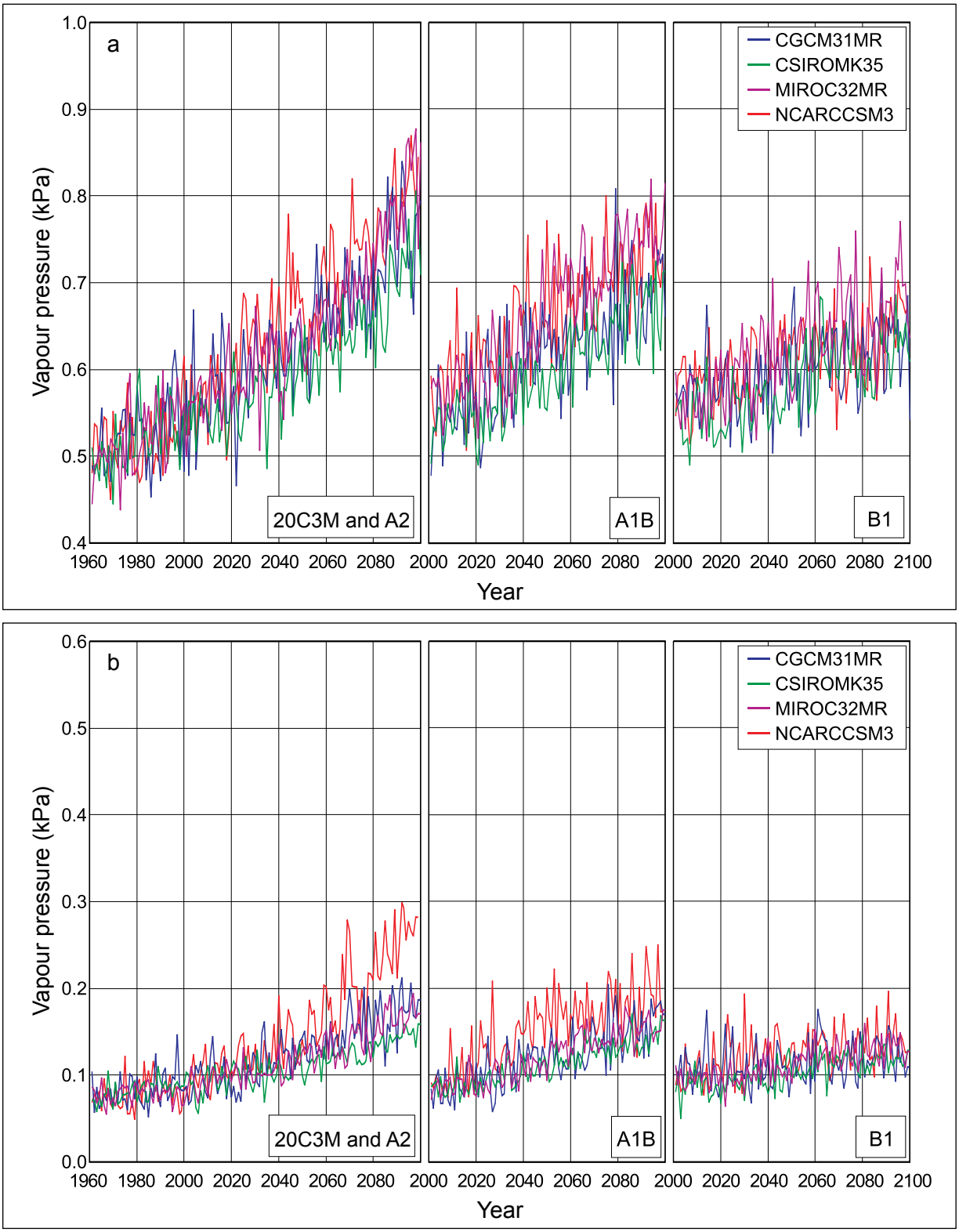

Figure 29. Projections of spatially averaged fall (a) and winter (b) mean vapor pressure (kPa) for the Taiga Shield East ecozone for four greenhouse gas forcing scenarios. The simulated historical data (20C3M scenario) are shown only in the leftmost panels but are common to all three future projections. Model abbreviations are as in Figure 4.

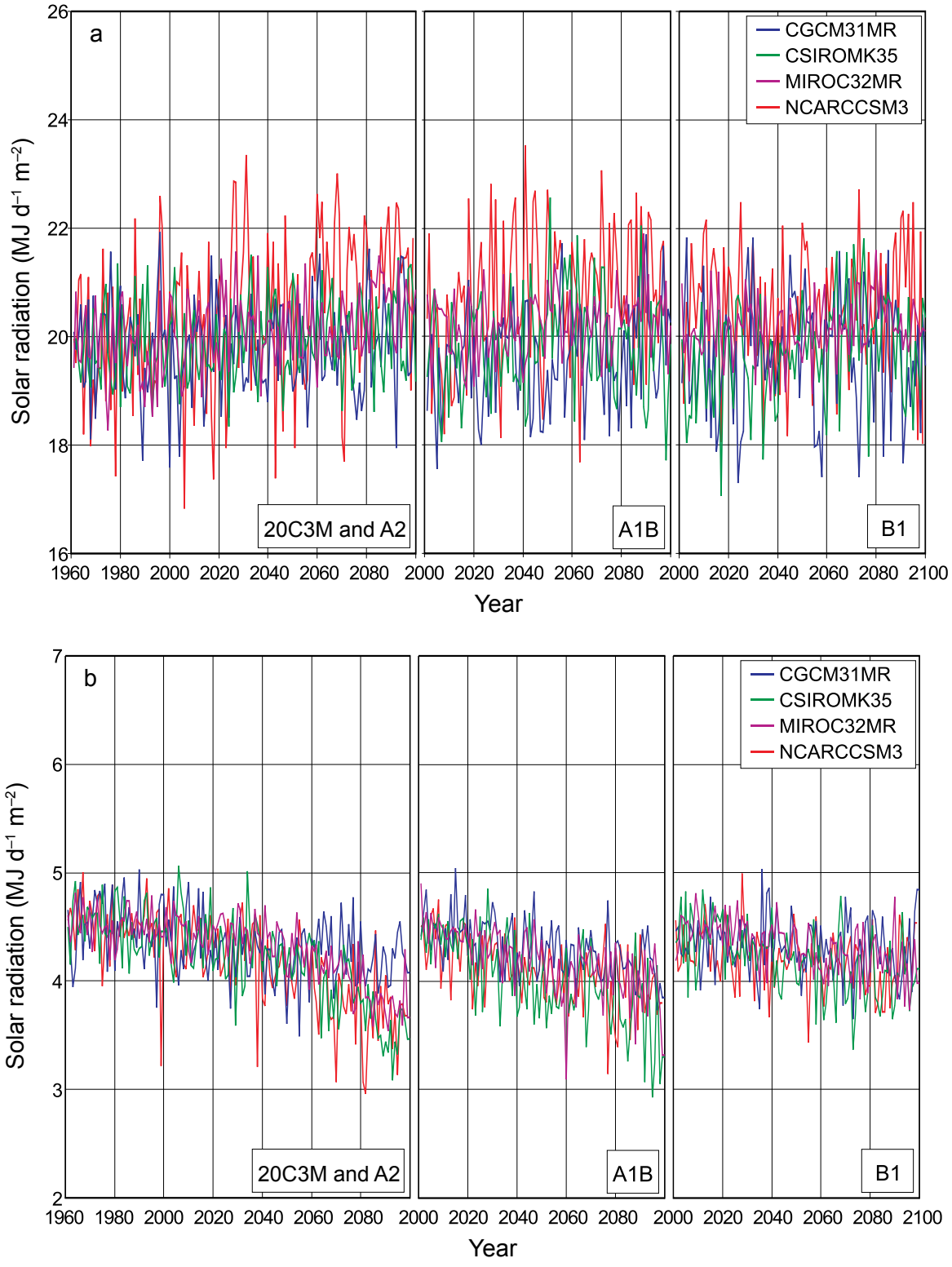

Figure 30. Projections of spatially averaged summer (a) and winter (b) mean global solar radiation (MJ m^{-2} d^{-1}) for the Boreal Shield West ecozone for four greenhouse gas forcing scenarios. The simulated historical data (20C3M scenario) are shown only in the leftmost panels but are common to all three future projections. Model abbreviations are as in Figure 4.

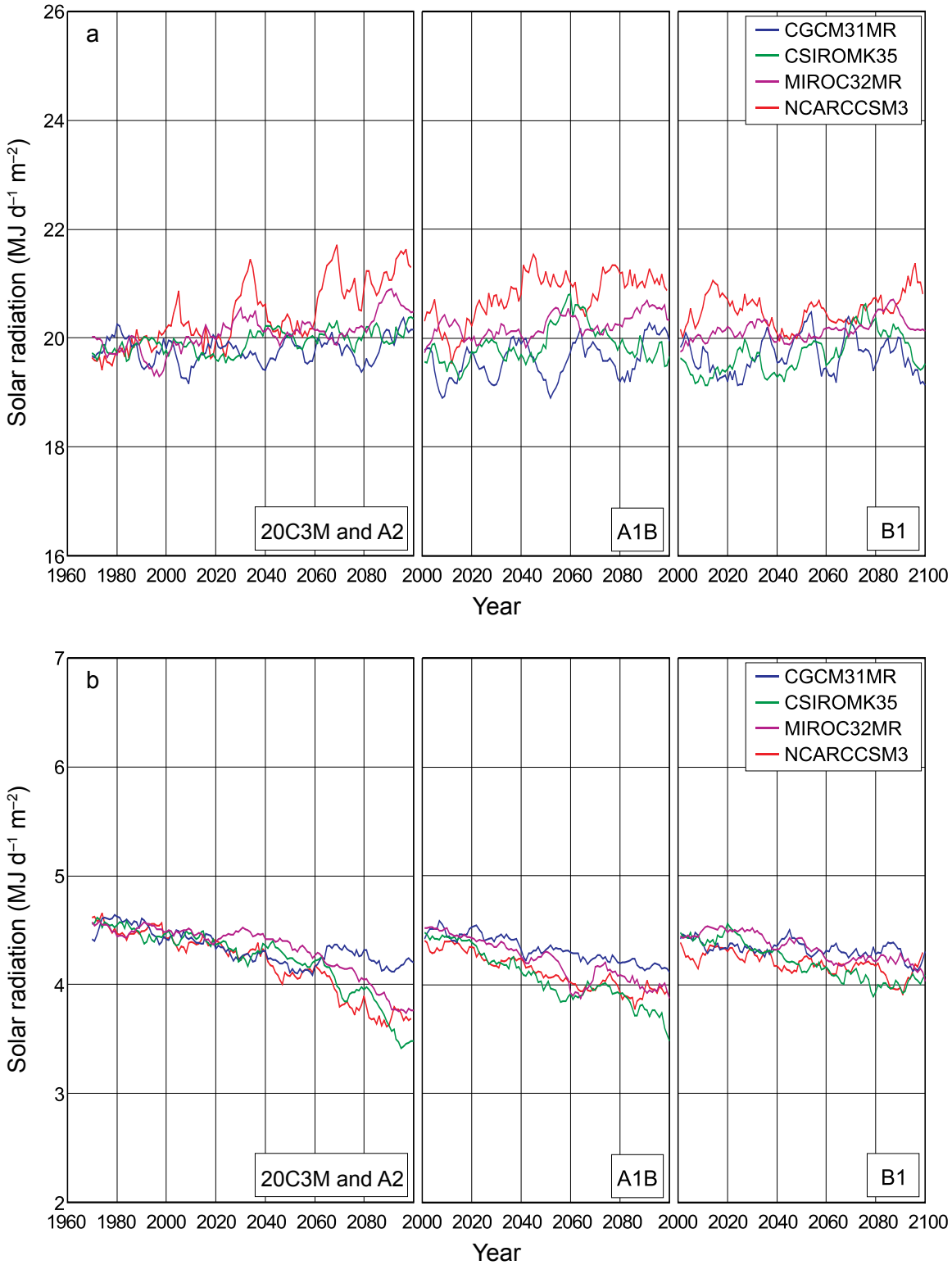

Figure 31. Projections of spatially averaged summer (a) and winter (b) mean global solar radiation (MJ m^{-2} d^{-1}) for the Boreal Shield West ecozone for four greenhouse gas forcing scenarios. Annual data have been smoothed as 10-year moving means. The simulated historical data (20C3M scenario) are shown only in the leftmost panels but are common to all three future projections. Model abbreviations are as in Figure 4.

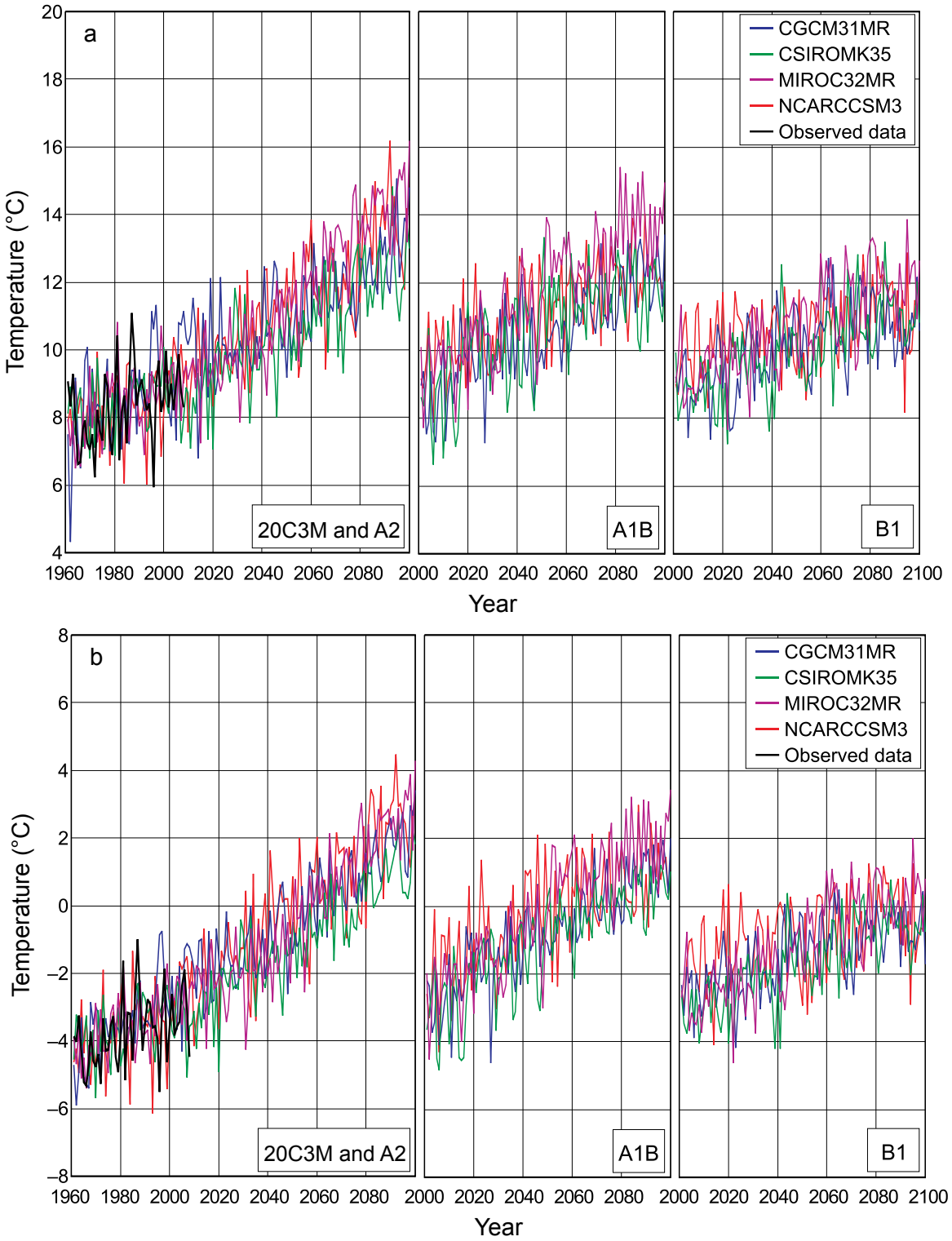

Figure 32. Projections of spatially averaged annual mean daily maximum (a) and minimum (b) temperature (°C) for the Prairies Subhumid ecozone for four greenhouse gas forcing scenarios, relative to interpolated observed data for 1961–2008. The simulated historical data (20C3M scenario) and observed data are shown only in the leftmost panels but are common to all three future projections. Model abbreviations are as in Figure 4.

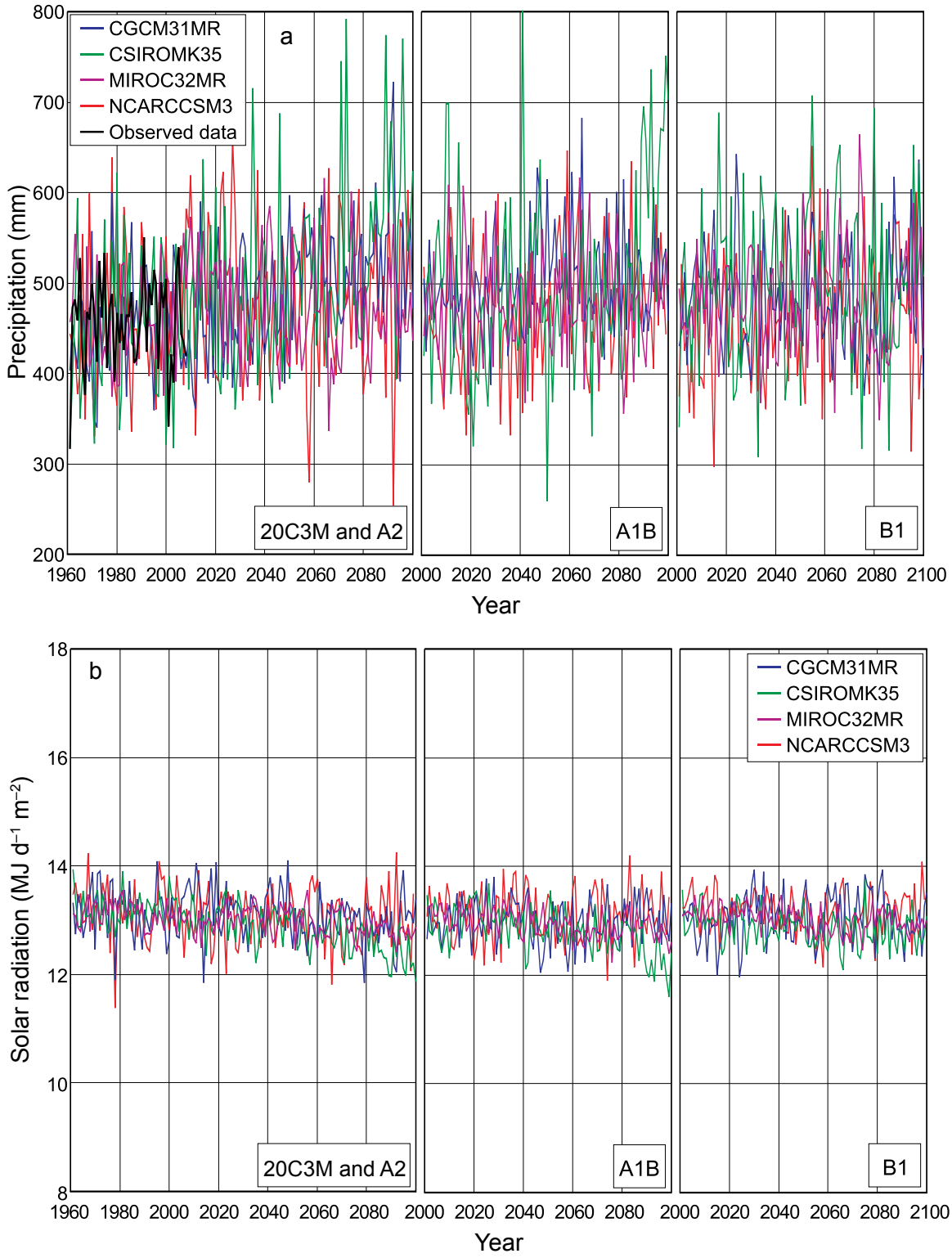

Figure 33. Projections of spatially averaged annual total precipitation (a) (mm) and daily global solar radiation (b) (MJ m^{-2} d^{-1}) for the Prairies Subhumid ecozone, for four greenhouse gas forcing scenarios. Precipitation projections are also compared with interpolated observed data for 1961–2008. The simulated historical data (20C3M scenario) and observed data are shown only in the leftmost panels but are common to all three future projections. Model abbreviations are as in Figure 4.

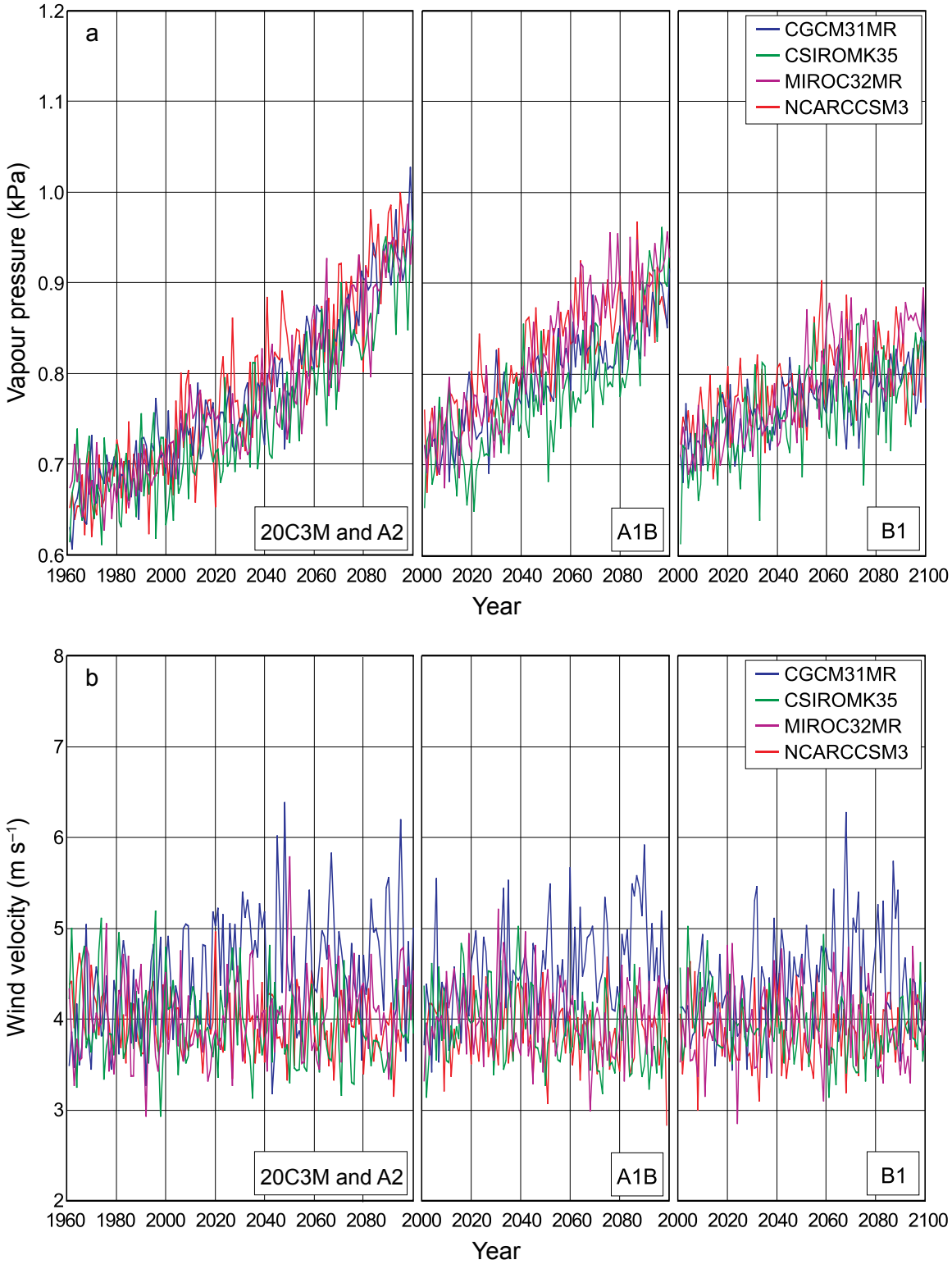

Figure 34. Projections of spatially averaged annual mean vapor pressure (a) (kPa) and wind speed (b) (m s^{-1}) for the Prairies Subhumid ecozone, for four greenhouse gas forcing scenarios. The simulated historical data (20C3M scenario) are shown only in the leftmost panels but are common to all three future projections. Model abbreviations are as in Figure 4.

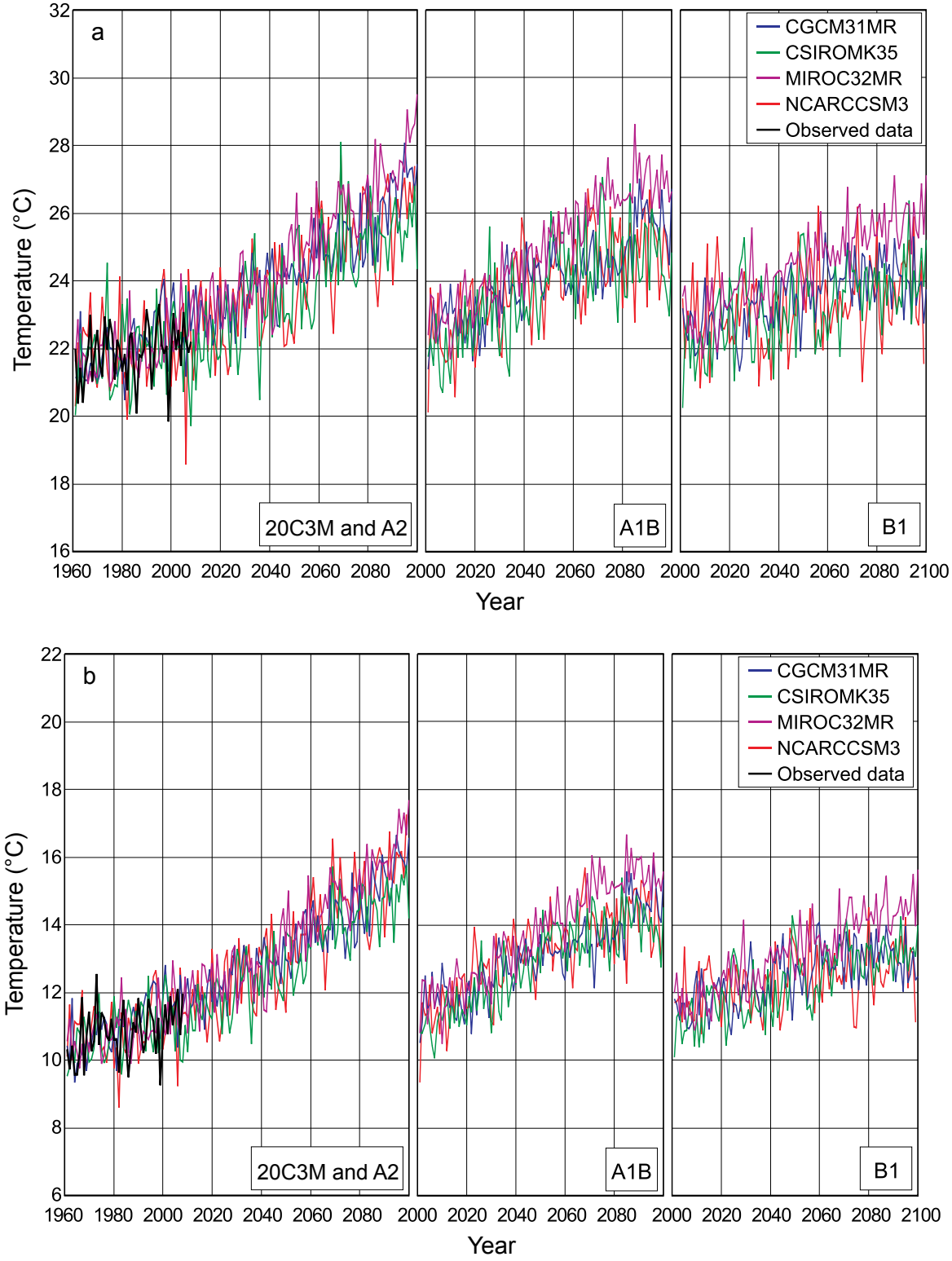

Figure 35. Projections of spatially averaged summer (June–August) mean daily maximum (a) and minimum (b) temperature (°C) for the Atlantic Maritime ecozone for four greenhouse gas forcing scenarios, relative to interpolated observed data for 1961–2008. The simulated historical data (20C3M scenario) and observed data are shown only in the leftmost panels but are common to all three future projections. Model abbreviations are as in Figure 4.

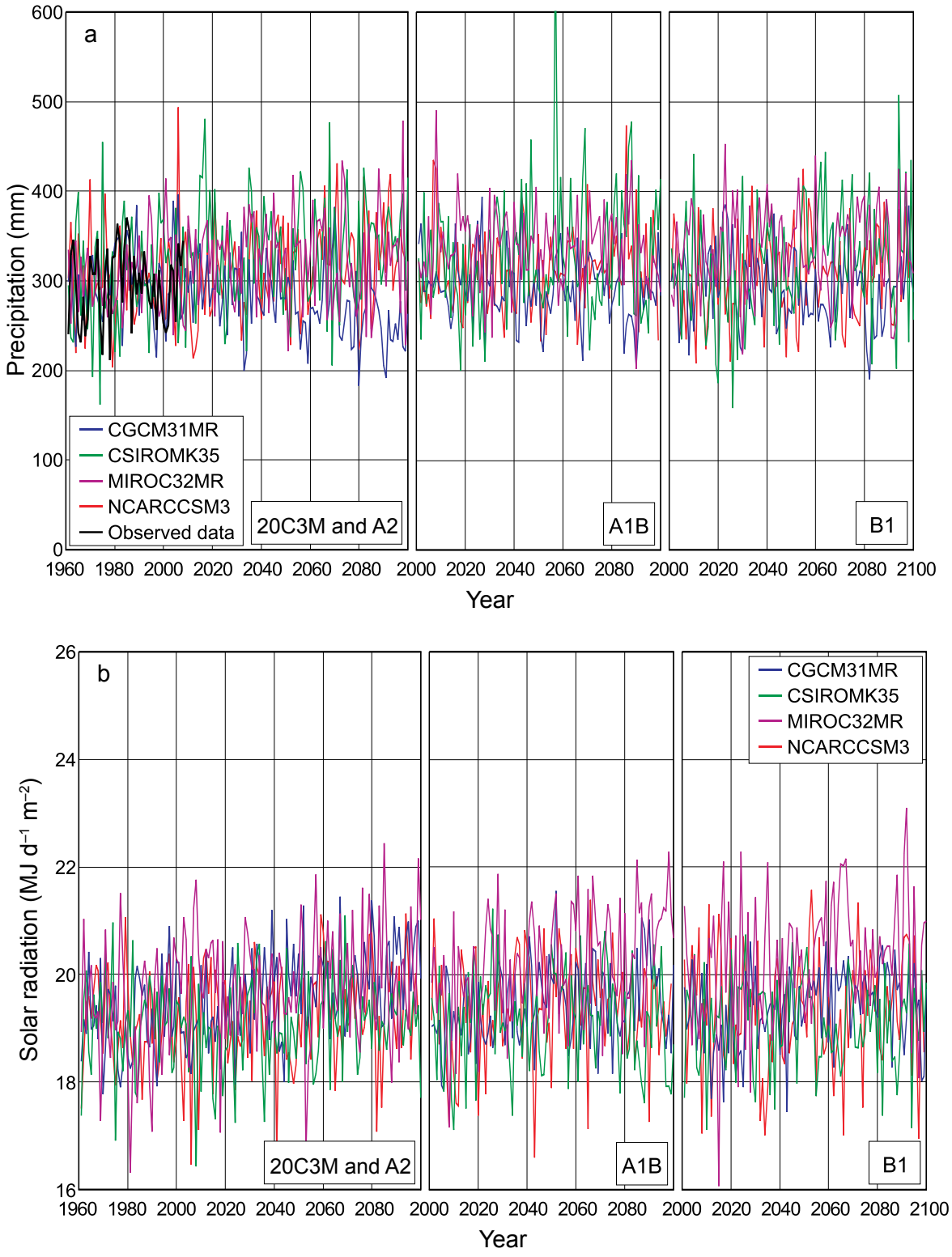

Figure 36. Projections of spatially averaged summer (June–August) total precipitation (a) (mm) and daily global solar radiation (b) (MJ m^{-2} d^{-1}) for the Atlantic Maritime ecozone, for four greenhouse gas forcing scenarios. Precipitation projections are also compared with interpolated observed data for 1961–2008. The simulated historical data (20C3M scenario) and observed data are shown only in the leftmost panels but are common to all three future projections. Model abbreviations are as in Figure 4.

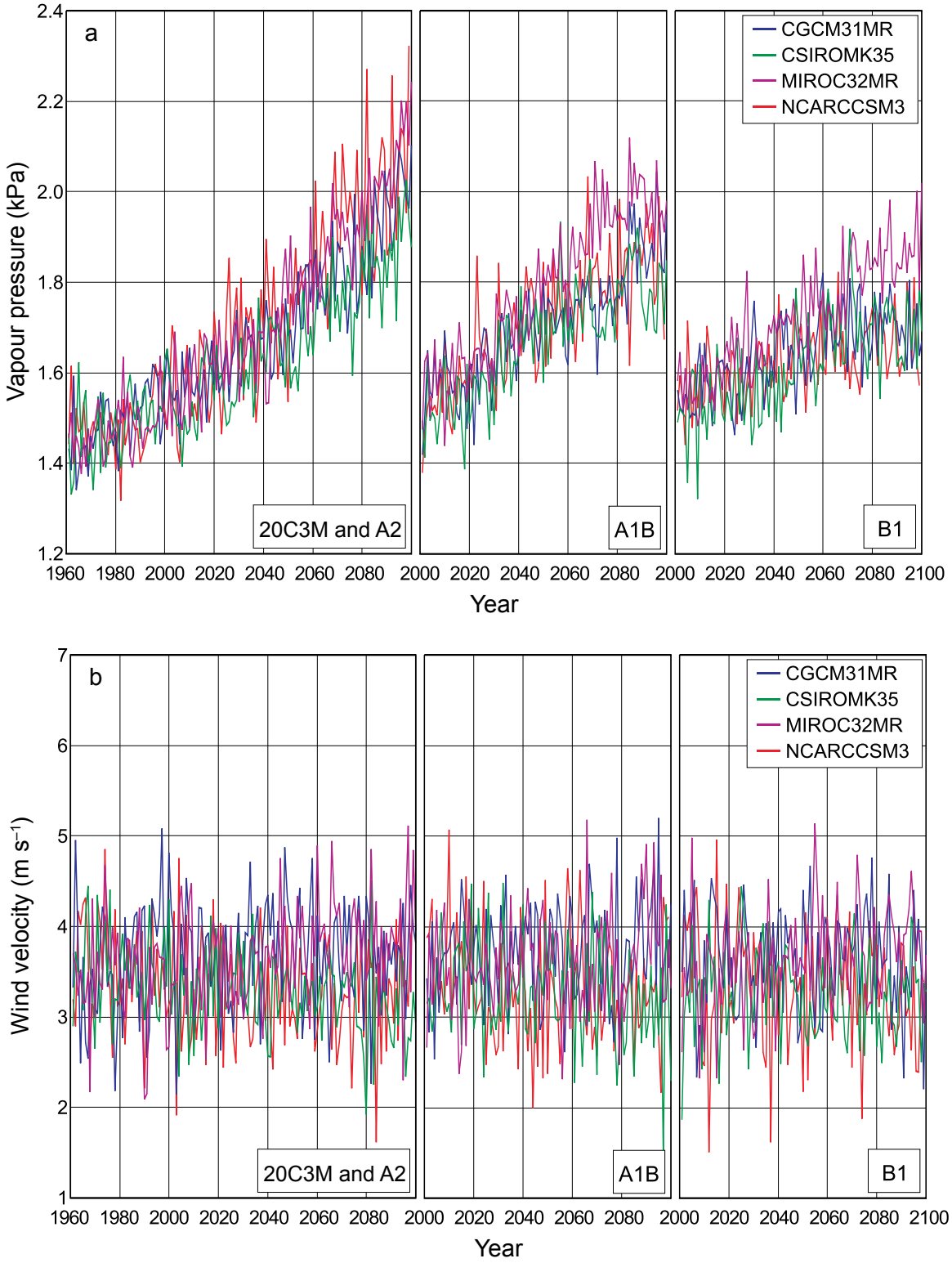

Figure 37. Projections of spatially averaged summer (June–August) mean vapor pressure (a) (kPa) and wind speed (b) (m s^{-1}) for the Atlantic Maritime ecozone, for four greenhouse gas forcing scenarios. The simulated historical data (20C3M scenario) are shown only in the leftmost panels but are common to all three future projections. Model abbreviations are as in Figure 4.

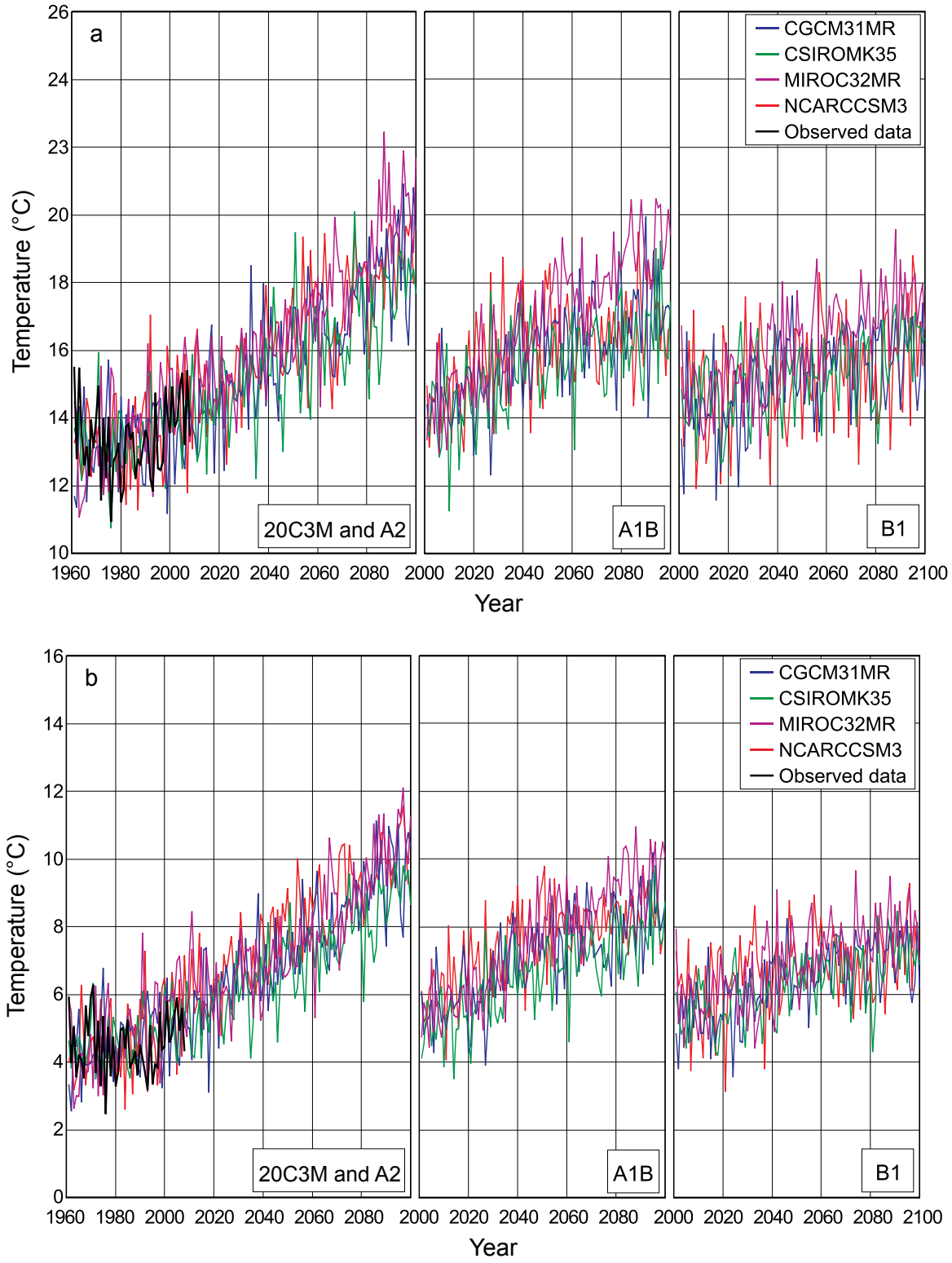

Figure 38. Projections of spatially averaged fall (September–November) mean daily maximum (a) and minimum (b) temperature (°C) for the Mixedwood Plains ecozone for four greenhouse gas forcing scenarios, relative to interpolated observed data for 1961–2008. The simulated historical data (20C3M scenario) and observed data are shown only in the leftmost panels but are common to all three future projections. Model abbreviations are as in Figure 4.

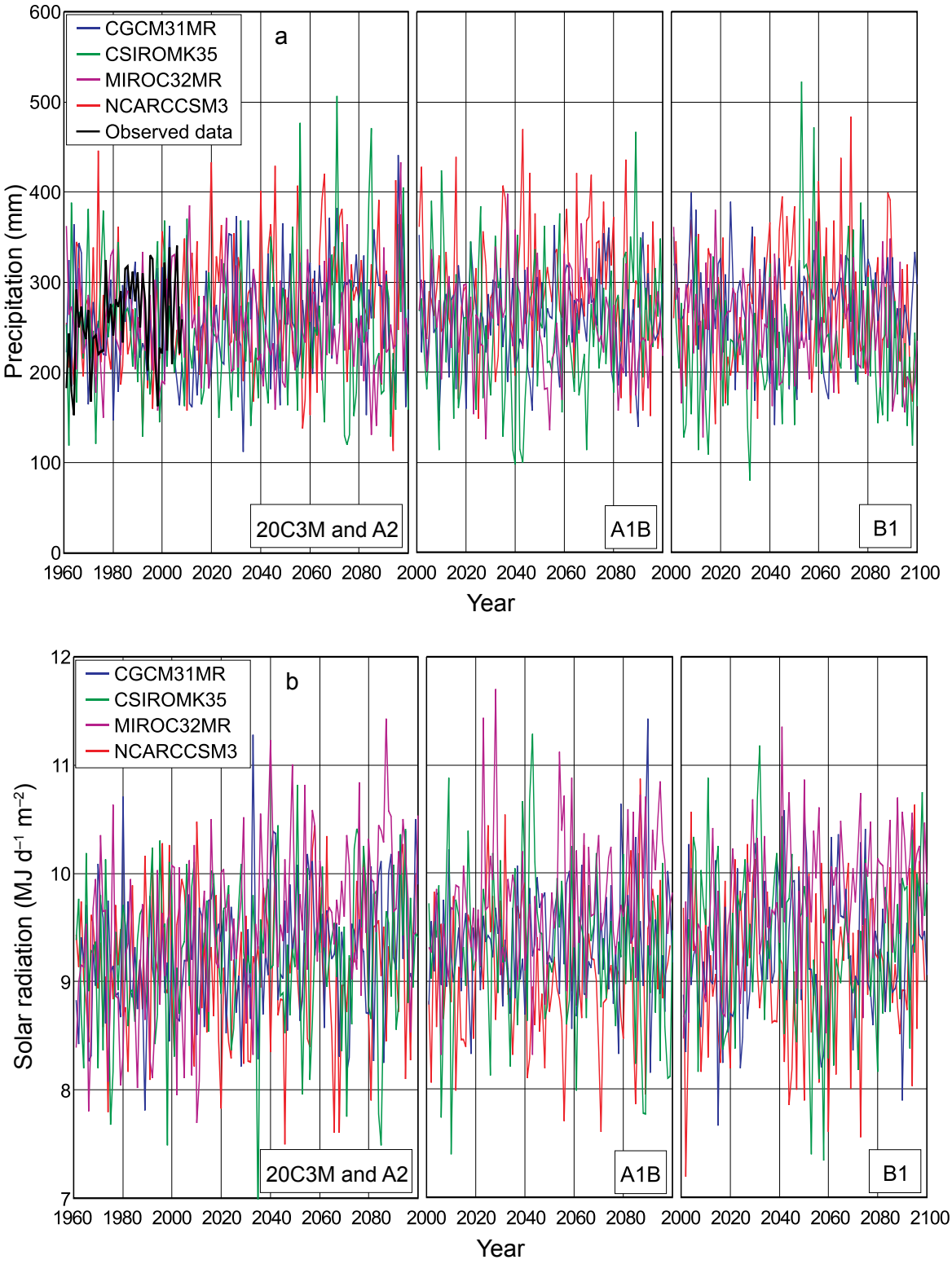

Figure 39. Projections of spatially averaged fall (September–November) total precipitation (a) (mm) and daily global solar radiation (b) (MJ m^{-2} d^{-1}) for the Mixedwood Plains ecozone, for four greenhouse gas forcing scenarios. Precipitation projections are also compared with interpolated observed data for 1961–2008. The simulated historical data (20C3M scenario) and observed data are shown only in the leftmost panels but are common to all three future projections. Model abbreviations are as in Figure 4.

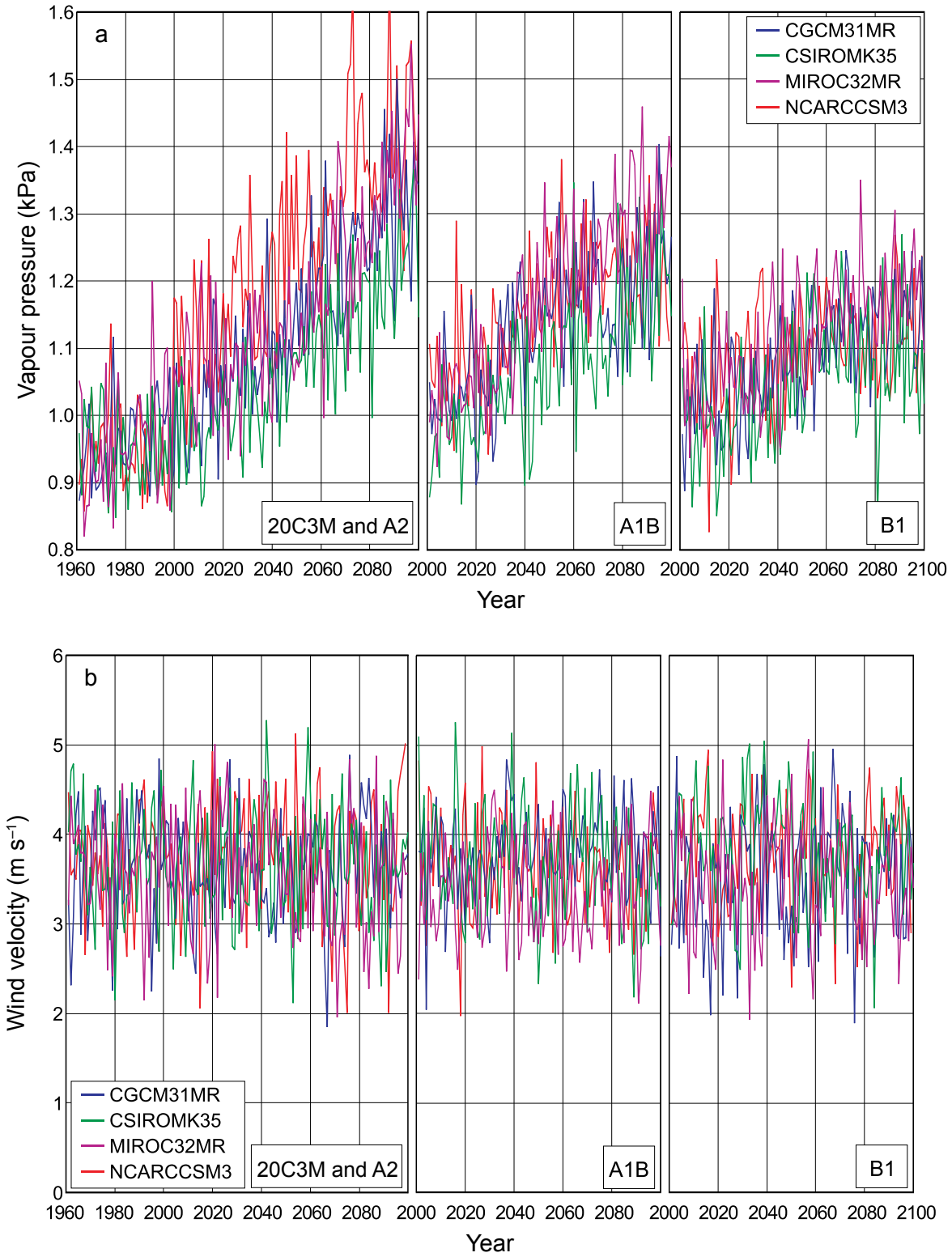

Figure 40. Projections of spatially averaged fall (September–November) mean vapor pressure (a) (kPa) and wind speed (b) (m s^{-1}) for the Mixedwood Plains ecozone, for four greenhouse gas forcing scenarios. The simulated historical data (20C3M scenario) are shown only in the leftmost panels but are common to all three future projections. Model abbreviations are as in Figure 4.

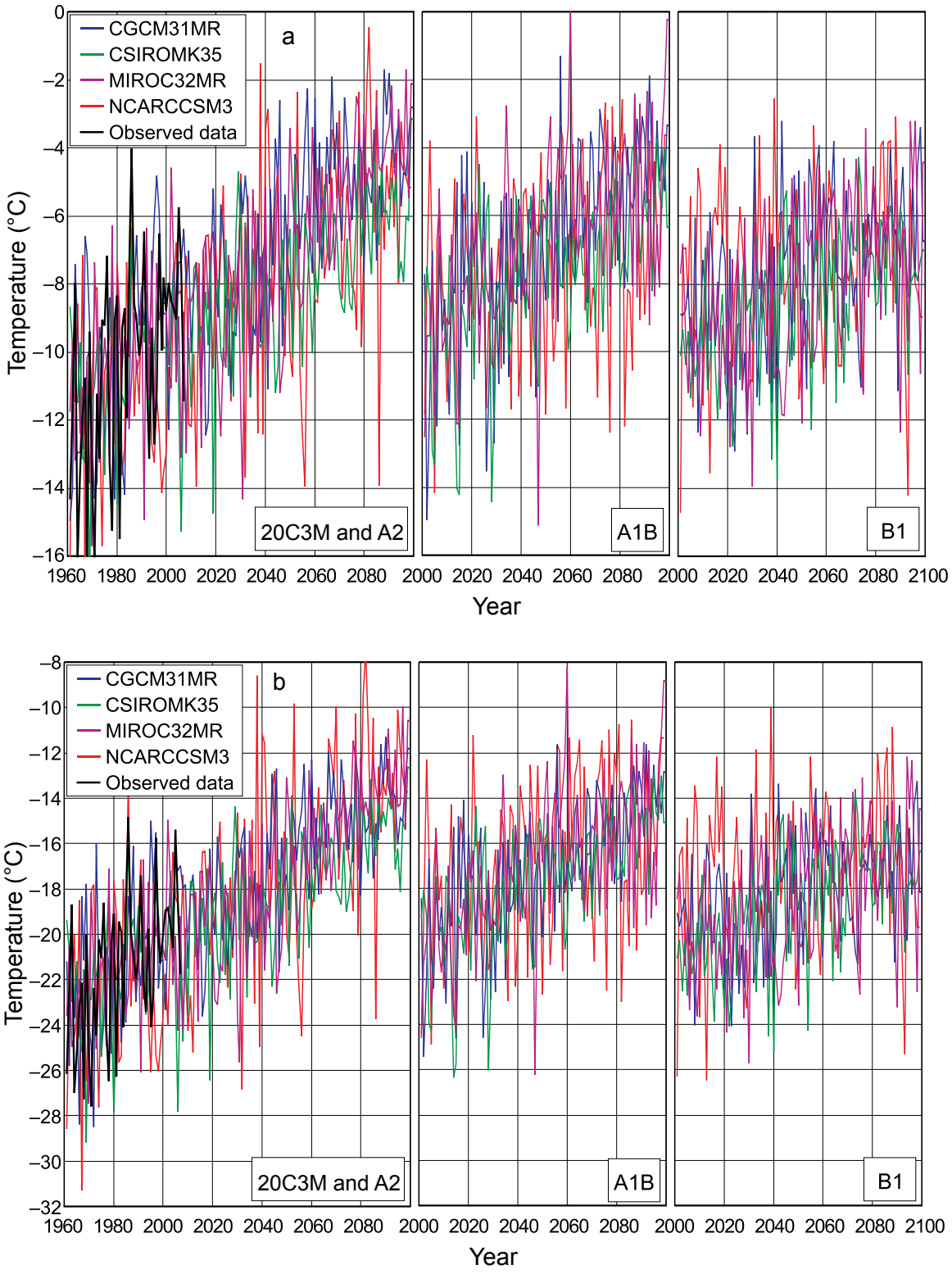

Figure 41. Projections of spatially averaged winter (December–February) mean daily maximum (a) and minimum (b) temperature (°C) for the Boreal Plains ecozone for four greenhouse gas forcing scenarios, relative to interpolated observed data for 1961–2008. The simulated historical data (20C3M scenario) and observed data are shown only in the leftmost panels but are common to all three future projections. Model abbreviations are as in Figure 4.

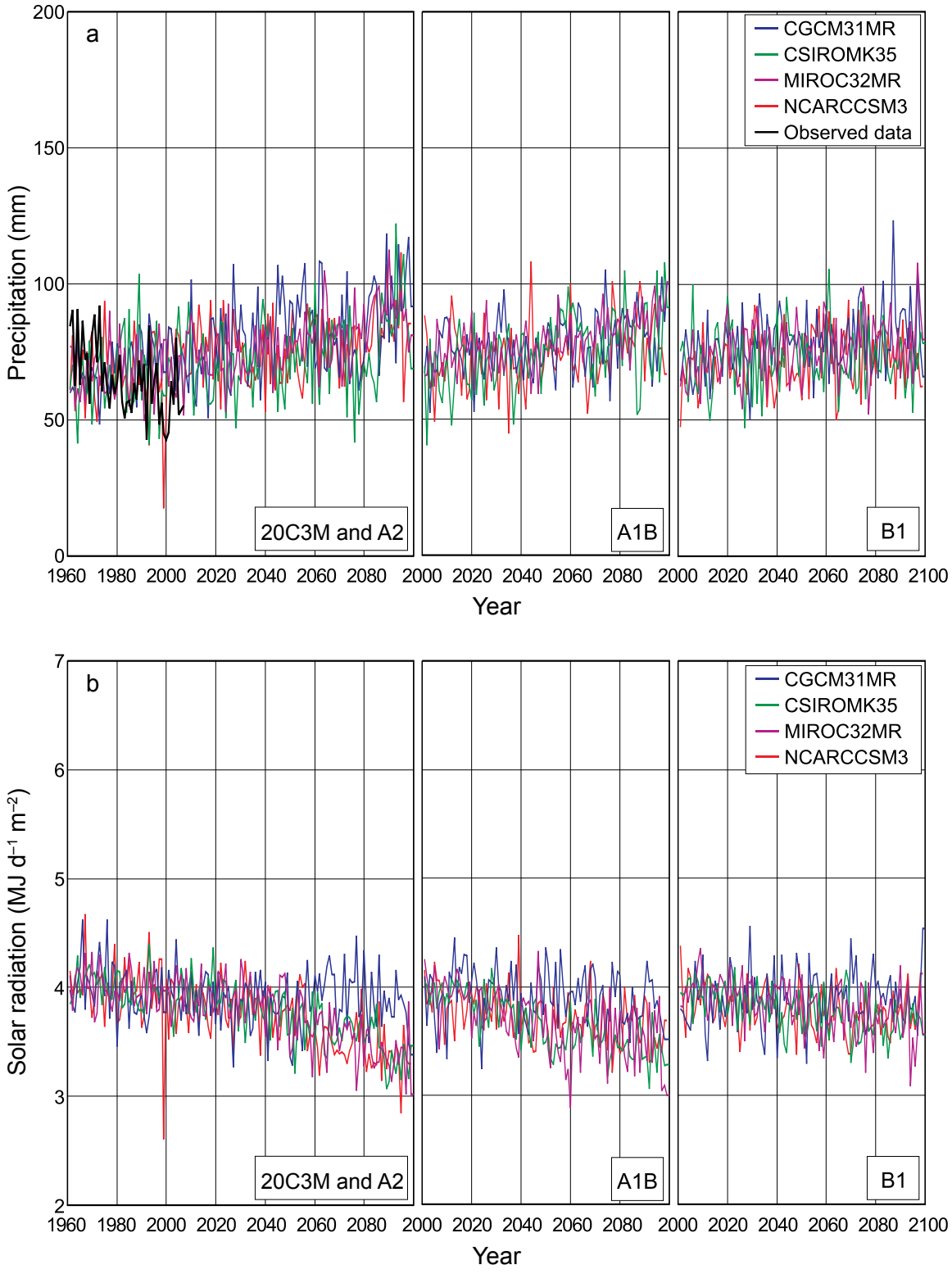

Figure 42. Projections of spatially averaged winter (December–February) total precipitation (a) (mm) and daily global solar radiation (b) (MJ m^{-2} d^{-1}) for the Boreal Plains ecozone, for four greenhouse gas forcing scenarios. Precipitation projections are also compared with interpolated observed data for 1961–2008. The simulated historical data (20C3M scenario) and observed data are shown only in the leftmost panels but are common to all three future projections. Model abbreviations are as in Figure 4.

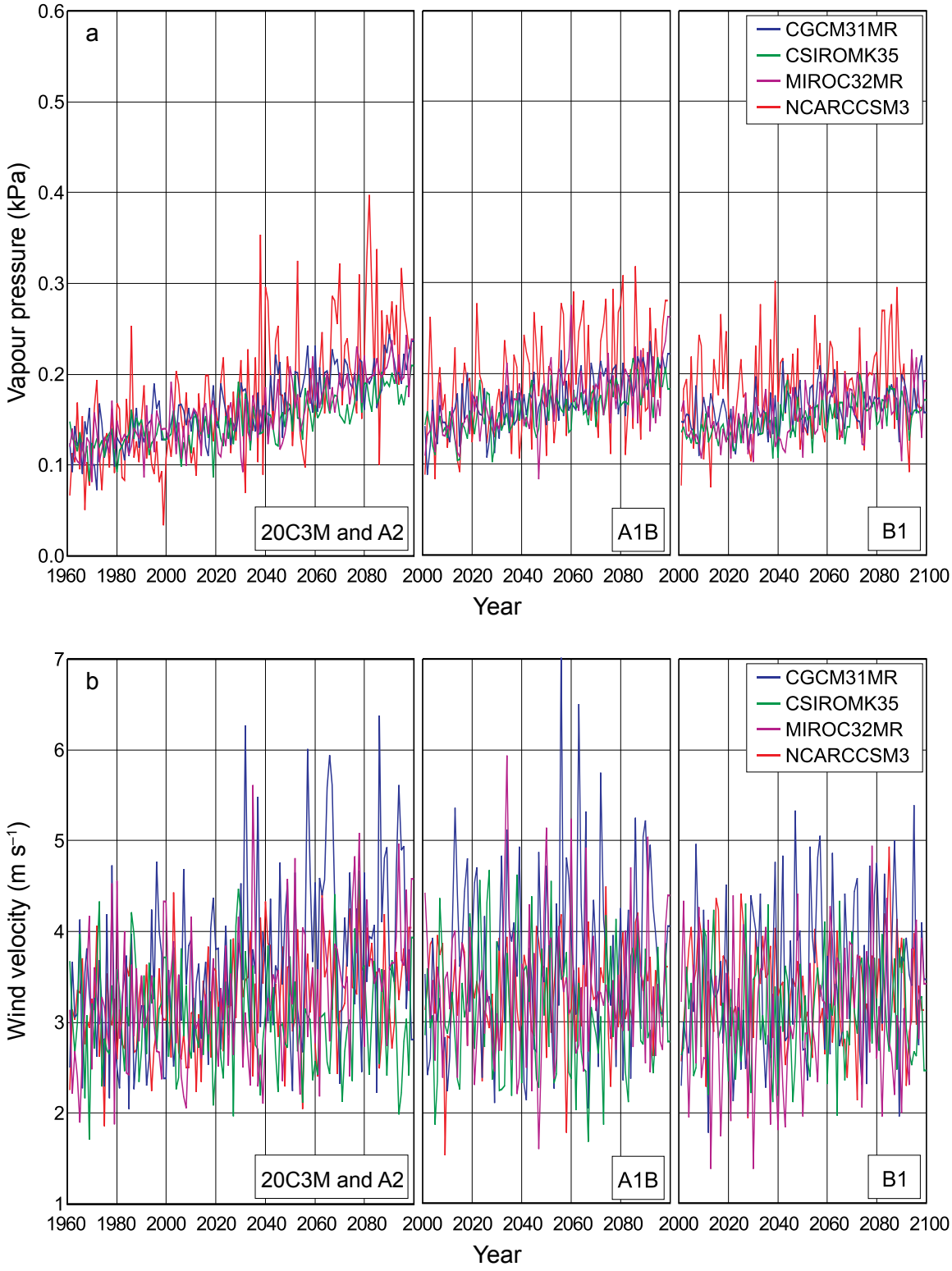

Figure 43. Projections of spatially averaged winter (December–February) mean vapor pressure (a) (kPa) and wind speed (b) (m s^{-1}) for the Boreal Plains ecozone, for four greenhouse gas forcing scenarios. The simulated historical data (20C3M scenario) are shown only in the leftmost panels but are common to all three future projections. Model abbreviations are as in Figure 4.

INTERPRETING THE DOWNSCALED CLIMATE SCENARIOS FOR INDIVIDUAL ECOZONES

Tables 5–22 present summaries of future projections for each climate variable by ecozone. The data shown in these tables deserve careful study, but some key results for each ecozone are summarized in the sections that follow, which could be interpreted as a "national climate outlook" for Canada, somewhat analogous to a long-term weather forecast based on multiple sources of information. Where ranges for future projections are reported in the text, they generally represent the range from the minimum change (obtained with the B1 emissions scenario) to the maximum change (obtained with the A2 scenario), expressed as a change from "present-day," circa 2000. It must be remembered that these outlooks represent results generated by a suite of imperfect models projecting an uncertain future and should be treated with skepticism: they are indications of what is possible rather than predictions of what is likely. Ultimately what really happens will depend on how the global human population acts over the next few decades.

In Tables 5–22, the area-weighted mean for each climate variable is the mean of the values projected by the four GCMs and therefore represents a "best guess," assuming that the GCMs are equally skillful (or equally believable). Each table presents results for a total of six climate variables (maximum and minimum temperature, precipitation, global solar radiation, vapor pressure and wind speed) for a single ecozone derived from the Terrestrial Ecozones of Canada classification of the Ecological Stratification Working Group (1995; see also Wiken 1986), as adopted by Kurz et al. (2009) and listed in Table 4.

For each variable, the data are organized across the page, in three sets of five columns. Each set of columns represents a single GHG emissions scenario (in the order A2, A1B, and B1), with the columns containing the means of the four GCM projections of monthly values for spring, summer, fall, winter, and the entire year.

The rows of data are labeled in the left-most column according to the period represented. "Baseline 1980–2009" refers to the 30-year mean for the period 1980–2009. This period was selected as the baseline because it represents current climate and immediately precedes the three consecutive 30-year periods reported as projections for the future (starting with 2010). It is important to distinguish this 30-year baseline period from the period 1961–1990, which was used as the baseline for combining scenario data with observed climate normals for 1961–1990. Although any differences between the periods 1961–1990 and 1980–2009 are probably small, there is evidence of a general warming trend over this entire period that is apparent in many of the graphs shown previously (both in the observed temperature records and in the GCM projections). Notably, the baseline 1980–2009 mean values differ slightly among the three emissions scenarios, because data for the nine years from 2001 to 2009 originated from the different GHG scenario simulations, which led to different calculated means.

These historical (baseline) means can be compared with those reported elsewhere for the Canadian Terrestrial Ecozones (e.g., http://www.pc.gc.ca/apprendre-learn/prof/itm2-crp-trc/htm/ecozone_e.asp). Differences may be attributed to the use of different periods as the baseline, but more particularly to different methods of estimating the mean values. The data reported here are area-weighted means of gridded data interpolated primarily from the station records generated by ANUSPLIN. Earlier estimates were probably based on more subjective averaging of the available climate station records (for example, see http://atlas.nrcan.gc.ca/auth/english/maps/environment/climate).

The rows labeled "Change by 2010–2039," "Change by 2040–2069," and "Change by 2070–2099" give the mean net changes in the projected 30-year means relative to 1980–2009. In these rows, a positive value indicates an increase, and a negative value indicates a decrease.

The rows labeled "100-year forcing" and "100-year variability (%)" represent the changes in 30-year means and 30-year standard deviations (SDs), respectively, between the periods 1970–1999 and 2070–2099. The changes in SD are reported as percentages relative to 100% for 1970–1999.

Arctic Cordillera

Projected temperature increases for the Arctic Cordillera ecozone (Table 5) were among the largest for the 18 ecozones identified in this report, with only the lower-elevation Northern and Southern Arctic ecozones (Tables 6 and 7, respectively) projected to experience slightly greater increases. Annual mean minimum temperature was projected to increase by about 5.5°C to 7.0°C and annual mean maximum temperature by 3.0°C to 6.5°C by 2100. Winter daily minimum temperature was expected to increase the most (5.0°C to 9.5°C), whereas summer temperatures (both minimum and maximum) were projected to increase by a relatively modest 1.5°C to 3.5°C. Fall temperatures were also projected to increase dramatically, by 5.0°C to 9.0°C, whereas spring temperatures were projected to rise by 2.5°C to 6.0°C. Interannual variability in annual and seasonal temperature was generally projected to decline in all seasons except summer, when increases in variability of up to 40% for daily minimum temperature and 70% for daily maximum temperature might occur with the A1B and A2 emissions scenarios.

Precipitation was projected to increase year-round by as much as 15%–30%, accompanied by increases in interannual variability, particularly in summer and fall. Related to these increases in precipitation, mean vapor pressure was projected to increase by 10%–35% on average (more in spring and summer), whereas solar radiation was expected to decline by 6%–10% year-round, presumably because of increased cloudiness. There were no consistent trends in the projections for mean wind speed, but overall changes appeared to be slight increases in spring and summer and slight decreases with the A2 scenario in winter and fall.

Northern Arctic

As with the Arctic Cordillera (Table 5) and Southern Arctic (Table 7) ecozones, temperatures in the Northern Arctic ecozone (Table 6) were projected to increase substantially year-round by 2100, with the smallest increases in summer (1.5°C to 3.5°C). Annual mean minimum temperature was projected to increase by 3.5°C to 7.5°C by 2100, slightly more than the projected 3.0°C to 6.5°C increase for mean maximum temperature. According to the optimistic B1 emissions scenario, increases in winter mean minimum temperature would be at least 5.0°C to 6.0°C, but winter increases in both mean minimum and maximum temperatures could exceed 10.0°C with the A2 scenario. Significantly more than half of this warming was projected to occur by the mid-2050s, in all scenarios and all seasons. Interannual variability in summer temperatures was projected to increase by 30%–75%, but the general trend was for slight decreases in most other seasons.

The Northern Arctic is the driest ecozone in Canada, with present-day annual precipitation totals averaging only 200 mm. Hence, relatively small increases in total precipitation amount would represent relatively large proportional increases, projected to be 15%–30% annually by 2100. The largest absolute increases were projected to occur mainly in summer and fall, although larger proportionate increases were projected for winter and spring (as much as 50% in winter with the A2 scenario). Increased variability in precipitation was projected for all seasons under most emissions scenarios. These increases were highly correlated with projected increases in mean vapor pressure (up to 30% by 2100) and decreases in solar radiation (approaching 10% in spring and summer with the A2 scenario, by 2100). Interannual variability in solar radiation was projected to increase substantially, particularly in summer. Greatly increased variability in vapor pressure was also projected for all seasons, but particularly in winter. Projected changes in average wind speed were generally positive, amounting to 10%–15% in summer, whereas interannual variability in this variable was generally projected to increase by only a few percentage points.

Southern Arctic

In the Southern Arctic ecozone (Table 7), projected increases in winter temperatures were very large (up to 11°C for mean minimum temperature with the A2 scenario), but, unlike the Northern Arctic (Table 5) and Arctic Cordillera (Table 6) ecozones, the warming in spring, summer, and fall was projected to be more even and generally less, typically ranging from 2.0°C to 6.0°C by 2100, depending on the emissions scenario. Interannual variation in temperature was projected to increase, according to the A2 scenario (particularly during summer), but the general trend was for a decrease of 10%–15%, according to the A1B and B1 scenarios. Present-day annual precipitation in the Southern Arctic is higher than in the Northern

Arctic, averaging about 270 mm, with close to half of this precipitation falling during summer. The GCMs generally projected year-round increases consistent with the level of GHG forcing, with the largest increase occurring in fall (20%–25%). However, as for the Northern Arctic (Table 6), winter and spring were projected to experience larger proportionate increases (as much as 50% for winter with the A2 scenario). Interannual variability in precipitation was projected to increase in all seasons, but particularly in spring and fall.

Annual mean atmospheric vapor pressure was projected to increase by 10%–30% depending on the emissions scenario, with the greatest proportionate increases occurring in winter, presumably related to the very large increases in winter mean minimum temperature. Variability in mean vapor pressure was also projected to increase year-round, with the greatest increase in winter and the least in spring. Solar radiation was projected to decrease in all seasons, presumably because increasing humidity would promote more cloud and precipitation. The largest proportionate decreases were projected to occur in winter, when total inputs would already be very low because of the short daylight periods. Variability in solar radiation was generally projected to increase slightly, but there was no clear trend across scenarios or among seasons. Projected trends for wind speed suggested a general increase, particularly in summer and winter, but inconsistent changes in interannual variability.

Taiga Plains

Projected increases by 2100 were in the range of 3.0°C to 5.5°C for mean daily minimum temperature and 2.5°C to 4.5°C for mean daily maximum temperature (Table 8). Winter increases in minimum temperature ranged from 4.0°C to 8.0°C, depending on the scenario, with increases for other seasons being more consistent across scenarios, within the range 2.0°C (B1 scenario, summer) to 5.0°C (A2 scenario, fall). Interannual variability in temperature was projected to decrease with all scenarios, but it appears that summer temperatures may become more variable. The Taiga Plains ecozone currently receives higher annual precipitation than the Arctic regions, with about two-thirds of the total falling in summer and fall. Annual precipitation was projected to increase by 40–75 mm per year by 2100, distributed fairly evenly across all seasons. However, the largest proportionate increases were projected for the fall (15%–30%), followed by winter and spring, with the summer increases being relatively insignificant (5%–15%). The general trend was for slight increases in interannual variability in precipitation, except with the B1 scenario, which showed smaller or negative changes.

The projected trends in solar radiation were related to those for precipitation, with relatively large changes in winter and spring (as much as a 15% decrease) and marginal decreases in summer. Projected decreases in the fall were proportionately even larger (about 20%), although present-day solar radiation is very low in fall (averaging about 4 MJ m^{-2} d^{-1}). Trends in interannual variability in solar radiation inputs were not clear, but the results suggested decreases in fall and increases in other seasons. Projections for annual mean vapor pressure were for substantial increases in means (as much as 35% with the A2 scenario). These increases were projected to occur throughout the year, with the greatest proportional increases of 30%–60% occurring during winter. Similarly, interannual variability was projected to increase year-round, but particularly in winter and summer. Projected changes in mean wind speed were less clear, with generally small increases, particularly in winter and summer, and a suggestion of increased variability in spring.

Taiga Shield West

Projected increases in mean annual temperature by 2100 for the Taiga Shield West ecozone (Table 9) were in the range of 3.5°C to 6.0°C for the daily minimum and 3.0°C to 5.0°C for the daily maximum, depending on the scenario. Over the same period, daily minimum temperature in winter was projected to warm by 5.0°C to 9.0°C, and daily maximum temperature in the same season by 4.0°C to 7.5°C, again depending on the scenario. Projected warming in the remaining seasons was more even, with fall generally warming the most, and spring, slightly less.

Present-day annual precipitation in the western Taiga Shield averages about 350 mm, less than half that received in the east (see Table 10). With the most extreme (A2) emissions scenario, projected increases by 2100 were about 18% for both regions; hence, the potential for serious droughts in the western part of the ecozone can only increase, given the similar

temperature increases projected across the entire ecozone. Furthermore, in the western Taiga Shield, the increases in precipitation were projected to occur mainly in winter and fall (25% and 30%, respectively), whereas summer amounts were projected to increase by less than 10%. Related to these changes, mean solar radiation was projected to increase slightly in summer (along with a decrease in interannual variability) and to decrease in other seasons. This trend suggests that summer storms will intensify and occur more regularly, since an increase in mean radiation indicates generally clearer skies on average and brings the likelihood of greater surface heating and more convective rainfall.

Mean vapor pressure was projected to increase year-round, with the largest absolute increases in summer. By 2100, these increases would typically represent 25%–30% of present-day levels with both the A1B and A2 scenarios, but winter increases were about double in proportional terms. Curiously, the projected increases were often larger with the A1B scenario than with the A2, but the B1 projected consistently smaller increases. The models projected fairly consistent increases in wind speed typically in the range 5–10% by 2100, for all seasons except spring (which changed little) for all emissions scenarios. However, there were no consistent trends in interannual variability.

Extending the conjecture about summer conditions further, the generally drier conditions combined with higher humidity and higher solar radiation suggest increased occurrence of convective storms and hence lightning activity, which would create the potential for more wildfire activity in this region (e.g., Stocks et al. 2002).

Taiga Shield East

Mean annual temperatures in the Taiga Shield East ecozone (Table 10) were projected to increase by 3.5°C to 6.0°C (minimum) and 2.5°C to 5.0°C (maximum) by 2100, depending on the emissions scenario. These increases, particularly for daily minimum temperature, are similar to those projected for the western portion of the Taiga Shield (see Table 9). Projected seasonal warming was also comparable to that for the western Taiga Shield, but with a more even distribution of increases over spring, summer, and fall. Winter warming was projected to be somewhat greater, however, as much as 10.0°C for the daily minimum and about 7.0°C for the daily maximum by 2100 with the A2 scenario.

As previously noted, mean annual precipitation in this region (about 770 mm) is more than double that of the western Taiga Shield (see Table 9), but the GCM-projected increases were generally proportional (about 18% for the annual mean, by 2100). The largest increases were projected for winter and the smallest for summer, but with summer and fall accounting for about two-thirds of the present-day annual total, the likelihood of frequent extensive droughts in the future seems relatively low. Also similar to the trend noted for the western Taiga Shield, solar radiation was projected to increase slightly in summer, which would suggest a shift in precipitation patterns to fewer but more intense summer storms. Radiation input was projected to decrease in other seasons, which correlates well with the projected general increases in precipitation (particularly in spring, when radiation was projected to decline by more than 10% with the A2 scenario).

Vapor pressure was projected to increase in all seasons under all three GHG emissions scenarios. Annual means would increase by 10%–30% by 2100, depending on the scenario, with winter means potentially doubling and summer and fall levels increasing by 25%–40% under the A2 and A1B scenarios. Interannual variability in atmospheric humidity was projected to increase in all seasons, but mainly in summer and winter. Projections for changes in wind speed indicated relatively small and inconsistent changes.

Boreal Shield West

The general north-to-south trend observed in this study was for progressively smaller increases in mean annual temperatures, consistent with many global-scale GCM projections. This trend was reflected in comparisons of the boreal ecozones with the Arctic and taiga ecozones, as discussed in previous sections. For the Boreal Shield West ecozone (Table 11), projected increases by 2100 were 3.0°C to 5.5°C for mean annual minimum temperature and 2.5°C to 4.5°C for mean annual maximum temperature. Winter minima were projected to increase by 4.5°C to 8.0°C, depending on the emissions scenario, whereas winter maxima would increase by 3.5°C to 5.5°C, with consistent decreases in interannual variation. All other seasons were projected to experience

increases of about 2.5°C to 4.5°C for both minimum and maximum temperatures, accompanied by inconsistent changes in interannual variability.

Present-day annual precipitation in the western Boreal Shield averages about 600 mm and is therefore appreciably higher than in the western Taiga Shield (see Table 9) and the more southerly Boreal Plains (see Table 15). Projected increases were comparatively small, however (about 11% by 2100 for both the A2 and A1B scenarios), with most of the increase occurring in winter and spring and rather less in summer and fall. As for the Taiga Shield, projected solar radiation inputs showed a consistent increase in summer (about 5%) but general decreases in other seasons, particularly winter and spring. Projected interannual variability in radiation showed little change in summer but increases in fall and winter.

Year-round projected increases in mean vapor pressure generally fell in the range 10%–25%, depending on the scenario. Winter vapor pressure was projected to increase by 30%–60% without appreciably affecting the annual mean change, because present-day winter values are typically much lower than in other seasons. Wind speed, in terms of both means and interannual variability, was projected to change little, either annually or seasonally.

Boreal Shield East

Projected increases in mean annual temperature by 2100 for the Boreal Shield East ecozone (Table 12) ranged from 3.0°C to 5.0°C for the minimum and from 2.5°C to 4.5°C for the maximum, depending on the scenario. As for other midcontinental ecozones, the projected warming was fairly uniform across spring, summer, and fall. However, the projected increases in winter maxima were only slightly greater than those in other seasons, whereas winter minima were projected to increase by as much 4.0°C to 7.0°C, depending on the scenario. There did not appear to be a general trend for changes in interannual temperature variability, except that spring and summer might become more variable with the extreme A2 scenario.

As with the Taiga Shield ecozone to the north, the eastern portion of the Boreal Shield ecozone receives significantly more annual precipitation than the west (compare Table 11). The projected increases for the two subzones were similar, at about 11% and 13% for west and east, respectively, by 2100 with both the A2 and A1B scenarios. These total increases were distributed unevenly, with the largest increases occurring in winter and spring and the smallest in summer. Again, similar to the Taiga Shield and the western Boreal Shield, radiation levels in the eastern Boreal Shield were projected to increase in summer (by 6%–7%) and to decrease in winter (by 10%–15%) and spring (by 3%–5%). Little change in interannual variability was projected, although winter radiation levels showed a trend of increasing variability with increasing GHG warming.

Present-day vapor pressure levels are generally similar to those in the western Boreal Shield, with the exception of winter, when the air is appreciably less humid in the west. Hence, the projected increases in vapor pressure for the eastern Boreal Shield were less dramatic than those in other northern ecozones, particularly in winter. Annual mean vapor pressure was projected to increase by 12%–25%, with increases of 20%–50% in winter and generally smaller increases in other seasons. Interannual variability in vapor pressure levels seemed likely to increase year-round, but there were no consistent trends among the three emissions scenarios. Wind speeds show little consistent change in terms of either means or variability.

Atlantic Maritime

The southeastern coastal region of Canada, the Atlantic Maritime ecozone (Table 13), is subject to the moderating effects of cool temperatures and high humidity from the North Atlantic Ocean. In this ecozone, projected increases in temperature by 2100 were nevertheless quite large, ranging from 2.5°C to 4.5°C for annual mean minimum temperature and from 2.0°C to 4.0°C for annual mean maximum temperature, depending on the emissions scenario. In particular, the minimum temperature in winter was projected to increase by as much as 6.0°C, with other seasons typically warming by about 4.0°C, according to the A2 scenario. Maximum temperatures were projected to increase by 2.0°C to 4.0°C year-round, depending on the scenario. Projected changes in interannual variability of temperature were inconsistent but suggested a general increase, particularly in spring, with increasing severity of the emissions scenario.

Present-day annual precipitation averages about 1200 mm, with an even seasonal distribution.

Projected increases were remarkably consistent for all emissions scenarios, ranging from about 8% to about 10%, with most of the increase occurring in winter and spring and the smallest increase in summer. Interannual variation was generally projected to increase with increasing GHG emissions, but the trend for individual seasons was less clear. Mean annual solar radiation was projected to change very little, but shifts in the seasonal distribution were forecast (possibly related to the trends in precipitation): summer radiation was projected to increase and winter radiation to decrease, with little change in fall and spring. This trend suggests that winters will generally be darker (by 5%–10%, depending on the scenario), whereas summer storms will be somewhat less frequent but more intense.

Present-day mean annual vapor pressure in the Atlantic Maritime ecozone is about 0.8 kPa, which is similar to that for the Pacific coast region (see Table 20) and second only to the Mixedwood Plains ecozone, which experiences considerable influence from the Great Lakes (see Table 14). With increasing GHG warming, the projected increases in vapor pressure in the Atlantic Maritime ecozone were 8%–30%, distributed fairly evenly throughout the year. Winter vapor pressure was still projected to increase the most in relative terms (by 15%–45%), but increasing in other seasons by 5%–25%, depending on the emissions scenario. In contrast, the general projection was for greater interannual variability, independent of the emissions scenario. Projections for changes in wind speed suggested slightly more wind in spring and winter, but less in other seasons, with little change in interannual variability, although these trends were not definitive.

Mixedwood Plains

The Mixedwood Plains ecozone (Table 14) occupies a relatively small area in southern Ontario (including the Niagara peninsula) and a corner of southern Quebec, making it the southernmost Canadian ecozone. The current climate is characterized by warm summers, long growing seasons, and high humidity because of the proximity to three of the Great Lakes. Projected increases in mean annual minimum and maximum temperatures were similar with the B1 scenario, but the increase in minimum temperature was projected to occur more quickly with the A1B and A2 scenarios. Hence, mean minimum and maximum temperatures were projected to increase by about 4.5°C and 4.0°C, respectively, by 2100. By then, assuming that the A2 scenario occurs, mean summer daily maximum temperatures will be about 30.0°C, with little change in interannual variability from the present day. This implies that midsummer heat waves, with daytime air temperatures exceeding 40.0°C, will be regular events. At the same time, atmospheric vapor pressure was projected to increase by about 25% over present-day values, regularly exceeding 2 kPa, which would imply extremely high humidity for much of the summer.

With all of the emissions scenarios, mean daily winter maxima in the Mixedwood Plains were projected to be above 0.0°C by 2100, which suggests that snow cover will persist only rarely in this region. Total annual precipitation was projected to increase by 5%–10% over present-day levels, with more than two-thirds of this increase occurring in winter and spring (although the MIROC32MR model exceptionally projected decreases in this variable). Interannual variability in rainfall events was projected to increase year-round. Annual radiation inputs were projected to change very little, but the seasonal distribution was projected to change markedly, related to the changes in distribution of precipitation. In particular, radiation levels were projected to increase in summer and fall and decrease by about 20% in winter with the A2 emissions scenario, which suggests that winters will be much darker and wetter than in the present day.

Projected trends in wind speed suggested small changes in annual means, but a tendency for more wind in winter and spring and less in summer and fall. Slight decreases in interannual variability were projected with the B1 and A1B scenarios, but the A2 scenario generally projected increases.

Boreal Plains

Located south of the western Boreal Shield, the Boreal Plains ecozone (Table 15) has a similar climate to that of the Boreal Shield West, although temperatures are about 1°C warmer on average. Projected increases in annual means were 2.5°C to 5.0°C for minimum temperature and 2.5°C to 4.0°C for maximum temperature by 2100, depending on the emissions scenario. Winter minima were projected to increase by 4.0°C to 6.5°C and winter maxima by 3.0°C to 4.5°C,

whereas summer temperatures, both minimum and maximum, were projected to increase by 2.5°C to 4.0°C. General projected trends also suggested that summer temperatures would become more variable and winter temperatures less so; trends for spring and fall were unclear.

Annual precipitation is about 500 mm at present and is projected to increase by 6%–12% by 2100, depending on the scenario. The increases were projected to be distributed fairly evenly across the seasons, with a general increase in interannual variability, particularly in summer and fall. Total solar radiation inputs were projected to decrease slightly (by 1%–2%), with much of the decrease occurring in winter but mostly offset by marginal increases in summer. Projections for interannual variation in solar radiation indicated slight increases for most of the year, but an inconsistent trend for summer. Annual vapor pressure was projected to increase by 8%–15%, with increases of 25%–50% during winter, accompanied by increased variability year-round. Wind speeds were projected to increase slightly in fall, winter, and spring and to change little in summer, with unclear changes in interannual variability.

Prairies Semiarid

The Prairies ecozone has been split into two regions for the purposes of forest carbon accounting: the Prairies Semiarid subzone (Table 16; discussed here) and the peripheral Prairies Subhumid subzone (see Table 17), which borders the Rocky Mountains to the west, the boreal forest to the north, and the mixedwood regions around Lake Winnipeg to the east. The semiarid subzone consists of largely treeless central grasslands, which extend south into the Great Plains region of the United States; in contrast, the subhumid subzone has significant tree cover.

The semiarid subzone of the Prairies is characterized by higher temperatures (and hence high evaporative demand) and relatively low annual precipitation. Present-day summer daily maximum temperatures average above 25°C, whereas winter minima average about –16.5°C, making this the warmest midcontinental ecozone in Canada. Mean annual precipitation is about 365 mm, which is higher than in the Arctic and comparable to the Taiga ecozones. Aridity results in the prairies because in most years, annual precipitation input is less than potential evapotranspiration.

By 2100, increases in annual minimum temperature in the semiarid subzone were projected to fall in the range 2.5°C to 4.5°C, and those for annual maximum temperature in the range 2.5°C to 4.0°C, depending on the emissions scenario. As for other Canadian ecozones, winter was projected to warm the most, with minimum temperature increasing by up to 5.5°C (A2 scenario), less than the projected summer increases of up to 4.5°C. Of particular interest is the projection that maximum temperature in summer will increase more than in winter, also by up to 4.5°C (A2 scenario). Projections for annual precipitation suggest relatively modest increases of 8%–15%, spread evenly throughout the year, coupled with some increase in interannual variation. Such trends imply that multiyear droughts will become more common and more intense in a region that was probably unusually humid during much of the 20th century (e.g., Sauchyn and Skinner 2001; Sauchyn et al. 2003).

At the same time, solar radiation levels were projected to increase slightly in summer, but to decrease in other seasons, particularly spring, with the changes being relatively consistent for all emissions scenarios. Vapor pressure levels were also projected to increase relatively uniformly: 12%–25% for the yearly mean, but 20%–30% during winter, depending on the scenario. These increases would offset some of the effects of warming on evaporative demand but would not prevent overall evaporation rates from increasing; as such, more frequent and severe droughts could be expected. Projections for wind speed appeared fairly consistent: little change occurred on average, but there were slight reductions in summer and increases in spring. However, the projected effects on interannual variation were inconsistent for all seasons.

Prairies Subhumid

In the subhumid subzone of the Prairies (Table 17), annual precipitation is currently about 100 mm higher than in the semiarid subzone (see Table 16), while mean temperatures are somewhat lower (about 2°C in winter and 1°C in summer for daily maximum). These differences generally allow evaporative demand to be met in most years, and hence the subhumid region supports more tree cover. (See discussion of the Prairies Semiarid ecozone and Table 16, above,

for the implications of low annual precipitation in the Prairie ecozone.)

The projected increases in temperature for the subhumid Prairies were similar in magnitude and pattern to those for the semiarid subzone (Table 16), although with the most extreme A2 scenario, winter values were projected to increase by about 1.0°C more (i.e., 6.5°C and 4.5°C for minimum and maximum, respectively), by 2100. Maximum temperature was generally projected to increase more in summer than in other seasons, although the differences between summer and winter warming were smaller and less consistent than projected for the Prairies Semiarid ecozone (Table 16).

Projected annual precipitation increases ranged from 5% to 12%, depending on the emissions scenario, with the increases occurring mainly in spring and rather less in other seasons. Summer in particular showed little consistent increase. This trend implies that the treed regions of the Canadian Prairie provinces are likely to come under increasingly frequent water stress, and the more southerly areas of this region may become subject to permanent dieback (see, for example, Hogg et al. 2008). These projected trends in precipitation change seem to correlate well with projected overall slight decreases in solar radiation by 2100: although solar inputs in summer were projected to increase slightly (by 1%–2%), those in winter and spring may decline by as much as 5%–10%, depending on the scenario. There was some suggestion that winter radiation will become more variable but that summer variability may decrease slightly. In addition, atmospheric vapor pressure levels were projected to increase by 2100, typically by 12%–25%, depending on the scenario, with larger increases (20%–40%) during winter and some suggestion of increased interannual variability, particularly in summer. Projected changes in wind speed suggest that summer may become slightly less windy, whereas spring may become more so, with increasing severity of the GHG forcing scenario; projections for interannual variability were inconsistent.

Taiga Cordillera

The Taiga Cordillera ecozone (Table 18) borders the Taiga Plains (Table 8) to the north and east, the Boreal Cordillera (Table 19) to the south, and Alaska to the west. Present-day annual mean daily minimum and maximum temperatures are about –13°C and –3°C, respectively, and total precipitation averages 420 mm. Projected temperature increases by 2100 ranged from 3.0°C to 5.5°C for the daily minimum and from 2.5°C to 4.5°C for the daily maximum, depending on the emissions scenario. For example, with the extreme A2 scenario, winter minimum temperature was projected to increase by up to 7.5°C, while summer maximum temperature was projected to increase by about 4.0°C. Interannual variability in summer temperatures was projected to increase, whereas all other seasons were projected to become appreciably less variable, although variability was projected to increase with the severity of GHG forcing (from the B1 to the A2 scenario).

Relative to the present day, annual precipitation was projected to increase by 12%–25% by 2100, depending on the scenario, with about two-thirds of the extra precipitation arriving in summer and fall, as typically projected for higher-latitude regions. Interannual variability in annual precipitation was also projected to increase, again in approximate proportion to the level of GHG forcing. Annual solar radiation input was projected to decrease appreciably, presumably in relation to the increased precipitation, with the largest proportional decreases in spring, fall, and winter. With the A2 scenario, radiation in these three seasons was projected to decrease by about 10% by 2100, with summer levels decreasing by about 5%. These changes in radiation were also correlated with projected increases in mean vapor pressure of up to 30% for spring, summer, and fall (according to both the A2 and A1B scenarios). The projected increases for winter ranged from 25% to more than 50%, depending on the scenario. Projections of changes in wind speed suggested slight increases in all seasons except fall, but no clear trends for changes in interannual variability.

Boreal Cordillera

Located south of the Taiga Cordillera ecozone (see Table 18), the western portions of the Boreal Cordillera ecozone (Table 19) have close proximity to the Pacific Ocean and hence are exposed to relatively moist maritime air and high annual precipitation. However, much of the ecozone lies further inland, where the climate is more closely related to that of

the Taiga Plains ecozone (see Table 8), and annual precipitation is therefore much lower. The area-weighted present-day mean annual precipitation in the Boreal Cordillera ecozone is about 460 mm, and precipitation was projected to increase by 10%–22% (depending on the emissions scenario) by 2100. Most of this increase was projected to occur in summer and fall, along with general increases in interannual variability, particularly in summer.

Projected increases in annual minimum temperature by 2100 ranged from about 2.5°C to 4.5°C, both yearly and during spring, summer, and fall, with the winter minimum projected to increase by 3.0°C to 6.0°C, depending on the emissions scenario. Increases of 2.0°C to 3.5°C were projected for annual mean maximum temperature, with both summer and winter means increasing rather more and the fall mean increasing less. Interannual variability was projected to increase for summer temperatures but generally to decrease in other seasons.

Projected changes in solar radiation were similar in pattern to those projected for the Taiga Cordillera (Table 18): general decreases of up to 10% annually (A2 scenario), with the largest proportional decreases occurring in spring and the smallest in summer. Interannual variability of radiation input was projected to increase in spring and summer but decrease in fall and winter. Annual mean vapor pressure was projected to increase by 15%–30% by 2100, depending on the scenario, with winter values increasing by 20%–45%. Large increases in interannual variability were also projected for vapor pressure, particularly in spring and summer. Slight increases were projected for mean wind speeds with no clear relation to the emission scenarios and small, inconsistent changes in variability.

Pacific Maritime

The Pacific coast experiences a uniquely mild and moist climate within Canada, reflected in the moderate mean temperatures and high precipitation amounts for the Pacific Maritime ecozone (Table 20). Present-day spatially weighted annual mean minimum temperature is about +1.0°C and maximum temperature about +9.0°C. Winter minimum temperature in this region averages about –5°C. Projected increases in annual means by 2100 were in the range 2.0°C to 3.5°C for the maximum, depending on the emissions scenario, and about 0.5°C greater for the minimum. The greatest increases were about 2.5°C to 4.0°C, projected for winter minima, but summer temperatures were projected to increase nearly as much. Interannual variability was projected to increase slightly in summer but decrease in other seasons, although the projections were inconsistent.

Present-day annual precipitation is just below 1850 mm per year (with considerable spatial variability). The projected increases ranged from 5% to 10%, with little difference between the A2 and A1B scenarios. There was a clear pattern suggesting that most of the increase would be distributed between fall and winter (with greater interannual variability), whereas spring precipitation would change little and summers would become slightly drier. These trends were confirmed by the projections of future solar radiation inputs: by 2100, this ecozone was projected to receive about 5% more radiation in summer (surprisingly consistent across all scenarios) but less in other seasons, particularly spring, when levels were projected to decrease by about 7% with the A2 scenario. Interannual variability in solar radiation levels was projected to decrease annually, but the seasonal distribution of this reduction showed no obvious trend.

The projected changes in vapor pressure were characterized by similar increases year-round, mainly because present-day winter temperatures are much warmer than in most other parts of Canada. These increases ranged from about 10% (B1 scenario) to 20% (A1B and A2 scenarios). Increased interannual variability was projected for spring and summer, with little change in fall and winter, but again the trends were inconsistent among the various GHG scenarios. Projections for changes in wind speed generally indicated slight increases, particularly in winter, but there were no consistent trends in variability.

Montane Cordillera

The Montane Cordillera ecozone (Table 21) is frequently exposed to relatively warm moist air from the Pacific ocean, which results in present-day mean temperatures only a few degrees cooler than those of the Pacific Maritime ecozone (Table 20) to the west and significantly warmer than those of the Boreal Plains (Table 15) to the east. Projected increases in both minimum and maximum temperatures by

2100 generally ranged from about 2.5°C to 4.0°C, depending on the emissions scenario. With the A2 scenario, the only exceptions were winter minimum temperature, projected to increase by about 5.0°C, and summer maximum temperature, projected to increase by about 4.5°C. Interannual variability in winter temperatures was projected to decline slightly, but changes in other seasons were projected to be smaller and less consistent.

Annual precipitation in the Montane Cordillera is markedly lower than in the Pacific Maritime ecozone (Table 21), averaging about 730 mm. Projected increases by 2100 ranged from about 6% to 12%, depending on the emissions scenario, distributed mainly through winter and fall, with marginal increases in summer and variability increasing slightly in all seasons. As noted for other ecozones, these changes in precipitation were correlated with projected changes in the solar radiation regime. Annual radiation inputs were projected to decline by up to 3% by 2100, with decreases of 5%–10% in winter and spring and increases of as much as 5% in summer with both the A1B and A2 scenarios. Interannual variability in radiation was projected to increase slightly, particularly in winter and fall. These projections suggest that rainfall events will become less frequent and more intense, leading to more frequent summer droughts and probable increased occurrence of wildfires.

Vapor pressure was projected to increase uniformly year-round, by as much as 25% (summer) to 30% (winter) by 2100, according to the A2 scenario, accompanied by increases in interannual variability, particularly in spring and summer. There were no apparent trends for projected changes in wind speeds or interannual variability in this variable.

Hudson Plains

The lowland regions immediately south of Hudson Bay are surrounded mainly by the western and eastern portions of the Boreal Shield ecozone (Tables 11 and 12, respectively), but the climate in the Hudson Plains (Table 22) is both cooler and drier than in the Boreal Shield, in spite of the proximity of Hudson Bay. Projected increases in annual mean temperatures by 2100 ranged from 3.5°C to 6.0°C for the minimum and from 3.0°C to 5.0°C for the maximum, depending on the emissions scenario. Increases in winter were projected to be about 9.5°C (minimum) and 7.0°C (maximum) with the A2 scenario, with warming of 5.0°C (minimum) and 4.0°C (maximum) projected for other seasons. Interannual variability in temperature was projected to decline in winter. Increases in interannual variability seem more probable in other seasons, but the trends were inconsistent among the emissions scenarios.

About two-thirds of present-day annual precipitation arrives in summer and fall. Projected increases by 2100 ranged from 6%–12%, depending on the emissions scenario. Of these, the largest proportional increases were projected for winter (20%–40%), with only marginal increases projected for summer. Interannual variability in precipitation was projected to increase generally, particularly in spring, fall, and winter. Consistent with these trends, solar radiation levels were projected to decrease by 10%–15% in winter and by 5%–10% in spring, depending on the emissions scenario, with summer levels expected to increase by 1%–5%. Interannual variability in solar radiation inputs was projected to increase, mainly in fall and winter.

Consistent with other northern continental ecozones, the relatively large projected increases in winter temperatures will drive major increases in winter vapor pressure, ranging from 40% (B1 scenario) to nearly 100% (A2 scenario) by 2100. Projected increases for other seasons ranged from about 10% to about 30%, depending on the scenario, with interannual variability projected to increase generally and quite substantially. Projections of changes in wind speeds suggested relatively consistent increases in mean values during fall, winter, and spring, and a general increase in interannual variability, particularly in fall and winter.

Table 5. Summary of projected climatic changes for the Arctic Cordillera ecozone (average of four general circulation models), measuring temperature, precipitation, solar radiation, vapor pressure, and wind speed

Climate variable	A2 emissions scenario ("pessimistic")					A1B emissions scenario ("medium")					B1 emissions scenario ("optimistic")				
	Spring	Summer	Fall	Winter	Year	Spring	Summer	Fall	Winter	Year	Spring	Summer	Fall	Winter	Year
Mean daily minimum temperature (°C)															
Baseline 1980–2009	−24.88	−1.92	−16.76	−33.19	−19.17	−24.95	−1.88	−16.70	−33.30	−19.20	−24.85	−1.86	−16.71	-33.00	-19.10
Change by 2010–2039	1.03	0.78	1.93	2.18	1.46	1.14	0.72	1.87	2.28	1.49	1.08	0.70	2.04	1.95	1.43
Change by 2040–2069	2.87	1.84	5.03	5.61	3.81	3.06	1.73	4.73	5.60	3.76	2.00	1.20	3.71	3.80	2.65
Change by 2070–2099	5.55	3.23	8.37	9.78	6.69	4.55	2.53	6.90	8.25	5.54	2.84	1.60	4.55	4.60	3.40
100-year forcing	6.08	3.50	9.24	10.46	7.30	5.01	2.84	7.84	8.82	6.12	3.40	1.93	5.47	5.47	4.09
100-year variability (%)	11.06	42.59	−1.16	28.94	47.34	−7.05	39.73	−17.27	−9.02	5.80	−14.27	−7.24	−19.76	-6.70	-19.51
Mean daily maximum temperature (°C)															
Baseline 1980–2009	−18.25	3.57	−11.43	−26.55	−13.15	−18.37	3.61	−11.35	−26.70	−13.20	−18.24	3.61	−11.38	-26.41	-13.10
Change by 2010–2039	0.75	0.70	1.69	1.64	1.18	0.89	0.64	1.65	1.83	1.24	0.80	0.65	1.76	1.53	1.17
Change by 2040–2069	2.22	1.68	4.46	4.99	3.31	2.52	1.59	4.16	5.05	3.32	1.54	1.09	3.27	3.35	2.29
Change by 2070–2099	4.45	3.03	7.44	8.98	5.93	3.72	2.37	6.14	7.63	4.95	2.24	1.46	4.04	4.00	2.95
100-year forcing	4.91	3.30	8.25	9.39	6.45	4.06	2.67	7.03	7.89	5.42	2.72	1.77	4.89	4.55	3.52
100-year variability (%)	5.82	76.74	-9.07	15.16	37.45	−6.38	69.45	−22.76	−13.84	2.63	−10.19	8.10	−22.36	-8.29	-19.95
Total precipitation (mm)															
Baseline 1980–2009	50	104	99	46	301	51	103	101	45	300	52	103	101	46	303
Change by 2010–2039	2	5	4	3	13	2	7	5	6	19	1	6	6	5	18
Change by 2040–2069	5	12	19	12	47	5	15	17	14	51	3	10	12	10	34
Change by 2070–2099	14	22	35	22	93	9	18	24	21	71	4	14	15	9	43
100-year forcing	14	24	38	24	99	9	19	29	21	77	6	16	20	11	52
100-year variability (%)	31.60	34.52	35.24	19.11	35.85	11.37	27.47	2.72	1.43	25.33	13.93	32.50	4.43	-15.16	20.98
Mean global solar radiation (MJ m^{-2} d^{-1})															
Baseline 1980–2009	13.50	17.43	2.36	0.89	8.55	13.39	17.45	2.34	0.89	8.52	13.40	17.41	2.34	0.89	8.51
Change by 2010–2039	−0.19	−0.52	−0.15	−0.02	−0.22	−0.13	−0.44	−0.14	−0.02	−0.18	−0.24	−0.41	−0.14	-0.02	-0.20
Change by 2040–2069	−0.59	−1.06	−0.35	−0.07	−0.52	−0.52	−1.09	−0.30	−0.06	−0.49	−0.38	−0.76	−0.27	-0.04	-0.36
Change by 2070–2099	−1.32	−1.73	−0.53	−0.12	−0.92	−0.95	−1.33	−0.42	−0.11	−0.70	−0.49	−1.02	−0.29	-0.05	-0.46
100-year forcing	−1.31	−1.85	−0.57	−0.12	−0.96	−1.05	−1.43	−0.48	−0.11	−0.77	−0.58	−1.16	−0.34	-0.06	-0.54
100-year variability (%)	18.39	24.04	−14.07	26.74	25.45	−3.51	21.16	−18.16	−7.14	9.35	2.13	15.30	−13.98	-9.23	7.97
Mean vapor pressure (kPa)															
Baseline 1980–2009	0.12	0.63	0.23	0.04	0.25	0.12	0.63	0.23	0.04	0.25	0.12	0.63	0.23	0.04	0.25
Change by 2010–2039	0.005	0.040	0.034	0.008	0.022	0.009	0.041	0.033	0.009	0.023	0.007	0.023	0.033	0.008	0.018
Change by 2040–2069	0.019	0.080	0.075	0.026	0.050	0.025	0.097	0.088	0.028	0.059	0.009	0.025	0.052	0.014	0.025
Change by 2070–2099	0.044	0.151	0.144	0.055	0.098	0.038	0.141	0.131	0.044	0.088	0.012	0.023	0.054	0.014	0.026
100-year forcing	0.048	0.163	0.152	0.057	0.105	0.041	0.154	0.144	0.045	0.096	0.016	0.038	0.061	0.017	0.033
100-year variability (%)	21.362	80.297	53.238	227.615	112.355	6.844	66.947	16.080	59.678	58.450	25.571	70.498	32.825	85.894	92.542
Mean wind speed (m s^{-1})															
Baseline 1980–2009	3.15	3.64	3.70	3.25	3.43	3.17	3.62	3.77	3.23	3.45	3.17	3.71	3.70	3.26	3.46
Change by 2010–2039	0.09	0.13	−0.03	−0.03	0.04	0.02	0.09	−0.02	0.00	0.02	0.16	0.05	0.06	0.01	0.07
Change by 2040–2069	0.13	0.04	0.00	−0.06	0.03	0.09	0.13	0.01	−0.03	0.06	0.11	−0.05	0.03	-0.02	0.02
Change by 2070–2099	0.10	0.28	0.06	−0.06	0.10	0.05	0.29	−0.05	−0.02	0.07	0.06	0.08	0.08	-0.03	0.05
100-year forcing	0.10	0.23	0.04	−0.04	0.09	0.07	0.22	0.00	−0.01	0.07	0.07	0.10	0.06	0.01	0.07
100-year variability (%)	0.05	−15.25	10.15	−10.48	−16.55	−3.13	8.01	6.07	6.63	6.33	−8.20	0.31	2.44	-9.04	-0.59

Table 6. Summary of projected climatic changes for the Northern Arctic ecozone (average of four general circulation models), measuring temperature, precipitation, solar radiation, vapor pressure, and wind speed

Climate variable	A2 emissions scenario ("pessimistic")					A1B emissions scenario ("medium")					B1 emissions scenario ("optimistic")				
	Spring	Summer	Fall	Winter	Year	Spring	Summer	Fall	Winter	Year	Spring	Summer	Fall	Winter	Year
Mean daily minimum temperature (°C)															
Baseline 1980–2009	−23.11	0.72	−14.10	−32.81	−17.31	−23.16	0.75	−14.04	−32.87	−17.32	−23.04	0.73	−14.07	−32.66	−17.25
Change by 2010–2039	1.02	0.78	1.90	2.35	1.50	1.13	0.71	1.78	2.40	1.48	1.02	0.73	2.00	2.00	1.42
Change by 2040–2069	3.05	1.81	4.91	5.87	3.87	3.16	1.77	4.58	5.93	3.83	2.04	1.22	3.50	3.90	2.63
Change by 2070–2099	5.60	3.35	8.16	10.83	6.93	4.59	2.66	6.81	8.92	5.72	2.92	1.60	4.45	5.14	3.53
100-year forcing	6.09	3.64	8.93	11.54	7.52	5.04	2.99	7.66	9.57	6.30	3.49	1.90	5.26	6.00	4.18
100-year variability (%)	9.83	65.76	−4.51	30.17	51.69	−3.41	60.60	−22.17	−0.13	12.91	−13.28	34.99	−15.35	−7.99	−13.68
Mean daily maximum temperature (°C)															
Baseline 1980–2009	−15.81	6.70	−8.48	−25.88	−10.85	−15.87	6.72	−8.40	−25.95	−10.87	−15.73	6.68	−8.45	−25.77	−10.81
Change by 2010–2039	0.76	0.77	1.58	1.91	1.25	0.85	0.69	1.47	2.00	1.23	0.71	0.80	1.65	1.63	1.18
Change by 2040–2069	2.34	1.79	4.18	5.32	3.37	2.49	1.82	3.85	5.45	3.37	1.52	1.23	2.95	3.49	2.27
Change by 2070–2099	4.27	3.49	6.96	10.00	6.13	3.55	2.73	5.77	8.25	5.05	2.23	1.60	3.80	4.67	3.08
100-year forcing	4.68	3.83	7.64	10.42	6.62	3.89	3.10	6.54	8.60	5.53	2.72	1.92	4.53	5.21	3.62
100-year variability (%)	0.57	75.23	−13.12	13.68	38.50	−7.25	67.39	−27.87	−4.86	9.55	−12.66	52.89	−20.00	−9.45	−14.01
Total precipitation (mm)															
Baseline 1980–2009	32	81	69	23	204	32	81	69	22	204	32	81	69	23	205
Change by 2010–2039	2	6	4	3	14	2	5	5	3	14	2	5	3	4	13
Change by 2040–2069	5	10	12	7	34	4	12	12	8	36	2	8	9	6	25
Change by 2070–2099	9	17	24	14	63	6	15	18	12	51	4	10	11	6	31
100-year forcing	10	17	26	14	67	7	15	21	12	55	5	11	14	7	36
100-year variability (%)	40.85	21.34	43.30	29.44	57.83	24.43	35.81	21.35	23.19	53.54	31.29	20.55	24.56	1.68	47.11
Mean global solar radiation (MJ m^{-2} d^{-1})															
Baseline 1980–2009	14.50	17.85	2.79	0.85	9.00	14.43	17.89	2.78	0.85	8.99	14.44	17.84	2.78	0.84	8.98
Change by 2010–2039	−0.17	−0.55	−0.19	−0.01	−0.23	−0.18	−0.54	−0.19	−0.01	−0.23	−0.23	−0.29	−0.18	−0.01	−0.18
Change by 2040–2069	−0.70	−1.21	−0.43	−0.04	−0.60	−0.58	−1.09	−0.39	−0.04	−0.53	−0.43	−0.81	−0.33	−0.02	−0.40
Change by 2070–2099	−1.33	−1.42	−0.66	−0.09	−0.88	−1.00	−1.19	−0.56	−0.08	−0.71	−0.63	−1.08	−0.39	−0.03	−0.53
100-year forcing	−1.36	−1.50	−0.71	−0.09	−0.92	−1.11	−1.23	−0.62	−0.08	−0.76	−0.73	−1.16	−0.44	−0.04	−0.59
100-year variability (%)	18.63	57.53	−21.68	3.70	43.95	3.31	55.86	−29.90	−4.89	31.14	1.43	42.55	−13.21	−16.68	24.84
Mean vapor pressure (kPa)															
Baseline 1980–2009	0.12	0.69	0.25	0.03	0.28	0.12	0.69	0.26	0.03	0.28	0.12	0.69	0.25	0.03	0.28
Change by 2010–2039	0.007	0.040	0.041	0.008	0.024	0.010	0.047	0.037	0.009	0.026	0.007	0.030	0.039	0.008	0.021
Change by 2040–2069	0.024	0.085	0.088	0.026	0.056	0.029	0.114	0.100	0.027	0.067	0.011	0.030	0.058	0.013	0.028
Change by 2070–2099	0.050	0.171	0.166	0.060	0.112	0.041	0.166	0.153	0.044	0.101	0.012	0.018	0.059	0.016	0.026
100-year forcing	0.054	0.185	0.173	0.062	0.118	0.045	0.182	0.168	0.046	0.110	0.016	0.031	0.066	0.018	0.033
100-year variability (%)	33.873	95.299	86.867	287.135	141.976	21.116	84.932	23.809	85.021	83.503	54.544	110.982	57.876	122.574	126.308
Mean wind speed (m s^{-1})															
Baseline 1980–2009	4.75	4.71	5.37	4.92	4.94	4.72	4.64	5.37	4.89	4.91	4.73	4.76	5.38	4.95	4.96
Change by 2010–2039	0.16	0.33	−0.20	0.02	0.07	0.09	0.32	−0.13	0.07	0.08	0.25	0.27	−0.08	−0.05	0.09
Change by 2040–2069	0.23	0.18	−0.06	0.19	0.13	0.24	0.43	0.20	0.23	0.27	0.24	0.22	0.02	0.15	0.15
Change by 2070–2099	0.26	0.69	0.20	0.43	0.39	0.17	0.65	0.25	0.37	0.36	0.25	0.47	0.09	0.16	0.24
100-year forcing	0.35	0.68	0.23	0.48	0.44	0.23	0.57	0.29	0.39	0.38	0.31	0.51	0.13	0.24	0.31
100-year variability (%)	14.18	12.41	11.30	13.47	5.37	−1.06	9.11	5.54	1.76	5.67	8.21	20.17	5.21	−8.80	0.84

Table 7. Summary of projected climatic changes for the Southern Arctic ecozone (average of four general circulation models), measuring temperature, precipitation, solar radiation, vapor pressure, and wind speed

Climate variable	A2 emissions scenario ("pessimistic")					A1B emissions scenario ("medium")					B1 emissions scenario ("optimistic")				
	Spring	Summer	Fall	Winter	Year	Spring	Summer	Fall	Winter	Year	Spring	Summer	Fall	Winter	Year
Mean daily minimum temperature (°C)															
Baseline 1980–2009	−19.26	3.62	−9.57	−30.62	−13.93	−19.29	3.60	−9.52	−30.64	−13.95	−19.05	3.57	−9.52	−30.44	−13.86
Change by 2010–2039	0.97	0.82	1.51	2.45	1.42	1.02	0.85	1.21	2.36	1.32	0.86	0.88	1.49	1.94	1.29
Change by 2040–2069	3.03	2.07	3.50	5.77	3.54	3.10	2.18	3.22	5.91	3.57	1.84	1.51	2.47	3.75	2.37
Change by 2070–2099	5.33	3.91	5.86	10.38	6.32	4.51	3.14	4.89	8.63	5.26	2.90	1.96	3.21	5.34	3.35
100-year forcing	5.79	4.27	6.33	11.14	6.86	4.94	3.49	5.41	9.37	5.79	3.57	2.28	3.73	6.29	3.97
100-year variability (%)	2.46	41.67	−7.74	−3.61	22.60	−8.51	11.43	−18.82	−10.82	3.01	−0.94	27.69	−14.92	−14.96	−9.67
Mean daily maximum temperature (°C)															
Baseline 1980–2009	−10.71	11.68	−3.69	−23.14	−6.45	−10.75	11.64	−3.61	−23.13	−6.44	−10.52	11.60	−3.64	−22.99	−6.38
Change by 2010–2039	0.74	0.77	1.26	1.91	1.16	0.77	0.87	0.94	1.81	1.05	0.61	0.95	1.21	1.46	1.05
Change by 2040–2069	2.37	1.97	2.96	4.91	3.00	2.38	2.27	2.62	5.08	3.05	1.39	1.45	2.05	3.14	1.99
Change by 2070–2099	4.03	4.06	5.02	8.96	5.47	3.44	3.18	4.11	7.41	4.51	2.19	1.94	2.72	4.66	2.87
100-year forcing	4.39	4.53	5.40	9.40	5.92	3.77	3.60	4.58	7.88	4.96	2.74	2.32	3.15	5.26	3.38
100-year variability (%)	−1.10	23.94	−8.80	−15.24	11.15	−11.22	0.37	−17.82	−15.43	−2.27	0.20	21.73	−12.33	−17.85	−12.34
Total precipitation (mm)															
Baseline 1980–2009	39	107	88	34	268	40	107	88	34	270	40	107	89	34	269
Change by 2010–2039	3	7	6	4	19	3	5	5	4	16	2	6	5	4	17
Change by 2040–2069	6	13	13	9	41	6	13	15	10	43	3	9	11	7	30
Change by 2070–2099	12	16	24	17	70	8	14	21	14	57	5	9	13	9	36
100-year forcing	13	16	27	18	74	10	15	23	15	62	6	9	16	10	41
100-year variability (%)	55.64	18.39	42.10	34.72	40.52	29.49	23.11	30.99	25.47	26.17	27.53	17.86	17.75	16.31	11.05
Mean global solar radiation (MJ m^{-2} d^{-1})															
Baseline 1980–2009	15.74	18.58	3.95	1.71	10.00	15.69	18.53	3.95	1.70	9.97	15.70	18.57	3.96	1.70	9.98
Change by 2010–2039	−0.26	−0.48	−0.21	−0.05	−0.25	−0.26	−0.27	−0.18	−0.04	−0.19	−0.31	−0.17	−0.22	−0.03	−0.18
Change by 2040–2069	−0.84	−0.79	−0.39	−0.12	−0.54	−0.82	−0.39	−0.40	−0.11	−0.43	−0.53	−0.57	−0.34	−0.07	−0.38
Change by 2070–2099	−1.65	−0.27	−0.59	−0.22	−0.68	−1.30	−0.36	−0.54	−0.19	−0.60	−0.83	−0.53	−0.42	−0.10	−0.47
100-year forcing	−1.73	−0.13	−0.64	−0.23	−0.68	−1.43	−0.28	−0.59	−0.19	−0.62	−0.95	−0.41	−0.46	−0.11	−0.49
100-year variability (%)	17.11	15.33	−17.06	26.49	16.13	11.56	6.90	−7.01	15.47	1.48	6.98	15.32	−9.45	−2.37	15.99
Mean vapor pressure (kPa)															
Baseline 1980–2009	0.17	0.81	0.36	0.04	0.34	0.17	0.81	0.37	0.04	0.35	0.17	0.81	0.35	0.04	0.34
Change by 2010–2039	0.007	0.045	0.041	0.010	0.026	0.011	0.057	0.036	0.011	0.029	0.006	0.041	0.036	0.009	0.023
Change by 2040–2069	0.028	0.103	0.085	0.028	0.061	0.038	0.142	0.097	0.032	0.077	0.013	0.057	0.053	0.014	0.034
Change by 2070–2099	0.057	0.209	0.153	0.060	0.120	0.054	0.198	0.147	0.048	0.112	0.017	0.051	0.055	0.019	0.035
100-year forcing	0.063	0.227	0.160	0.063	0.128	0.058	0.214	0.162	0.051	0.121	0.023	0.066	0.061	0.022	0.043
100-year variability (%)	17.457	77.714	68.886	152.384	100.632	14.376	45.654	31.133	69.566	58.128	30.486	124.348	42.661	102.084	109.325
Mean wind speed (m s^{-1})															
Baseline 1980–2009	5.22	4.88	5.73	5.13	5.25	5.25	4.85	5.78	5.16	5.26	5.16	4.88	5.70	5.18	5.23
Change by 2010–2039	0.09	0.36	−0.07	0.19	0.14	−0.01	0.37	−0.08	0.06	0.08	0.16	0.28	0.03	0.00	0.11
Change by 2040–2069	0.28	0.34	0.00	0.31	0.23	0.03	0.50	0.25	0.27	0.26	0.16	0.25	−0.01	0.16	0.14
Change by 2070–2099	0.25	0.68	0.34	0.73	0.50	0.12	0.71	0.27	0.53	0.41	0.23	0.50	0.20	0.22	0.29
100-year forcing	0.35	0.78	0.38	0.72	0.56	0.25	0.77	0.35	0.54	0.49	0.26	0.59	0.21	0.26	0.34
100-year variability (%)	16.20	17.89	−3.85	9.82	8.59	0.79	10.34	−13.16	13.02	−4.97	10.11	7.60	−8.54	−9.08	−12.36

Table 8. Summary of projected climatic changes for the Taiga Plains ecozone (average of four general circulation models), measuring temperature, precipitation, solar radiation, vapor pressure, and wind speed

Climate variable	A2 emissions scenario ("pessimistic")					A1B emissions scenario ("medium")					B1 emissions scenario ("optimistic")				
	Spring	Summer	Fall	Winter	Year	Spring	Summer	Fall	Winter	Year	Spring	Summer	Fall	Winter	Year
Mean daily minimum temperature (°C)															
Baseline 1980–2009	−11.44	7.64	−8.21	−27.67	−9.89	−11.50	7.56	−8.16	−27.54	−9.89	−11.27	7.54	−8.29	−27.56	−9.89
Change by 2010–2039	0.87	0.80	1.12	1.46	1.03	1.11	0.92	0.74	1.76	1.08	0.79	0.83	1.08	1.12	0.95
Change by 2040–2069	2.43	2.06	2.66	4.17	2.78	2.70	2.20	2.49	4.29	2.89	1.74	1.69	2.15	2.63	2.04
Change by 2070–2099	4.33	3.90	4.76	7.27	5.02	3.65	3.15	4.00	5.88	4.14	2.45	2.06	2.74	3.83	2.76
100-year forcing	4.87	4.28	5.07	7.97	5.54	4.14	3.44	4.36	6.71	4.66	3.17	2.34	2.97	4.65	3.28
100-year variability (%)	7.59	25.78	−24.80	−25.45	−8.30	−6.45	5.08	−21.56	−22.99	−7.80	3.29	10.51	−17.83	−21.42	−12.12
Mean daily maximum temperature (°C)															
Baseline 1980–2009	0.55	19.44	−0.03	−18.71	0.33	0.46	19.33	0.03	−18.58	0.33	0.69	19.27	−0.11	−18.63	0.31
Change by 2010–2039	0.70	0.74	0.94	1.15	0.86	0.82	0.87	0.59	1.36	0.86	0.64	0.77	0.93	0.81	0.79
Change by 2040–2069	1.91	1.90	2.23	3.39	2.32	2.08	2.11	2.07	3.46	2.40	1.39	1.62	1.79	2.04	1.70
Change by 2070–2099	3.31	3.68	4.03	5.84	4.18	2.85	2.87	3.35	4.74	3.43	1.98	1.89	2.37	3.18	2.35
100-year forcing	3.78	4.09	4.28	6.34	4.62	3.23	3.16	3.66	5.38	3.86	2.58	2.12	2.54	3.77	2.76
100-year variability (%)	3.77	14.86	−20.75	−30.00	−15.90	−8.46	3.43	−18.50	−24.66	−12.03	1.69	11.69	−18.48	−22.80	−18.43
Total precipitation (mm)															
Baseline 1980–2009	60	152	92	59	364	60	154	92	59	365	60	157	91	59	366
Change by 2010–2039	1	2	5	3	10	4	4	6	3	17	3	1	6	4	13
Change by 2040–2069	6	11	15	9	41	7	13	15	8	42	5	6	10	6	28
Change by 2070–2099	13	21	25	14	72	12	21	20	13	67	5	9	14	9	38
100-year forcing	14	20	27	16	76	14	22	23	15	73	6	13	16	10	44
100-year variability (%)	28.59	18.92	14.04	9.47	25.23	13.94	29.39	11.95	3.56	25.25	−9.75	21.45	−0.39	−13.05	6.56
Mean global solar radiation (MJ m^{-2} d^{-1})															
Baseline 1980–2009	14.94	19.04	4.51	1.71	10.05	14.89	19.00	4.51	1.71	10.03	14.95	18.92	4.53	1.71	10.03
Change by 2010–2039	−0.19	−0.17	−0.14	0.01	−0.12	−0.29	−0.16	−0.10	−0.01	−0.14	−0.26	−0.01	−0.12	0.01	−0.10
Change by 2040–2069	−0.63	−0.23	−0.27	−0.08	−0.30	−0.71	−0.06	−0.29	−0.04	−0.28	−0.53	−0.04	−0.24	−0.03	−0.21
Change by 2070–2099	−1.28	0.05	−0.41	−0.12	−0.44	−1.03	−0.18	−0.37	−0.11	−0.43	−0.61	−0.21	−0.27	−0.05	−0.29
100-year forcing	−1.35	0.12	−0.47	−0.13	−0.46	−1.15	−0.15	−0.42	−0.12	−0.46	−0.68	−0.26	−0.30	−0.07	−0.33
100-year variability (%)	31.67	3.57	3.09	−21.87	13.57	27.40	4.87	−0.78	−8.95	12.41	3.17	5.63	2.09	−14.33	7.29
Mean vapor pressure (kPa)															
Baseline 1980–2009	0.33	1.07	0.43	0.06	0.47	0.33	1.07	0.44	0.06	0.48	0.33	1.06	0.43	0.06	0.47
Change by 2010–2039	0.014	0.039	0.023	0.006	0.021	0.026	0.074	0.026	0.010	0.034	0.014	0.048	0.032	0.006	0.025
Change by 2040–2069	0.045	0.119	0.068	0.019	0.063	0.069	0.183	0.090	0.028	0.092	0.030	0.099	0.057	0.011	0.049
Change by 2070–2099	0.088	0.242	0.130	0.039	0.124	0.093	0.260	0.141	0.036	0.132	0.044	0.119	0.068	0.016	0.062
100-year forcing	0.096	0.262	0.139	0.041	0.134	0.101	0.281	0.157	0.040	0.145	0.056	0.138	0.075	0.019	0.072
100-year variability (%)	50.086	88.108	37.225	−0.055	63.008	18.199	50.662	4.903	18.840	26.491	6.690	45.550	−6.162	23.265	30.005
Mean wind speed (m s^{-1})															
Baseline 1980–2009	3.32	3.20	3.30	2.72	3.13	3.41	3.22	3.29	2.76	3.17	3.37	3.13	3.26	2.75	3.12
Change by 2010–2039	0.09	0.14	−0.12	0.11	0.05	−0.02	0.17	−0.08	0.09	0.04	−0.12	0.17	0.00	0.02	0.02
Change by 2040–2069	0.19	0.23	0.00	0.18	0.15	−0.07	0.23	0.00	0.18	0.09	0.07	0.22	0.03	0.00	0.08
Change by 2070–2099	0.24	0.32	0.16	0.41	0.28	0.01	0.18	0.04	0.24	0.12	0.05	0.23	0.07	0.17	0.14
100-year forcing	0.28	0.37	0.24	0.42	0.33	0.13	0.25	0.11	0.29	0.20	0.14	0.21	0.11	0.21	0.17
100-year variability (%)	22.56	7.67	7.95	8.07	7.69	13.64	−0.87	−0.64	1.80	7.37	−3.01	4.65	−5.54	−6.07	−4.39

Table 9. Summary of projected climatic changes for the Taiga Shield West ecozone (average of four general circulation models), measuring temperature, precipitation, solar radiation, vapor pressure, and wind speed

Climate variable	A2 emissions scenario ("pessimistic")					A1B emissions scenario ("medium")					B1 emissions scenario ("optimistic")				
	Spring	Summer	Fall	Winter	Year	Spring	Summer	Fall	Winter	Year	Spring	Summer	Fall	Winter	Year
Mean daily minimum temperature (°C)															
Baseline 1980–2009	−14.85	6.95	−7.25	−29.90	−11.23	−14.80	6.92	−7.20	−29.86	−11.21	−14.55	6.89	−7.26	−29.73	−11.15
Change by 2010–2039	0.83	0.84	1.28	1.88	1.19	0.99	0.97	0.99	2.18	1.23	0.82	0.94	1.34	1.57	1.15
Change by 2040–2069	2.62	2.22	3.14	4.74	3.12	2.83	2.52	2.85	5.23	3.31	1.58	1.66	2.32	3.14	2.16
Change by 2070–2099	4.59	4.15	5.27	8.65	5.62	3.89	3.36	4.47	7.23	4.69	2.50	2.13	2.96	4.59	3.03
100-year forcing	5.01	4.48	5.65	9.34	6.10	4.35	3.65	4.91	7.96	5.19	3.21	2.40	3.33	5.45	3.58
100-year variability (%)	2.80	27.75	−5.48	−20.05	13.07	−16.46	−2.45	−19.59	−11.74	−2.35	−0.24	16.39	−6.25	−17.07	−2.37
Mean daily maximum temperature (°C)															
Baseline 1980–2009	−3.82	17.01	−0.47	−21.12	−2.08	−3.82	16.97	−0.37	−21.07	−2.05	−3.52	16.90	−0.47	−20.99	−2.02
Change by 2010–2039	0.62	0.79	1.11	1.42	0.97	0.82	0.97	0.78	1.73	1.03	0.62	0.99	1.15	1.19	0.98
Change by 2040–2069	2.17	2.18	2.72	3.97	2.71	2.27	2.62	2.33	4.37	2.86	1.21	1.63	1.93	2.55	1.81
Change by 2070–2099	3.65	4.22	4.51	7.17	4.85	3.18	3.35	3.76	5.93	4.01	1.94	2.21	2.60	3.90	2.65
100-year forcing	3.97	4.59	4.81	7.63	5.24	3.51	3.67	4.16	6.45	4.43	2.56	2.47	2.90	4.50	3.10
100-year variability (%)	−0.31	10.85	−3.23	−28.80	−2.48	−16.90	−2.99	−13.11	−17.01	−7.10	−0.86	13.50	−3.10	−19.09	−9.92
Total precipitation (mm)															
Baseline 1980–2009	57	141	105	48	351	58	142	104	48	352	57	144	104	49	353
Change by 2010–2039	3	0	7	3	14	3	3	8	5	19	2	1	6	4	13
Change by 2040–2069	5	9	16	9	38	6	7	16	11	40	3	5	11	7	26
Change by 2070–2099	13	11	25	16	65	9	9	22	14	53	5	1	13	10	29
100-year forcing	14	9	29	17	70	11	9	25	14	58	6	3	15	11	35
100-year variability (%)	10.76	20.83	21.84	12.67	18.65	10.51	8.23	18.52	2.00	11.70	0.02	34.60	12.52	9.98	14.33
Mean global solar radiation (MJ m^{-2} d^{-1})															
Baseline 1980–2009	16.12	19.60	4.92	2.44	10.78	16.04	19.57	4.96	2.45	10.76	16.14	19.56	4.96	2.44	10.78
Change by 2010–2039	−0.29	−0.10	−0.17	−0.02	−0.15	−0.22	−0.05	−0.16	−0.05	−0.12	−0.34	0.10	−0.17	−0.02	−0.11
Change by 2040–2069	−0.65	−0.04	−0.31	−0.13	−0.28	−0.83	0.29	−0.38	−0.15	−0.27	−0.55	−0.07	−0.28	−0.08	−0.25
Change by 2070–2099	−1.38	0.42	−0.49	−0.25	−0.43	−1.05	0.25	−0.46	−0.23	−0.38	−0.79	0.11	−0.34	−0.12	−0.29
100-year forcing	−1.50	0.60	−0.55	−0.27	−0.43	−1.25	0.39	−0.49	−0.25	−0.40	−0.89	0.25	−0.36	−0.15	−0.29
100-year variability (%)	7.78	−4.93	−1.52	−1.85	3.57	−1.34	−2.11	9.99	8.53	2.97	5.06	7.78	12.66	9.31	13.82
Mean vapor pressure (kPa)															
Baseline 1980–2009	0.26	1.04	0.43	0.04	0.45	0.26	1.04	0.45	0.04	0.45	0.27	1.04	0.43	0.04	0.44
Change by 2010–2039	0.006	0.047	0.035	0.006	0.024	0.017	0.075	0.037	0.011	0.035	0.008	0.056	0.041	0.007	0.028
Change by 2040–2069	0.034	0.104	0.088	0.019	0.061	0.054	0.179	0.102	0.028	0.091	0.018	0.087	0.061	0.011	0.044
Change by 2070–2099	0.064	0.223	0.155	0.040	0.120	0.075	0.244	0.157	0.037	0.128	0.026	0.079	0.069	0.015	0.047
100-year forcing	0.070	0.238	0.164	0.042	0.129	0.081	0.259	0.174	0.039	0.138	0.035	0.089	0.077	0.018	0.055
100-year variability (%)	14.035	55.643	55.689	81.020	72.637	8.053	26.666	25.991	49.089	38.164	2.614	13.269	15.711	36.139	17.546
Mean wind speed (m s^{-1})															
Baseline 1980–2009	4.44	4.20	4.80	4.00	4.36	4.53	4.21	4.77	4.16	4.42	4.38	4.15	4.75	4.06	4.33
Change by 2010–2039	0.03	0.27	−0.02	0.30	0.14	−0.14	0.23	0.05	0.03	0.04	−0.03	0.22	0.19	0.11	0.12
Change by 2040–2069	0.25	0.31	0.23	0.28	0.27	−0.26	0.36	0.21	0.17	0.12	0.07	0.12	0.10	0.13	0.11
Change by 2070–2099	0.03	0.42	0.44	0.78	0.41	−0.04	0.42	0.30	0.31	0.25	−0.02	0.28	0.26	0.24	0.20
100-year forcing	0.11	0.52	0.53	0.72	0.47	0.14	0.53	0.37	0.41	0.37	0.00	0.33	0.31	0.23	0.23
100-year variability (%)	−4.15	6.34	5.25	26.34	5.94	2.63	6.72	−8.44	14.31	−2.10	5.47	0.88	1.17	3.52	0.45

Table 10. Summary of projected climatic changes for the Taiga Shield East ecozone (average of four general circulation models), measuring temperature, precipitation, solar radiation, vapor pressure, and wind speed

Climate variable	A2 emissions scenario ("pessimistic")					A1B emissions scenario ("medium")					B1 emissions scenario ("optimistic")				
	Spring	Summer	Fall	Winter	Year	Spring	Summer	Fall	Winter	Year	Spring	Summer	Fall	Winter	Year
Mean daily minimum temperature (°C)															
Baseline 1980–2009	−11.53	5.19	−3.44	−24.26	−8.49	−11.51	5.23	−3.46	−24.40	−8.52	−11.40	5.24	−3.37	−23.91	−8.36
Change by 2010–2039	0.64	1.02	1.28	2.62	1.37	0.67	0.91	1.10	2.19	1.19	0.75	0.94	0.94	1.97	1.16
Change by 2040–2069	2.57	2.47	2.70	5.61	3.29	2.64	2.51	2.64	5.78	3.35	1.66	1.64	1.84	3.65	2.18
Change by 2070–2099	4.77	4.31	4.55	9.31	5.70	3.96	3.43	3.83	8.10	4.80	2.62	2.28	2.44	4.80	3.04
100-year forcing	5.12	4.61	4.93	9.99	6.15	4.32	3.78	4.19	8.64	5.22	3.10	2.63	2.89	5.83	3.62
100-year variability (%)	1.33	49.81	4.98	−5.53	33.51	−22.21	12.96	−16.13	−13.35	−5.46	−6.79	12.38	−12.52	−14.53	−2.85
Mean daily maximum temperature (°C)															
Baseline 1980–2009	−1.41	15.48	3.23	−14.87	0.62	−1.42	15.49	3.22	−14.98	0.59	−1.26	15.51	3.31	−14.56	0.75
Change by 2010–2039	0.46	1.04	1.17	1.58	1.05	0.51	1.05	1.03	1.32	0.95	0.55	1.06	0.82	1.11	0.89
Change by 2040–2069	1.91	2.56	2.38	4.00	2.68	2.02	2.79	2.40	4.11	2.80	1.22	1.70	1.59	2.53	1.75
Change by 2070–2099	3.55	4.41	4.12	6.84	4.70	2.97	3.55	3.39	5.93	3.94	1.89	2.37	2.16	3.40	2.47
100-year forcing	3.78	4.75	4.46	7.11	5.02	3.19	3.90	3.73	6.09	4.22	2.27	2.74	2.59	3.97	2.91
100-year variability (%)	12.62	49.21	7.43	−14.83	30.91	−9.82	22.10	−1.74	−19.91	−1.81	2.73	17.59	−1.19	−19.16	0.86
Total precipitation (mm)															
Baseline 1980–2009	139	263	231	140	775	138	262	231	139	772	139	258	232	142	772
Change by 2010–2039	8	3	3	11	23	8	6	5	11	29	6	8	4	8	25
Change by 2040–2069	16	9	18	34	74	19	13	21	30	80	14	15	17	24	69
Change by 2070–2099	39	19	36	52	145	33	18	27	45	122	17	14	13	27	70
100-year forcing	42	24	39	55	160	35	22	30	48	134	20	14	17	31	82
100-year variability (%)	31.28	33.68	17.92	36.54	50.93	22.54	21.75	−0.01	22.19	20.32	4.97	15.40	1.74	11.24	17.32
Mean global solar radiation (MJ m^{-2} d^{-1})															
Baseline 1980–2009	15.73	17.23	5.61	3.90	10.62	15.70	17.17	5.62	3.92	10.60	15.75	17.24	5.62	3.87	10.62
Change by 2010–2039	−0.17	0.00	−0.08	−0.15	−0.10	−0.21	0.15	−0.07	−0.10	−0.06	−0.30	0.05	−0.08	−0.09	−0.11
Change by 2040–2069	−0.75	0.18	−0.27	−0.36	−0.30	−0.77	0.64	−0.23	−0.36	−0.18	−0.53	0.03	−0.21	−0.21	−0.23
Change by 2070–2099	−1.70	0.44	−0.39	−0.62	−0.57	−1.41	0.41	−0.38	−0.54	−0.48	−0.90	0.21	−0.23	−0.28	−0.30
100-year forcing	−1.84	0.52	−0.40	−0.65	−0.59	−1.58	0.43	−0.39	−0.56	−0.53	−1.02	0.31	−0.24	−0.34	−0.33
100-year variability (%)	24.02	10.15	−2.66	18.37	1.29	2.69	2.06	10.14	9.81	3.19	3.07	−2.86	0.29	8.15	1.98
Mean vapor pressure (kPa)															
Baseline 1980–2009	0.32	1.00	0.53	0.08	0.49	0.33	1.01	0.54	0.09	0.49	0.32	1.01	0.53	0.09	0.49
Change by 2010–2039	0.005	0.056	0.049	0.017	0.031	0.014	0.075	0.053	0.020	0.040	0.014	0.048	0.031	0.015	0.027
Change by 2040–2069	0.049	0.143	0.096	0.042	0.082	0.060	0.180	0.120	0.054	0.103	0.023	0.083	0.056	0.024	0.046
Change by 2070–2099	0.088	0.269	0.196	0.081	0.158	0.087	0.256	0.170	0.077	0.147	0.035	0.088	0.065	0.028	0.054
100-year forcing	0.093	0.289	0.201	0.085	0.167	0.097	0.277	0.185	0.081	0.160	0.042	0.109	0.076	0.034	0.065
100-year variability (%)	24.030	76.554	48.804	93.134	82.544	12.112	47.868	20.345	55.045	43.160	18.843	36.827	26.490	47.112	54.085
Mean wind speed (m s^{-1})															
Baseline 1980–2009	4.70	4.22	5.16	4.85	4.73	4.80	4.27	5.11	4.83	4.76	4.68	4.20	5.11	4.88	4.71
Change by 2010–2039	0.03	0.13	0.17	0.10	0.10	0.14	0.24	0.26	0.17	0.19	0.40	0.17	0.23	0.08	0.22
Change by 2040–2069	0.30	0.24	0.28	−0.01	0.21	−0.02	0.34	0.56	0.01	0.22	0.21	0.18	0.35	−0.05	0.19
Change by 2070–2099	0.43	0.37	0.47	0.21	0.37	0.17	0.30	0.39	0.14	0.25	0.21	0.31	0.45	−0.03	0.24
100-year forcing	0.46	0.38	0.51	0.22	0.39	0.30	0.35	0.38	0.13	0.29	0.23	0.30	0.44	0.01	0.24
100-year variability (%)	6.68	12.18	26.96	9.36	13.11	0.28	13.27	26.91	0.76	28.25	11.48	−0.96	19.27	−7.28	−4.50

Table 11. Summary of projected climatic changes for the Boreal Shield West ecozone (average of four general circulation models), measuring temperature, precipitation, solar radiation, vapor pressure, and wind speed

Climate variable	A2 emissions scenario ("pessimistic")					A1B emissions scenario ("medium")					B1 emissions scenario ("optimistic")				
	Spring	Summer	Fall	Winter	Year	Spring	Summer	Fall	Winter	Year	Spring	Summer	Fall	Winter	Year
Mean daily minimum temperature (°C)															
Baseline 1980–2009	−7.42	9.79	−2.26	−23.90	−5.93	−7.33	9.82	−2.24	−23.91	−5.89	−7.15	9.82	−2.30	−23.68	−5.83
Change by 2010–2039	0.87	1.03	1.24	1.86	1.24	1.00	1.19	1.02	2.15	1.31	0.64	0.97	1.10	1.49	1.05
Change by 2040–2069	2.35	2.59	2.78	4.39	2.98	2.56	2.77	2.65	4.84	3.17	1.41	1.79	2.04	3.08	2.07
Change by 2070–2099	4.28	4.41	4.50	7.47	5.14	3.47	3.51	3.79	6.47	4.26	2.14	2.33	2.58	4.17	2.80
100-year forcing	4.56	4.68	4.90	8.08	5.53	3.84	3.81	4.22	7.09	4.69	2.68	2.63	2.95	5.00	3.29
100-year variability (%)	11.72	31.79	9.99	−17.81	11.95	−16.05	6.51	−19.12	−8.42	−11.61	−1.72	2.24	−2.21	−16.50	−10.54
Mean daily maximum temperature (°C)															
Baseline 1980–2009	5.55	21.40	6.02	−12.92	5.02	5.68	21.42	6.03	−12.96	5.06	5.85	21.46	5.95	−12.76	5.12
Change by 2010–2039	0.67	1.07	1.16	1.22	1.03	0.85	1.27	1.07	1.57	1.16	0.54	0.95	1.06	0.91	0.87
Change by 2040–2069	2.04	2.71	2.67	3.21	2.62	2.10	2.92	2.50	3.47	2.72	1.14	1.82	1.86	2.17	1.74
Change by 2070–2099	3.64	4.61	4.24	5.35	4.44	2.89	3.61	3.57	4.65	3.64	1.78	2.49	2.55	3.04	2.46
100-year forcing	3.84	4.81	4.63	5.82	4.75	3.22	3.83	3.97	5.07	3.99	2.28	2.75	2.87	3.67	2.88
100-year variability (%)	7.56	20.25	15.77	−27.36	5.40	−11.66	12.53	−2.17	−17.69	−12.07	−6.69	6.63	8.03	−21.93	−11.60
Total precipitation (mm)															
Baseline 1980–2009	112	254	159	83	608	110	254	163	82	609	111	253	163	84	610
Change by 2010–2039	7	−5	6	4	11	5	3	1	8	17	2	3	2	3	10
Change by 2040–2069	9	1	11	12	33	16	−2	10	16	40	8	4	11	10	33
Change by 2070–2099	20	−2	19	22	59	20	5	12	18	55	10	−2	3	14	26
100-year forcing	23	5	17	24	69	21	13	15	19	67	12	6	5	16	38
100-year variability (%)	21.28	12.61	44.02	20.76	20.54	13.46	17.52	35.04	31.60	18.75	3.58	22.80	34.23	23.73	16.22
Mean global solar radiation (MJ m^{-2} d^{-1})															
Baseline 1980–2009	16.71	19.83	6.94	4.47	11.99	16.74	19.79	6.92	4.47	11.98	16.74	19.84	6.92	4.44	11.99
Change by 2010–2039	−0.25	0.19	−0.07	−0.11	−0.06	−0.19	0.20	0.06	−0.14	−0.02	−0.11	0.07	−0.02	−0.08	−0.04
Change by 2040–2069	−0.37	0.37	−0.04	−0.30	−0.08	−0.68	0.49	−0.11	−0.38	−0.17	−0.34	0.20	−0.07	−0.21	−0.11
Change by 2070–2099	−0.89	0.55	−0.20	−0.59	−0.29	−0.81	0.45	−0.16	−0.50	−0.26	−0.51	0.31	−0.06	−0.29	−0.14
100-year forcing	−0.98	0.57	−0.17	−0.62	−0.30	−0.87	0.43	−0.15	−0.53	−0.28	−0.56	0.34	−0.05	−0.34	−0.16
100-year variability (%)	5.59	−2.37	31.49	16.68	−4.15	5.48	1.37	31.28	31.76	6.35	−3.08	5.26	29.57	17.13	−0.18
Mean vapor pressure (kPa)															
Baseline 1980–2009	0.44	1.32	0.62	0.10	0.62	0.45	1.33	0.64	0.10	0.63	0.45	1.32	0.62	0.10	0.62
Change by 2010–2039	0.015	0.064	0.044	0.010	0.033	0.027	0.089	0.048	0.020	0.046	0.013	0.058	0.036	0.010	0.029
Change by 2040–2069	0.052	0.152	0.097	0.031	0.083	0.084	0.211	0.129	0.046	0.117	0.033	0.105	0.067	0.019	0.056
Change by 2070–2099	0.100	0.266	0.170	0.057	0.148	0.110	0.283	0.176	0.060	0.156	0.046	0.121	0.082	0.025	0.068
100-year forcing	0.109	0.286	0.182	0.061	0.159	0.121	0.307	0.196	0.064	0.172	0.058	0.141	0.093	0.031	0.080
100-year variability (%)	20.575	53.157	46.570	81.657	56.062	12.397	17.618	20.285	56.369	27.638	−0.075	19.338	6.071	17.601	12.503
Mean wind speed (m s^{-1})															
Baseline 1980–2009	3.70	3.29	3.95	3.32	3.56	3.66	3.33	3.82	3.37	3.55	3.62	3.32	3.87	3.37	3.54
Change by 2010–2039	0.02	0.14	0.01	0.23	0.10	−0.01	0.13	0.16	0.17	0.11	0.01	0.02	0.06	0.09	0.04
Change by 2040–2069	0.16	0.15	0.16	0.31	0.20	−0.15	0.21	0.17	0.26	0.12	0.13	0.09	0.08	0.12	0.11
Change by 2070–2099	0.10	0.16	0.16	0.63	0.26	0.07	0.10	0.33	0.27	0.19	0.02	0.03	0.13	0.21	0.10
100-year forcing	0.22	0.07	0.27	0.64	0.29	0.16	0.04	0.31	0.32	0.21	0.06	-0.04	0.17	0.26	0.11
100-year variability (%)	7.11	−1.12	12.17	24.95	6.82	7.97	−10.60	4.83	5.72	5.06	−0.49	−9.49	14.79	5.71	6.81

Table 12. Summary of projected climatic changes for the Boreal Shield East ecozone (average of four general circulation models), measuring temperature, precipitation, solar radiation, vapor pressure, and wind speed

Climate variable	A2 emissions scenario ("pessimistic")					A1B emissions scenario ("medium")					B1 emissions scenario ("optimistic")				
	Spring	Summer	Fall	Winter	Year	Spring	Summer	Fall	Winter	Year	Spring	Summer	Fall	Winter	Year
Mean daily minimum temperature (°C)															
Baseline 1980–2009	−5.79	8.91	−0.17	−18.98	−4.01	−5.76	8.93	−0.17	−19.06	−4.02	−5.57	8.94	−0.11	−18.69	−3.87
Change by 2010–2039	0.79	0.96	1.21	1.84	1.20	0.89	1.06	1.09	1.88	1.23	0.62	0.88	0.86	1.31	0.94
Change by 2040–2069	2.44	2.44	2.51	4.22	2.87	2.55	2.45	2.49	4.46	2.97	1.64	1.63	1.72	2.84	1.97
Change by 2070–2099	4.46	4.13	4.22	6.92	4.92	3.72	3.29	3.46	6.11	4.13	2.29	2.19	2.20	3.69	2.61
100-year forcing	4.73	4.39	4.57	7.46	5.28	4.02	3.57	3.80	6.58	4.48	2.78	2.48	2.61	4.52	3.10
100-year variability (%)	22.42	34.29	16.50	−4.89	29.67	−12.39	0.54	−6.49	−10.70	−4.41	2.47	−7.14	−9.24	−18.65	−7.76
Mean daily maximum temperature (°C)															
Baseline 1980–2009	5.69	20.42	8.34	−8.03	6.60	5.72	20.43	8.33	−8.10	6.59	5.91	20.50	8.40	−7.82	6.73
Change by 2010–2039	0.74	0.99	1.11	0.98	0.95	0.85	1.16	1.11	1.13	1.06	0.56	0.92	0.86	0.61	0.76
Change by 2040–2069	2.14	2.54	2.39	2.70	2.43	2.21	2.62	2.45	2.83	2.52	1.42	1.63	1.60	1.79	1.62
Change by 2070–2099	3.92	4.26	4.07	4.60	4.21	3.23	3.40	3.27	4.06	3.48	1.92	2.23	2.13	2.38	2.18
100-year forcing	4.14	4.51	4.46	4.85	4.48	3.49	3.66	3.64	4.24	3.74	2.37	2.56	2.58	2.83	2.58
100-year variability (%)	33.86	24.78	6.14	2.71	29.29	3.41	6.62	3.53	−3.90	7.00	13.59	−1.70	1.32	−10.07	−1.33
Total precipitation (mm)															
Baseline 1980–2009	209	313	277	212	1012	208	315	280	214	1018	209	308	281	216	1015
Change by 2010–2039	11	4	5	15	32	5	−3	8	16	26	0	0	1	7	7
Change by 2040–2069	18	2	16	38	71	24	2	13	32	70	16	16	18	28	77
Change by 2070–2099	33	2	29	58	120	36	4	22	48	110	22	9	8	30	67
100-year forcing	36	9	26	61	131	38	14	24	52	127	25	11	10	36	81
100-year variability (%)	14.75	28.28	47.57	30.66	52.73	22.75	24.84	13.75	11.01	10.25	4.76	6.25	29.23	9.58	7.41
Mean global solar radiation (MJ m^{-2} d^{-1})															
Baseline 1980–2009	15.66	18.75	7.41	5.17	11.75	15.69	18.72	7.38	5.14	11.74	15.68	18.82	7.39	5.10	11.75
Change by 2010–2039	−0.04	0.23	−0.01	−0.19	0.00	−0.02	0.33	0.08	−0.18	0.04	−0.04	0.18	0.08	−0.08	0.03
Change by 2040–2069	−0.28	0.47	−0.02	−0.48	−0.07	−0.48	0.71	0.06	−0.47	−0.05	−0.27	0.34	−0.03	−0.30	−0.07
Change by 2070–2099	−0.69	0.82	−0.05	−0.80	−0.18	−0.78	0.67	−0.04	−0.68	−0.21	−0.50	0.40	0.02	−0.37	−0.12
100-year forcing	−0.76	0.87	0.01	−0.83	−0.18	−0.82	0.71	0.00	−0.74	−0.21	−0.55	0.54	0.07	−0.47	−0.11
100-year variability (%)	0.91	0.23	10.49	15.52	10.68	0.61	9.99	3.86	9.70	19.45	9.59	−1.12	5.48	4.12	18.17
Mean vapor pressure (kPa)															
Baseline 1980–2009	0.48	1.31	0.72	0.16	0.67	0.49	1.32	0.73	0.16	0.68	0.49	1.31	0.72	0.16	0.67
Change by 2010–2039	0.021	0.081	0.057	0.018	0.044	0.029	0.093	0.065	0.028	0.054	0.016	0.056	0.033	0.015	0.030
Change by 2040–2069	0.073	0.172	0.115	0.048	0.102	0.090	0.210	0.149	0.064	0.128	0.042	0.100	0.061	0.027	0.058
Change by 2070–2099	0.130	0.311	0.209	0.087	0.184	0.132	0.300	0.200	0.090	0.180	0.052	0.119	0.073	0.033	0.069
100-year forcing	0.139	0.335	0.222	0.092	0.197	0.148	0.328	0.217	0.097	0.197	0.068	0.146	0.090	0.041	0.086
100-year variability (%)	52.968	95.494	39.818	45.418	86.359	23.141	29.772	21.427	38.391	46.210	45.479	65.752	39.267	46.697	102.680
Mean wind speed (m s^{-1})															
Baseline 1980–2009	4.15	3.52	4.18	4.30	4.03	4.19	3.57	4.13	4.30	4.05	4.13	3.53	4.13	4.36	4.03
Change by 2010–2039	0.04	−0.03	0.04	0.12	0.04	0.04	0.01	0.10	0.07	0.05	0.23	−0.04	0.08	−0.02	0.06
Change by 2040–2069	0.19	0.03	0.04	0.15	0.10	0.06	0.01	0.13	0.11	0.07	0.22	−0.03	0.11	−0.01	0.08
Change by 2070–2099	0.42	0.00	0.07	0.33	0.20	0.19	−0.07	0.08	0.20	0.10	0.14	−0.03	0.13	0.05	0.08
100-year forcing	0.44	−0.03	0.13	0.39	0.23	0.26	−0.05	0.09	0.26	0.14	0.14	−0.05	0.13	0.17	0.09
100-year variability (%)	13.75	−1.95	20.46	4.72	12.30	−5.63	−4.32	16.17	13.37	19.42	−4.00	−11.84	13.02	−1.70	10.23

Table 13. Summary of projected climatic changes for the Atlantic Maritime ecozone (average of four general circulation models), measuring temperature, precipitation, solar radiation, vapor pressure, and wind speed

Climate variable	A2 emissions scenario ("pessimistic")					A1B emissions scenario ("medium")					B1 emissions scenario ("optimistic")				
	Spring	Summer	Fall	Winter	Year	Spring	Summer	Fall	Winter	Year	Spring	Summer	Fall	Winter	Year
Mean daily minimum temperature (°C)															
Baseline 1980–2009	–2.06	11.17	2.59	–12.43	–0.19	–2.03	11.18	2.54	–12.50	–0.22	–1.86	11.19	2.64	–12.23	–0.09
Change by 2010–2039	0.74	0.92	1.09	1.43	1.05	0.79	1.02	1.08	1.59	1.14	0.46	0.80	0.80	1.06	0.81
Change by 2040–2069	2.16	2.28	2.33	3.42	2.53	2.25	2.34	2.39	3.58	2.64	1.50	1.59	1.64	2.34	1.78
Change by 2070–2099	3.94	3.86	4.00	5.57	4.35	3.36	3.22	3.35	4.93	3.73	2.02	2.11	2.07	2.96	2.31
100-year forcing	4.16	4.10	4.34	6.02	4.66	3.60	3.48	3.64	5.32	4.01	2.43	2.38	2.46	3.60	2.72
100-year variability (%)	22.35	26.72	13.32	0.79	31.00	–4.74	2.63	–6.00	–12.80	–3.80	5.62	–13.08	–13.36	–7.17	–6.79
Mean daily maximum temperature (°C)															
Baseline 1980–2009	7.97	22.17	11.63	–3.13	9.65	7.96	22.19	11.58	–3.18	9.62	8.13	22.21	11.67	–2.98	9.74
Change by 2010–2039	0.81	0.94	0.95	0.83	0.89	0.85	1.04	1.07	0.99	1.01	0.51	0.83	0.81	0.43	0.68
Change by 2040–2069	2.11	2.27	2.20	2.40	2.24	2.16	2.37	2.31	2.45	2.33	1.48	1.61	1.52	1.57	1.56
Change by 2070–2099	3.75	3.83	3.79	4.08	3.87	3.25	3.19	3.13	3.62	3.31	1.89	2.10	1.96	2.07	2.02
100-year forcing	3.99	4.04	4.17	4.26	4.11	3.48	3.42	3.46	3.75	3.53	2.29	2.35	2.37	2.40	2.35
100-year variability (%)	34.56	12.59	0.69	17.91	32.18	8.36	1.05	–4.51	2.80	8.74	18.60	–7.29	–11.93	7.19	–1.28
Total precipitation (mm)															
Baseline 1980–2009	285	308	315	310	1219	290	312	318	314	1234	290	307	317	311	1229
Change by 2010–2039	8	6	6	16	33	7	0	0	21	27	0	1	–4	9	4
Change by 2040–2069	21	6	–1	45	67	17	7	0	34	56	13	9	14	28	60
Change by 2070–2099	34	5	22	54	114	26	7	23	57	113	20	13	15	40	84
100-year forcing	34	10	20	56	119	32	16	25	62	134	26	17	15	43	99
100-year variability (%)	5.72	21.78	33.79	27.10	37.23	5.46	11.60	25.18	21.44	15.21	8.45	20.36	13.74	8.49	11.11
Mean global solar radiation (MJ m^{-2} d^{-1})															
Baseline 1980–2009	15.28	19.14	8.80	5.72	12.24	15.21	19.11	8.78	5.68	12.21	15.21	19.19	8.77	5.67	12.22
Change by 2010–2039	0.20	0.24	–0.04	–0.08	0.07	0.30	0.30	0.10	–0.12	0.13	0.23	0.17	0.11	–0.03	0.11
Change by 2040–2069	0.03	0.33	0.04	–0.32	0.02	0.02	0.60	0.14	–0.32	0.10	0.11	0.43	0.02	–0.17	0.09
Change by 2070–2099	–0.11	0.55	–0.01	–0.50	–0.02	–0.13	0.56	0.03	–0.42	0.00	–0.07	0.43	0.07	–0.24	0.04
100-year forcing	–0.06	0.59	0.09	–0.52	0.02	–0.15	0.55	0.10	–0.48	0.00	–0.09	0.50	0.13	–0.31	0.05
100-year variability (%)	–14.48	–12.49	2.12	1.97	–4.55	–8.61	–6.90	12.32	–5.47	–7.05	6.98	–2.71	–7.01	–3.34	11.05
Mean vapor pressure (kPa)															
Baseline 1980–2009	0.60	1.52	0.85	0.26	0.81	0.61	1.52	0.85	0.26	0.81	0.62	1.52	0.86	0.26	0.81
Change by 2010–2039	0.032	0.093	0.062	0.022	0.053	0.033	0.104	0.071	0.038	0.062	0.033	0.062	0.040	0.018	0.039
Change by 2040–2069	0.133	0.215	0.140	0.066	0.138	0.099	0.238	0.159	0.078	0.144	0.061	0.106	0.053	0.031	0.064
Change by 2070–2099	0.167	0.376	0.257	0.116	0.229	0.155	0.351	0.220	0.114	0.210	0.039	0.079	0.043	0.035	0.049
100-year forcing	0.178	0.394	0.274	0.120	0.242	0.173	0.379	0.235	0.123	0.227	0.062	0.100	0.063	0.044	0.067
100-year variability (%)	36.859	61.310	44.341	49.395	59.689	21.251	37.772	21.130	29.179	36.497	37.659	82.037	140.192	70.211	127.486
Mean wind speed (m s^{-1})															
Baseline 1980–2009	4.24	3.48	3.94	4.56	4.06	4.28	3.50	3.93	4.57	4.07	4.25	3.47	3.90	4.62	4.06
Change by 2010–2039	0.25	–0.04	0.04	0.15	0.09	0.13	–0.01	0.06	0.02	0.04	0.18	0.01	0.11	–0.07	0.06
Change by 2040–2069	0.35	0.05	0.03	0.18	0.15	0.30	–0.01	0.01	0.06	0.08	0.27	0.02	0.09	0.00	0.10
Change by 2070–2099	0.61	0.00	0.02	0.28	0.23	0.37	–0.03	0.01	0.17	0.13	0.26	0.00	0.08	0.02	0.09
100-year forcing	0.61	–0.03	0.04	0.33	0.24	0.42	–0.04	0.02	0.22	0.16	0.28	–0.03	0.06	0.12	0.11
100-year variability (%)	–3.91	–0.07	4.83	–5.21	0.61	–19.05	6.84	–6.54	2.21	–7.50	–8.54	–5.90	–10.13	–7.42	–0.59

Table 14. Summary of projected climatic changes for the Mixedwood Plains ecozone (average of four general circulation models), measuring temperature, precipitation, solar radiation, vapor pressure, and wind speed

Climate variable	A2 emissions scenario ("pessimistic")					A1B emissions scenario ("medium")					B1 emissions scenario ("optimistic")				
	Spring	Summer	Fall	Winter	Year	Spring	Summer	Fall	Winter	Year	Spring	Summer	Fall	Winter	Year
Mean daily minimum temperature (°C)															
Baseline 1980–2009	0.75	13.71	5.01	–9.81	2.40	0.79	13.76	5.01	–9.82	2.41	0.99	13.74	5.06	–9.59	2.52
Change by 2010–2039	1.12	1.01	1.19	1.36	1.18	1.22	1.15	1.24	1.74	1.36	0.62	0.89	0.87	0.88	0.85
Change by 2040–2069	2.58	2.45	2.48	3.22	2.67	2.73	2.42	2.57	3.42	2.79	1.84	1.71	1.78	2.31	1.94
Change by 2070–2099	4.35	4.14	4.21	5.26	4.50	3.72	3.25	3.30	4.70	3.76	2.30	2.23	2.15	2.81	2.39
100-year forcing	4.57	4.39	4.56	5.75	4.81	3.98	3.56	3.64	5.19	4.08	2.76	2.51	2.55	3.53	2.83
100-year variability (%)	4.37	6.17	11.13	–10.17	9.15	–27.96	–14.50	–9.26	–13.45	–12.76	–13.70	–22.17	–6.46	–17.13	–17.60
Mean daily maximum temperature (°C)															
Baseline 1980–2009	10.95	24.72	13.79	–1.78	11.90	10.99	24.82	13.83	–1.81	11.94	11.15	24.87	13.87	–1.63	12.04
Change by 2010–2039	1.13	1.03	1.17	0.75	1.04	1.20	1.18	1.38	1.11	1.24	0.69	0.88	0.97	0.38	0.76
Change by 2040–2069	2.49	2.57	2.65	2.20	2.48	2.65	2.47	2.65	2.30	2.53	1.81	1.55	1.82	1.55	1.70
Change by 2070–2099	4.35	4.27	4.42	3.88	4.24	3.64	3.33	3.36	3.47	3.46	2.20	2.29	2.28	1.93	2.20
100-year forcing	4.61	4.48	4.78	4.15	4.49	3.95	3.64	3.75	3.70	3.74	2.67	2.64	2.72	2.34	2.58
100-year variability (%)	20.03	5.17	12.13	21.13	25.91	–15.87	–2.70	–0.44	10.64	5.09	0.61	–6.45	–3.40	7.17	–7.03
Total precipitation (mm)															
Baseline 1980–2009	215	254	249	220	940	215	252	253	220	938	216	249	254	223	941
Change by 2010–2039	14	6	6	14	38	12	5	10	12	40	3	1	–2	7	8
Change by 2040–2069	20	–1	14	30	63	20	9	10	23	62	16	25	12	20	72
Change by 2070–2099	26	4	18	48	94	26	11	15	37	90	26	4	0	20	50
100-year forcing	27	11	19	49	104	27	16	19	38	98	28	5	5	24	62
100-year variability (%)	12.41	19.49	35.76	30.74	37.44	9.05	14.24	6.17	18.18	13.36	–0.07	3.14	11.44	20.42	6.95
Mean global solar radiation (MJ m^{-2} d^{-1})															
Baseline 1980–2009	16.42	20.90	9.18	6.18	13.18	16.45	20.96	9.20	6.13	13.19	16.38	21.03	9.18	6.11	13.19
Change by 2010–2039	–0.10	0.25	0.06	–0.26	–0.02	–0.08	0.25	0.18	–0.24	0.01	0.00	0.14	0.18	–0.09	0.04
Change by 2040–2069	–0.21	0.43	0.21	–0.54	–0.03	–0.25	0.49	0.17	–0.50	–0.03	–0.13	0.19	0.14	–0.34	–0.04
Change by 2070–2099	–0.13	0.58	0.28	–0.89	–0.05	–0.27	0.42	0.18	–0.71	–0.11	–0.25	0.39	0.26	–0.38	0.00
100-year forcing	–0.07	0.61	0.32	–0.94	–0.03	–0.19	0.50	0.24	–0.82	–0.07	–0.23	0.55	0.30	–0.50	0.03
100-year variability (%)	–13.68	–1.07	4.41	–17.42	–13.38	–17.79	0.23	0.35	–13.88	–14.79	–7.17	–1.13	–11.61	–17.84	–10.74
Mean vapor pressure (kPa)															
Baseline 1980–2009	0.70	1.69	0.99	0.31	0.92	0.71	1.69	0.99	0.31	0.92	0.70	1.66	0.99	0.31	0.92
Change by 2010–2039	0.042	0.125	0.082	0.024	0.069	0.055	0.128	0.090	0.046	0.081	0.016	0.079	0.045	0.018	0.040
Change by 2040–2069	0.091	0.226	0.174	0.066	0.139	0.126	0.256	0.198	0.090	0.168	0.067	0.145	0.076	0.045	0.084
Change by 2070–2099	0.164	0.387	0.262	0.117	0.233	0.178	0.354	0.247	0.132	0.228	0.081	0.180	0.098	0.052	0.103
100-year forcing	0.178	0.433	0.293	0.128	0.258	0.199	0.392	0.271	0.146	0.252	0.099	0.201	0.133	0.066	0.125
100-year variability (%)	70.429	64.308	86.412	34.145	119.982	19.218	21.373	12.209	30.784	23.246	27.791	4.350	–4.552	16.712	2.305
Mean wind speed (m s^{-1})															
Baseline 1980–2009	3.98	3.07	3.65	4.27	3.74	3.95	3.16	3.68	4.29	3.76	3.95	3.06	3.65	4.38	3.76
Change by 2010–2039	0.20	–0.11	0.01	0.25	0.08	–0.01	–0.08	–0.04	0.25	0.04	0.12	–0.08	–0.03	–0.06	–0.01
Change by 2040–2069	0.21	–0.02	–0.02	0.36	0.14	0.16	–0.18	–0.06	0.19	0.03	0.16	–0.07	0.04	0.09	0.06
Change by 2070–2099	0.52	–0.23	–0.04	0.45	0.18	0.33	–0.19	–0.07	0.24	0.08	0.09	–0.08	–0.04	0.12	0.02
100-year forcing	0.53	–0.29	–0.03	0.48	0.17	0.30	–0.17	–0.04	0.29	0.10	0.07	–0.15	–0.02	0.26	0.04
100-year variability (%)	6.09	1.17	11.25	11.58	12.73	–11.45	2.14	–10.87	14.54	8.43	–1.60	–1.38	–9.31	25.49	11.60

Table 15. Summary of projected climatic changes for the Boreal Plains ecozone (average of four general circulation models, measuring temperature, precipitation, solar radiation, vapor pressure, and wind speed

Climate variable	A2 emissions scenario ("pessimistic")					A1B emissions scenario ("medium")					B1 emissions scenario ("optimistic")				
	Spring	Summer	Fall	Winter	Year	Spring	Summer	Fall	Winter	Year	Spring	Summer	Fall	Winter	Year
Mean daily minimum temperature (°C)															
Baseline 1980–2009	–4.92	9.10	–3.12	–20.76	–4.92	–4.90	9.07	–3.07	–20.59	–4.87	–4.80	9.06	–3.23	–20.56	–4.90
Change by 2010–2039	0.60	0.91	1.08	1.44	1.01	1.04	1.12	0.73	1.73	1.14	0.72	0.89	1.01	1.18	0.96
Change by 2040–2069	2.11	2.36	2.41	3.93	2.66	2.36	2.52	2.36	4.00	2.80	1.27	1.76	1.88	2.62	1.90
Change by 2070–2099	3.89	4.18	4.00	6.28	4.58	3.10	3.40	3.51	5.36	3.82	2.05	2.30	2.45	3.51	2.59
100-year forcing	4.28	4.49	4.31	6.88	4.99	3.51	3.68	3.88	6.10	4.28	2.56	2.57	2.66	4.28	3.03
100-year variability (%)	0.80	21.25	–3.33	–26.92	–0.97	–7.31	6.36	–24.00	–12.05	–4.69	–9.70	12.65	–15.38	–15.47	–11.83
Mean daily minimum temperature (°C)															
Baseline 1980–2009	7.91	21.75	7.19	–9.70	6.78	7.97	21.70	7.21	–9.61	6.81	8.07	21.70	7.04	–9.57	6.79
Change by 2010–2039	0.46	0.96	0.91	1.03	0.85	0.88	1.14	0.71	1.30	1.00	0.62	0.78	0.94	0.74	0.78
Change by 2040–2069	1.81	2.43	2.22	2.87	2.30	1.88	2.55	2.17	2.83	2.35	1.03	1.80	1.73	1.83	1.61
Change by 2070–2099	3.27	4.13	3.61	4.50	3.88	2.57	3.38	3.30	3.90	3.27	1.77	2.37	2.41	2.59	2.30
100-year forcing	3.57	4.33	3.90	4.98	4.20	2.93	3.53	3.60	4.46	3.63	2.23	2.51	2.55	3.19	2.63
100-year variability (%)	1.96	3.23	9.32	–23.98	1.62	–4.77	12.05	–9.62	–10.97	–0.55	–9.11	8.27	–2.89	–14.54	–5.75
Total precipitation (mm)															
Baseline 1980–2009	92	231	104	70	497	92	229	105	70	495	90	232	106	69	498
Change by 2010–2039	2	–8	6	3	3	4	3	3	4	14	2	8	2	4	16
Change by 2040–2069	8	0	8	8	24	9	5	9	7	30	6	6	9	6	26
Change by 2070–2099	18	6	19	13	55	15	10	12	13	50	6	2	4	8	21
100-year forcing	20	14	19	15	68	17	16	14	14	60	7	12	6	9	33
100-year variability (%)	7.62	20.64	35.44	24.64	25.46	25.96	20.12	21.65	–8.08	28.82	6.30	13.13	13.56	1.41	14.62
Mean global solar radiation (MJ m^{-2} d^{-1})															
Baseline 1980–2009	16.46	20.54	7.20	3.94	12.04	16.44	20.51	7.19	3.93	12.02	16.51	20.49	7.16	3.94	12.03
Change by 2010–2039	–0.17	0.17	–0.14	–0.05	–0.05	–0.20	0.14	–0.03	–0.05	–0.04	–0.18	0.04	–0.03	–0.05	–0.06
Change by 2040–2069	–0.47	0.31	–0.12	–0.20	–0.12	–0.66	0.40	–0.19	–0.22	–0.17	–0.44	0.23	–0.09	–0.14	–0.11
Change by 2070–2099	–0.97	0.44	–0.32	–0.39	–0.31	–0.84	0.40	–0.21	–0.33	–0.25	–0.47	0.28	–0.08	–0.18	–0.12
100-year forcing	–1.05	0.40	–0.31	–0.42	–0.35	–0.94	0.32	–0.21	–0.37	–0.30	–0.50	0.17	–0.10	–0.21	–0.17
100-year variability (%)	6.40	–5.27	17.02	7.06	–1.72	12.45	3.52	19.18	8.08	11.64	7.67	4.04	9.85	4.44	10.34
Mean vapor pressure (kPa)															
Baseline 1980–2009	0.51	1.28	0.60	0.13	0.63	0.51	1.29	0.62	0.14	0.64	0.51	1.28	0.60	0.14	0.63
Change by 2010–2039	0.009	0.059	0.039	0.011	0.030	0.038	0.092	0.036	0.021	0.047	0.019	0.058	0.036	0.014	0.031
Change by 2040–2069	0.056	0.141	0.085	0.037	0.079	0.093	0.210	0.111	0.048	0.115	0.035	0.107	0.061	0.021	0.056
Change by 2070–2099	0.108	0.267	0.157	0.061	0.148	0.120	0.291	0.164	0.063	0.159	0.053	0.128	0.078	0.028	0.072
100-year forcing	0.120	0.289	0.164	0.066	0.160	0.131	0.314	0.182	0.070	0.174	0.065	0.147	0.083	0.035	0.083
100-year variability (%)	17.767	52.092	33.663	25.584	58.393	20.828	20.312	3.000	23.985	21.976	5.128	31.231	–3.285	13.990	26.178
Mean wind speed (m s^{-1})															
Baseline 1980–2009	3.54	3.04	3.51	3.15	3.31	3.58	3.10	3.42	3.17	3.32	3.55	3.05	3.42	3.20	3.30
Change by 2010–2039	0.05	0.13	–0.04	0.13	0.07	–0.06	0.10	0.08	0.23	0.08	–0.05	0.05	0.05	0.00	0.01
Change by 2040–2069	0.13	0.14	0.10	0.28	0.16	–0.03	0.06	0.08	0.23	0.08	0.06	0.09	0.10	0.02	0.07
Change by 2070–2099	0.18	0.15	0.12	0.41	0.22	0.05	0.02	0.21	0.25	0.13	–0.06	0.05	0.08	0.16	0.06
100-year forcing	0.27	0.06	0.23	0.42	0.24	0.18	–0.02	0.22	0.28	0.16	0.04	–0.04	0.09	0.22	0.07
100-year variability (%)	–0.82	4.45	3.27	10.79	–6.84	4.30	–14.87	–4.11	6.67	–3.23	–1.13	–3.55	4.72	9.78	–4.21

Table 16. Summary of projected climatic changes for the Prairies Semiarid ecozone (average of four general circulation models), measuring temperature, precipitation, solar radiation, vapor pressure, and wind speed

Climate variable	A2 emissions scenario ("pessimistic")					A1B emissions scenario ("medium")					B1 emissions scenario ("optimistic")				
	Spring	Summer	Fall	Winter	Year	Spring	Summer	Fall	Winter	Year	Spring	Summer	Fall	Winter	Year
Mean daily minimum temperature (°C)															
Baseline 1980–2009	–2.14	10.46	–1.66	–16.41	–2.42	–2.04	10.45	–1.59	–16.37	–2.37	–2.05	10.51	–1.76	–16.36	–2.40
Change by 2010–2039	0.49	1.06	1.08	1.50	1.03	1.04	1.31	0.83	1.89	1.26	0.74	0.96	1.01	1.30	0.98
Change by 2040–2069	2.05	2.66	2.34	3.56	2.59	2.16	2.80	2.36	3.64	2.71	1.22	1.81	1.83	2.72	1.89
Change by 2070–2099	3.63	4.52	3.83	5.29	4.30	2.79	3.70	3.42	4.78	3.64	1.92	2.51	2.46	3.46	2.57
100-year forcing	3.85	4.81	4.11	5.82	4.63	3.11	3.99	3.76	5.34	4.01	2.24	2.85	2.63	4.04	2.91
100-year variability (%)	–8.01	29.81	18.28	–27.70	6.08	–12.09	8.27	–12.48	–14.02	–4.29	–14.56	14.45	–7.14	–18.84	–11.05
Mean daily maximum temperature (°C)															
Baseline 1980–2009	10.72	25.34	11.39	–5.76	10.43	10.86	25.25	11.37	–5.74	10.45	10.86	25.36	11.16	–5.72	10.42
Change by 2010–2039	0.36	1.04	0.90	0.98	0.82	0.98	1.31	0.79	1.31	1.09	0.66	0.95	1.04	0.82	0.86
Change by 2040–2069	1.90	2.78	2.33	2.47	2.33	1.95	2.86	2.27	2.48	2.37	1.06	1.82	1.86	1.89	1.66
Change by 2070–2099	3.42	4.45	3.63	3.84	3.83	2.61	3.89	3.54	3.47	3.35	1.78	2.63	2.61	2.44	2.35
100-year forcing	3.65	4.73	4.00	4.27	4.15	2.98	4.09	3.90	3.92	3.69	2.14	2.94	2.76	2.90	2.66
100-year variability (%)	4.50	11.42	15.34	–19.66	14.91	–2.03	4.49	–3.38	–7.16	–1.92	–14.78	9.99	–0.90	–15.75	–0.11
Total precipitation (mm)															
Baseline 1980–2009	91	162	61	51	365	89	160	63	52	364	87	160	63	50	361
Change by 2010–2039	6	5	4	4	19	5	3	3	2	13	5	5	4	4	17
Change by 2040–2069	11	–6	5	6	16	9	6	8	4	28	10	10	5	6	30
Change by 2070–2099	17	5	15	11	47	15	5	4	8	32	10	8	1	7	26
100-year forcing	19	12	11	12	54	16	10	3	9	38	8	13	1	6	28
100-year variability (%)	38.04	3.91	26.94	55.00	20.16	11.10	9.92	17.11	17.80	12.87	4.07	23.25	10.14	13.67	19.94
Mean global solar radiation (MJ m^{-2} d^{-1})															
Baseline 1980–2009	17.43	22.40	9.42	5.46	13.68	17.44	22.31	9.37	5.45	13.65	17.54	22.36	9.35	5.48	13.68
Change by 2010–2039	–0.25	0.10	–0.12	–0.11	–0.10	–0.18	0.20	–0.07	–0.12	–0.05	–0.31	0.12	–0.06	–0.09	–0.09
Change by 2040–2069	–0.44	0.37	–0.10	–0.28	–0.11	–0.50	0.39	–0.16	–0.31	–0.15	–0.46	0.16	–0.05	–0.25	–0.15
Change by 2070–2099	–0.81	0.34	–0.31	–0.46	–0.32	–0.72	0.45	–0.12	–0.39	–0.20	–0.54	0.32	–0.02	–0.28	–0.13
100-year forcing	–0.85	0.34	–0.21	–0.49	–0.31	–0.75	0.36	–0.06	–0.43	–0.22	–0.48	0.29	0.02	–0.29	–0.12
100-year variability (%)	3.81	–6.95	–5.84	13.75	–3.92	1.02	–5.83	–1.04	12.82	–0.48	4.98	–9.90	–12.09	–0.88	–11.65
Mean vapor pressure (kPa)															
Baseline 1980–2009	0.61	1.33	0.66	0.20	0.70	0.62	1.34	0.67	0.20	0.71	0.61	1.33	0.66	0.20	0.70
Change by 2010–2039	0.016	0.068	0.029	0.016	0.032	0.045	0.100	0.045	0.030	0.055	0.028	0.054	0.031	0.017	0.033
Change by 2040–2069	0.057	0.130	0.074	0.044	0.075	0.094	0.210	0.118	0.055	0.119	0.047	0.127	0.063	0.030	0.067
Change by 2070–2099	0.116	0.259	0.146	0.066	0.147	0.128	0.287	0.165	0.073	0.162	0.068	0.145	0.083	0.038	0.083
100-year forcing	0.125	0.286	0.155	0.074	0.160	0.137	0.313	0.180	0.082	0.177	0.074	0.165	0.091	0.046	0.094
100-year variability (%)	14.809	50.187	44.260	16.366	65.439	13.063	25.212	18.170	21.450	34.095	14.104	20.865	4.295	7.468	28.379
Mean wind speed (m s^{-1})															
Baseline 1980–2009	4.95	4.13	4.65	4.70	4.60	4.91	4.17	4.52	4.69	4.58	4.94	4.15	4.59	4.77	4.60
Change by 2010–2039	0.09	0.01	–0.07	0.10	0.03	–0.07	0.02	0.01	0.20	0.04	–0.13	–0.08	–0.12	–0.15	–0.11
Change by 2040–2069	–0.02	–0.02	–0.13	0.18	0.00	0.11	–0.14	–0.03	0.03	–0.01	–0.08	–0.13	–0.03	–0.02	–0.05
Change by 2070–2099	0.15	–0.15	–0.21	0.03	–0.04	–0.04	–0.28	0.02	0.10	–0.05	–0.17	–0.18	–0.13	–0.06	–0.13
100-year forcing	0.30	–0.26	–0.09	0.05	0.00	0.08	–0.35	0.01	0.12	–0.04	–0.02	–0.27	–0.07	0.04	–0.09
100-year variability (%)	–4.26	13.32	0.36	12.60	–9.15	–2.67	–8.53	–14.15	12.06	–1.40	11.92	–3.82	–6.62	20.23	–7.32

Table 17. Summary of projected climatic changes for the Prairies Subhumid ecozone (average of four general circulation models), measuring temperature, precipitation, solar radiation, vapor pressure, and wind speed

Climate variable	A2 emissions scenario ("pessimistic")					A1B emissions scenario ("medium")					B1 emissions scenario ("optimistic")				
	Spring	Summer	Fall	Winter	Year	Spring	Summer	Fall	Winter	Year	Spring	Summer	Fall	Winter	Year
Mean daily minimum temperature (°C)															
Baseline 1980–2009	−2.87	10.44	−1.62	−18.36	−3.09	−2.78	10.44	−1.57	−18.29	−3.03	−2.75	10.48	−1.72	−18.20	−3.04
Change by 2010–2039	0.64	1.04	1.11	1.70	1.12	1.10	1.29	0.86	2.07	1.31	0.74	0.97	1.02	1.36	1.01
Change by 2040–2069	2.20	2.62	2.41	3.94	2.73	2.30	2.77	2.42	4.09	2.86	1.31	1.82	1.85	2.90	1.96
Change by 2070–2099	3.90	4.51	3.97	6.00	4.57	3.05	3.66	3.50	5.34	3.85	2.03	2.47	2.49	3.71	2.66
100-year forcing	4.17	4.80	4.29	6.57	4.94	3.41	3.94	3.87	5.98	4.26	2.42	2.80	2.71	4.44	3.07
100-year variability (%)	−6.10	30.65	11.53	−28.87	4.22	−15.44	13.20	−19.06	−15.86	−8.08	−14.24	12.55	−8.88	−20.21	−11.06
Mean daily maximum temperature (°C)															
Baseline 1980–2009	9.33	23.92	9.88	−7.94	8.80	9.47	23.84	9.86	−7.92	8.82	9.50	23.96	9.70	−7.84	8.83
Change by 2010–2039	0.52	1.06	0.95	1.10	0.91	1.03	1.34	0.85	1.45	1.16	0.72	0.88	0.97	0.82	0.84
Change by 2040–2069	2.01	2.68	2.39	2.70	2.41	2.04	2.82	2.32	2.75	2.46	1.12	1.76	1.80	1.99	1.67
Change by 2070–2099	3.63	4.48	3.77	4.24	4.02	2.77	3.77	3.54	3.80	3.44	1.88	2.55	2.60	2.59	2.40
100-year forcing	3.86	4.71	4.14	4.71	4.34	3.15	3.92	3.90	4.29	3.78	2.29	2.82	2.80	3.16	2.75
100-year variability (%)	3.92	12.12	18.63	−22.44	12.71	−3.40	7.20	−3.00	−10.83	−2.07	−14.60	7.61	1.74	−17.60	−1.49
Total precipitation (mm)															
Baseline 1980–2009	102	217	85	60	465	102	215	88	60	465	100	213	88	59	460
Change by 2010–2039	7	0	6	2	15	5	0	4	2	11	3	6	6	4	19
Change by 2040–2069	13	−6	6	6	18	12	3	7	6	29	10	8	10	5	33
Change by 2070–2099	19	−1	18	11	46	19	2	6	9	37	10	6	1	7	24
100-year forcing	21	8	15	11	55	20	10	7	9	46	10	11	1	6	28
100-year variability (%)	23.73	8.95	15.90	34.94	13.49	18.09	−0.74	14.62	1.22	2.93	6.27	18.65	4.62	9.99	15.47
Mean global solar radiation (MJ m^{-2} d^{-1})															
Baseline 1980–2009	17.09	21.58	8.73	5.16	13.14	17.10	21.51	8.70	5.16	13.12	17.16	21.58	8.68	5.17	13.15
Change by 2010–2039	−0.26	0.12	−0.12	−0.09	−0.09	−0.18	0.18	−0.06	−0.13	−0.05	−0.20	0.04	−0.07	−0.10	−0.08
Change by 2040–2069	−0.44	0.31	−0.09	−0.29	−0.12	−0.59	0.33	−0.17	−0.34	−0.20	−0.44	0.11	−0.09	−0.23	−0.16
Change by 2070–2099	−0.83	0.36	−0.31	−0.52	−0.33	−0.77	0.39	−0.15	−0.45	−0.25	−0.49	0.24	−0.04	−0.29	−0.15
100-year forcing	−0.88	0.33	−0.23	−0.55	−0.34	−0.82	0.29	−0.11	−0.49	−0.28	−0.47	0.20	−0.02	−0.31	−0.16
100-year variability (%)	1.40	−6.02	4.12	19.43	−4.39	5.63	−3.55	14.12	13.47	2.00	4.28	−5.86	−1.79	2.77	−6.10
Mean vapor pressure (kPa)															
Baseline 1980–2009	0.58	1.39	0.66	0.16	0.70	0.59	1.39	0.67	0.17	0.71	0.58	1.39	0.66	0.17	0.70
Change by 2010–2039	0.018	0.069	0.038	0.015	0.035	0.043	0.101	0.045	0.028	0.054	0.023	0.059	0.036	0.016	0.033
Change by 2040–2069	0.055	0.145	0.080	0.042	0.080	0.099	0.219	0.124	0.054	0.123	0.046	0.123	0.064	0.027	0.065
Change by 2070–2099	0.117	0.270	0.153	0.065	0.151	0.129	0.296	0.170	0.071	0.166	0.065	0.141	0.083	0.034	0.081
100-year forcing	0.127	0.296	0.161	0.072	0.164	0.140	0.323	0.188	0.079	0.182	0.073	0.165	0.090	0.043	0.092
100-year variability (%)	13.737	49.008	38.602	62.944	60.747	11.415	28.705	10.365	27.411	30.094	2.816	35.473	−14.47	−6.466	12.754
Mean wind speed (m s^{-1})															
Baseline 1980–2009	4.41	3.57	4.23	4.10	4.07	4.39	3.63	4.12	4.09	4.06	4.39	3.59	4.15	4.17	4.07
Change by 2010–2039	0.04	0.09	−0.06	0.16	0.06	−0.05	0.00	0.04	0.29	0.06	−0.10	0.00	−0.09	−0.04	−0.05
Change by 2040–2069	0.00	0.08	−0.07	0.26	0.07	−0.02	−0.03	−0.03	0.18	0.02	−0.02	0.03	0.01	0.06	0.03
Change by 2070–2099	0.07	0.04	−0.14	0.25	0.06	−0.06	−0.15	0.08	0.20	0.02	−0.14	−0.04	−0.07	0.08	−0.04
100-year forcing	0.22	−0.09	−0.03	0.29	0.09	0.07	−0.23	0.08	0.22	0.03	−0.02	−0.15	−0.04	0.18	−0.01
100-year variability (%)	−6.84	8.69	−1.90	16.46	−6.26	−2.46	−19.37	−12.65	9.07	−4.07	3.56	−10.78	−4.38	14.67	−9.22

Table 18. Summary of projected climatic changes for the Taiga Cordillera ecozone (average of four general circulation models), measuring temperature, precipitation, solar radiation, vapor pressure, and wind speed

Climate variable	A2 emissions scenario ("pessimistic")					A1B emissions scenario ("medium")					B1 emissions scenario ("optimistic")				
	Spring	Summer	Fall	Winter	Year	Spring	Summer	Fall	Winter	Year	Spring	Summer	Fall	Winter	Year
Mean daily minimum temperature (°C)															
Baseline 1980–2009	−15.22	3.83	−12.52	−29.07	−13.21	−15.30	3.73	−12.46	−28.94	−13.21	−15.15	3.78	−12.56	−29.00	−13.22
Change by 2010–2039	0.96	0.76	1.21	1.43	1.05	1.17	0.87	0.79	1.63	1.05	0.95	0.75	1.01	1.07	0.93
Change by 2040–2069	2.44	2.07	2.50	3.91	2.67	2.68	2.09	2.56	4.01	2.80	1.98	1.70	2.09	2.49	2.05
Change by 2070–2099	4.38	3.89	4.81	6.91	4.95	3.74	3.14	4.08	5.49	4.07	2.66	2.07	2.72	3.70	2.77
100-year forcing	4.98	4.28	5.15	7.61	5.50	4.25	3.43	4.46	6.33	4.62	3.32	2.41	3.01	4.46	3.30
100-year variability (%)	6.74	35.66	−29.03	−25.33	−13.11	−7.96	12.23	−23.84	−27.21	−14.90	1.47	14.68	−22.77	−22.30	−16.75
Mean daily maximum temperature (°C)															
Baseline 1980–2009	−3.45	15.60	−4.26	−19.60	−2.90	−3.55	15.49	−4.17	−19.45	−2.90	−3.44	15.54	−4.29	−19.55	−2.93
Change by 2010–2039	0.74	0.69	0.99	1.08	0.85	0.74	0.78	0.58	1.20	0.76	0.73	0.67	0.84	0.75	0.74
Change by 2040–2069	1.70	1.94	2.00	3.12	2.14	1.92	1.97	2.05	3.16	2.24	1.46	1.60	1.69	1.89	1.65
Change by 2070–2099	3.09	3.70	3.93	5.51	4.01	2.71	2.95	3.27	4.41	3.30	1.99	1.94	2.25	3.06	2.30
100-year forcing	3.56	4.08	4.18	5.99	4.45	3.08	3.22	3.60	5.04	3.75	2.47	2.26	2.47	3.60	2.71
100-year variability (%)	5.33	24.30	−27.00	−29.81	−20.11	−9.92	9.86	−21.35	−28.30	−19.18	−3.12	16.32	−24.04	−22.94	−22.84
Total precipitation (mm)															
Baseline 1980–2009	63	176	114	67	420	63	177	114	68	422	63	178	113	67	420
Change by 2010–2039	2	8	6	4	20	6	7	6	4	22	3	9	8	5	25
Change by 2040–2069	8	19	20	12	60	9	21	19	11	59	8	16	12	8	44
Change by 2070–2099	17	38	34	19	108	13	39	26	16	94	8	19	20	13	60
100-year forcing	19	38	37	20	114	15	40	29	18	102	9	21	22	13	66
100-year variability (%)	40.89	44.99	18.14	5.27	38.03	27.78	21.23	15.91	15.33	19.76	29.77	32.86	19.53	3.39	10.32
Mean global solar radiation (MJ m^{-2} d^{-1})															
Baseline 1980–2009	14.09	17.36	3.66	1.11	9.06	14.09	17.41	3.65	1.11	9.07	14.11	17.35	3.69	1.11	9.07
Change by 2010–2039	−0.17	−0.26	−0.15	0.00	−0.14	−0.33	−0.51	−0.13	−0.01	−0.25	−0.19	−0.30	−0.17	0.01	−0.17
Change by 2040–2069	−0.71	−0.59	−0.35	−0.05	−0.43	−0.73	−0.70	−0.32	−0.02	−0.45	−0.56	−0.46	−0.28	−0.02	−0.33
Change by 2070–2099	−1.46	−0.60	−0.51	−0.07	−0.66	−1.14	−0.68	−0.43	−0.07	−0.58	−0.69	−0.50	−0.36	−0.04	−0.40
100-year forcing	−1.54	−0.72	−0.57	−0.09	−0.73	−1.22	−0.76	−0.50	−0.08	−0.64	−0.75	−0.64	−0.39	−0.05	−0.46
100-year variability (%)	31.20	19.61	6.56	−21.71	32.42	21.53	10.02	2.72	−19.58	12.59	10.46	18.09	0.66	−18.32	23.89
Mean vapor pressure (kPa)															
Baseline 1980–2009	0.22	0.79	0.31	0.06	0.35	0.22	0.79	0.32	0.06	0.35	0.22	0.79	0.31	0.06	0.35
Change by 2010–2039	0.010	0.028	0.019	0.005	0.015	0.019	0.053	0.019	0.008	0.025	0.009	0.033	0.023	0.006	0.018
Change by 2040–2069	0.030	0.100	0.048	0.017	0.049	0.047	0.137	0.071	0.024	0.070	0.022	0.078	0.040	0.010	0.037
Change by 2070–2099	0.061	0.192	0.097	0.036	0.096	0.063	0.200	0.109	0.032	0.101	0.029	0.091	0.049	0.014	0.046
100-year forcing	0.068	0.209	0.105	0.038	0.105	0.070	0.218	0.120	0.036	0.111	0.038	0.108	0.055	0.017	0.054
100-year variability (%)	25.284	95.237	15.698	31.849	39.893	19.387	61.100	9.315	9.160	26.334	19.196	178.892	10.001	22.569	89.359
Mean wind speed (m s^{-1})															
Baseline 1980–2009	3.09	2.90	2.88	2.55	2.86	3.16	2.93	2.90	2.59	2.90	3.17	2.81	2.87	2.60	2.86
Change by 2010–2039	0.13	0.17	−0.10	0.09	0.07	0.05	0.17	−0.09	0.04	0.03	−0.06	0.20	−0.06	−0.01	0.02
Change by 2040–2069	0.12	0.23	−0.10	0.11	0.09	−0.06	0.34	−0.08	0.12	0.07	0.07	0.33	−0.03	−0.05	0.08
Change by 2070–2099	0.18	0.32	−0.03	0.28	0.18	0.06	0.18	−0.06	0.18	0.08	0.05	0.26	−0.03	0.11	0.10
100-year forcing	0.23	0.37	0.02	0.26	0.22	0.17	0.26	0.01	0.20	0.16	0.17	0.21	0.00	0.14	0.13
100-year variability (%)	12.58	12.31	3.30	−2.93	10.58	25.24	−4.76	−2.43	−2.87	9.87	−0.87	3.18	−5.88	−6.09	3.00

Table 19. Summary of projected climatic changes for the Boreal Cordillera ecozone (average of four general circulation models), measuring temperature, precipitation, solar radiation, vapor pressure, and wind speed

Climate variable	A2 emissions scenario ("pessimistic")					A1B emissions scenario ("medium")					B1 emissions scenario ("optimistic")				
	Spring	Summer	Fall	Winter	Year	Spring	Summer	Fall	Winter	Year	Spring	Summer	Fall	Winter	Year
Mean daily minimum temperature (°C)															
Baseline 1980–2009	–8.89	4.28	–8.19	–22.79	–8.86	–8.84	4.20	–8.07	–22.61	–8.79	–8.85	4.23	–8.25	–22.71	–8.88
Change by 2010–2039	0.71	0.83	1.10	1.23	0.93	1.16	1.07	0.66	1.49	1.03	1.05	0.90	0.97	1.15	0.99
Change by 2040–2069	2.13	2.33	2.33	3.38	2.48	2.40	2.37	2.37	3.31	2.57	1.78	1.87	1.97	2.24	1.95
Change by 2070–2099	4.07	4.14	4.27	5.72	4.50	3.26	3.54	3.69	4.69	3.74	2.47	2.35	2.58	3.29	2.65
100-year forcing	4.55	4.54	4.50	6.30	4.96	3.79	3.86	4.04	5.45	4.27	3.00	2.69	2.75	3.96	3.09
100-year variability (%)	12.42	22.19	–23.57	–23.81	–8.85	3.56	6.68	–23.54	–25.46	–7.73	2.52	9.35	–18.48	–22.46	–15.70
Mean daily maximum temperature (°C)															
Baseline 1980–2009	3.44	16.86	1.01	–12.65	2.19	3.42	16.75	1.10	–12.49	2.22	3.41	16.79	0.95	–12.60	2.15
Change by 2010–2039	0.46	0.76	0.86	0.92	0.73	0.67	1.05	0.49	1.05	0.76	0.74	0.88	0.74	0.79	0.77
Change by 2040–2069	1.42	2.29	1.83	2.53	1.97	1.58	2.36	1.91	2.37	2.02	1.25	1.87	1.56	1.57	1.55
Change by 2070–2099	2.71	4.10	3.40	4.13	3.55	2.31	3.57	2.99	3.44	3.03	1.74	2.39	2.06	2.44	2.14
100-year forcing	3.10	4.48	3.59	4.55	3.93	2.68	3.84	3.26	4.02	3.44	2.10	2.71	2.19	2.91	2.47
100-year variability (%)	19.28	24.95	–17.74	–25.41	–14.51	4.91	16.91	–15.73	–27.06	–12.12	3.69	20.48	–21.87	–21.71	–19.44
Total precipitation (mm)															
Baseline 1980–2009	71	172	124	93	460	72	172	124	94	463	72	172	122	94	459
Change by 2010–2039	2	7	4	5	17	4	4	3	6	16	3	8	6	6	22
Change by 2040–2069	10	14	14	13	50	9	14	12	10	45	6	9	10	8	33
Change by 2070–2099	19	26	24	22	90	11	24	21	19	73	8	12	15	13	49
100-year forcing	19	28	27	24	98	14	25	24	22	84	10	14	16	16	55
100-year variability (%)	20.56	28.07	14.92	4.96	46.39	1.47	22.27	19.76	10.27	27.60	6.64	26.61	11.03	–1.00	19.04
Mean global solar radiation (MJ m^{-2} d^{-1})															
Baseline 1980–2009	14.36	17.50	4.88	1.89	9.66	14.32	17.54	4.87	1.90	9.66	14.35	17.43	4.90	1.89	9.65
Change by 2010–2039	–0.22	–0.32	–0.20	0.00	–0.19	–0.42	–0.33	–0.17	–0.06	–0.25	–0.31	–0.13	–0.27	0.00	–0.18
Change by 2040–2069	–0.88	–0.50	–0.44	–0.10	–0.48	–0.98	–0.59	–0.43	–0.07	–0.52	–0.63	–0.37	–0.38	–0.03	–0.35
Change by 2070–2099	–1.87	–0.65	–0.69	–0.19	–0.85	–1.35	–0.48	–0.53	–0.19	–0.64	–1.03	–0.13	–0.48	–0.10	–0.44
100-year forcing	–1.93	–0.84	–0.77	–0.22	–0.94	–1.46	–0.63	–0.62	–0.22	–0.73	–1.11	–0.40	–0.53	–0.14	–0.55
100-year variability (%)	17.48	18.98	–8.91	–14.54	37.28	15.98	20.59	–11.88	–6.47	22.05	14.45	27.16	–2.38	–10.19	30.81
Mean vapor pressure (kPa)															
Baseline 1980–2009	0.39	0.96	0.47	0.12	0.49	0.39	0.97	0.48	0.13	0.49	0.39	0.96	0.47	0.12	0.49
Change by 2010–2039	0.015	0.042	0.024	0.008	0.022	0.034	0.079	0.028	0.015	0.038	0.022	0.047	0.030	0.012	0.027
Change by 2040–2069	0.049	0.135	0.065	0.027	0.068	0.078	0.187	0.098	0.035	0.099	0.037	0.105	0.055	0.018	0.054
Change by 2070–2099	0.100	0.247	0.125	0.049	0.130	0.101	0.274	0.147	0.049	0.142	0.054	0.131	0.069	0.025	0.069
100-year forcing	0.110	0.269	0.135	0.053	0.142	0.112	0.296	0.162	0.056	0.156	0.065	0.152	0.077	0.029	0.081
100-year variability (%)	61.636	56.535	10.575	–5.009	37.532	28.433	41.114	6.027	–0.885	19.441	84.667	191.122	24.316	–1.387	80.745
Mean wind speed (m s^{-1})															
Baseline 1980–2009	2.68	2.55	2.45	2.21	2.48	2.73	2.58	2.47	2.22	2.51	2.76	2.48	2.43	2.23	2.48
Change by 2010–2039	0.08	0.05	–0.05	0.04	0.03	0.03	0.06	–0.08	0.12	0.02	–0.07	0.09	0.04	0.06	0.03
Change by 2040–2069	0.07	0.09	0.02	0.12	0.07	0.06	0.17	–0.02	0.11	0.07	0.02	0.18	0.03	0.03	0.06
Change by 2070–2099	0.23	0.16	0.02	0.16	0.14	0.02	0.10	0.00	0.16	0.06	0.02	0.13	0.07	0.14	0.09
100-year forcing	0.19	0.16	0.03	0.20	0.14	0.04	0.14	0.03	0.20	0.09	0.07	0.06	0.06	0.19	0.09
100-year variability (%)	7.68	8.65	–12.14	–8.46	7.04	11.94	–8.52	–17.55	0.53	13.59	10.01	–4.51	–6.59	5.93	9.26

Table 20. Summary of projected climatic changes for the Pacific Maritime ecozone (average of four general circulation models), measuring temperature, precipitation, solar radiation, vapor pressure, and wind speed

Climate variable	A2 emissions scenario ("pessimistic")					A1B emissions scenario ("medium")					B1 emissions scenario ("optimistic")				
	Spring	Summer	Fall	Winter	Year	Spring	Summer	Fall	Winter	Year	Spring	Summer	Fall	Winter	Year
Mean daily minimum temperature (°C)															
Baseline 1980–2009	−0.57	7.02	1.45	−5.13	0.71	−0.56	7.01	1.51	−4.95	0.77	−0.66	6.95	1.39	−5.09	0.67
Change by 2010–2039	0.62	0.78	0.86	1.06	0.82	0.95	0.99	0.70	1.10	0.91	1.09	0.83	0.80	1.10	0.92
Change by 2040–2069	1.81	2.08	1.97	2.55	2.06	2.02	2.09	2.04	2.41	2.12	1.49	1.61	1.61	1.91	1.63
Change by 2070–2099	3.29	3.58	3.34	3.93	3.52	2.69	3.03	3.06	3.34	2.99	2.04	2.13	2.12	2.45	2.17
100-year forcing	3.64	3.88	3.56	4.34	3.84	3.05	3.32	3.35	3.92	3.38	2.31	2.36	2.29	2.89	2.45
100-year variability (%)	−2.37	22.18	4.43	−23.14	−1.75	−1.25	7.55	−9.93	−19.26	−6.09	−5.44	0.07	−8.02	−22.26	−15.18
Mean daily maximum temperature (°C)															
Baseline 1980–2009	8.07	16.99	8.70	1.11	8.73	8.03	16.91	8.69	1.27	8.74	7.94	16.83	8.57	1.12	8.63
Change by 2010–2039	0.48	0.84	0.72	0.85	0.72	0.84	1.09	0.57	0.80	0.81	0.95	0.89	0.73	0.84	0.83
Change by 2040–2069	1.61	2.24	1.75	2.06	1.88	1.76	2.45	1.92	1.90	1.99	1.41	1.83	1.51	1.52	1.55
Change by 2070–2099	2.79	3.87	3.05	3.18	3.21	2.43	3.41	2.94	2.66	2.84	1.98	2.46	2.09	1.97	2.11
100-year forcing	3.15	4.21	3.28	3.47	3.52	2.74	3.68	3.16	3.11	3.15	2.20	2.65	2.18	2.28	2.32
100-year variability (%)	6.58	5.88	6.15	−19.86	−3.62	−3.64	8.57	−0.46	−17.47	−11.28	1.68	3.04	−2.16	−23.06	−13.80
Total precipitation (mm)															
Baseline 1980–2009	352	228	619	628	1827	358	231	623	629	1842	359	234	617	638	1849
Change by 2010–2039	10	−5	21	37	61	11	0	18	52	83	−3	0	30	13	39
Change by 2040–2069	11	−7	63	61	124	15	−11	57	68	126	−6	−12	57	46	85
Change by 2070–2099	36	−12	87	91	202	13	−12	97	97	190	−6	−14	52	56	89
100-year forcing	35	−16	95	98	210	17	−12	109	105	213	0	−12	59	73	119
100-year variability (%)	1.71	0.82	26.77	20.11	9.68	4.14	2.34	−1.90	16.33	5.88	15.82	7.68	0.53	9.91	−6.57
Mean global solar radiation (MJ m^{-2} d^{-1})															
Baseline 1980–2009	13.17	18.37	6.28	2.68	10.13	13.07	18.23	6.23	2.69	10.06	13.11	18.16	6.21	2.65	10.04
Change by 2010–2039	−0.22	0.15	−0.09	−0.06	−0.06	−0.13	0.36	−0.18	−0.14	−0.03	−0.22	0.23	−0.07	0.02	−0.02
Change by 2040–2069	−0.43	0.48	−0.22	−0.14	−0.08	−0.48	0.84	−0.09	−0.11	0.03	−0.18	0.63	−0.09	−0.05	0.07
Change by 2070–2099	−0.97	0.85	−0.16	−0.19	−0.12	−0.54	0.99	−0.08	−0.25	0.03	−0.19	0.91	0.02	−0.09	0.15
100-year forcing	−0.92	0.94	−0.17	−0.22	−0.09	−0.60	0.95	−0.13	−0.27	−0.01	−0.22	0.81	−0.06	−0.16	0.09
100-year variability (%)	−9.61	−12.20	15.85	0.50	−13.17	−8.16	3.66	−3.38	0.76	−6.54	2.28	2.79	−6.41	8.85	−1.40
Mean vapor pressure (kPa)															
Baseline 1980–2009	0.70	1.21	0.87	0.53	0.83	0.70	1.22	0.88	0.53	0.83	0.69	1.21	0.86	0.53	0.82
Change by 2010–2039	0.025	0.052	0.039	0.010	0.032	0.048	0.082	0.045	0.039	0.053	0.045	0.050	0.035	0.021	0.038
Change by 2040–2069	0.079	0.145	0.100	0.064	0.096	0.110	0.174	0.133	0.091	0.125	0.053	0.093	0.065	0.022	0.059
Change by 2070–2099	0.143	0.257	0.180	0.099	0.170	0.141	0.258	0.204	0.125	0.180	0.070	0.110	0.076	0.031	0.072
100-year forcing	0.158	0.274	0.191	0.117	0.185	0.156	0.282	0.222	0.147	0.200	0.079	0.122	0.082	0.052	0.084
100-year variability (%)	26.648	35.482	23.018	−4.681	27.668	10.789	32.799	4.011	12.254	17.171	59.346	89.020	8.393	−10.92	38.191
Mean wind speed (m s^{-1})															
Baseline 1980–2009	3.57	3.16	3.66	4.26	3.67	3.69	3.11	3.66	4.23	3.69	3.69	3.11	3.62	4.28	3.68
Change by 2010–2039	0.05	0.07	−0.07	0.04	0.02	−0.07	0.08	−0.06	0.26	0.04	−0.11	0.02	0.01	0.08	−0.01
Change by 2040–2069	−0.03	0.12	0.06	0.24	0.08	−0.02	0.15	−0.02	0.21	0.07	−0.20	0.03	0.10	0.16	0.02
Change by 2070–2099	0.23	0.16	0.00	0.28	0.17	−0.08	0.11	0.11	0.34	0.10	−0.21	0.08	0.03	0.13	0.00
100-year forcing	0.13	0.22	0.06	0.37	0.19	−0.06	0.13	0.17	0.39	0.14	−0.20	0.10	0.04	0.24	0.04
100-year variability (%)	−14.57	14.32	15.76	−8.49	2.93	−9.04	7.87	−9.66	−0.06	9.54	5.97	24.97	−2.47	−4.65	−2.59

Table 21. Summary of projected climatic changes for the Montane Cordillera ecozone (average of four general circulation models), measuring temperature, precipitation, solar radiation, vapor pressure, and wind speed

Climate variable	A2 emissions scenario ("pessimistic")					A1B emissions scenario ("medium")					B1 emissions scenario ("optimistic")				
	Spring	Summer	Fall	Winter	Year	Spring	Summer	Fall	Winter	Year	Spring	Summer	Fall	Winter	Year
Mean daily minimum temperature (°C)															
Baseline 1980–2009	−4.13	5.33	−2.90	−12.79	−3.60	−4.09	5.29	−2.83	−12.61	−3.54	−4.21	5.26	−3.00	−12.78	−3.66
Change by 2010–2039	0.61	0.92	0.99	1.21	0.92	1.12	1.13	0.76	1.34	1.07	1.14	0.90	0.88	1.25	1.01
Change by 2040–2069	2.17	2.33	2.21	3.06	2.39	2.37	2.42	2.27	2.86	2.45	1.63	1.77	1.77	2.29	1.85
Change by 2070–2099	3.90	4.01	3.70	4.75	4.07	3.12	3.36	3.37	4.03	3.43	2.34	2.35	2.36	2.96	2.48
100-year forcing	4.24	4.36	3.94	5.20	4.42	3.50	3.66	3.68	4.67	3.84	2.59	2.62	2.51	3.43	2.77
100-year variability (%)	3.65	21.88	6.85	−19.56	7.18	10.91	3.37	−9.48	−15.63	2.73	3.31	6.89	−7.81	−20.77	−11.18
Mean daily maximum temperature (°C)															
Baseline 1980–2009	7.15	18.46	6.71	−3.95	7.11	7.16	18.37	6.71	−3.80	7.12	7.05	18.32	6.54	−3.94	7.00
Change by 2010–2039	0.46	1.00	0.79	0.88	0.78	0.91	1.20	0.60	0.89	0.88	0.95	0.99	0.80	0.87	0.88
Change by 2040–2069	1.84	2.55	1.87	2.14	2.06	1.92	2.86	2.06	1.93	2.17	1.43	2.02	1.61	1.56	1.64
Change by 2070–2099	3.19	4.34	3.27	3.25	3.50	2.63	3.81	3.13	2.72	3.05	2.13	2.70	2.28	2.03	2.27
100-year forcing	3.49	4.71	3.51	3.59	3.82	2.95	4.09	3.37	3.21	3.38	2.34	2.93	2.35	2.38	2.48
100-year variability (%)	15.28	5.32	13.58	−20.35	1.28	11.10	−0.99	0.53	−16.15	−3.83	9.37	5.12	1.09	−23.71	−9.34
Total precipitation (mm)															
Baseline 1980–2009	142	192	192	205	731	144	190	192	206	732	142	193	193	208	735
Change by 2010–2039	2	−2	10	15	25	4	2	10	16	33	4	1	7	7	18
Change by 2040–2069	9	−2	20	24	50	8	−3	21	22	49	6	−1	18	21	43
Change by 2070–2099	21	2	30	39	92	13	−3	32	35	78	5	1	15	21	43
100-year forcing	21	5	32	41	98	16	−2	35	39	85	5	4	19	26	53
100-year variability (%)	16.40	22.50	13.94	26.87	27.90	11.57	3.61	9.62	8.91	19.85	12.77	3.80	3.00	6.73	−2.45
Mean global solar radiation (MJ m^{-2} d^{-1})															
Baseline 1980–2009	15.20	20.35	7.41	3.49	11.62	15.14	20.26	7.38	3.48	11.57	15.25	20.19	7.32	3.46	11.56
Change by 2010–2039	−0.24	0.22	−0.17	−0.11	−0.08	−0.29	0.31	−0.24	−0.15	−0.10	−0.37	0.29	−0.08	−0.03	−0.06
Change by 2040–2069	−0.70	0.66	−0.37	−0.26	−0.17	−0.83	1.03	−0.25	−0.24	−0.08	−0.63	0.67	−0.15	−0.16	−0.07
Change by 2070–2099	−1.43	1.13	−0.41	−0.43	−0.29	−1.07	1.19	−0.29	−0.43	−0.15	−0.66	0.93	−0.08	−0.24	−0.02
100-year forcing	−1.48	1.19	−0.41	−0.46	−0.29	−1.17	1.16	−0.32	−0.46	−0.20	−0.67	0.83	−0.16	−0.30	−0.08
100-year variability (%)	1.10	−5.72	15.50	11.90	1.09	3.99	−3.73	6.89	13.56	2.44	−0.64	8.68	−5.57	12.99	1.04
Mean vapor pressure (kPa)															
Baseline 1980–2009	0.53	1.07	0.67	0.29	0.64	0.54	1.08	0.67	0.30	0.65	0.53	1.06	0.66	0.29	0.64
Change by 2010–2039	0.020	0.046	0.030	0.018	0.028	0.051	0.081	0.040	0.030	0.050	0.039	0.044	0.034	0.023	0.035
Change by 2040–2069	0.074	0.128	0.082	0.053	0.083	0.110	0.173	0.118	0.065	0.115	0.056	0.100	0.068	0.039	0.065
Change by 2070–2099	0.137	0.233	0.149	0.084	0.151	0.142	0.249	0.180	0.091	0.164	0.084	0.130	0.088	0.048	0.087
100-year forcing	0.149	0.252	0.161	0.094	0.164	0.155	0.271	0.197	0.105	0.181	0.091	0.145	0.096	0.058	0.097
100-year variability (%)	23.750	27.532	15.348	7.014	36.319	30.520	24.281	8.850	22.651	27.000	25.457	16.889	−7.161	4.548	14.742
Mean wind speed (m s^{-1})															
Baseline 1980–2009	2.45	2.34	2.40	2.48	2.42	2.52	2.33	2.39	2.48	2.43	2.54	2.35	2.37	2.51	2.44
Change by 2010–2039	0.07	0.02	0.01	0.07	0.04	−0.07	0.04	0.02	0.11	0.02	−0.11	−0.02	0.01	0.02	−0.03
Change by 2040–2069	0.06	0.02	0.06	0.11	0.06	0.03	0.00	0.04	0.03	0.02	−0.13	−0.06	0.08	0.04	−0.02
Change by 2070–2099	0.19	−0.04	0.03	0.07	0.07	−0.02	−0.05	0.10	0.13	0.03	−0.17	−0.07	0.02	0.05	−0.04
100-year forcing	0.13	−0.04	0.09	0.10	0.07	−0.02	−0.06	0.14	0.16	0.05	−0.14	−0.06	0.05	0.10	−0.02
100-year variability (%)	1.31	10.76	3.11	−2.48	0.18	−7.25	6.73	−11.36	0.05	14.22	16.31	15.01	−9.37	7.18	1.37

Table 22. Summary of projected climatic changes for the Hudson Plains ecozone (average of four general circulation models), measuring temperature, precipitation, solar radiation, vapor pressure, and wind speed

Climate variable	A2 emissions scenario ("pessimistic")					A1B emissions scenario ("medium")					B1 emissions scenario ("optimistic")				
	Spring	Summer	Fall	Winter	Year	Spring	Summer	Fall	Winter	Year	Spring	Summer	Fall	Winter	Year
Mean daily minimum temperature (°C)															
Baseline 1980–2009	−10.67	7.33	−2.30	−25.38	−7.75	−10.57	7.40	−2.25	−25.44	−7.70	−10.34	7.38	−2.22	−25.09	−7.57
Change by 2010–2039	1.04	1.14	1.32	2.58	1.51	0.97	1.12	1.06	2.34	1.35	0.69	0.98	1.03	1.88	1.15
Change by 2040–2069	2.93	2.72	2.77	5.59	3.45	3.01	2.87	2.66	5.94	3.59	1.65	1.81	1.85	3.76	2.26
Change by 2070–2099	5.22	4.60	4.51	9.19	5.86	4.26	3.67	3.75	7.99	4.88	2.69	2.41	2.45	5.13	3.17
100-year forcing	5.52	4.91	4.88	9.91	6.28	4.66	4.04	4.16	8.64	5.34	3.32	2.76	2.90	6.14	3.77
100-year variability (%)	11.80	35.55	13.68	−14.78	18.85	−10.22	−0.18	−14.73	−15.64	−10.47	3.32	5.04	−3.78	−16.53	−10.71
Mean daily maximum temperature (°C)															
Baseline 1980–2009	1.40	18.91	5.53	−14.75	2.78	1.52	18.98	5.57	−14.81	2.84	1.75	18.98	5.59	−14.49	2.95
Change by 2010–2039	0.83	1.16	1.23	1.57	1.19	0.87	1.20	1.09	1.53	1.15	0.57	1.02	0.99	1.09	0.93
Change by 2040–2069	2.38	2.74	2.63	3.96	2.89	2.37	3.03	2.55	4.16	2.99	1.26	1.84	1.72	2.57	1.84
Change by 2070–2099	4.18	4.72	4.32	6.64	4.95	3.31	3.67	3.52	5.72	4.02	2.02	2.42	2.36	3.64	2.61
100-year forcing	4.35	4.95	4.68	7.01	5.23	3.59	3.98	3.91	6.03	4.35	2.53	2.73	2.77	4.26	3.06
100-year variability (%)	16.49	27.70	11.69	−24.84	13.18	−2.22	3.39	−2.50	−23.70	−13.56	3.26	4.47	7.61	−23.91	−12.73
Total precipitation (mm)															
Baseline 1980–2009	91	237	174	73	575	89	235	177	72	574	90	236	179	74	579
Change by 2010–2039	6	−6	6	6	12	5	3	0	7	14	5	−5	−3	4	2
Change by 2040–2069	11	−3	13	16	36	17	−1	11	20	46	10	1	11	13	35
Change by 2070–2099	23	−4	20	28	66	22	1	11	23	57	13	−1	4	16	33
100-year forcing	26	4	18	30	77	23	8	12	24	66	15	7	7	19	48
100-year variability (%)	41.64	19.31	44.43	33.39	39.16	20.36	12.81	14.76	30.04	12.00	26.19	17.73	27.62	25.10	15.15
Mean global solar radiation (MJ m^{-2} d^{-1})															
Baseline 1980–2009	16.85	18.94	6.45	4.38	11.66	16.89	18.94	6.43	4.40	11.67	16.86	18.97	6.41	4.35	11.65
Change by 2010–2039	−0.21	0.28	−0.02	−0.18	−0.04	−0.19	0.26	0.04	−0.16	−0.02	−0.25	0.21	0.02	−0.08	−0.03
Change by 2040–2069	−0.63	0.42	−0.05	−0.41	−0.17	−0.87	0.71	−0.06	−0.49	−0.18	−0.43	0.22	−0.03	−0.27	−0.13
Change by 2070–2099	−1.40	0.74	−0.09	−0.74	−0.38	−1.35	0.55	−0.11	−0.64	−0.39	−0.79	0.32	−0.05	−0.38	−0.23
100-year forcing	−1.56	0.72	−0.05	−0.78	−0.42	−1.47	0.53	−0.08	−0.66	−0.42	−0.94	0.32	−0.05	−0.45	−0.28
100-year variability (%)	12.44	5.17	32.02	17.02	6.68	−3.21	3.38	30.69	20.74	12.29	2.40	2.42	34.27	9.55	14.63
Mean vapor pressure (kPa)															
Baseline 1980–2009	0.34	1.17	0.60	0.08	0.55	0.35	1.16	0.62	0.08	0.55	0.35	1.16	0.61	0.08	0.55
Change by 2010–2039	0.016	0.085	0.061	0.015	0.044	0.016	0.077	0.052	0.018	0.041	0.014	0.057	0.041	0.012	0.031
Change by 2040–2069	0.062	0.163	0.122	0.038	0.096	0.068	0.200	0.131	0.049	0.112	0.023	0.094	0.048	0.022	0.047
Change by 2070–2099	0.105	0.311	0.220	0.071	0.177	0.093	0.268	0.179	0.065	0.151	0.029	0.068	0.066	0.027	0.047
100-year forcing	0.112	0.341	0.227	0.075	0.189	0.104	0.296	0.196	0.070	0.166	0.041	0.088	0.077	0.032	0.059
100-year variability (%)	38.656	57.068	62.710	59.330	68.328	21.109	21.606	21.084	54.921	35.644	36.997	19.847	36.693	42.902	43.339
Mean wind speed (m s^{-1})															
Baseline 1980–2009	4.15	3.91	4.61	4.06	4.18	4.14	3.95	4.51	4.16	4.19	4.05	3.93	4.56	4.12	4.17
Change by 2010–2039	0.00	−0.09	0.07	0.36	0.08	−0.05	0.06	0.23	0.11	0.08	0.16	0.03	0.13	0.20	0.12
Change by 2040–2069	0.12	−0.08	0.12	0.52	0.17	−0.19	0.01	0.27	0.31	0.10	0.15	−0.12	0.10	0.27	0.11
Change by 2070–2099	0.32	−0.01	0.17	0.92	0.34	0.19	0.06	0.40	0.50	0.30	0.12	−0.11	0.25	0.30	0.14
100-year forcing	0.42	−0.03	0.23	0.92	0.38	0.29	0.09	0.36	0.60	0.34	0.13	−0.10	0.25	0.37	0.16
100-year variability (%)	−0.06	−4.00	23.52	20.67	24.83	0.39	6.26	15.26	14.68	34.27	−9.44	0.98	24.77	6.95	26.09

DISCUSSION

Interpolated climate scenarios derived from state-of-the-art GCMs provide an effective and reasonable means for comparing standardized climate projections in assessments of the impacts of climate change at high spatial resolution. The suite of 12 climate scenarios presented here were downscaled from simulations carried out with four well-established GCMs, each forced by three GHG emissions scenarios developed for the IPCC: the A2 scenario, derived from a "business-as-usual" storyline on global development during the 21st century, which provides the strongest GHG forcing; the B1 scenario, derived from a storyline with significant GHG mitigation, which provides the weakest forcing; and the A1B scenario, derived from an intermediate forcing scenario, which provides intermediate projections. The downscaled climate scenarios were developed in support of large-scale assessments of forest vulnerability to climate change. These scenarios also formed part of the effort by the US Department of Agriculture Forest Service to address the requirements of the US Resources Planning Act (1974) assessment for 2010. In both projects, a key objective was to follow recommendations on the selection and use of climate scenario data from the IPCC's AR4 (see http://www.ipcc-data.org/ddc_scen_selection.html). Each downscaled climate scenario comprised data for six monthly climate variables, reported as differences from or ratios in relation to mean values for 1961–1990. When combined with baseline interpolated climatologies (data for 1961–1990 normals), these data sets should provide a solid basis for exploring the potential effects of climate change anywhere in Canada.

Producing such a comprehensive data set requires an assessment of the quality and consistency of the data. With that in mind, the data were analyzed to highlight both consistencies and discrepancies among the different GCMs and their differential responses to the three GHG forcing scenarios. To make this analysis more informative, the land area of Canada was divided into 18 ecozones, based on the Terrestrial Ecozones of Canada (Wiken 1986; Ecological Stratification Working Group 1995), with three extra subdivisions identified for the Carbon Budget Model of the Canadian Forest Sector (Kurz et al. 2009).

The results across models generally were highly consistent, particularly with respect to temperature and solar radiation, both in terms of each model's response to the different forcing scenarios and in terms of the agreement among the four models. This is not to say that the models agreed completely in all cases, but in general, the various projections seemed plausible and those from any single model were rarely completely inconsistent with results from the other models. However, the divergence among model projections generally increased with time into the future and with increasing GHG forcing (i.e., from the B1 to the A1B to the A2 scenario). Hence, the uncertainty in projections of future climate must inevitably increase as the projected change from present-day conditions increases, which is consistent with many other assessments of climate scenarios.

Subjective comparisons for the period 1961–2008, for which both observed and modeled monthly temperature and precipitation data were available, strongly suggested that the magnitude and periodicity of interannual variations produced by all four GCMs were consistent with observations for all seasons and all ecozones. There was less consistency among the models in their predictions of changes in interannual variability over the 21st century, but time-dependent changes in amplitude and frequency generally were similar among models, and seasonal differences appeared consistent.

Aggregation of the scenario data for 18 ecozones showed some significant differences among regional trends that were broadly consistent with trends determined by visual inspection of the national-scale maps. However, some trends occurring over smaller regions (notably of decreasing precipitation) did not appear in the area-weighted ecozonal means. This suggests that the climatic limits defining present-day ecological classifications can be expected to change differentially in coming decades and, more importantly, that some regional assessments of the effects of climate change should be carried out at smaller spatial scales than entire ecozones.

Sources of Error and Uncertainty

Users of the data presented here should keep in mind that GCMs provide imperfect physical representations of observed climate, considered as key variables averaged over large areas, with little representation of the effects of surface topography. Furthermore, the global projections of future climate created by GCMs are based on an understanding of current global trends, such as eccentricities in earth's orbit and observed rates of increase of atmospheric GHGs—and the assumption that these trends will change only in predictable ways. For example, GCMs cannot capture future stochastic events, such as major volcanic eruptions, which could dramatically alter future climate at any time. Hence, the downscaled scenarios reported here should not be considered accurate predictions of future climate.

For each step in the process used for downscaling the data, there are areas of concern affecting the reliability of these predictions. These concerns begin with the assumptions that underlie each GCM, which represent the physical and chemical processes occurring in the global atmosphere, in the oceans, and on the land surface. These assumptions govern the responses of each GCM to the IPCC SRES forcing scenarios, which are themselves based on a set of socioeconomic assumptions that are unlikely to occur in reality. In addition, the documentation for and availability of GCM output data were sometimes incomplete. For example, as discussed in the Methods section, humidity data generated by the NCARCCSM3 model forced by the A2 emissions scenario for the 2070s were missing from the PCMDI data portal and had to be obtained from the Earth System Grid portal of the University Corporation for Atmospheric Research. Of these substitute data, humidity values for certain grid cells during the 2070s decade were completely out of range and required correction. The latter problem was fixed in more recent simulations, but the metadata did not document why the problem occurred or how it was resolved.

Any process of downscaling GCM grid-level "averages" to a finer scale incorporates further assumptions (see the section "Review of Spatial Downscaling of Global Climate Simulations," at the beginning of the Methods section). In the present study, GCM outputs were normalized and converted to change factors (relative to simulated means for 1961–1990) and were then downscaled by interpolation to a 5 arcminute grid. In the case of the Canadian data set reported here, these interpolated 5 arcminute geographic grids were also reprojected onto the commonly used Lambert conformal conic projection, which introduced further minor errors. Clearly, these downscaled change factors cannot be more accurate than the data from which they were derived. The interpolated change factors were applied to a historical climatology for 1961–1990 to produce future projections that more closely resembled climatic observations.

Basing projections of future climate on interpolated data from weather stations provides a realistic context within which to assess the GCM results; however, station data also are subject to problems with data quality, measurement errors, and missing values. Furthermore, observing stations are not uniformly distributed across a heterogeneous land surface. Canada has relatively few monitoring stations at high elevations and in the far north, which results in larger errors in interpolated data for these regions. Hence, any baseline value is only an estimate of the "truth" (though arguably a relatively accurate estimate compared with the errors inherent in the GCM projections). The implication is that the scenarios of future climate reported here must be considered not as forecasts, but as a range of plausible futures. In particular, as noted above, the influences of unpredictable climatic drivers, such as future volcanic eruptions, cannot be included in the GCM simulations, and biospheric feedbacks on GHG forcing, such as increased occurrence of forest fires and accelerated oxidation of peatland soils, are represented simplistically, if at all.

Carbon Dioxide Concentration Scenarios

Readers of this report might pose the question, "Which projections of increases in atmospheric CO_2 concentration are represented by the downscaled scenarios reported here?" This question is not as easy to answer as it might seem, because although the original NetCDF files downloaded from the PCMDI portal and other sites provide comprehensive metadata, in general these metadata do not explicitly state the source of the greenhouse gas emissions scenarios that were used to drive the GCM simulations.

The individual scenarios of future climate developed by GCM modeling groups for the IPCC AR4 resulted from projections of how the world will change during the 21st century. As mentioned in the Methods section, the assumptions supporting these projections were documented by Nakićenović et al. (2000) in the IPCC SRES developed by Working Group 3 as part of the IPCC Third Assessment Report. Two modeling groups developed separate global carbon cycle models (with components of GCMs, ocean carbon models, and dynamic vegetation models, including representations of the effects of historical land-use change, as well as climate change feedbacks on ocean and terrestrial processes) known as the Bern Carbon Cycle Model (Bern-CC) and Integrated Science Model for Assessment of Climate Change (ISAM) (see http://www.ipcc-data.org/ddc_co2.htmlfor an overview of these models and their underlying assumptions.) These two models were used to project future global emissions of carbon dioxide (CO_2) and other GHGs for six SRES scenarios (four "marker scenarios" and two additional "illustrative scenarios"). The projected range of CO_2 concentrations for 2100 is from 550 to 970 ppm according to ISAM and from 540 to 960 ppm according to Bern-CC, which implies close agreement between the two modeling approaches. Of course, as mentioned above, none of these scenarios can be considered an accurate prediction of what will actually happen. In principle, all six scenarios, and the underlying storylines of population growth and economic and technological development from which the concentration projections are derived, can be considered equally likely, depending on one's views of these possible paths for global society.

For all four GCMs considered in this report, the metadata refer to the "720 ppm stabilization experiment" for the A1B scenario and the "550 ppm stabilization experiment" for the B1 scenario. This implies closer agreement with the ISAM trajectories for A1B and B1, which reach 717 and 549 ppm by 2100, respectively (the Bern-CC trajectories project 703 and 540 ppm, respectively). However, in the specific case of the CGCM31MR model, the metadata for the A1B scenario (see Appendix 1) state, "The CO_2 concentrations are from the Bern-CC model." Stabilization concentrations are not given in the metadata for the A2 projections. This is because, according to the A2 scenario, GHG emissions are assumed to continue growing and stabilization in 2100 is unlikely. In general, it is recommended that the ISAM trajectories be used where CO_2 concentration data are needed for an impact assessment, although in practice either data set is likely to be acceptable.

CONCLUSIONS

The data sets presented here will be valuable for use in models and assessment frameworks that need climate variables as inputs. Twelve model–scenario combinations have been presented, to offer a variety of potential futures for assessing the possible effects of a changing climate on natural resources, ecosystems, human infrastructure, and communities. These data sets capture the trends of projected climate, and each should be considered a plausible outcome under a set of assumptions that the user is encouraged to study and understand. Data are presented as grids and may be used in other models to determine effects at scales similar to the grid-cell size. Reporting of spatial and temporal trends will be meaningful across an aggregation of these grid cells. For example, the timing of extreme values simulated for any given grid cell should be considered as a general indicator of future possibilities in that region, but not as a precise forecast of extreme events at that specific location.

Of the four GCMs studied here, the NCARCCSM3 model was generally the most sensitive to GHG concentration at the Canadian national scale. Hence, when forced by the A2 emissions scenario, the NCARCCSM3 model generally projected the greatest warming. However, maps comparing projections of increases in annual mean daily minimum temperature for the period 2071–2100 were remarkably similar for the NCARCCSM3 and MIROC32MR models. In general, the MIROC32MR model projected slightly less warming than the NCARCCSM3 model with forcing by the A2 scenario, except in the northeastern Arctic, taiga, and boreal ecozones. The CSIROMK35 model generally projected the least warming, whereas the CGCM31MR model had intermediate projections.

Differences in projected warming among the models were greatest in the north. In the southern ecozones, the models were generally more consistent in terms of projected temperature increases, but were less consistent in terms of projected precipitation change. The CGCM31MR and CSIROMK35 models both projected similar temperature increases on the Pacific and Atlantic coasts, whereas the MIROC32MR and NCARCCSM3 models generally projected more uniform warming across eastern Canada, extending into the Atlantic coastal regions.

Despite these variations, the models generally agreed that the Arctic and Hudson Bay regions would undergo the greatest temperature increases and the coastal regions of British Columbia and the Atlantic Provinces would experience the least. The distribution of warming from east to west across the Provinces was less consistent across models, although the general pattern was for the greatest warming to occur in Manitoba and western Ontario.

Given the less predictable nature of precipitation and the known limitations in the capacity of GCMs to simulate precipitation patterns accurately, the four GCMs were surprisingly similar in their simulations of observed data (when expressed at seasonal timescales). Furthermore, projections of future precipitation trends and variability were generally similar among models and forcing scenarios, with the greatest proportional increases occurring in the territories, particularly in the northern Arctic, with noticeable divergence in projected trends in the provinces to the south. These projected trends also were more variable among regions and among models than were the temperature projections.

In general, precipitation was projected to increase, but only the CGCM31MR model projected increases nationwide. The MIROCMR32 model projected the greatest increases in precipitation in the Arctic region when forced with the A2 emissions scenario, but it was also the only GCM to project a decrease in precipitation in any ecozone (the Mixedwood Plains; see Fig. 23f). Over smaller regions, the NCARCCSM3 model projected significant decreases in southern British Columbia (Figs. 17–20) and a more general decline on the west coast and in southern Saskatchewan and Manitoba. The CSIROMK35 model projected a less severe decrease in annual precipitation across much of southern British Columbia. With the A1B and A2 emissions scenarios, these precipitation decreases were projected to appear within the next 15–30 years.

The various GCMs generally projected small changes in solar radiation, which were typically inversely correlated with the projected trends in precipitation. This is to be expected, because trends in simulated precipitation are related to vapor condensation as cloud and hence inversely related to solar radiation arriving at the earth's surface.

The GCMs were generally similar in their projections of future changes in vapor pressure, although in many cases the MIROC32MR and NCARCCSM3 models projected larger increases in seasonal mean values than the other models. The larger increases in vapor pressure with these two models were generally reflective of the larger temperature increases that they projected for the north. Conversely, the MIROC32MR model projected small increases in solar radiation in the southern ecozones, where it also projected reduced summer precipitation.

There was general agreement among the models that changes in mean wind speeds would be relatively small, but this result varied both regionally and seasonally. There was some evidence that greater warming (i.e., such as would result from the A1B or A2 emissions scenarios) would cause greater increases in wind speed in regions and seasons where wind speeds were evidently sensitive to climate warming. In general, projected changes in interannual variability of wind speed were small, and the relations were inconsistent across regions, seasons, and GHG forcing scenarios.

LITERATURE CITED

Conway, D.; Jones, P.D. 1998. The use of weather types and air flow indices for GCM downscaling. J. Hydrol. 212–213(1–4):348–361.

Ecological Stratification Working Group. 1995. A national ecological framework for Canada. Agric. Agri-Food Can., Res. Branch, Cent. Land Biol. Resour. Res. and Environ. Can., State Environ. Dir., Ecozone Analys. Branch, Ottawa/Hull. 125 p. + map at 1:7 500 000 scale.

Gordon, H.B.; Rotstayn, L.D.; McGregor, J.L.; Dix, M.R.; Kowalczyk, E.A.; O'Farrell, S.P.; Waterman, L.J.; Hirst, A.C.; Wilson, S.G.; Collier, M.A.; Watterson, I.G.; Elliott, T.I. 2002. The CSIRO Mk3 Climate System Model. CSIRO Atmospheric Research Technical Paper No.60 CSIRO Atmospheric Research, Private Bag No. 1, Aspendale, Victoria, Australia. <http://www.cmar.csiro.au/e-print/open /gordon_2002a.pdf> Accessed 6 June 2011.

Hashmi, M.Z.; Shamseldin, A.Y.; Melville, B.W. 2009. Statistical downscaling of precipitation: state-of-the-art and application of Bayesian multi-model approach for uncertainty assessment. Hydrol. Earth Syst. Sci. Discuss. 6:6535–6579. Also available at: <http://www.hydrol-earth-syst-sci-discuss.net/6/6535/2009/hessd-6-6535-2009-discussion.html>. Accessed 28 July 2010.

Hasumi, H.; Emori, S. 2004. K-1 Coupled GCM (MIROC) Description. K-1 Technical Report No. 1. Center for Climate System Research, University of Tokyo; National Institute for Environmental Studies; Frontier Research Center for Global Change, Japan. <http://www.ccsr.u-tokyo.ac.jp/kyosei/hasumi/MIROC/tech-repo.pdf> Accessed 6 June 2011.

Hijmans, R.; Cameron, S.E.; Parra, J.; Jones, P.; Jarvis, A. 2005. Very high resolution interpolated climate surface for global land areas. Int. J. Climatol. 25:1965–1978.

Hogg, E.H.; Brandt, J.P.; Michaelian, M. 2008. Impacts of a regional drought on the productivity, dieback and biomass of western Canadian aspen forests. Can. J. For. Res. 38:1373–1384.

Houlder, D.J.; Hutchinson, M.F.; Nix, H.A.; McMahon, J.P. 2000. ANUCLIM User Guide, Version 5.1. Centre for Resource and Environmental Studies, Australian National University, Canberra, Australia.

Hutchinson, M.F. 1995. Interpolating mean rainfall using thin plate smoothing splines. Int. J. Geogr. Inf. Syst. 9(4):385–403.

Hutchinson M.F. 1998a. Interpolation of rainfall data with thin plate smoothing splines: I. Two dimensional smoothing of data with short range correlation. J. Geogr. Inf. Decis. Anal. 2(2):152–167.

Hutchinson M.F. 1998b. Interpolation of rainfall data with thin plate smoothing splines: II. Analysis of topographic dependence. J. Geogr. Inf. Decis. Anal. 2(2):168–185.

Hutchinson, M.F. 2009. ANUSPLIN. version 4.3. <http://fennerschool.anu.edu.au/publications/software/anusplin.php>. Accessed 13 April 2011.

Hutchinson, M.F.; Gessler, P.E. 1994. Splines—more than just a smooth interpolator. Geoderma 62:45–67.

Hutchinson, M.F.; McKenney D.W.; Lawrence, K.; Pedlar, J.H.; Hopkinson, R.F.; Milewska, E.; Papadopol, P. 2009. Development and testing of Canada-wide interpolated spatial models of daily minimum–maximum temperature and precipitation for 1961–2003. J. Appl. Meteorol. Climatol. 48:726–741.

Jensen, M.E.; Burman, R.D.; Allen, R.G., editors. 1990. Evapotranspiration and irrigation water requirements. Am. Soc. Civil Eng., New York.

Joyce, L.A.; Price, D.T.; McKenney, D.W.; Siltanen, R.M.; Papadopol, P.; Lawrence, K.; Coulson, D.P. 2011. High resolution interpolation of climate scenarios for the conterminous United States and Alaska. Rocky Mt. Res. Stn. Gen. Tech. Rep. RMRS-GTR-263. US Dep. Agric., For. Serv., Rocky Mt. Res. Stn., Ft. Collins, CO. 87 p.

Kittel, T.G.F.; Rosenbloom, N.A.; Painter, T.H.; Schimel, D.S.; VEMAP Modeling Participants (1995). The VEMAP integrated database for modeling United States ecosystem/vegetation sensitivity to climate change. J. Biogeogr. 22:857–862.

Kurz, W.A.; Dymond, C.C.; White. T.M.; Stinson, G.; Shaw, C.H.; Rampley, G.J.; Smyth, C.; Simpson, B.N.; Neilson, E.T.; Trofymow, J.A.; Metsarantaa, J.; Apps, M.J. 2009. CBM-CFS3: a model of carbon-dynamics in forestry and land-use change implementing IPCC standards. Ecol. Model. 220:480–504.

Lawrence, K.; Hutchinson, M.; McKenney, D. 2007. Multi-scale digital elevation models for Canada. Nat. Resour. Canada, Can. For. Serv., Great Lakes For. Cent., Sault Ste. Marie, ON. Frontline Tech. Rep. 109.

Mackey, B.G.; McKenney, D.W.; Yang, Y.Q.; McMahon, J.P.; Hutchinson, M.F. 1996. Site regions revisited: a climatic analysis of Hill's site regions for the province of Ontario using a parametric method. Can. J. For. Res. 26:333–354.

McKenney, D.W.; Hutchinson, M.F.; Kesteven, J.L.; Venier, L.A. 2001. Canada's plant hardiness zones revisited using modern climate interpolation techniques. Can. J. Plant Sci. 81:129–143.

McKenney, D.W.; Hutchinson, M.F.; Papadopol, P.; Price, D.T. 2004. Evaluation of alternative spatial models of vapour pressure in Canada. Pages 6.2.1–6.2.11 *in* Proceedings of the 26th Conference on Agricultural and Forest Meteorology, Vancouver, BC, 23–26 August 2004. Am. Meteorol. Soc., Boston, MA. <http://ams.confex.com/ams/AFAPURBBIO/techprogram/ paper_78201.htm>. Accessed 28 July 2010.

McKenney, D.; Papadapol, P.; Campbell, K.; Lawrence, K.; Hutchinson, M. 2006a. Spatial models of Canada- and North America-wide 1971/2000 minimum and maximum temperature, total precipitation and derived bioclimatic variables. Nat. Resour. Canada, Can. For. Serv., Great Lakes For. Cent., Sault Ste. Marie, ON. Frontline Tech. Note 106. 9 p.

McKenney, D.; Papadopol, P.; Lawrence, K.; Campbell, K.; Hutchinson, M. 2007. Customized spatial climate models for Canada. Nat. Resour. Canada, Can. For. Serv., Great Lakes For. Cent., Sault Ste. Marie, ON. Frontline Tech. Note 108. 7 p.

McKenney, D.W.; Pedlar, J.H.; Papadopol, P.; Hutchinson, M.F. 2006b. The development of 1901–2000 historical monthly climate models for Canada and the United States. Agric. For. Meteorol. 138:69–81.

McKenney, D.; Price, D.; Papadapol, P.; Siltanen, M; Lawrence, K. 2006c. High-resolution climate change scenarios for North America. Nat. Resour. Canada, Can. For. Serv., Great Lakes For. Cent., Sault Ste. Marie, ON. Frontline Tech. Note 107. 6 p.

Monteith, J.L.; Unsworth, M.H. 2008. Principles of environmental physics. 3rd ed. Academic Press, Elsevier, Amsterdam. 418 p.

Nakićenović, N.; Alcamo, J.; Davis, G.; de Vries, B.; Fenhann, J.; Gaffin, S.; Gregory, K.; Grübler, A.; Jung, T.Y.; Kram, T.; La Rovere, E.L.; Michaelis, L.; Mori, S.; Morita, T.; Pepper, W.; Pitcher, H.; Price, L.; Raihi, K.; Roehrl, A.; Rogner, H.-H.; Sankovski, A.; Schlesinger, M.; Shukla, P.; Smith, S.; Swart, R.; van Rooijen, S.; Victor, N.; Dadi, Z. 2000. Special report on emission scenarios. A special report of Working Group III of the Intergovernmental Panel on Climate Change. Cambridge Univ. Press, Cambridge, UK, and New York, NY. 599 p. Also available from <http://www.grida.no/publications/other/ipcc_sr/>. Accessed 28 July 2010.

NCAR Data Support Section. 2004. ERA-40 Horizontal Coordinate Conventions and Numerical Attributes. Scientific Computing Division, National Center for Atmospheric Research, Boulder, CO. <http://dss.ucar.edu/datasets/common/ecmwf/ERA40/docs/horizontal-coordinate/index.html> Accessed 12 July 2011.

New, M.; Lister, D.; Hulme, M.; Makin, I. 2002. A high-resolution data set of surface climate over global land areas. Clim. Res. 21(1):1–25.

Price, D.T.; McKenney, D.W.; Caya, D.; Flannigan, M.D.; Côté, H. 2001. Transient climate change scenarios for high resolution assessment of impacts on Canada's forest ecosystems. Final report to Climate Change Action Fund. Canadian Institute for Climate Studies, Victoria, BC. <http://www.cics.uvic.ca/scenarios/index.cgi?Other_Data#transienthighres>. Accessed 21 April 2011.

Price, D.T.; McKenney, D.W.; Nalder, I.A.; Hutchinson, M.F.; Kestevan, J.L. 2000. A comparison of statistical and thin-plate spline methods for spatial interpolation of Canadian monthly mean climate data. Agric. For. Meteorol. 101:81–94.

Price, D.T.; McKenney, D.W.; Papadopol, P.; Logan, T.; Hutchinson, M.F. 2004. High resolution future scenario climate data for North America. Pages 7.7.1–7.7.13 *in* Proceedings of the 26th Conference on Agricultural and Forest Meteorology, Vancouver, BC, 23–26 August 2004. Am. Meteorol. Soc., Boston, MA. <http://ams.confex.com/ams/AFAPURBBIO/techprogram/paper_78202.htm>. Accessed 28 July 2010.

Price, D.T.; Scott, D. 2006. Final report to Government of Canada: Climate Change Impacts and Adaptation Program. Project A636: Large scale modelling of Canada's forest ecosystem responses to climate change. 2nd ed. <http://adaptation.nrcan.gc.ca/projdb/pdf/116_e.pdf>. Accessed 28 July 2010.

Rehfeldt, G.E. 2006. A spline model of climate for the western United States. Rocky Mt. Res. Stn. Gen. Tech. Rep. 165. US Dep. Agric., For. Serv., Rocky Mt. Res. Stn., Ft. Collins, CO. 21 p.

Sauchyn, D.J.; Skinner, W.R. 2001. A proxy record of drought severity for the southwestern Canadian plains. Can. Wat. Resour. J. 26(2):253–272.

Sauchyn, D.J.; Stroich, J.; Beriault, A. 2003. A paleoclimatic context for the drought of 1999–2001 in the northern Great Plains of North America. Geogr. J. 169(2):158–167.

Semenov, M.A.; Barrow, E.M. 1997. Use of a stochastic weather generator in the development of climate change scenarios. Clim. Chang. 35:397–414.

Solomon, S.; Qin, D.; Manning, M.; Chen, Z.; Marquis, M.; Averyt, K.B.; Tignor, M.; Miller, H.L., editors. 2007. Climate change 2007: the physical science basis. Contribution of Working Group I to the Fourth Assessment Report of the Intergovernmental Panel on Climate Change. Cambridge Univ. Press, Cambridge, UK. 996 p.

Snyder, J.P. 1987. Map projections—a working manual. U.S. Geol. Surv. Prof. Pap. 1395. U.S. Gov. Print. Off., Washington, DC. 383 p.

Stocks, B.J.; Mason, J.A.;Todd, J.B.; Bosch, E.M.; Wotton, B.M.; Amiro, B.D.; Flannigan, M.D.; Hirsch, K.G.; Logan, K.A.; Martell, D.L.; Skinner, W.R. 2002. Large forest fires in Canada, 1959–1997. J. Geophys. Res. 108:8149–60. DOI:10.1029/2001JD000484.

Wiken, E.B., compiler. 1986. Terrestrial ecozones of Canada. Environ. Can., Ecol. Land Classif. Ser. 19. Environ. Can. Hull, QC. 26 p.

Wilby, R.L.; Charles, S.P.; Zorita, E.; Timbal, B.; Whetton, P.; Mearns, L.O. 2004. Guidelines for use of climate scenarios developed from statistical downscaling methods. Supporting material for Intergovernmental Panel on Climate Change, Task Group on Data and Scenario Support for Impacts and Climate Analysis (TGICA). 27 p. <http://www.ipcc-data.org/guidelines/dgm_no2_v1_09_2004.pdf>. Accessed 28 July 2010.

Wilby, R.L.; Dawson, C.W.; Barrow, E.M. 2002. SDSM—a decision support tool for the assessment of regional climate change impacts. Environ. Model. Softw. 17:145–157.

Wilks, D.S.; Wilby, R.L. 1999. The weather generation game: a review of stochastic weather models. Prog. Phys. Geogr. 23(3):329–357.

Williams, J.W.; Jackson, S.T.; Kutzbach, J.E. 2007. Projected distributions of novel and disappearing climates by 2100 AD. Proc. Natl. Acad. Sci. U. S. A. 104(14):5738–5742.

APPENDIX 1

EXAMPLES OF METADATA

Examples of metadata embedded in the general circulation model (GCM) NetCDF files downloaded from the data portal of the Program for Climate Model Diagnosis and Intercomparison Coupled Model Intercomparison Project 3. These metadata were obtained directly from the data files that were used to create the input data for interpolation by the ANUSPLIN software package (using ncdump –h <fname>) and hence can be considered sample documentation of the GCM simulation results used to create all of the climate scenario products described in the main report.

NCAR-CCSM3.0 (Community Climate System Model, version 3.0, US National Center for Atmospheric Research)

```
:table_id = “Table A1” ;
:title = “model output prepared for IPCC AR4” ;
:institution = “NCAR (National Center for Atmospheric \n”,
       “Research, Boulder, CO, USA)” ;
:source = “CCSM3.0, version beta19 (2004): \n”,
       “atmosphere: CAM3.0, T85L26;\n”,
       “ocean : POP1.4.3 (modified), gx1v3\n”,
       “sea ice : CSIM5.0, T85;\n”,
       “land : CLM3.0, gx1v3” ;
:contact = “ccsm@ucar.edu” ;
:project_id = “IPCC Fourth Assessment” ;
:Conventions = “CF-1.0” ;
:references = “Collins, W.D., et al., 2005:\n”,
       “ The Community Climate System Model, Version 3\n”,
       “ Journal of Climate\n”,
       “ \n”,
       “ Main website: http://www.ccsm.ucar.edu” ;
:acknowledgment = “ Any use of CCSM data should acknowledge the contribution\n”,
       “ of the CCSM project and CCSM sponsor agencies with the \n”,
       “ following citation:\n”,
       “ \’This research uses data provided by the Community Climate\n”,
       “ System Model project (www.ccsm.ucar.edu), supported by the\n”,
       “ Directorate for Geosciences of the National Science Foundation\n”,
       “ and the Office of Biological and Environmental Research of\n”,
       “ the U.S. Department of Energy.\’\n”,
       “In addition, the words \’Community Climate System Model\’ and\n”,
       “ \’CCSM\’ should be included as metadata for webpages referencing\n”,
       “ work using CCSM data or as keywords provided to journal or book\n”,
       “publishers of your manuscripts.\n”,
       “Users of CCSM data accept the responsibility of emailing\n”,
       “ citations of publications of research using CCSM data to\n”,
       “ ccsm@ucar.edu.\n”,
       “Any redistribution of CCSM data must include this data\n”,
       “ acknowledgement statement.” ;
:realization = 5 ;
:experiment_id = “720 ppm stabilization experiment (SRES A1B)” ;
:history = “Created from CCSM3 case b30.040e\n”,
       “ by strandwg@ucar.edu\n”,
       “ on Thu Dec 9 12:52:07 MST 2004\n”,
       “ \n”,
       “ For all data, added IPCC requested metadata” ;
:comment = “This simulation was initiated from year 2000 of \n”,
       “ CCSM3 model run b30.030e and executed on \n”,
       “ hardware bluesky.ucar.edu. The input external forcings are\n”,
       “ozone forcing: A1B.ozone.128x64_L18_1991-2100_c040528.nc\n”,
       “aerosol optics : AerosolOptics_c040105.nc\n”,
       “aerosol MMR : AerosolMass_V_128x256_clim_c031022.nc\n”,
       “carbon scaling : carbonscaling_A1B_1990-2100_c040609.nc\n”,
       “solar forcing: Fixed at 1366.5 W m-2\n”,
       “GHGs : ghg_ipcc_A1B_1870-2100_c040521.nc\n”,
       “GHG loss rates : noaamisc.r8.nc\n”,
       “volcanic forcing : none\n”,
       “DMS emissions: DMS_emissions_128x256_clim_c040122.nc\n”,
       “oxidants : oxid_128x256_L26_clim_c040112.nc\n”,
       “SOx emissions: SOx_emissions_A1B_128x256_L2_1990-2100_c040608.nc\n”,
```

```
“ Physical constants used for derived data:\n»,
“ Lv (latent heat of evaporation): 2.501e6 J kg-1\n»,
“ Lf (latent heat of fusion ): 3.337e5 J kg-1\n»,
“ r[h2o] (density of water ): 1000 kg m-3\n»,
“ g2kg (grams to kilograms ): 1000 g kg-1\n»,
“ \n»,
“ Integrations were performed by NCAR and CRIEPI with support\n»,
“ and facilities provided by NSF, DOE, MEXT and ESC/JAMSTEC.» ;
```

MIROC3.2mr (Model for Interdisciplinary Research on Climate, version 3.2, medium resolution, Center for Climate System Research, Japan)

```
:title = “CCSR/NIES/FRCGC model output prepared for IPCC Fourth Assessment climate
of the 20th Century experiment (20C3M)”
institution = “CCSR/NIES/FRCGC (Center for Climate System Research, Tokyo, Japan /
National Institute for
Environmental Studies, Ibaraki, Japan / Frontier Research Center for Global Change,
Kanagawa, Japan)”
:source = “MIROC3.2 (2004): atmosphere: AGCM (AGCM5.7b, T42 L20); ocean & sea ice:
COCO (COCO3.3, 256x192 L44); land: MATSIRO (T42)” ;
:contact = “Toru Nozawa (nozawa@nies.go.jp)”
:project_id = “IPCC Fourth Assessment” ;
:table_id = “Table A1 (8 October 2004)” ;
:experiment_id = “climate of the 20th Century experiment (20C3M)” ;
:realization = 3 ;
:cmor_version = 0.96f ;
:Conventions = “CF-1.0” ;
:history = “output from MIROC3.2 At 20:53:37 on 10/14/2004, CMOR rewrote data to
comply with CF standards and IPCC Fourth Assessment requirements” ;
:references = “K-1 Coupled GCM Description (K-1 Technical Report No.1) in
preparation” ;
:comment = “This run was initiated after 300-year spin-up of the coupled model from
an arbitrary chosen initial condition (a snapshot result of a previous version of
the model). The preceding spinup was forced by fixed external conditions for the year
1850, including solar and volcanic forcings, GHGs concentration, various aerosols
emissions and land use, while all those conditions were changed according to
historical data during the 20C in the course of this run.” ;
```

CGCM3.1mr (Third Generation Coupled Global Climate Model, version 3.1, medium resolution, Canadian Centre for Climate Modelling and Analysis)

```
:title = “CCCma model output prepared for IPCC Fourth Assessment 720 ppm
stabilization experiment (SRES A1B)” ;
:institution = “CCCma (Canadian Centre for Climate Modelling and Analysis, Victoria,
BC, Canada)” ;
:source = “CGCM3.1 (2004): atmosphere: AGCM3 (GCM13d, T47L31); ocean: CCCMA
(OGCM3.1,192x96L29)” ;
:contact = “Greg Flato (Greg.Flato@ec.gc.ca)” ;
:project_id = “IPCC Fourth Assessment” ;
:table_id = “Table A1 (17 November 2004)” ;
:experiment_id = “720 ppm stabilization experiment (SRES A1B)” ;
:realization = 5 ;
:cmor_version = 0.96f ;
:Conventions = “CF-1.0” ;
:history = “ At 20:30:10 on 06/07/2005, CMOR rewrote data to comply with CF
standards and IPCC Fourth Assessment requirements” ;
:comment = “This model run continues from the end of the 20th century simulation
```

with GHG and aerosol loadings for the IPCC SRES A1B scenario as tabulated in the IPCC Third Assessment Report, Appendix II. The CO2 concentrations are from the Bern-CC model (Contribution of Working Group I to the Third Assesment Report of IPCC, p808) and the aerosol loadings are from O. Boucher, Laboratoire d\'Optique Atmospherique, France. For years 2101-2300, all GHG concentrations and the aerosol loading are held constant at the values obtained by extrapolation to year 2101." ;

CSIRO Mark 3.5 (Australian Commonwealth Scientific and Industrial Research Organisation Mark 3.5 Climate System Model)

:title = "CSIRO model output prepared for IPCC Fourth Assessment" ;
:institution = "CSIRO (CSIRO Atmospheric Research, Melbourne, Australia)" ;
:source = "CSIRO Mk3.5d (2005): atmosphere: spectral (T63L18); ocean: MOM2.2 (1.875x0.925L31)" ;
:contact = "Mark Collier (Mark.Collier@csiro.au), Martin Dix (Martin.Dix@csiro.au), Tony Hirst (Tony.Hirst@csiro.au)" ;
:project_id = "IPCC Fourth Assessment" ;
:experiment_id = "720 ppm stabilization experiment (SRES A1B)" ;
:realization = 1 ;
:Conventions = "CF-1.0" ;
:references = "Model described by Gordon et al. The CSIRO Mk3 Climate System Model, 2002, www.dar.csiro.au/publications/gordon_2002a.pdf" ;
:comment = "SRES A1B experiment with CSIRO Mk 3.5d model, starting from year 2000 (model year 300) of 20C3M experiment. Radiative forcings held constant from year 2100." ;
:history = "Date/Time stamp=year:2006:month:04:day:11:hour:06:minute:04:second:59:UTC. Processed from model output using tcl-nap version 8.4." ;
:table_id = "Table A1a" ;